



Escuela de Doctorado de la Universitat Jaume I

**Design of catalytic systems for sustainable
processes development: hydrogen storage and
biomass transformation**

Andrés Mollar Cuni

Directors:

Prof. José A. Mata Martínez
Dr. Gregorio Guisado barrios

Tutor:

Prof. José A. Mata Martínez

Castellón de la Plana, January 2023



Programa de Doctorado en Ciencias

Escuela de Doctorado de la Universitat Jaume I

**Design of catalytic systems for sustainable processes
development: hydrogen storage and biomass transformation**

**Memòria presentada per Andrés Mollar Cuni per a optar al grau
de doctor/a per la Universitat Jaume I**

Andrés Mollar Cuni

José A. Mata Martínez

Gregorio Guisado Barrios

Castellón de la Plana, January 2023

Financial support

The present Doctoral thesis has been carried out thanks to the “Subvenciones para la contratación de personal investigador de carácter predoctoral” (Reference: ACIF/2019/100), and the short stages program (Reference: BEFPI/2021/065) which allowed me to carry out a stage from 06/09/2021 to 06/12/2022 in the Laboratory of Coordination Chemistry (LCC) of CNRS in Toulouse under the supervision of Prof. Rosa M. Axet. Both programs have been financed by Generalitat Valenciana Government.

The work developed in this Doctoral Thesis has been possible thanks to the financial support from the following research projects:

- MICIU (Ref. RTI2018-098237-B-C22)
- Generalitat Valencia (Ref. PROMETEU/2020/028)
- Universitat Jaume I (Ref. UJI-B2018-23)



License

Llicència CC Reconeixement - Compartir igual (BY-SA).

Es pot reutilitzar contingut de la teua tesi indicant expressament que tu eres l'autor/a. També es poden crear altres obres a partir de la teua, sempre amb la mateixa llicència que la teua tesi. És la llicència recomanada per TDX i Repositori UJI.

Scientific Divulcation

The results obtained throughout the development of the current PhD Thesis have led to four publications in high impact scientific journals and one submitted:

- (1) Mollar-Cuni, A.; Ventura-Espinosa, D.; Martín, S.; García, H.; Mata, J. A.; Reduced Graphene Oxides as Carbocatalysts in Acceptorless Dehydrogenation of N-Heterocycles. *ACS Catal.* **2021**, *11*, 14688–14693. <https://doi.org/10.1021/acscatal.1c04649>. Impact Factor: 13.700
- (2) Mollar-Cuni, A.; Borja, P.; Martin, S.; Guisado-Barrios, G.; Mata, J. A.: A Platinum Molecular Complex Immobilised on the Surface of Graphene as Active Catalyst in Alkyne Hydrosilylation. *Eur. J. Inorg. Chem.* **2020**, 4254–4262. <https://doi.org/10.1002/ejic.202000356>. Impact Factor: 2.524
- (3) Mollar-Cuni, A.; Ventura-Espinosa, D.; Martín, S.; Mayoral, Á.; Borja, P.; Mata, J. A.; Stabilization of Nanoparticles Produced by Hydrogenation of Palladium-N-Heterocyclic Carbene Complexes on the Surface of Graphene and Implications in Catalysis. *ACS Omega* **2018**, *3*, 15217–15228. <https://doi.org/10.1021/acsomega.8b02193>. Impact factor: 2.584
- (4) Mollar-Cuni, A.; Byrne, J. P.; Borja, P.; Vicent, C.; Albrecht, M.; Mata, J. A.; Selective Conversion of Various Monosaccharaides into Sugar Acids by Additive-Free Dehydrogenation in Water. *ChemCatChem* **2020**, *12*, 3746–3752. <https://doi.org/10.1002/cctc.202000544>. Impact Factor: 5.686
- (5) Mollar-Cuni, A; Martín, S.; Guisado-Barrios, G.; Mata, J. A.; Dual role of graphene as support of ligand-stabilized palladium nanoparticles and carbocatalyst for (de)hydrogenation of N-Heterocycles. *Carbon*, **2022**, Submitted (CARBON-D-22-04236).

This thesis has been accepted by the co-authors of the publications listed above that have waved the right to present them as a part of another PhD thesis.

During the PhD process the following works have also been published:

- (1) Mollar-Cuni, A.; Mejuto, C.; Ventura-Espinosa, D.; Borja, P.; Mata, J. A. Introducing Catalysis to Undergraduate Chemistry Students: Testing a Ru-NHC Complex in the Selective Dehydrogenative Coupling of Hydrosilanes and Alcohols. *J. Chem. Educ.* **2021**, *98*, 2638–2642. <https://doi.org/10.1021/acs.jchemed.1c00032>. Impact factor: 3.208
- (2) Porcar, R.; Mollar-Cuni, A.; Ventura-Espinosa, D.; Luis, S. V.; García-Verdugo, E.; Mata, J. A. A Simple, Safe and Robust System for Hydrogenation “without High-Pressure Gases” under Batch and Flow Conditions Using a Liquid Organic Hydrogen Carrier. *Green Chem.* **2022**, *24*, 2036–2043. <https://doi.org/10.1039/D1GC03850H>.
- (3) García-Zaragoza, A.; Cerezo-Navarrete, C.; Mollar-Cuni, A.; Oña-Burgos, P.; Mata, J. A.; Corma, A.; Martínez-Prieto, L. M. Tailoring Graphene-Supported Ru Nanoparticles by Functionalization with Pyrene-Tagged N-Heterocyclic Carbenes. *Catal. Sci. Technol.* **2022**, *12*, 1257–1270. <https://doi.org/10.1039/d1cy02063c>.
- (4) Martínez-Laguna, J.; Mollar-Cuni, A.; Ventura-Espinosa, D.; Martín, S.; Caballero, A.; Mata, J. A.; Pérez, P. J. Gold Nanoparticle-Catalysed Functionalization of Carbon–hydrogen Bonds by Carbene Transfer Reactions. *Dalt. Trans.* **2022**, *51*, 5250–5256. <https://doi.org/10.1039/D1DT04351J>.
- (5) Mollar-Cuni, A.; Ibáñez-Ibáñez, L.; Guisado-Barrios, G.; Mata, J. A.; Vicent, C. Introducing Ion Mobility Mass Spectrometry to Identify Site-Selective C–H Bond Activation in N-Heterocyclic Carbene Metal Complexes. *J. Am. Soc. Mass Spectrom.* **2022**, *33*, 2291–2300. <https://doi.org/10.1021/jasms.2c00257>

And the following patents:

- (1) Mata, J. A.; Mejuto-Nieblas, C.; Mollar-Cuni, A.; Ibáñez-Ibáñez, L.; Baya, M.; Guisado-Barrios, G. Procedimiento de almacenamiento de hidrógeno en forma líquida (fenol/ciclohexanol). Patent number: P202131178 (20/12/2021)
- (2) Mata, J. A.; Mas-Marzá, E.; Fabregat, F.; Guerrero, A.; Mejuto-Nieblas, C.; Mollar-Cuni, A.; El Guenani, N.; Carvajal, D. Procedimiento reversible de almacenamiento-liberación de hidrógeno en forma líquida (almacenamiento de hidrógeno utilizando derivados de aminas/nitrilos). Patent number: P202230632 (11/07/2022)

Index	i
List of abbreviatons	vi
Abstract	viii
CHAPTER 1: Introduction & Objectives	1
1.1 TOWARDS A SUSTAINABLE SOCIETY	3
1.1.1 The principles of green chemistry	5
1.1.2 The role of catalysis in sustainable chemistry	8
1.2 ENERGY PRODUCTION vs SUSTAINABILITY	18
1.2.1 Hydrogen economy	22
1.3 SUSTAINABLE TRANSFORMATIONS AND BIOMASS AS FEEDSTOCK FOR CHEMICALS PRODUCTIONS	25
1.3.1 Sustainable catalytic reactions	26
1.3.2 Revalorization of biomass	35
1.4 OBJECTIVES	38
1.5 REFERENCES	39
CHAPTER 2: Reduced Graphene Oxides as Carbocatalysts in Acceptorless Dehydrogenation of N-Heterocycles	53
2.1 INTRODUCTION	55
2.2 RESULTS AND DISCUSSION	57
2.3 CONCLUSIONS	64
2.4 SUPPORTING INFORMATION	65
2.5 REFERENCES	79

CHAPTER 3: A platinum molecular complex immobilized on the surface of graphene as active catalyst in alkyne hydrosilylation	83
3.1 INTRODUCTION	85
3.2 RESULTS AND DISCUSSION	87
3.3 CONCLUSIONS	101
3.4 SUPPORTING INFORMATION	102
3.5 REFERENCES	110
CHAPTER 4: Stabilization of nanoparticles produced by hydrogenation of Palladium-NHC complexes on the surface of graphene and implications in catalysis	115
4.1 INTRODUCTION	117
4.2 RESULTS AND DISCUSSION	118
4.3 CONCLUSIONS	134
4.4 SUPPORTING INFORMATION	135
4.5 REFERENCES	143
CHAPTER 5: Selective conversion of various monosaccharaides into sugar acids by additive-free hydrogenation in water	149
5.1 INTRODUCTION	151
5.2 RESULTS AND DISCUSSION	153
5.3 CONCLUSIONS	164
5.4 SUPPORTING INFORMATION	165
5.5 REFERENCES	175

CHAPTER 6: Dual role of graphene as support of ligand-stabilized palladium nanoparticles and carbocatalyst for (de)hydrogenation of N-heterocycles	179
6.1 INTRODUCTION	181
6.2 RESULTS AND DISCUSSION	183
6.3 CONCLUSIONS	195
6.4 SUPPORTING INFORMATION	196
6.5 REFERENCES	203
CHAPTER 7: Conclusions	207
APPENDIX	211

List of abbreviations

4-ADPA	4-aminodiphenylamine
AC	Activated carbon
ADH	Acceptorless dehydrogenation reaction
AE	Atom economy
a. u.	Arbitrary units
Ca.	Circa
C ₃ N ₄	Carbon nitride
CDGs	Chemically derived graphenes
CID	Collision induced dissociation
CNTs	Carbon nanotubes
COD	Cyclooctadiene
DBT	Dibenzyltoluene
DIPB	1,3-diisopropylbenzene
DIPEA	N,N-diisopropylethylamine
DMF	N,N-dimethylformamide
DMS	Dimethylsulfide
DMSO	Dimethylsulfoxide
dvtms	Divinyltetramethyldisiloxane
E _a	Activation energy
ECB	European central bank
EDX	Energy dispersive X-Ray spectrometer
E-Factor	Environmental Impact Factor
eq	Equivalent

ESI/MS	Mass spectrometry with electrospray ionization
Et	Ethyl
eV	Electron volts
G	Graphene
GO	Graphene oxide
GC/FID	Gas chromatography with flame ionization detector
h	Hour
^1H or ^{13}C	Proton or carbon nuclear magnetic resonance
δ	Chemical shift
d	Doublet
t	Triplet
m	Multiplet
HMF	Hydroxymethylfurfural
HPLC	High performance liquid chromatography
HRTEM	High resolution transmission electron microscopy
HSC	Hydrogen storage capacity
ICP/MS	Inductively coupled plasma mass spectrometry
kcal	Kilocalorie
kg	Kilogram
kJ	Kilojoule
kW	Kilowatts
LOHCs	Liquid organic hydrogen carriers
H_o -LOHCs	Hydrogen poor molecule of a LOHC
H_r -LOHCs	Hydrogen rich molecule of a LOHC
Me	Methyl
MeOH	Methanol

MHC	Methyl cyclohexane
MHz	Megahertz
min	Minutes
mL	Milliliter
NHCs	N-heterocyclic carbenes
nPr	n-Propyl
<i>o</i> -DCB	1,2-dichlorobenzene
ODH	Oxidative dehydrogenation reaction
OMC	Ordered mesoporous carbon
Pd/C	Palladium over carbon
PEPSI	Pyridine-enhanced precatalyst preparation
Ph	Phenyl
phDBT	Perhydrodibenzyltoluene
PMS	Peroxymonosulfate
POP	Phosphorous-oxygen-phosphorous
ppm	Parts per million
PVP	Poly(4-vinylpyridine)
Q	Quinoline
rGO	Reduced graphene oxide
rGO ^t	Graphene oxide thermally reduced
rGO ^{COOH}	Reduced graphene oxide with masked carboxylic acid groups
rGO ^{CO}	Reduced graphene oxide with masked carbonyl groups
rGO ^{OH}	Reduced graphene oxide with masked hydroxyl groups
R. T.	Room temperature
STEM	Scanning transmission electron microscopy
ta	Tones

TASF	Tris(dimethylamino)sulfonium difluorotrimethylsilicate
TCD	Thermal conductivity detector
TGA	Thermogravimetric analysis
THQ	Tetrahydroquinoline
TMS	Trimethylsilyl
TNT	Trinitrotoluene
TOF	Turnover frequency
TON	Turnover number
Tol	Toluene
Trz	1,2,3-triazolyliedene
US	Ultrasounds
UV-Vis	Ultraviolet-visible spectroscopy
wt%	Weight per cent
XPS	X-Ray photoelectron spectroscopy

ABSTRACT

The objective of this PhD Thesis is the design and development of more sustainable catalytic processes trying to address some of the current challenges that today our society is facing such as the seek for clean energy alternatives, the reduction of environmental pollution and industrial waste (greenhouse gases, sewage). To contribute to this arduous task, the 12 principles of Green Chemistry have been followed as a guide. Special attention has been paid to the use of catalysis, the development of atom economical processes, design for efficient energy relevant to the hydrogen economy and the use of biomass transformation.

The catalytic properties of graphene-derived materials as carbocatalysts are evaluated in acceptorless dehydrogenation of N-heterocycles. Among them, reduced graphene oxides (**rGOs**) are active under mild conditions acting as efficient heterogeneous systems. This reaction is important from the synthetic viewpoint as N-heterocycles are found in many added-value organic compounds. They are also considered interesting potential Liquid Organic Hydrogen Carriers (LOHCs) for hydrogen storage.

Classical synthetic methodologies employed in the chemical sector produce high quantity of waste, making this scenario unsustainable. For this reason, there is a growing necessity to develop sustainable methodologies with high atom economy (AE) and selectivity. For instance, hydrosilylation and semi-hydrogenation of alkynes are good examples of this. To carry out these transformations in a sustainable-manner, different supported catalysts onto **rGO** have been developed. The properties of such hybrid materials are discussed in terms of activity, stability and reusability.

Abundant sugars of five and six carbon atoms are promising candidates to produce valuable platform chemicals. In chapter 5, it is described the catalytic dehydrogenation of several pentoses and hexoses into their corresponding aldonic acids with the concomitant formation of molecular hydrogen (H₂). This biomass transformation is catalyzed by highly active and selective catalysts based on iridium-(III) complexes containing a 1,2,3-triazolylidene (trz) as ligand. Monosaccharides are converted into sugar acids in an easy and sustainable manner using only catalyst and water under reflux conditions.

Finally, the use of **rGO** as support to immobilize PdNPs results an efficient catalytic material towards hydrogenation and dehydrogenation of N-heterocycles. The **rGO** plays a dual role by acting as a carbocatalyst in acceptorless dehydrogenation of N-

heterocycles and as a support for the palladium nanoparticles. The mild conditions used in both transformations represent a potential application of this system for hydrogen storage technologies in the form of liquid organic hydrogen carriers (LOHCs). The use of a single solid catalyst that is recyclable in hydrogen conversion and reconversion through (de)hydrogenation of N-heterocycles paves the way for the development of efficient hydrogen storage materials.

ABSTRACT

El objetivo de esta tesis doctoral es el diseño y desarrollo de procesos catalíticos más sostenibles enfocados a algunos de los principales desafíos a los que se enfrenta nuestra sociedad actualmente. Entre tales desafíos esta la búsqueda de fuentes de energía alternativas más limpias, la reducción de la contaminación ambiental y los residuos industriales. Para realizar esta ardua tarea se han utilizado los 12 principios de la química verde como guía. Entre ellos hay que destacar el uso de procesos catalíticos, sistemas de almacenamiento de hidrógeno y el uso de biomasa como materia prima.

En primer lugar, se han evaluado las propiedades catalíticas de materiales derivados del grafeno en la deshidrogenación (sin aceptor de hidrogeno) de N-Heterociclos. Entre ellos, el óxido de grafeno reducido (**rGO**) es activo bajo condiciones suaves actuando como un eficiente carbocatalizador en dicha transformación. La deshidrogenación de N-Heterociclos es una reacción importante desde el punto de vista sintético ya que los N-heterociclos se encuentran en muchos compuestos orgánicos de alto valor añadido. Además, a este tipo de moléculas se les considera potenciales líquidos orgánicos transportadores de hidrogeno (LOHCs) para su utilización en almacenamiento de hidrogeno.

Las metodologías clásicas empleadas en el sector químico producen una gran cantidad de desechos, siendo este escenario insostenible. Por esta razón, hay una creciente necesidad por desarrollar metodologías sostenibles que presenten una alta economía atómica (AE) y sean selectivas. Las reacciones de hidrosililación y la semihidrogenación de alquinos son buenos ejemplos de ello. Para llevar a cabo estas transformaciones de una forma sostenible, se han desarrollado catalizadores soportados utilizando rGO. Las propiedades catalíticas de estos materiales híbridos se han estudiado en términos de actividad, estabilidad y reciclabilidad.

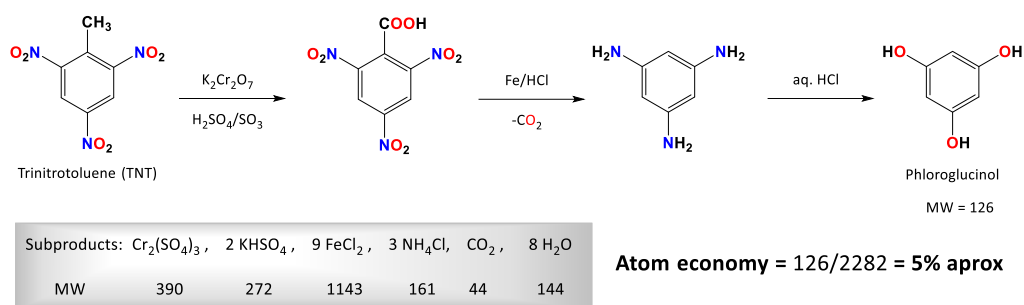
Los azúcares de cinco o seis carbonos, pentosas y hexosas respectivamente, son candidatos potenciales como materia prima en la obtención de productos de valor añadido. En el capítulo 5 se describe la deshidrogenación catalítica de varias pentosas y hexosas en sus correspondientes ácidos aldonicos con la correspondiente formación de hidrogeno molecular (H_2). La transformación de biomasa se lleva a cabo mediante el empleo de complejos de iridio (III) con un ligando 1,2,3-triazolylidene (trz) que resultan ser unos catalizadores altamente activos y sobre todo selectivos. Los monosacáridos son convertidos en los correspondientes ácidos de forma sencilla y sostenible utilizando únicamente el catalizador en medio acuoso a 100 °C.

Finalmente, se utilizó el rGO como soporte para inmovilizar nanopartículas de paladio. Este material híbrido resultó ser un catalizador eficiente tanto para la deshidrogenación de quinoleínas como para su posterior hidrogenación. En este caso el rGO juega un papel dual, actuando como carbocatalizador en la reacción de deshidrogenación y como soporte y estabilizador de las nanopartículas en la reacción de hidrogenación. Las condiciones suaves empleadas para ambas reacciones hacen de este sistema un candidato ideal para ser utilizado como LOHCs. El uso de un solo catalizador que sea reciclable tanto para el paso de hidrogenación como de deshidrogenación de N-heterociclos facilita el desarrollo de sistemas de almacenamiento de hidrogeno eficientes.

CHAPTER 1:

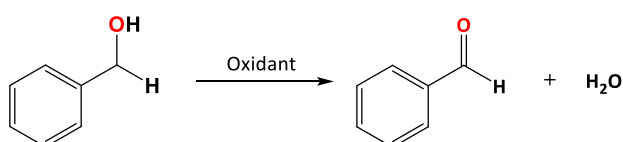
Introduction & Objectives

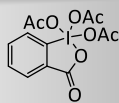
The present PhD. Thesis is the result of research efforts directed towards the design and development of more sustainable catalytic processes trying to address some of the current challenges that today our society is facing such as the seek for clean energy alternatives, the reduction of environmental pollution and industrial waste (greenhouse gases, sewage), as well as to increase the use of renewable resources. To contribute to this arduous task, the 12 principles of Green Chemistry have been followed as a guide. Special attention has been paid to the use of catalysis, the development of atom economical processes, design for efficient energy relevant to the hydrogen economy and the use of biomass transformation. For this purpose, novel strategies to improve both, heterogeneous and homogeneous catalytic processes have been studied and are now found within this PhD Thesis, which is comprised of 7 chapters. Each one includes a more in-depth introduction complementary to this first general introduction.



Scheme 1.2 Reaction equation of classical synthesis of phloroglucinol with the molecular weight of products and byproducts.

A neater example of AE utility is obtained when applying this factor in the alcohol oxidation reaction. Classical oxidants such as Dess-Martin periodinane, Jones's reagent or Swern oxidation have low atom economy producing high quantity of waste (high E-Value, see *infra*), making the process inefficient. Alternatively, the use of O_2 and H_2O_2 could be considered as a cleaner solution, which not only would afford higher AE values, but also because they are least expensive oxidants (per mole).¹ As counter example is the more recent and efficient acceptorless dehydrogenation reaction of alcohols. Through this procedure, alcohols are oxidized without the necessity of any stoichiometric oxidant. This methodology has an AE of 98% and produces only H_2 as byproduct (Scheme 1.3).



Oxidant	-*	O_2	NaOCl	$\text{CrO}_3/\text{H}_2\text{SO}_4$	$\text{DMSO}/(\text{COCl})_2$	
AE (%)	98	87	48	44	37	22

* H_2 as byproduct

Scheme 1.3 Different procedures to oxidized alcohols with its AE.

In 1992, only one year later, R.A. Sheldon introduced the concept of “Environmental Impact Factor” or “E-Factor”, which could be defined as the mass ratio of waste to the desired product.⁷ A higher rate of E-factor means more waste and, consequently, greater negative environmental impact. When this factor is applied to the different areas of the chemical industry (Table 1.1), it reveals the necessity, particularly for the fine chemistry and pharmaceutical sectors, to reduce the huge amount of waste formed in their manufacturing processes.

Table 1.1 E Factors in the chemical industry.

Industry Sector	Tonnage	E-Factor (Kgs waste/Kgs product)
Oil refining	10^6 - 10^8	<0.1
Bulk chemicals	10^4 - 10^6	<1 - 5
Fine chemicals	10^2 - 10^4	5 - >50
Pharmaceuticals	10 - 10^3	25 - >100

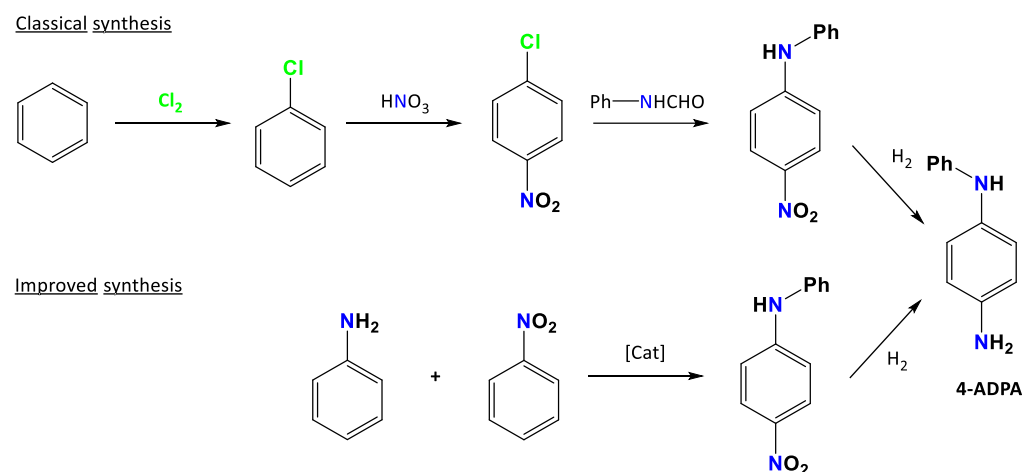
1.1.1 The principles of green chemistry

Clearly a new paradigm was needed to define the efficiency in organic synthesis.⁸ Classical methodologies produced high quantity of waste and consumed huge amounts of energy. This environmentally unfriendly situation could not be sustained any longer.⁹ Under this scenario, it was introduced the term “Green Chemistry” used to describe minimum impact in chemistry or “benign by design chemistry”.¹⁰ The term gained popularity and got worldwide recognition in 1998 when Anastas and Warner published the 12 principles of green chemistry.¹¹ They constitute a guiding framework for the design of new chemical products and transformations, which can be extended to all aspects of the process life-cycle ranging from the type of raw materials used, to the efficiency and safety of the transformation or the toxicity and biodegradability of products and reagents used.⁶

1. **Prevention:** It is better to prevent waste than to treat or clean up waste after it is formed.
2. **Atom economy:** Synthetic methods should be designed to maximize the incorporation of all materials used in the process into the final product.
3. **Less hazardous Chemical Synthesis:** Whenever practicable, synthetic methodologies should be designed to use and generate substances that pose little or no toxicity to human health and the environment.
4. **Designing safer chemicals:** Chemical products should be designed to preserve efficacy of the function while reducing toxicity.
5. **Safer solvents and auxiliaries:** The use of auxiliary substances (e.g. solvents, separation agents, etc.) should be made unnecessary whenever possible and, when used, innocuous.
6. **Design for efficiency energy:** Energy requirements of chemical processes should be recognized for their environmental and economic impacts and should be minimized. If possible, synthetic methods should be conducted at ambient temperature and pressure.
7. **Use of renewable feedstocks:** A raw material of feedstock should be renewable rather than depleting whenever technically and economically practicable.
8. **Reduce Derivatives:** Unnecessary derivatization (use of blocking groups, protection/deprotection, and temporary modification of physical/chemical processes) should be minimized or avoided, if possible, because such steps require additional reagents.
9. **Catalysis:** Catalytic reagents (as selective as possible) are superior to stoichiometric reagents.
10. **Design for degradation:** Chemical products should be designed so that at the end of their function they break down into innocuous degradation products and do not persist in the environment.
11. **Real-time analysis for pollution prevention:** Analytical methodologies need to be further developed to allow for real-time, in-process monitoring and control prior to the formation of hazardous substances.

12. Inherently safer chemistry for accident prevention: Substances and the form of a substance used in chemical process should be chosen to minimize the potential for chemical accidents, including releases, explosions, and fires.

The “Green Chemistry” approach is now widely accepted evidenced by the efficient and sustainable procedures at the molecular level. The concept has become firmly entrenched in both industrial and academic circles and it is a guide for the development of the chemistry in particular and the science in general.¹² A clear example is the modification of synthetic route for the synthesis of 4-aminodiphenylamine (4-ADPA) by Solutia. Traditionally, toxic and hazard chlorine gas was being employed for this transformation, as a result aqueous waste containing high quantity of inorganic salts were produced. The improved procedure consists of a base catalyzed coupling of aniline and nitrobenzene preventing the use of chlorine and reducing the waste generated (Scheme 1.4).¹³⁻¹⁵



Scheme 1.4 Classical (top) and improved (bottom) synthesis of 4-ADPA.

1.1.2 The role of catalysis in sustainable chemistry

Among the 12 principles of green chemistry, catalysis stands out being probably one of the most important. It implies the use of catalytic reagents (as selective as possible) which are superior to stoichiometric reagents. Nowadays, its use is considered gateway to green and sustainable chemistry in organic synthesis.¹⁶ A proof of its current vital importance can be seen in the last 2001, 2005, 2010 chemistry Nobel prizes, which have been awarded to catalysis-related

contributions.¹⁷ By definition, according to the IUPAC, a catalyst is “A substance that increases the rate of a reaction without modifying the overall standard Gibbs energy change in the reaction. The catalyst is both a reactant and product, is not consumed during the reaction”.¹⁸

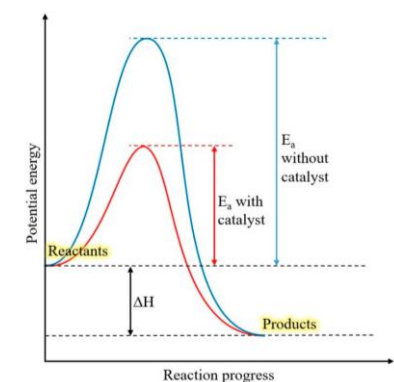


Figure 1.1 Differences in energetic profile for no-catalyzed (blue) and catalyzed (red) reaction.¹⁹

A catalyst does not modify the overall standard Gibbs energy change of the reaction but provides an alternative reaction pathway with a lower energy transition state (Figure 1.1). In other words, a catalyst does not affect the thermodynamics of the reaction, but it has a deep effect on the kinetics. For that reason, catalysis can improve the efficiency of a reaction by reducing the energy needed, by avoiding the use of stoichiometric reagents, and by increasing the selectivity towards the desired product.²⁰ This implies less energy consumption and less production of waste. Moreover, the use of catalyst opens the door to new transformations that seemed impossible with traditional methodologies. For these reasons, its use is widely spread in academics and industry, and catalyst design and development are a topic of great interest.

Catalysis can be divided into two main types, homogeneous and heterogeneous depending on the physical state of the reagents and the catalyst employed in the chemical reaction. The main differences between them are summarized in table 1.2.

Table 1.2 Differences between homogeneous and heterogeneous catalysis.

Homogeneous	Heterogeneous
Mild conditions	Harsh conditions
High activity	High activity (diffusivity can be an issue)
High selectivity	Low selectivity
Difficult catalyst separation (Difficult recycling)	Easy catalyst separation (Simply recycling)
Low stability	High stability
Well-defined active sites	Poorly defined active sites
Easy to understand the mechanism	Difficult to understand the mechanism

Homogeneous catalysis

In the case of homogeneous catalysis, the catalyst is in the same phase than the reactants. For that reason, the interaction of catalytic active centers and the reactants is easy. In this way, homogeneous catalysts tend to show better activity and selectivity than heterogeneous catalysts. In addition, homogeneous catalysts are usually well-defined molecules that can be characterized with relative ease, facilitating the study of the reaction mechanism. This information allows the design of more active and selective catalyst. However, homogeneous catalysts have a main drawback: the difficulty in catalyst recovery, being this procedure inefficient or impossible in most cases. At the same time, homogeneous catalysts sometimes show poor stability, which implies the catalyst deactivation along reaction progress and hinder its possible recovery. These types of catalysts usually are Lewis acids/bases, organic molecules (organocatalysts), ionic liquids or metal complexes.

Notably, among the latest are organometallic complexes, compounds containing at least one chemical bond between a carbon atom of an organic molecule (ligand) and a metal. These metal complexes are widely used as catalysts due to its high activity and selectivity in a huge variety of organic reactions such as olefin polymerization,²¹ hydrogenations,²² cross-coupling,^{23–25} and olefin metathesis.^{26,27} An important feature of these complexes is its versatility and modularity given, in part, by the ligands. One type of useful ligands in catalysis are N-heterocyclic carbene ligands (NHCs). NHCs are by definition cyclic carbenes (organic species with a divalent carbon with six valence electrons) bearing at least one α -amino substituent. They display higher σ -donating capacity when compared to other phosphorus or nitrogen based ligands that confer them stronger metal to ligand bond.²⁸ Imidazolylidenes are

among the most studied carbenes for that purpose due to the fine-tuning of electronic and steric properties along with the possibility of the functionalization through the backbone.²⁹ In addition, due to its carbene nature and its strong interaction with the metal, these types of ligands provide a strong stability to the complex avoiding its decomposition during the reaction progress.³⁰



Figure 1.2 Fine tuning of electronic properties and steric control of imidazolylidines.

Heterogeneous catalysis

In contrast, in the case of heterogeneous catalysis, substrates and catalysis are found in different phase. (The catalyst is usually a solid and reactants are liquids or gases). The use of biphasic system usually hampers the approximation of reactants to the active center due to mass transfer problems, producing a negative effect in the catalytic activity and as a result, harder reactions conditions (temperature or pressure) are needed in comparison with homogenous catalysis. However, despite of all these drawbacks, around 90 % of industrial catalytic processes are carried out by heterogeneous catalysts.³¹ The solid nature of the catalyst and its major stability allows its easy recyclability, making these catalysts more efficient and attractive for industry. Typical heterogeneous materials are based on zeolites, metal oxides or metal nanoparticles.

The latest of this type of materials has gained strong interest in scientific research as well as industrial applications due to their unusual properties. Thanks to their intrinsic large surface-to-volume ratios, which provide a large number of active sites per unit area, these materials shows extraordinary catalytic properties.³² Its immobilization not only prevents the agglomeration of metallic nanoparticles avoiding its deactivation but it can also produce a synergy between surface nanoparticle and support with positive effect in the catalytic properties.³³ For that

reason these types of materials are widely used as catalysts in different organic transformations.^{34,35}

Carbocatalysis

The use of carbon based materials as catalysts (carbocatalysts) is an attractive approach in this regard because of their low cost and natural abundance.³⁶ They can be defined as those catalysts whose elemental composition contains predominantly carbon, which plays an active role. It could be considered the heterogeneous version of an organocatalysts to some extent, where a homogeneous organic molecule is the active species. In carbocatalysts the key point is to incorporate the active sites into the carbon network by suitable modifications.³⁷

The term carbocatalysis encompasses a wide variety of materials such as activated carbon (AC),³⁸ CNTs,^{39,40} ordered mesoporous carbon (OMC),^{41,42} nanodiamonds,⁴³ carbon dots⁴⁴ and carbon nitride (C₃N₄).⁴⁵ Among them, it is worth highlighting the important role of chemically derived graphenes (CDGs) as carbocatalyst and particularly reduced graphene oxide (rGO).

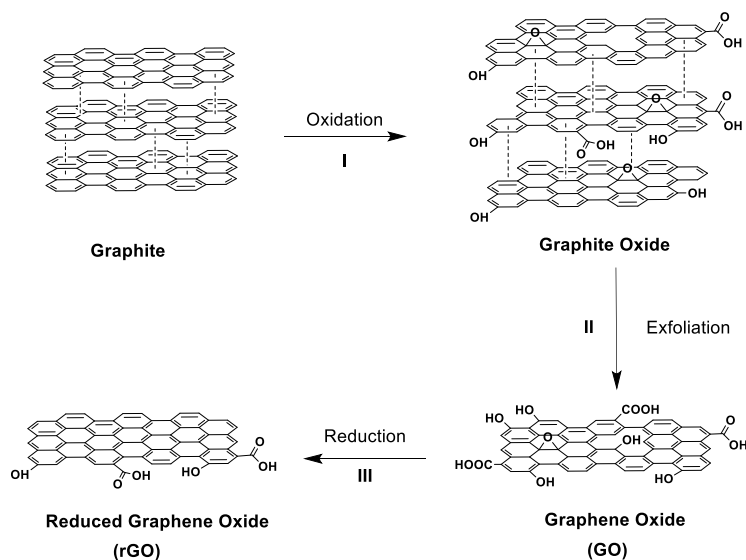
Graphene is a bidimensional layer of one atom thick sp² carbons in a hexagonal arrangement. It was obtained for the first time in 2004 by A. Geim and K. Novoselov, who were awarded with the Nobel Prize in Physics in 2010.⁴⁶ Pristine graphene shows excellent mechanical, electric, thermal, and optical properties. However, it is very expensive and unreactive so it cannot be considered a good candidate to be used as carbocatalyst. In contrast, CDGs (graphenes with a certain degree of functionalization) are more reactive and are cheaper maintaining the properties of pristine graphene. Among the existing CGD graphene oxide (GO) and reduced graphene oxide (rGO) are two of the most widely used. Pristine graphene and the related CDGs derivatives present different physical properties in terms of surface area, electrical conductivity, C/O ratio and number of layers which values are summarized in Table 1.3.

Table 1.3 Properties of pristine graphene and CDGs.

	Graphite	Graphite oxide	GO	rGO*	Graphene
Surface Area (m ² /g)	4-10	4-10	20-30	400-500	2600
Electrical conductivity (S/m)	1x10 ⁵	Insulator	Insulator	600-2400	1x10 ⁸
C/O relation	-	2-4	2-4	10-14	-
Dimensionality	3D	3D	2D	2D	2D
Number of layers	Multilayer	Multilayer	<10	<10	1

*Properties of CDGs vary depending on the synthetic route preparation

There are different synthetic routes to obtain these CGDs but from a chemical point of view the most common methodology is based on a series of sequential redox reactions and exfoliation processes.

**Scheme 1.5** Synthetic route to obtain GO and rGO from graphite.

Initially, graphite is oxidized to obtain graphite oxide (I), usually the Hummers method is used to carry out this transformation.⁴⁷ This new material now contains oxygen functionalities that reduce π - π interactions between the carbon layers facilitating its exfoliation and yielding graphene oxide (II). Then, GO can be reduced by chemical^{48,49} or thermal reduction⁵⁰ to yield the reduced graphene oxide (III),

whose properties are between GO and pristine graphene. Due to the reduction step many oxygenated functional groups are removed while resetting the π network. Thus, the material shows higher surface area, major thermal stability and major conductivity. In addition, depending on the reduction process the structure and composition can be modified and it can suffer post-synthesis functionalization, making the material tunable.^{36,50,51}

This material shows high thermal and chemical stability, high surface area and contains oxygen functionalities at the surface. Moreover, it exhibits a great facility to incorporate dopant atoms (such as N, B, P and S in less than 10 wt%) and the possibility to modify its surface with pendant units making rGO a material with potential applications in carbocatalysis. The surface defects in rGO may also act as active sites in catalysis. In addition, if dopant atoms or pendant groups are present in the material, the catalytic properties may improve (Figure 1.3).

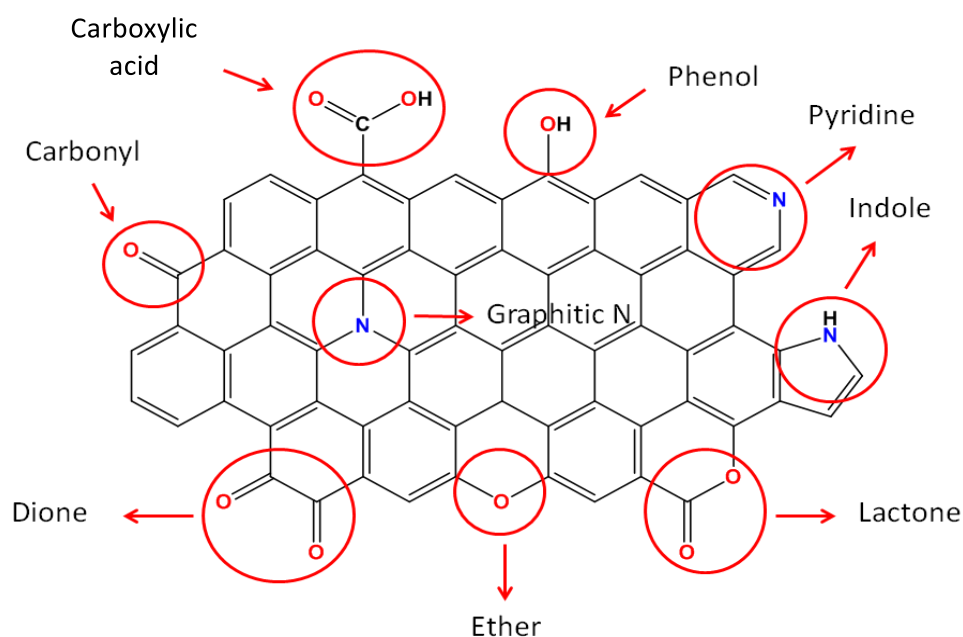


Figure 1.3 Possible catalytic active sites in rGO.

Reduced graphene oxide, has been used as carbocatalyst in different reactions such as cross coupling,⁸⁴ reduction reactions,^{53,54} photophemton reactions,⁵⁵

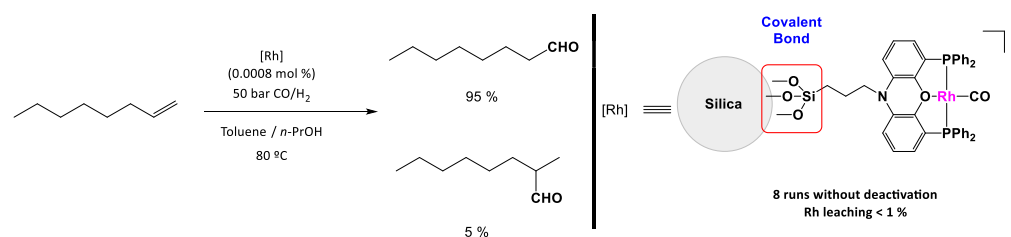
peroxymonosulfate (PMS) activation in pollutant degradation,⁵⁶ and water splitting.⁵⁷ Remark that material is widely used in oxidative dehydrogenation reactions (ODH) of different type of molecules: amines,^{36,58} N-Heterocycles⁵⁹ and alcohols.⁶⁰

Heterogenization of Homogeneous Catalysts for recycling

Transition metal-based catalysts are usually based on precious and rare metals, which are expensive and scarce, or/and by molecules obtained by complex procedures. A key factor to develop greener catalytic processes is to have an effective method to recycle them. For that reason, heterogeneous catalysts are the most used in the industry. However, to obtain more efficient catalysts, an important part of the academic research is trying to merge the benefits of homogeneous and heterogeneous catalysis, combining the activity and selectivity of homogeneous catalysts with the stability and recyclability of heterogeneous catalysts. These methodologies allow the heterogenization of traditional homogeneous catalysts and open the possibility of easy-isolation and reutilization.^{61,62}

Although different recycling strategies to heterogenize a homogenous catalyst are available, anchoring of a transition metal-based complex onto a solid support is one of the most commonly used. In this manner, the new solid catalytic material can be easily separated from the reaction media and reused. Still, the main drawback of this strategy is that the catalyst may show less activity than its homogeneous counterpart due to mass transfer problems and difficulty to access the active sites. This problem is closely related to the support used for the heterogenization of the homogeneous catalysts.

In general, the two main methodologies employed in the immobilization differ on the type of interaction between homogeneous catalyst and the solid support which can be: via covalent bond or non-covalent bond. The first one is the most extended and consists in the formation of covalent bonds between the homogenous catalyst and the support. Modification of the molecular species and surface functionalization of the support is usually needed to ensure a proper immobilization. In addition, the variation of the catalyst can alter its activity and selectivity. A clarifying example of this strategy was reported by Prof. P. Van Leeuwen in 1999, where a cationic rhodium (I) complex bearing a POP ligand was supported onto silica is active in the hydroformylation reaction.^{63,64} That catalyst can be reused 8 runs without deactivation by simple filtration (Scheme 1.6)

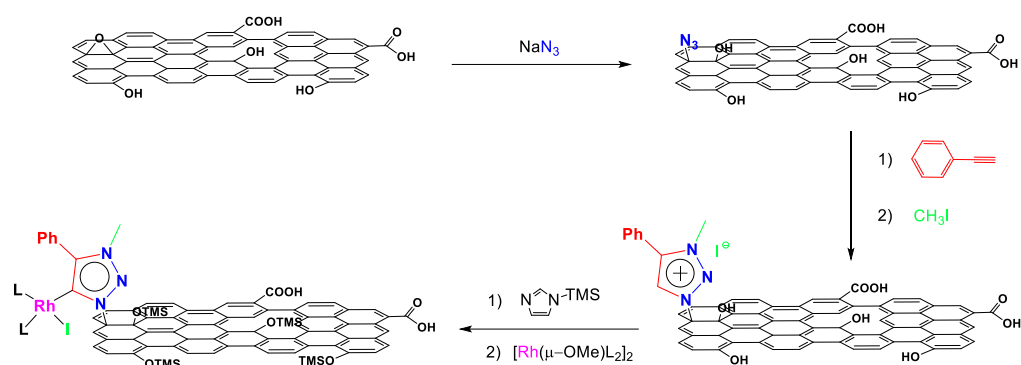


Scheme 1.6 1-Octene hydroformylation catalyzed by heterogenized Rh catalyst.

The second strategy consists in immobilizing the homogeneous system onto a solid support through non-covalent forces such as physisorption,⁶⁵ electrostatic interactions,⁶⁶ and π - π stacking.⁶⁷ Through this methodology the nature of the homogeneous catalyst is better preserved, maintaining its catalytic properties and no further functionalization steps are required. However, the interaction between homogeneous species and the support are weaker than in covalent anchoring. For that reason, it is more prone to suffer leaching. Thus, careful catalyst design is needed to ensure strong interactions between the catalyst and the support to avoid this problem.

Traditionally, the common supports to immobilize homogeneous catalysts have been silica, polymeric supports and metal nanoparticles.^{68–71} However, carbon based materials are considered promising candidates in its field. The increasing interest in the use of these materials as catalyst supports is due to its advanced properties such as inertness, mechanical and thermal stability, high surface area and the possibility to modulate and control the composition and surface functionalization.⁷² Specifically, graphene and chemically derived graphenes like rGO (above described) are considered one of the most interesting carbon based materials. Thanks to the excellent properties of rGO in terms of stability, high surface area and tuneability, it is considered an ideal material for supporting catalysis. In addition, their particular electronic properties convert rGO in an optimal material for photo- and electrocatalysis.^{73,74}

Both, covalent and no-covalent approaches have been investigated. In the first case, the presence of oxygen functionalities allows after further derivatization the incorporation of the catalyst via covalent bond facilitating the direct interaction with the support (Scheme 1.7).⁷⁵



Scheme 1.7 Synthesis of Rh-Triazole complex covalently anchored to reduced graphene oxide.

In the second case, non-covalent interactions such as electrostatic, adsorption and supramolecular forces have also been studied. Thanks to the extended π -cloud of reduced graphene oxide, it is considered an ideal material to support molecular catalysts bearing an aromatic auxiliary through π stacking interactions. This interaction is a Van der Waals forces and the energy of a single interaction is low, about 2 kJ/mol.⁷⁶ However, the complete strength between a polyaromatic system and rGO depends on the number of aromatic rings of the molecule aromatic region and the curvature contact with rGO surface. For these reasons, molecular catalyst must possess a polyaromatic moiety such as pyrene to strength the interaction with graphene and ensure immobilization. The advantage of this methodology is that neither the catalyst nor the support needs to be modified during the immobilization process.

Immobilization of homogeneous catalyst over carbon surfaces through π stacking interactions is well studied for grafting metal complexes onto carbon nanotubes (a graphene sheet rolled into a cylindrical shape).⁷⁷⁻⁷⁹ However, the use of rGO for this purpose is a novel strategy pioneered by our research group and only a few examples can be found in the literature.^{67,80,81} One of them is a Ru-NHC complex with a pyrene moiety that is immobilized over rGO by π stacking interactions. This catalyst shows better activity than its homogeneous counterpart. In addition it can be reused 10 times without deactivation.⁸²

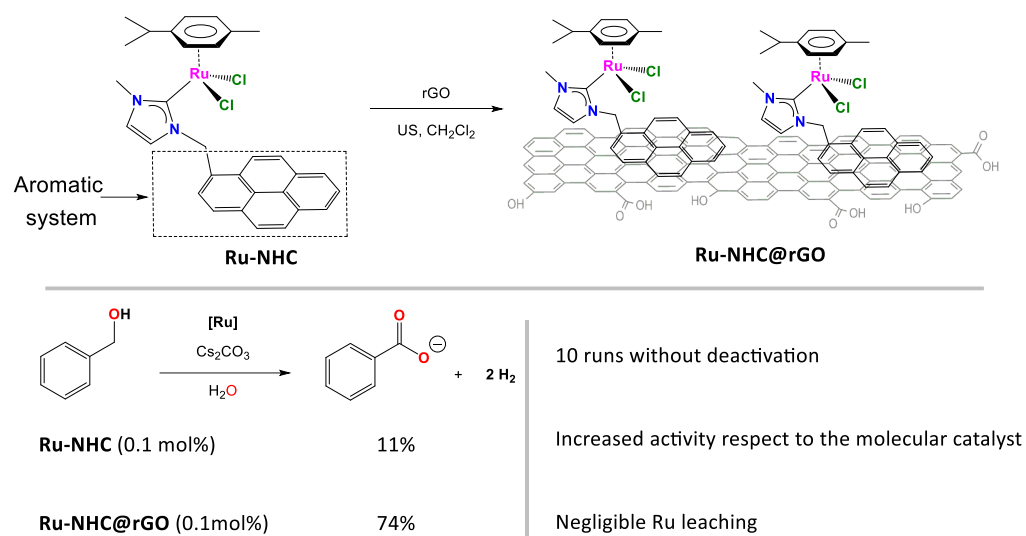


Figure 1.4 Non-covalent immobilization of Ru complex over rGO and its catalytic properties.

1.2 ENERGY PRODUCTION vs SUSTAINABILITY

The current overpopulation and growing energy consumption per capita imply an unsustainable energy production system that does not stop growing in the last years (Figure 1.5).⁸³

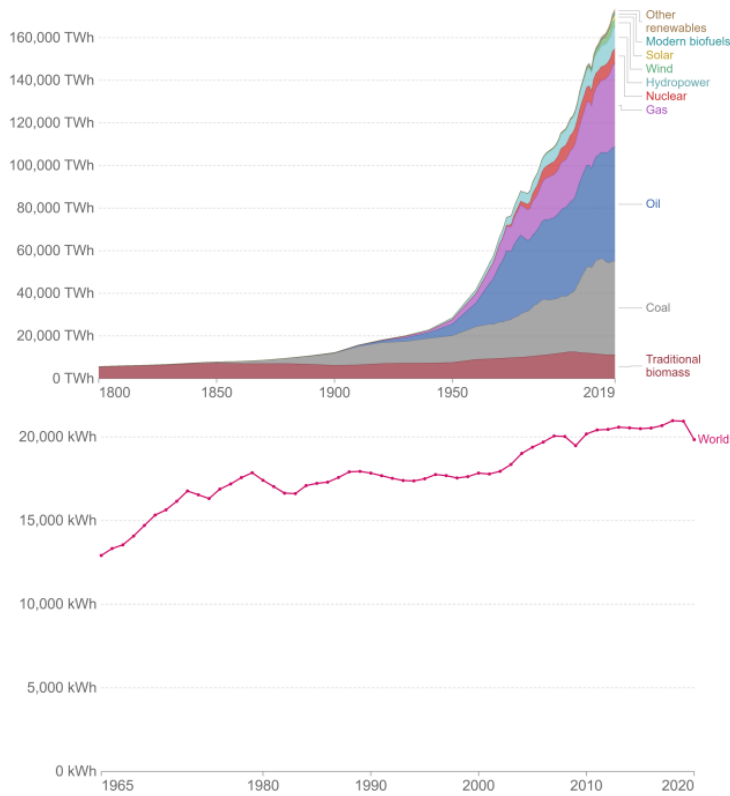


Figure 1.5 Total energy consumption and its source (top) and energy consumption per capita in the world (down).⁸⁴

The current energy sector (either to produce electricity, to use as transport combustible or to heat water) is mainly based on the use of fossil fuels such as coal, oil and gas (Figure 1.5), which is no longer sustainable due to their limited availability and negative environmental impact (Figure 1.6).

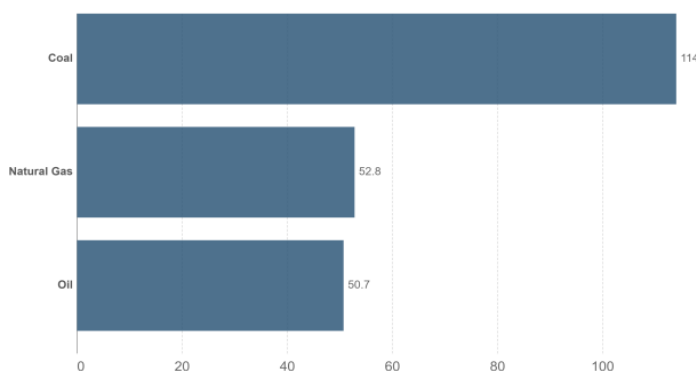
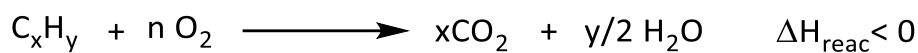


Figure 1.6 Years of fossil fuels reserves left according with the current demand in year 2016.⁸⁴

Fossil fuels (coal, natural gas and oil) are composed basically of carbon and hydrogen with variable amounts of other elements such as sulfur, oxygen and nitrogen. Depending on the fuel these elements are found in varying degree. For example, coal contains high quantity of sulfur and oxygen. In contrast, natural gas shows very low amount of these contaminants. Generally, the energy from fossil fuels is obtained through combustion where a fossil fuel acts as fuel and atmospheric oxygen as oxidant to obtain CO₂ and H₂O as products (Scheme 1.8).



Scheme 1.8 General reaction for fossil fuels combustion.

Unfortunately, CO₂ is one of the side products, a non-toxic gas and one of the main responsible of the greenhouse effect.⁸⁵ In parallel, CO₂ is produced by the major part of the living beings, but its concentration, in the atmosphere, remains constant due to the fact that autotroph beings re-absorb part of it achieving equilibrium. However, if this equilibrium is broken and CO₂ (or other greenhouse gas) accumulates in excess, the earth temperature will increase exceeding the optimal range due to the greenhouse effect. Since the eighteen centuries, the world population is increasing as well as the energy demand (Figure 1.5) causing an exorbitant production of CO₂. These anthropogenic (originated by human activity) emissions of CO₂ have broken the equilibrium and it is accumulating in the atmosphere. The atmospheric CO₂ concentration between years 1000 and 1800 was

around 280 ppm, but nowadays it has achieved a value of 419 ppm.⁸⁶ These facts produce an amplification of the greenhouse effect and an increase of the world temperature as final consequence (Figure 1.7).^{87,88}

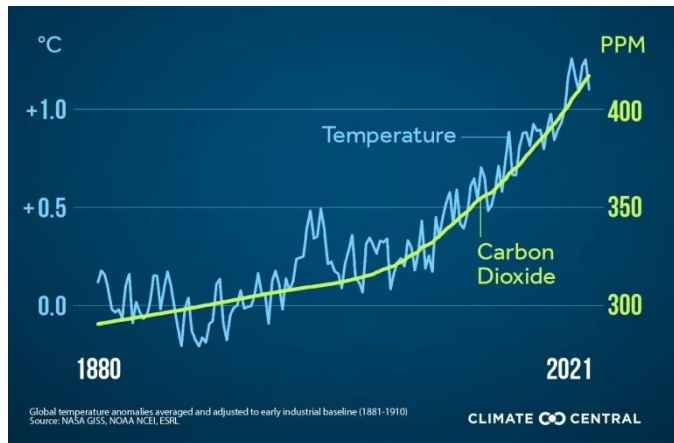


Figure 1.7 Relation between CO₂ concentration in atmosphere and global temperature.⁸⁹

That increase of CO₂ concentration and the world temperature has various negative implications:

1.- Increment of sea temperature. According with the Henry's law, an increment of water temperature reduces the oxygen solubility. It plays a crucial role in all aerobic aquatic life. For that reason, a reduction of dissolved O₂ could be lethal for these beings (hypoxia). Thus, the amplification of global warming is producing that fishery sources are decreasing and aquatic ecosystems are being seriously affected.^{90,91}

2.- Reduction of water availability. Saturation vapor pressure of water in air is highly sensitive to temperature, for that reason perturbations in the global water cycle are expected as consequence to increase of world temperature.⁹² It has been estimated an increase of the runoff, the differences between precipitation and evapotranspiration, among 10-30% in North America and Eurasia by the year 2050,⁹³ reducing the water availability.⁹⁴

3.- Sea-level rise. Thermal expansion, glacier loss and mass loss from Greenland and Antarctic, due to the high temperatures, are the main responsible of the increase of sea-level.⁹⁵ The measures, since 1993 until 2018, indicated that global sea level rise 3 mm per year, more than 7 cm in 25 years.⁹⁶

4.- Increment of extreme climate events. It has been demonstrated that human-induced increases in greenhouse gases have contributed to the observed intensification of extreme climate events such as heavy precipitation events, storms and extreme temperatures.^{97–100}

5.- Plants, crops and animals need specific conditions to survive and grow including the suitable ambient temperature where the increase in the global temperature will disturb the growth and the breed of these creatures.¹⁰¹ In addition, lack of water and extreme events (see above) make this situation worse.

6.- Physico-chemical changes in water chemistry. Half of the anthropogenic CO₂ has been absorbed with the time by oceans. When it dissolves in water, carbonic acidic is formed which will cause a drop in the surface water's pH, this change will affect the life cycle of many marine creatures.^{102,103}

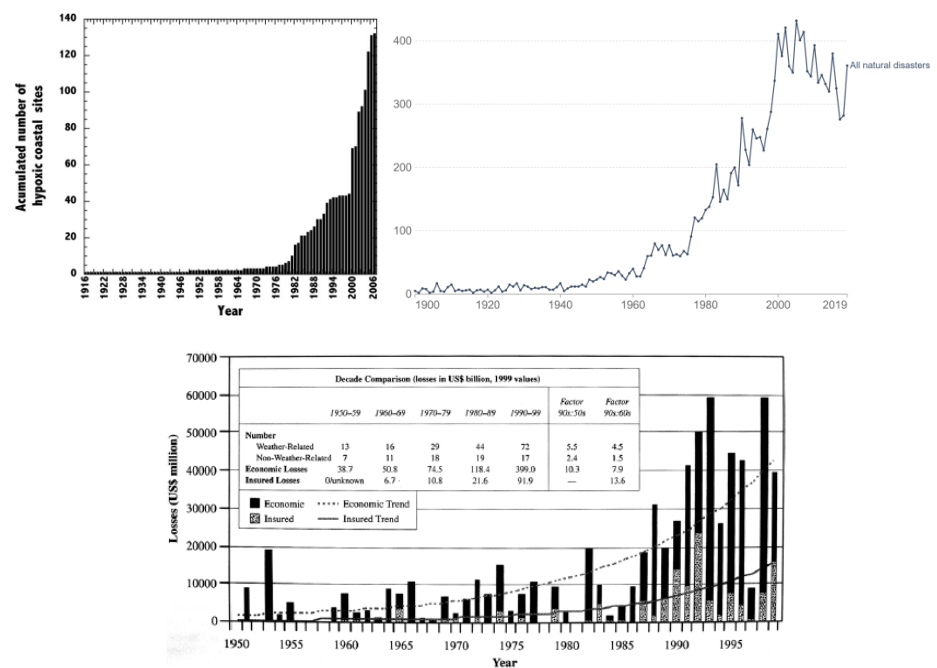


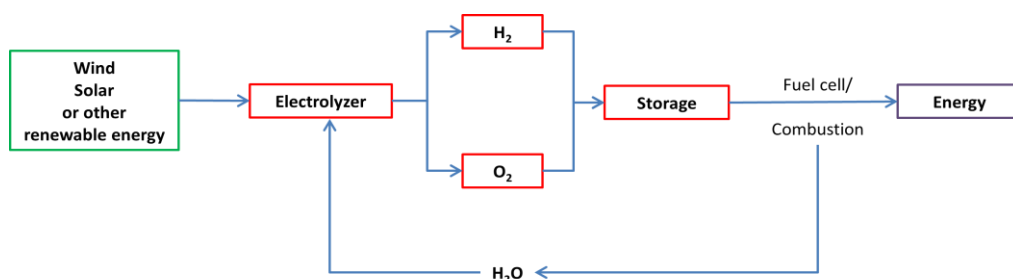
Figure 1.8 Accumulated numbers of reported hypoxia sites since 1916 to 2006. Exponential growth rate of 5.54% per year. (a) Number of global recorded natural disaster events since 1900 to 2019. (b) The total economic costs and the insured costs of catastrophic weather events for the second half of the 20th century as recorded by the Munich Reinsurance company⁸⁵ (c).

All the implications derived from global warming mentioned above have as final consequences important ecologic, economic and human losses.¹⁰⁴ Due to these problematic, global warming becomes one of the most important issues for the scientific and politic community.⁸⁸ Along with carbon dioxide, there are other greenhouse gases like NO_x (nitrogen oxides) that are produced by reaction with oxygen at high temperatures, commonly during fossil fuels combustion. Another one is methane, which is the mainly constituent of natural gas. Its presence in the atmosphere is due to leaks of natural gas.

In this context, renewable energies such as wind or solar energy are considered as an alternative energy source to overcome these problems. The main drawback of these technologies is their intermittent character. For example, solar technology only produces energy during the day. This fact makes impossible to satisfy the constant demand of energy. For this reason, energy storage is experiencing a surge of interest by the scientific community.

1.2.1 Hydrogen economy

Among all the possibilities, the use of molecular hydrogen as an energy vector is a promising clean energy alternative. The hydrogen economy consists in the use of hydrogen as reservoir of energy. The methodology consists of the production of green hydrogen from the energy surpluses of renewable sources, mainly by water electrolysis. Then, it can be storage and/or transport and used when needed. Energy recovery from green hydrogen can be obtained by combustion or used in a fuel cell but the most important is that the only by product is water (Scheme 1.9).



Scheme 1.9 Schematic procedure of the use hydrogen as energetic vector.

Hydrogen is used due to its high gravimetric energy density (33 kW·h/kg). Furthermore, the use of hydrogen as fuel is very efficient. For example, hydrogen powered cars using a fuel cell shows efficiencies of energy conversion around 50–60%, much higher than today's cars using fossil which has maximum efficiencies of 25%.^{105,106} In addition, when it is used to obtain energy, water is the only by-product avoiding the carbon footprint ligated to present energy generation. However, this technology has also some drawbacks. First, H₂ is extremely flammable and explosive, which makes it difficult to manipulate. In addition, it shows low gravimetric density (0.0899 kg/m³) under standard conditions. For that reason, conventionally, high pressures (usually 700 bar) or cryogenic temperatures (-253 °C) are used to store it in a reasonable amount. These methodologies require an important energy intake (approx. 15 and 30% of the total stored energy respectively) as well as complex, expensive materials and procedures to store the hydrogen in an efficient and safe manner.¹⁰⁷

Hydrogen storage

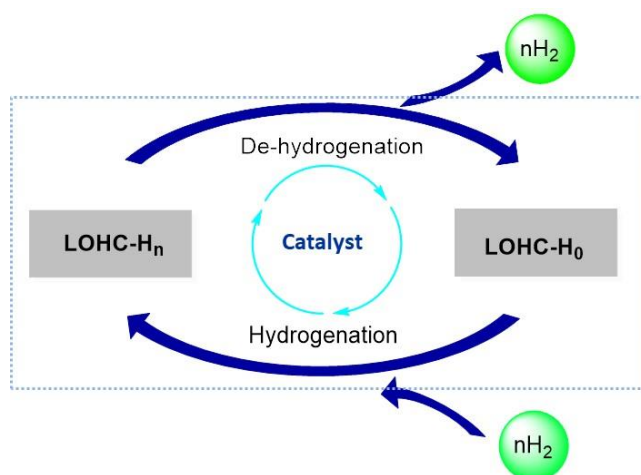
To overcome the limitations of these traditional methodologies various storage methods have been proposed. For instance physisorption of H₂ onto surface of solid materials, which has been studied for many years,¹⁰⁸ consists in a physical and reversible process in which H₂ is adsorbed onto a surface through van der Waals forces without the creation or activation of any type of bound.^{109,110} Hydrogen storage of this methodology is mainly governed by specific surface area and pore volume of the material.¹¹¹ For that reason, metal-organic frameworks, zeolites, chlathrate hydrates, organic polymers and carbon materials are used for this purpose.¹⁰⁷ This methodology shows fast kinetics and good reversibility due to of the weak interactions between hydrogen and support. However, it makes that high storage capacities are only achieved employing extreme low temperatures (≈-196 °C) and high pressures.

Another alternative is the storage of H₂ as solid hydrides. In this case, hydrogen is chemisorbed in a solid material. The bond of the hydrogen molecule is activated and reacts with the support forming bonds and giving a new material. This reaction is reversible and the H₂ can be obtained on demand when is needed. Different materials are employed for this purpose such as metal hydrides, metal alloy hydrides, alanates, metal borohydrides and alkali imides/amides systems. As usual, these materials show a storage capacity between 2 to 8 wt%. This methodology,

usually, is limited by the high temperatures needed to activate and/or release the molecular hydrogen (in some cases over 300 °C).¹¹² In addition, in the major part of the cases low recyclability of the material has been achieved.¹⁰⁷

Liquid Organic Hydrogen Carriers (LOHCs)

A promising alternative that has gained ground in this field is storage of hydrogen in the form of liquid organic hydrogen carriers (LOHC).^{113,114} It is a similar approach that solid hydrides but using liquid molecules as carriers. A LOHC system is formed by a hydrogen rich molecule (H_n -LOHC) and its dehydrogenate counterpart (H_0 -LOHC). H_2 is loaded in the system through the catalytic hydrogenation of the H_0 -LOHC to obtain the H_n -LOHC. Then, this liquid molecule can be safely transported or stored during long periods of time. Once there is an energetic demand, hydrogen is discharged of the system by a catalytic dehydrogenation reaction recovering the initial molecule (H_0 -LOHC) (Scheme 1.10).



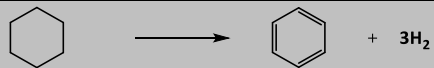
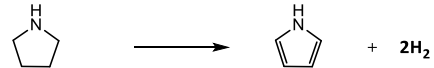
Scheme 1.10 Schematic use of LOHCs.

Two important characteristics of this technology must be taken into account. The first one is the dehydrogenation temperature (usually is the thermodynamic disfavored process of the system), the temperature at which hydrogen is release from the H_n -LOHC. For practical purposes and efficiency this temperature should be as low as possible. Another important aspect is the hydrogen storage capacity (HSC) which determines the amount of H_2 that can be stored in the system. This feature must be as high as possible to reduce the quantity of LOHC needed becoming the

system more efficient. This fact gains special importance if hydrogen is used as fuel for on-board storage system or other mobile functions where space is limited.¹¹³

The different efficient organic pairs have been summarized in table 1.4

Table 1.4 Different LOHC systems.

System	Reaction	T _{dehydro} (°C)	HSC (wt%)
Cycloalkanes		>250	7.2
N-heterocycles		>150	5.2
Methanol	MeOH + H ₂ O → CO ₂ + 3H ₂	>100	4.4
Formic acid	HCOOH → CO ₂ + H ₂	R.T.	4.4
Ammonia-borane			
Hydrolysis	NH ₃ BH ₃ + 3H ₂ O → NBO ₂ ·H ₂ O + 3H ₂	<100	7.1
Methanolysis	NH ₃ BH ₃ + 4MeOH → NB(OMe) ₃ + 3H ₂	<100	3.8
Silane/alcohol	R ₃ SiH + 3MeOH → RSi(OMe) ₃ + 3H ₂	<0	4.4

Historically, the first research activities toward hydrogen storage using LOHC systems date back to the 1980s. Taube and co-workers proposed a system based on the pair methylcyclohexane/toluene (MCH/TOL) for on-board applications.¹¹⁵ That pair shows an interesting HSC of 6.1 wt%. However, that system has an important drawback, the hydrogen recovery (the dehydrogenation of MCH) occurs at temperatures of ca. 300°C.¹¹⁶ Despite this limitation, the pair MCH/TOL is being used as a system to store energy by the Japanese company Chiyoda corporation.¹¹⁷ More recent studies have focused on the perhydrodibenzyltoluene/dibenzyltoluene pair (pHDBT/DBT). This pair is non-toxic and liquid in a wide range of temperatures (-30-390 °C). Its HSC is similar to the MCH/TOL pair (6.2 towards 6.1 wt%) but shows low dehydrogenation temperatures (around 250 °C) due to its lower dehydrogenation enthalpy (65.3 vs 68.3 kJ/mol) making pHDBT/DBT a good pair for hydrogen storage. In fact, there are two companies (Hydrogenious technologies and H₂ industries) that supply this type of technology for stationary power storage.^{118,119}

To improve the efficiency of LOHCs through the reduction of dehydrogenation temperature other systems were studied. Pez along with the company Air Products¹²⁰ and Crabtree^{121,122} demonstrated that the partial substitution of carbon

atoms by nitrogen in a cyclic compound reduce the energy required for the dehydrogenation reaction (Figure 1.9).

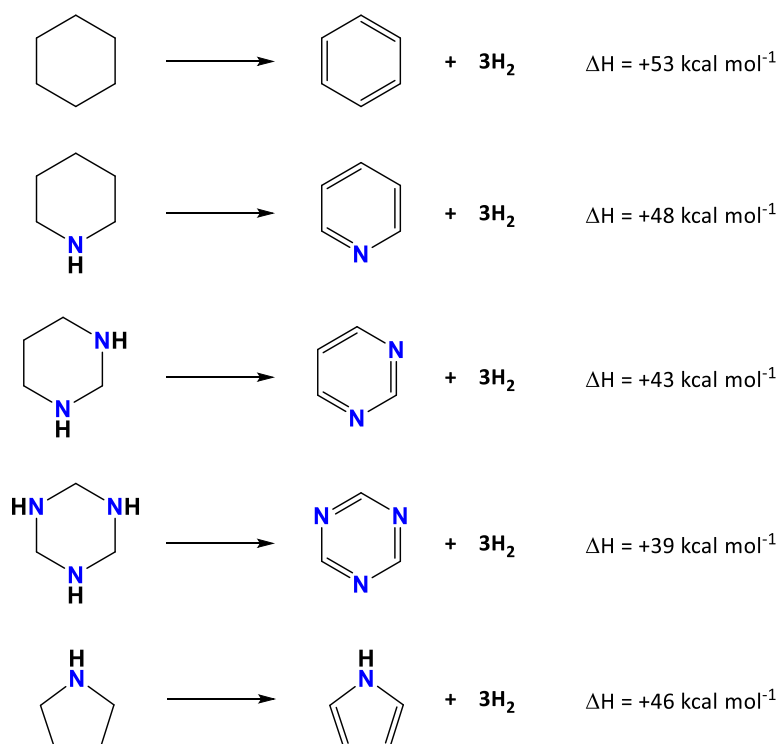


Figure 1.9 Calculated enthalpies of dehydrogenation for cyclohexane and structurally similar N-heterocycles.

Among all the N-heterocycles, dodecahydrocarbazole was found one of the most effective hydrogen storage carriers. It can be considered as an indoline moiety with two six-membered rings as substituents showing a low dehydrogenation enthalpy.¹²² The dehydrogenation reaction is carried out at ca. 200 °C catalyzed by noble metals. Although decahydrocarbazole has a HSC of 6.7 wt%, it shows low dehydrogenation reaction rates due to the nitrogen heteroatom is free to interact with the metal catalyst surface through the lone pair of electrons inhibiting the catalyst.^{123,124} For this reason, recent studies have focused in use N-ethyldecahydrocarbazole instead of decahydrocarbazole due to ethyl group prevents the strong adsorption onto metal surface. It has HSC slightly lower than decahydrocarbazole of 5.8 wt% but shows better reactions rates, no catalyst deactivation and it shows good stability in

repeated hydrogenation/dehydrogenation cycles. As in the case of decahydrocarbazole, the dehydrogenation of this molecule is mainly carried out by heterogeneous novel metals such as: Pd,¹²⁵ Pt,¹²⁶ Rh,¹²⁷ or Ir.¹²⁸ The main drawback of this N-ethyldecahydrocarbazole/N-ethylcarbazole pair is its high melting point, it is solid at ambient temperature. However, the eutectic mixture of different N-alkyl carbazoles has a melting point of 24 °C without having a high impact in the HSC.¹²⁹ Another issue that needs to solve is the lability of the N-alkyl bond that under high temperatures can be broken leading with substrate decomposition and inhibiting the catalyst.¹¹⁴

Other interesting N-heterocycles to be used as LOHC are piperidines and tetrahydroquinoleines (THQ). The first one, piperidines/pyridines system show a high storage capacity of 7 wt% for piperidine/pyridine pair (it decreases with the substitution of the molecule) and low dehydrogenation enthalpies. Milstein et al. dehydrogenate quantitatively piperidines to the correspondent dehydrogenated counterpart using Pd/C at 170 °C (reflux temperature of the substrate) in 2 days.¹³⁰ Although it is liquid in a wide range of temperatures, the boiling point of these pairs is usually low (between 100 and 150 °C). This fact could be a drawback from a practical point of view. On the other hand, tetrahydroquinoline (THQ)/quinoline (Q) pair shows a lower dehydrogenation enthalpy due to the aromatic fused ring allowing carrying out the reaction at low temperatures. There are examples that reaction occurs quantitatively at 110 °C in less than 24h.¹³¹ Although this pair shows low HSC of 3 wt%, it can be use as model substrate to understand the mechanism of the reactions involved and design more efficient catalysts. Thus, this reaction is widely studied in academics. To carry out the dehydrogenation of THQ to obtain Q and H₂ both homogeneous and heterogeneous catalysts are used, usually based on novel metals.¹³²⁻¹³⁴ In addition there are some examples where the catalysts are based on 3d metals such as Ni,¹³⁵ Co,¹³⁶ Cu,¹³⁷ or Fe¹³⁸ among others¹³⁹. Despite of this fact, it is more interesting carry out this transformation with a recyclable metal-free catalyst such as a carbocatalyst. However, this field has not been studied. There are few examples in metal-free dehydrogenation of THQ and in all cases an oxidant is used as hydrogen acceptor obtaining another product (H₂O or H₂O₂) instead of H₂.^{59,140,141} Only there is an example in the literature of acceptorless dehydrogenation (ADH) of THQ to obtain Q and H₂ using a metal-free catalyst.¹⁴²

1.3 SUSTAINABLE TRANSFORMATIONS AND BIOMASS AS FEEDSTOCK FOR CHEMICALS PRODUCTION

In parallel, still today, a major part of all chemical and material products obtained from the chemical industry is derived from seven simple building-block molecules (Figure 1.10), the ‘base chemicals’.

Most of chemicals produced by the chemical industry are derived from seven simple building-block molecules known as the ‘base chemicals’ (Figure 1.11). These chemicals are derived from fossil resources (predominately crude, oil and natural gas) via distillation, cracking, reforming and fractionation. All seven base chemicals are produced on a global annual scale exceeding 10 million tones, with ethene produced in more than 100 million tons (Table 1.5).¹⁴³

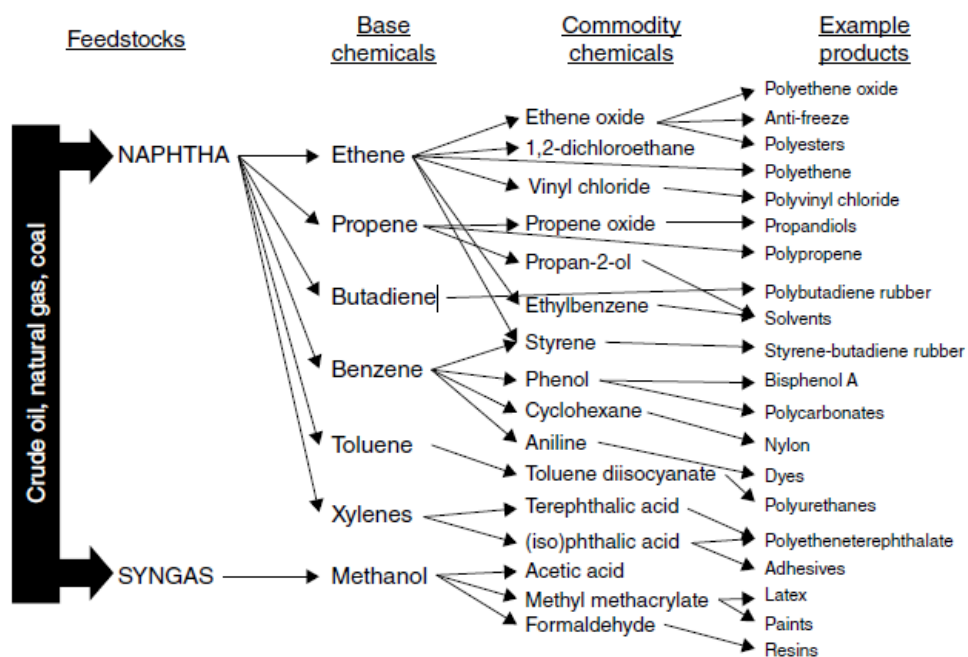


Figure 1.10 Basic fossil-fuel derived products.

Table 1.5 Global annual production (2010) of 7 “base chemicals” and its sources.

Base/Bulk chemical	Predominant feedstock	Annual production from fossil sources (ton)
Ethene	Oil, gas	123 300 000
Propene	Oil, gas	74 900 000
Butadiene	Oil, gas	10 200 000
Benzene	Oil	40 200 000
Toluene	Oil	19 800 000
Xylenes	Oil	42 500 000
Methanol	Syngas	49 100 000

The main problem of this current scenario is the non-renewable character of feedstock (coal, natural gas and predominantly oil). Around 10% of global crude oil is used to produce the base chemicals. As previously mentioned, its availability is limited and it has been estimated, with the actual production and demand that we will run off oil in less than 50 years (Figure 1.6). In addition, the use of this type of feedstock generates high quantities of CO₂.

On the other hand, apart from methanol (MeOH), all base chemicals are devoid of heteroatoms with only double bonds or aromatic rings as functional groups. As a result, further chemical modifications, such as oxidation, are required to introduce chemical complexity in the form of functional groups.¹⁴⁴ Normally, these transformations involve harsh conditions and strong reactants that are usually toxic and/or generate high quantity of waste.

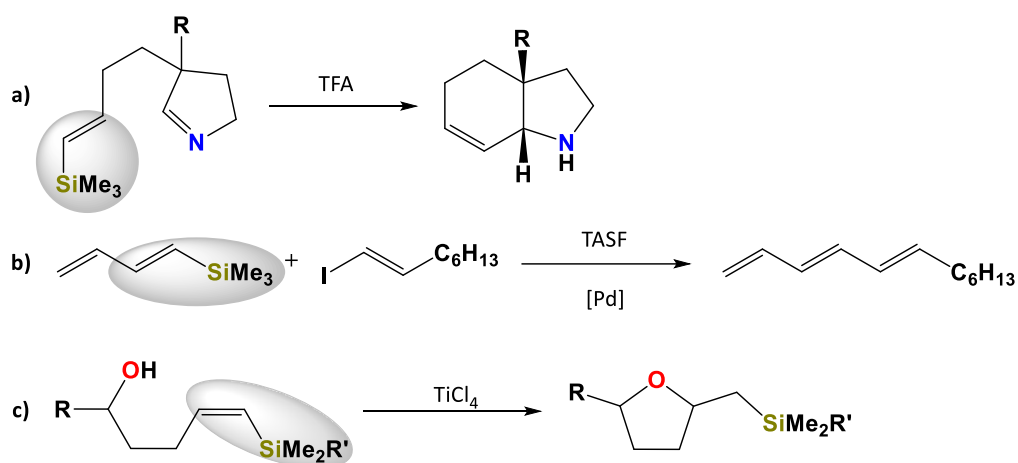
1.3.1 Sustainable catalytic reactions

The classical methodologies employed in the different organic transformations by the chemical sector produce high quantity of waste, making this scenario unsustainable. For this reason, there is a growing necessity to develop sustainable methodologies, based on the 12 principles of green chemistry to replace them.

Hydrosilylation reaction

From an industrial point of view, organosilanes are interesting type of molecules due to its versatile functionalities in the synthetic chemist's toolbox, offering a convenient and inexpensive procedure to create new carbon-carbon or carbon-heteroatom bonds.¹⁴⁵ In special vinylsilanes, a silyl moiety attached to double bond, due to its particular reactivity.

The silicon-carbon bond is generally robust towards many reagents used in organic synthesis but, under specific conditions can be easily activated.¹⁴⁶ The reactivity of vinylsilanes includes a wide variety of reactions such as substitution of silyl moiety by an electrophilic carbon (Scheme 1.11.a),¹⁴⁷ Heck reaction (Scheme 1.11.b)¹⁴⁸ or attack of hydroxyl group to the olefinic double bond (Scheme 1.11.c).¹⁴⁹ Moreover, configuration of the double bond after some reactions can be controlled.¹⁵⁰

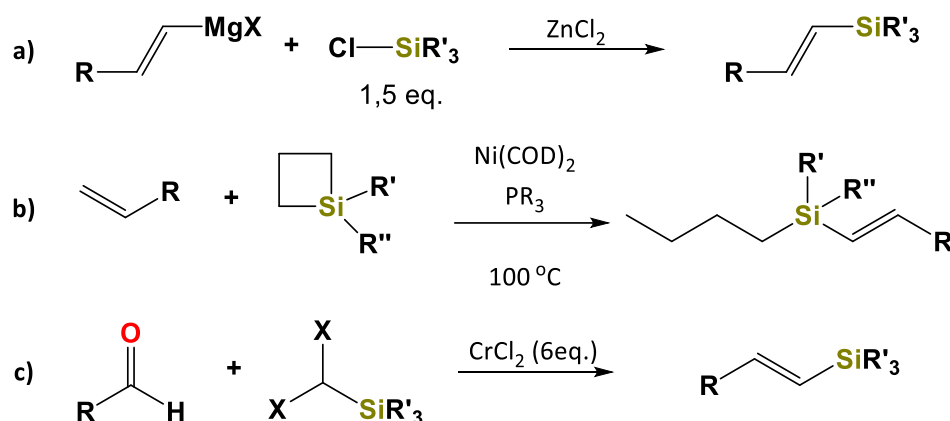


Scheme 1.11 Different reactivity of vinylsilane group. TASF = $(\text{Et}_2\text{N})_3\text{S}^+ \text{SiMe}_3\text{F}_2^-$.

Due to these properties vinylsilanes are extensively observed in many organic reactions as intermediates. An example of this is the synthesis of Pumiliotoxin 251D, an alkaloid isolated from the Ecuadoran poison-dart frog that could be used as toxin, from 1-heptyn-3-ona. In this synthetic route the key step is the vinylsilane cyclization.¹⁵¹

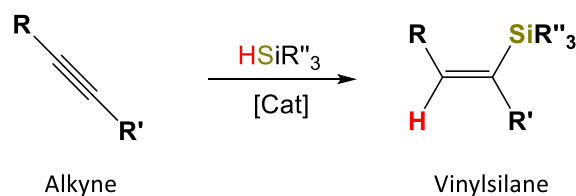
Vinylsilanes are obtained by different ways such as the reaction of organomagnesium reactants with chlorosilanes (Scheme 1.12.a),¹⁵² terminal alkenes

and cyclic silanes (Scheme 1.12.b),¹⁵³ or dihalomethylsilanes and aldehydes (Scheme 1.12.c).¹⁴⁵ These synthetic routes require several reaction steps producing undesired by-products.



Scheme 1.12 Different synthetic routes to obtain vinylsilanes.

Alternatively, there is a more sustainable synthetic route, the hydrosilylation of alkynes. This reaction occurs in one step, shows good yields and has an atom economy of 100%. Hydrosilylation consists in the reaction between a hydrosilane and an alkyne. In this way, the silane moiety and the hydrogen are inserted in the different *sp* carbons yielding the corresponding vinylsilane (Scheme 1.13).



Scheme 1.13 Schema of hydrosilylation of alkynes reaction.

However, the main drawback of this methodology is limited selectivity due to different products can be obtained such as α addition, β addition, disilylation or dehydrogenative product.¹⁵⁴ For that reason, the search for catalysts that can promote selective hydrosilylation processes under mild and aerobic conditions is one of the main goals in industry and academy. Traditionally, the Karstedt complex ($\text{Pt}_2(\text{dvtms})_3$, dvtms = divinyltetramethyldisiloxane) is the reference catalyst for hydrosilylation due to its good activity and selectivity for this reaction.¹⁵⁵ However,

this catalyst generates colloidal platinum species, which are responsible of a number of undesired reactions.¹⁵⁶ Then, Markó and co-workers demonstrated that NHC-platinum(0) complexes avoid the formation of platinum colloids catalyzing the hydrosilylation of alkynes in a more efficient way.^{157,158}

Although Marko catalysts (NHC-Platinum (0)) show excellent catalytic properties in hydrosilylation of alkynes reaction, it cannot be recycled after the reaction. To make the process more sustainable the development of efficient, stable and recyclable catalyst for that transformation is necessary. The last efforts in hydrosilylation reactions have focused in that field and different recyclable catalyst have appeared, but the examples are still scarce.¹⁵⁹⁻¹⁶¹ Chapter 3 is focused on achieve this target. For that purpose, a platinum complex is immobilized onto reduced graphene oxide and tested as reusable catalyst for alkynes hydrosilylation reaction.

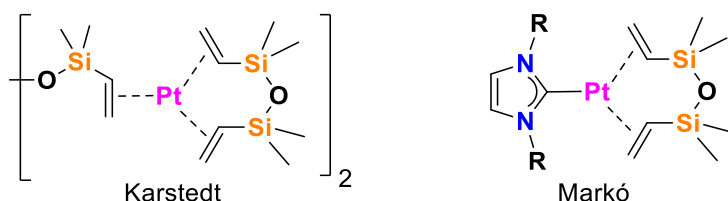


Figure 1.11 Structure of Karstedt and Markó catalysts.

Semihydrogenation of alkynes reaction

The preparation of bioactive natural products such as medicaments, drugs or pheromones containing Z-alkenes is an important issue in fine chemistry.¹⁶²⁻¹⁶⁴ However, methods for highly selective access to Z-alkenes are less established than those for the E-isomers. One of the reasons is thermodynamic control that favors the lower-in-energy E-alkenes.

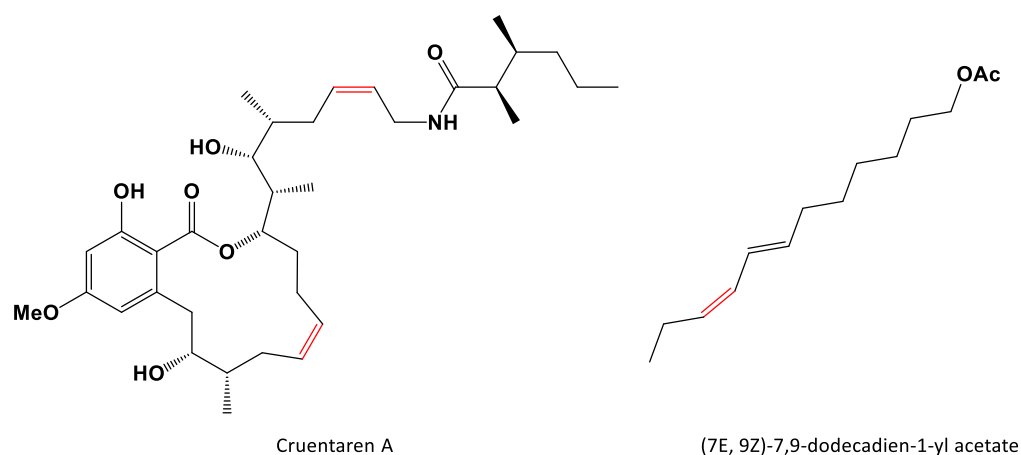
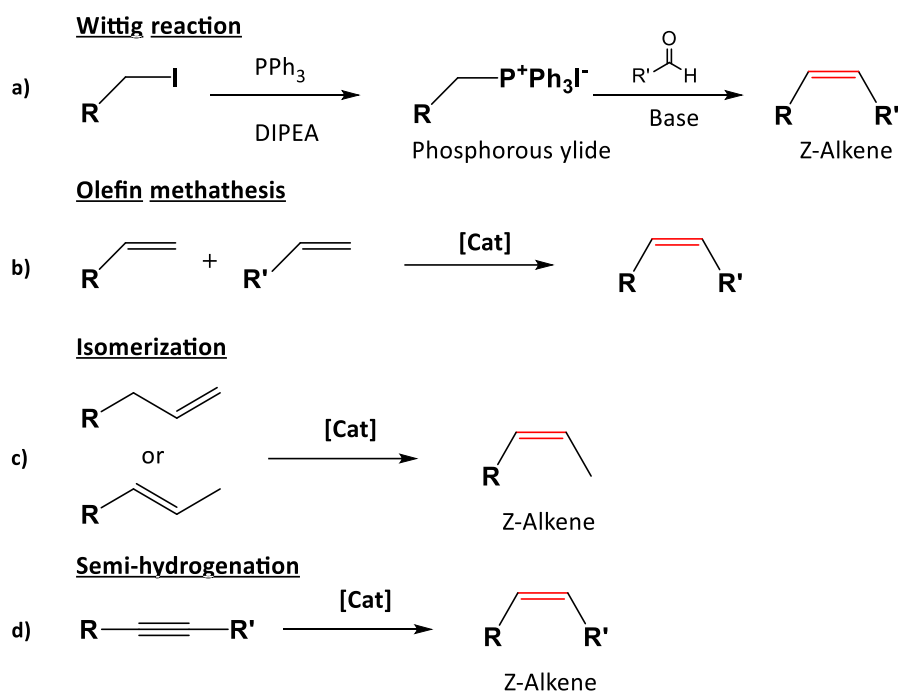


Figure 1.12 Structure of Cruentaren A (antifungal and antitumoral molecule) and 7,9-dodecadien-1-yl-acetate (sex pheromone). In red Z-alkene functionality.

The number of methodologies to obtain Z alkynes is limited. One of the most used in natural product synthesis is the Wittig reaction. This transformation consists in the reaction between a carbonyl compound and a phosphorous ylide (prepared in situ) to yield the corresponding alkene with the concomitant formation of phosphorous oxide as by-product (Scheme 1.15.a).¹⁶⁵ In general, selectivity of 90% towards Z isomer is achieved. The main drawback of this synthetic route is the undesired by-products formed. Other way to obtain Z-alkenes functionalities is through olefin metathesis reactions (Scheme 1.15.b). Although it is a methodology with enormous synthetic possibilities, the selectivity towards Z-alkene is low (usually Z:E relation is 2:1) with a big depending of the substrate.¹⁶⁶ However, in recent years, the Z-alkene selectivity have been improved by the development of better catalysts based on Mo, W and Ru.^{167–169}

An alternative to these methodologies is the isomerization of alkenes (terminal or E-alkenes) to obtain the desire Z-alkene (Scheme 1.14.c).^{170–172} The isomerization of terminal alkenes to internal alkenes is thermodynamically favorable but the E-isomer is more favored than Z which difficult the formation of Z-alkenes.



Scheme 1.14 Different methodologies to Z-Alkenes synthesis.

One promising and sustainable alternative to these methodologies is the catalytic semi-hydrogenation of alkynes (Scheme 1.15.d). This reaction consists in a partial hydrogenation of alkyne to obtain the corresponding Z-alkene without a completed hydrogenation to the corresponding alkane. It means, that the catalyst employed to carry out the reaction have to be selective towards Z-isomer¹⁷³ without overhydrogenate the substrate.¹⁷⁴ To carry out this transformation Lindlar's catalyst is widely use. It consists in Pd supported over CaCO_3 poisoned with lead co-catalyst and quinoline.¹⁷⁵ In contrast to Pd over carbon, no complete hydrogenation of alkyne towards alkane occurs when this catalyst is used. In addition, due to the nature of heterogeneous catalysts, H_2 is bound to the surface of the catalyst and Z-configured alkenes could be generated exclusively.¹⁷⁶ Although Lindlar's catalyst shows good catalytic properties for this reaction and is widely used for this purpose, it shows two important drawbacks:

- Rigorous control of catalyst loading. If the amount of catalyst is too low the reactions is not completed. On the other hand, an excess of catalyst produces the overhydrogenation of the substrate.

-The use of toxic lead co-catalyst poses problems in terms of environmentally and safety issues.

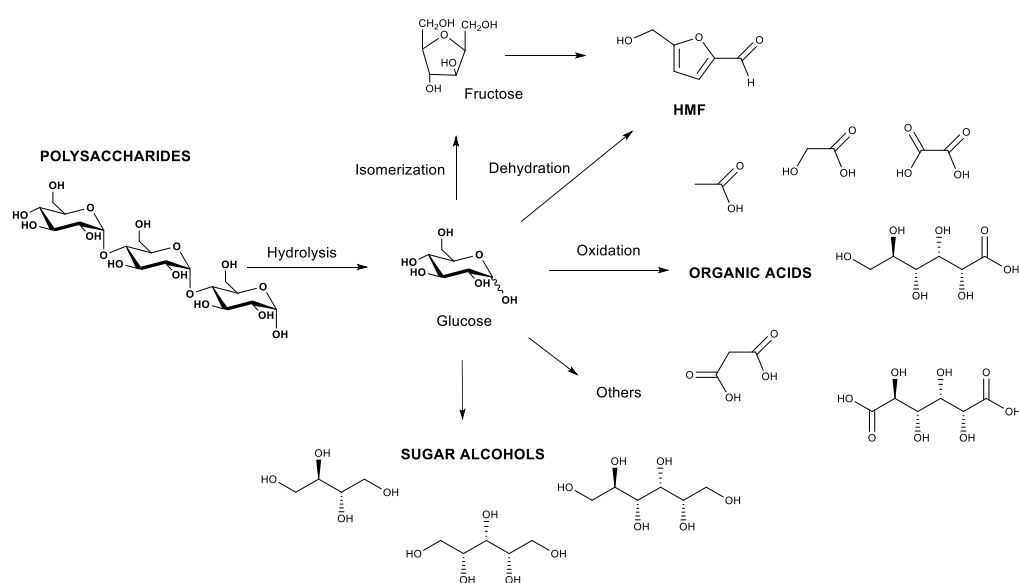
-Partial isomerization of Z to E-alkene.¹⁷⁷

Due to the potential of the semi-hydrogenation of alkynes to obtain Z-alkenes reaction in fine chemistry many efforts are directed towards the design of a catalytic system that overcomes these inconvenients.¹⁷⁸⁻¹⁸⁰ Consequently, chapter 4 it is devoted to the synthesis of palladium nanoparticles supported onto rGO and stabilized by NHC ligands to be applied as selective and reusable catalyst in the semi-hydrogenation of alkynes reaction.

1.3.2 Revalorization of Biomass

As early mentioned, a major part of chemical products proceeds from fossil fuels. This scenario is not sustainable because it generates considerable amounts of CO₂. In addition, they derive from non-renewable sources for that reason its availability is limited. Alternatively, the use of biomass as feedstock is a more sustainable alternative towards the synthesis of organic compounds.^{181,182} Moreover, biomass molecules show high grade of oxygenated functionalization (around of 45% of weight is oxygen).¹⁸³ From an economical and chemical point of view, this is an advantage due to it is typically more simple and inexpensive remove oxygen from a molecule than add oxygen via selective oxidization reactions.¹⁸⁴

Considering both economics and avoidance of competition with food production, biomass for platform chemical production should ideally be the “waste” originated from other industries and not specifically grown for chemicals.¹⁴⁴ The most abundant waste biomass is lignocelluloses,¹⁸⁵ material constituted by a mix of lignin, cellulose and hemicellulose in a variable concentration.¹⁸⁶ Lignins are bio-polymers made by cross-linking phenolic precursors.¹⁸⁷ On the other hand, cellulose and hemi-cellulose are polysaccharides, bio-polymers based on sugars. These types of molecules are interesting initial platform chemicals in organic synthesis due to the variety of products that can be obtained (Scheme 1.15).^{188,189}

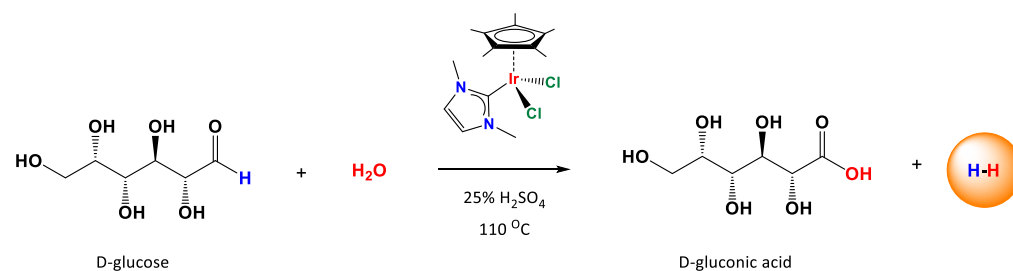


Scheme 1.15 Different products obtained from glucose.

An interesting example of these reactions is the conversion of sugars in its corresponding aldonic acid. In the case of glucose, gluconic acid is obtained, a biocompatible and biodegradable molecule (Scheme 1.15). For these reasons, it is widely used as food additive (E574),¹⁹⁰ medicines¹⁹¹ and biodegradable polymers.¹⁹² In addition, it is used in other fields such as building and construction¹⁹³ and chelating agent for extraction of rare earth elements.¹⁹⁴ The huge amount of gluconic acid applications converts it in a valuable chemical intermediate having an annual production of 60 000 ton.

The main challenge in the synthesis of gluconic acid, or any aldonic acid from its corresponding sugar, is selectivity due to presence of many oxygenated functionalities.¹⁹⁵ The Industrial obtainment of gluconic acid from glucose is carried out by enzymatic catalysis, concretely by *Aspergillus niger* enzyme.¹⁹⁶ Despite of this methodology shows high productivity, it has a few drawbacks: need of specific conditions for an optimal enzyme activity, waste-water removal and difficulties for reusing the catalyst.^{184,195} In the last years, it has been developed different heterogeneous catalysts based on noble metals (Pd, Pt and Au) that oxidase glucose to gluconic acid using O₂ as final oxidant. Among them, Au/TiO₂ based materials show the most interesting catalytic properties.^{184,197}

A promising and more sustainable alternative methodology is the acceptorless dehydrogenation of sugars. Through this synthetic procedure aldonic acids are obtained without the use of any oxidant. Only H₂ is obtained as byproduct that can be used in energy production or as reactant in other organic synthetic procedures. Despite the great potential of this technology only one example exists in the bibliography developed by our group. In that example, glucose is dehydrogenated at reflux in water using homogeneous iridium complexes with H₂SO₄ as additive yielding gluconic acid with good yield and selectivity.¹⁹⁵



Scheme 1.16 Acceptorless dehydrogenation of glucose to obtain gluconic acid and hydrogen using an iridium complex.

Carrying out with this work, different iridium complexes with a triazolylidene ligand are synthesized in Chapter 5. Then, these complexes are tested as additive-free catalysts in sugars dehydrogenation reaction in water media under reflux conditions.

1.4 OBJECTIVES

The general objective of this PhD. thesis is the development of more sustainable catalytic processes, using the 12 principles of Green Chemistry as a guide, to address the main current challenges of our society such as the seek for clean energy alternatives, the reduction of environmental pollution and industrial waste. To carry out this arduous task, special attention has been paid to the design and development of catalysts to make the processes more efficient. This general objective can be divided in the following:

- Evaluation of properties of graphene derived materials as carbocatalysts in hydrogenation transformations.
- Design and development of palladium and platinum-based catalysts to carry out sustainable synthetic procedures such as semi-hydrogenation of alkynes and hydrosilylation of alkynes.
- Development of selective transformation for biomass feedstocks. The synthesis of different iridium complexes and the study of its catalytic properties in the conversion of sugars in their corresponding aldonic acid in water media.
- Development and evaluation of catalytic properties of hybrid material based on graphene derivatives functionalized with organometallic or metal nanoparticles.

1.5 REFERENCES

- (1) Sheldon, R. A. *ACS Sustain. Chem. Eng.* **2018**, *6*, 32–48.
- (2) Kastens, M. L.; Kaplan, J. F. *Ind. Eng. Chem. Res.* **1950**, *4*, 402–413.
- (3) Sheldon, R. A. *Green Chem.* **2017**, *19*, 18–43.
- (4) Trost, B. M. *Science* **1991**, *254*, 1471–1477.
- (5) Trost, B. M. *Angew. Chem. Int. Ed.* **1995**, *34*, 259–281.
- (6) Anastas, P.; Eghbali, N. *Chem. Soc. Rev.* **2010**, *3*, 301–312.
- (7) Sheldon, R. A. *Green Chem.* **2007**, *9*, 1273–1283.
- (8) Sheldon, R. A. *Chem. Soc. Rev.* **2012**, *4*, 1437–1451.
- (9) Clark, J. H. *Green Chem.* **1999**, *1*, 1–8.
- (10) Anastas, P. T.; Farris C. A. *Benign by Design: Alternative Synthetic Design for Pollution Prevention*; American Chemical Society, **1993**.
- (11) Anastas, P. T.; Warner, J. *Green Chemistry: Theory and Practice*; Oxford University Press: Oxford, **1998**.
- (12) Anastas, P. T.; Zimmerman, J. B. *IEEE Eng. Manag. Rev.* **2007**, *35*, 16.
- (13) Office of Pollution Prevention and Toxics. The Presidential Green Chemistry Challenge Awards Program, Summary of 1998 Award Entries and Recipients. *US Environmental Protection Agency* **1998**, EPA 744R98001.
- (14) Stern, M. K.; Cheng, B. K.; Hileman, F. D.; Allman, J. M. *J. Org. Chem.* **1994**, *59*, 5627–5632.
- (15) Bashkin, J.; Rains, R.; Stern, M. *Green Chem.* **1999**, *1*, 41–43.
- (16) Sheldon, R. A.; Arends, I.; Hanefeld, U. *Green Chemistry and Catalysis*; Wiley-VCH, **2007**.
- (17) “The Nobel Prize” can be found under <https://www.nobelprize.org>, accessed 14/10/ 2022.

- (18) Laidler, K. J. *Pure Appl. Chemistry* **1996**, *68*, 149–192.
- (19) Mashuri, S. I. S.; Ibrahim, M. L.; Kasim, M. F.; Mastuli, M. S.; Rashid, U.; Abdullah, A. H.; Islam, A.; Asikin-Mijan, N.; Tan, Y. H.; Mansir, N.; Kaus, N. H. M.; Hin T. Y. Y. *Catalysts* **2020**, *10*, 1–29.
- (20) Cornils, B.; Herrmann, W. A.; Wong, C.; Zanthoff, H.; Eds, R. *Catalysis from A to Z*; **2013**.
- (21) Survey, G. Polyolefins. In *Ullmann's Encyclopedia of Industrial Chemistry*; John Wiley & Sons, **2000**.
- (22) James, B. R. *Homogeneous Hydrogenation*; John Wiley & Sons, **1973**.
- (23) Heck, R. F.; Nolley Jr, J. J. *J. Org. Chem.* **1972**, *37*, 2320–2322.
- (24) Miyaura, N.; Yamada, K.; Suzuki, A. *Tetrahedron Lett.* **1979**, *20*, 3437–3440.
- (25) King, A. O.; Okukando, N.; Negishi, E. I. *J. Chem. Soc., Chem. Commun.* **1977**, 683–684.
- (26) Schrock, R. R. *Acc. Chem. Res.* **1986**, *19*, 342–348.
- (27) Nguyen, S. T.; Johnson, L. K.; Grubbs, R. H.; Beckman, M.; Joseph, W. *J. Am. Chem. Soc.* **1992**, *114*, 3974–3975.
- (28) Díez-González, S.; Nolan, S. P. *Coord. Chem. Rev.* **2007**, *251*, 874–883.
- (29) Peris, E. *Chem. Rev.* **2018**, *118*, 9988–10031.
- (30) Jacobsen, H.; Correa, A.; Poater, A.; Costabile, C.; Cavallo, L.; Chimica, D.; Salerno, U.; Sa, I.-F. *Coord. Chem. Rev.* **2009**, *253*, 687–703.
- (31) Wegener, S. L.; Marks, T. J.; Stair, P. C. *Acc. Chem. Res.* **2012**, *45*, 206–214.
- (32) Ndolomingo, M. J.; Bingwa, N.; Meijboom, R. *J. Mater. Sci.* **2020**, *55*, 6195–6241.
- (33) Astruc, D. *Chem. Rev.* **2020**, *120*, 461–463.
- (34) Climent, M. J.; Corma, A.; Iborra, S. *Chem. Rev.* **2011**, 1072–1133.

- (35) Zhu, Q.; Xu, Q. *Chem* **2016**, *1*, 220–245.
- (36) Su, C.; Acik, M.; Takai, K.; Lu, J.; Hao, S. J.; Zheng, Y.; Wu, P.; Bao, Q.; Enoki, T.; Chabal, Y. J.; Loh, K. *Nat. Commun.* **2012**, *3*, 1–9.
- (37) Navalon, S.; Dhakshinamoorthy, A.; Alvaro, M.; Garcia, H. *Chem. Rev.* **2014**, *114*, 6179–6212.
- (38) Enders, L.; Casadio, D. S.; Aikonen, S.; Lenarda, A.; Wirtanen, T.; Hu, T.; Hietala, S.; Ribeiro, L. S.; Pereira, M. F. R.; Helaja, J. *Catal. Sci. Technol.* **2021**, *11*, 5962–5972.
- (39) Su, D. S.; Perathoner, S.; Centi, G. *Chem. Rev.* **2013**, *113*, 5782–5816.
- (40) Wang, S.; Iyyamperumal, E.; Roy, A.; Xue, Y.; Yu, D.; Dai, L. *Angew. Chem. Int. Ed.* **2011**, *50*, 11756–11760.
- (41) Su, D. S.; Delgado, J. J.; Liu, X.; Wang, D.; Schlögl, R.; Wang, L.; Zhang, Z.; Shan, Z.; Xiao, F. S. *Chem. - An Asian J.* **2009**, *4*, 1108–1113.
- (42) Taguchi, A.; Schüth, F. *Ordered Mesoporous Materials in Catalysis*, **2005**.
- (43) Qin, J. X.; Yang, X. G.; Lv, C. F.; Li, Y. Z.; Liu, K. K.; Zang, J. H.; Yang, X.; Dong, L.; Shan, C. X. *Mater. Des.* **2021**, *210*, 11009–11012.
- (44) Liu, J.; Li, R.; Yang, B. *ACS Cent. Sci.* **2020**, *6*, 2179–2195.
- (45) Sano, T.; Tsutsui, S.; Koike, K.; Hirakawa, T.; Teramoto, Y.; Negishi, N.; Takeuchi, K. *J. Mater. Chem. A* **2013**, *1*, 6489–6496.
- (46) K. S. Novoselov; Geim, A. K.; Morozov, S. V.; Jiang, D.; Zhang, Y.; Dubonos, S. V.; Grigorieva, I. V.; Firsov, A. A. *Science* **2004**, *306*, 666–669.
- (47) Hummers, W. S.; Offeman, R. E. *J. Am. Chem. Soc.* **1958**, *80*, 1339.
- (48) Stankovich, S.; Dikin, D. A.; Piner, R. D.; Kohlhaas, K. A.; Kleinhammes, A.; Jia, Y.; Wu, Y.; Nguyen, S. B. T.; Ruoff, R. S. *Carbon N. Y.* **2007**, *45*, 1558–1565.
- (49) Feng, H.; Cheng, R.; Zhao, X.; Duan, X.; Li, J. *Nat. Commun.* **2013**, *4*, 1–8.

- (50) Botas, C.; Álvarez, P.; Blanco, P.; Granda, M.; Blanco, C.; Santamaría, R.; Romasanta, L. J.; Verdejo, R.; López-Manchado, M. A.; Menéndez, R. *Carbon N. Y.* **2013**, *65*, 156–164.
- (51) Georgakilas, V.; Otyepka, M.; Bourlinos, A. B.; Chandra, V.; Kim, N.; Kemp, K. C.; Hobza, P.; Zboril, R.; Kim, K. S. *Chem. Rev.* **2012**, *112*, 6156–6214.
- (52) Morimoto, N.; Morioku, K.; Suzuki, H.; Nakai, Y.; Nishina, Y. *Chem. Commun.* **2017**, *53*, 7226–7229.
- (53) Presolski, S.; Pumera, M. *Angew. Chem. Int. Ed.* **2018**, *57*, 16713–16715.
- (54) Primo, A.; Neatu, F.; Florea, M.; Parvulescu, V.; Garcia, H. *Nat. Commun.* **2014**, *5*, 1–9.
- (55) Espinosa, J. C.; Navalón, S.; Álvaro, M.; García, H. *ChemCatChem* **2016**, *8*, 2642–2648.
- (56) Duan, X.; Ao, Z.; Zhou, L.; Sun, H.; Wang, G.; Wang, S. *Appl. Catal. B Environ.* **2016**, *188*, 98–105.
- (57) Wu, Q.; Zhu, M.; Cao, J.; Wang, X.; Liu, Y.; Xiang, C.; Shao, M.; Tian, H.; Kang, Z. *ACS Appl. Mater. Interfaces* **2020**, *12*, 30280–30288.
- (58) Espinosa, J. C.; Álvaro, M.; Dhakshinamoorthy, A.; Navalón, S.; García, H. *E ACS Sustain. Chem. Eng.* **2019**, *7*, 15948–15956.
- (59) Zhang, J.; Chen, S.; Chen, F.; Xu, W.; Deng, G. J.; Gong, H. *Adv. Synth. Catal.* **2017**, *359*, 2358–2363.
- (60) Xie, X.; Long, J.; Xu, J.; Chen, L.; Wang, Y.; Zhang, Z.; Wang, X. *ACS Catal.* **2012**, *2*, 622–631.
- (61) Ye, R.; Zhao, J.; Wickemeyer, B. B.; Toste, F. D.; Somorjai, G. A. *Nat. Catal.* **2018**, *1* (5), 318–325.
- (62) Axet, M. R.; Durand, J.; Gouygou, M.; Serp, P. *Coord. Chem. Rev.* **2016**, *308*, 236–345.

- (63) Sandee, A. J.; Van Der Veen, L. A.; Reek, J. N. H.; Kamer, P. C. J.; Lutz, M.; Spek, A. L.; Van Leeuwen, P. W. N. M. *Angew. Chem. Int. Ed.* **1999**, *38*, 3231–3235.
- (64) Sandee, A. J.; Reek, J. N. H.; Kamer, P. C. J.; Van Leeuwen, P. W. N. M. *J. Am. Chem. Soc.* **2001**, *123*, 8468–8476.
- (65) Carabineiro, S. A. C.; Martins, L. M. D. R. S.; Pombeiro, A. J. L.; Figueiredo, J. L. *ChemCatChem* **2018**, *10* (8), 1804–1813.
- (66) Rajabi, F.; Schaffner, D.; Follmann, S.; Wilhelm, C.; Ernst, S.; Thiel, W. R. *ChemCatChem* **2015**, *7*, 3513–3518.
- (67) Sabater, S.; Mata, J. A.; Peris, E. *ACS Catal.* **2014**, *4*, 2038–2047.
- (68) Wang, W.; Cui, L.; Sun, P.; Shi, L.; Yue, C.; Li, F. *Chem. Rev.* **2018**, *118*, 9843–9929.
- (69) Esteve, F.; Escrig, A.; Porcar, R.; Luis, S. V.; Altava, B.; García-Verdugo, E. *Adv. Sustain. Syst.* **2022**, *6*, 2100408–21004012.
- (70) Govan, J.; Gun'ko, Y. K. *Nanomaterials* **2014**, *4*, 222–241.
- (71) Fehrmann, R.; Riisager, A.; Marco Haumann. *Supported Ionic Liquids: Fundamentals and Applications*; Wiley-VCH, **2014**.
- (72) Axet, M. R.; Dechy-Cabaret, O.; Durand, J.; Gouygou, M.; Serp, P. *Coord. Chem. Rev.* **2016**, *308*, 236–345.
- (73) Choi, S.; Kim, C.; Suh, J. M.; Jang, H. W. *Carbon Energy* **2019**, *1*, 85–108.
- (74) Suresh, R.; Mangalaraja, R. V; Mansilla, H. D.; Santander, P.; Yáñez, J. Reduced Graphene Oxide-Based Photocatalysis In *Green Photocatalysts*; **2019**; 145–166.
- (75) Sánchez-Page, B.; Victoria Jiménez, M.; Pérez-Torrente, J. J.; Passarelli, V.; Blasco, J.; Subias, G.; Granda, M.; Álvarez, P. *ACS Appl. Nano Mater.* **2020**, *3*, 1640–1655.

- (76) Janiak, C. *J. Chem. Soc. Dalton Trans.* **2000**, 21, 3885–3896.
- (77) Suzuki, Y.; Laurino, P.; McQuade, D. T.; Seeberger, P. H. *Helv. Chim. Acta* **2012**, 95, 2578–2588.
- (78) Zhang, L.; Zhang, W.; Serp, P.; Sun, W. H.; Durand, J. *ChemCatChem* **2014**, 6, 1310–1316.
- (79) Campisciano, V.; Gruttadauria, M.; Giacalone, F. *ChemCatChem* **2019**, 11, 90–133.
- (80) Ventura-Espinosa, D.; Sabater, S.; Carretero-Cerdán, A.; Baya, M.; Mata, J. A. *ACS Catal.* **2018**, 8, 2558–2566.
- (81) Li, S.; Zhong, X.; Yang, H.; Hu, Y.; Zhang, F.; Niu, Z.; Hu, W.; Dong, Z.; Jin, J.; Li, R.; Ma, J. *Carbon N. Y.* **2011**, 49, 4239–4245.
- (82) Ventura-Espinosa, D.; Vicent, C.; Baya, M.; Mata, J. A. *Catal. Sci. Technol.* **2016**, 6, 8024–8035.
- (83) Dresselhaus, M. S.; Thomas, I. L. *Nature* **2001**, 414, 332–337.
- (84) “Our world in data” can be found under <https://ourworldindata.org> accessed 2/10/2022
- (85) Houghton, J. *Reports Prog. Phys.* **2005**, 68, 1343–1403.
- (86) “Earth’s CO₂” can be found under <https://www.co2.earth>, accessed 23/10/2022.
- (87) Abram, N. J.; McGregor, H. V.; Tierney, J. E.; Evans, M. N.; McKay, N. P.; Kaufman D. S. *Nature* **2016**, 536, 411–418.
- (88) Climate Change 2014 Synthesis Report. *IPCC* **2014**.
- (89) “Climate Central” can be found under <https://www.climatecentral.org>, accessed 17/11/2022.
- (90) Vaquer-Sunyer, R.; Duarte, C. M. *Proc. Natl. Acad. Sci. U. S. A.* **2008**, 105, 15452–15457.

- (91) Keeling, R. F.; Körtzinger, A.; Gruber, N. *Ann. Rev. Mar. Sci.* **2010**, *2*, 199–229.
- (92) Allen, M. R.; Ingram, W. J. *Nature* **2002**, *419*, 224–232.
- (93) Milly, P. C. D.; Dunne, K. A.; Vecchia, A. V. *Nature* **2005**, *438*, 347–350.
- (94) Barnett, T. P.; Adam, J. C.; Lettenmaier, D. P. *Nature* **2005**, *438*, 303–309.
- (95) Summary, R. *Science* **2015**, *349*, 4019–4026.
- (96) Nerem, R. S.; Beckley, B. D.; Fasullo, J. T.; Hamlington, B. D.; Masters, D.; Mitchum, G. T. *Proc. Natl. Acad. Sci. U. S. A.* **2018**, *115*, 2022–2025.
- (97) Hansen, J.; Sato, M. *Environ. Res. Lett.* **2016**, *11*.
- (98) Min, S. K.; Zhang, X.; Zwiers, F. W.; Hegerl, G. C. *Nature* **2011**, *470*, 378–381.
- (99) Prein, A. F.; Rasmussen, R. M.; Ikeda, K.; Liu, C.; Clark, M. P.; Holland, G. J. *Nat. Clim. Chang.* **2017**, *7*, 48–52.
- (100) Easterling, D. R.; Meehl, G. A.; Parmesan, C.; Changnon, S. A.; Karl, T. R.; Mearns, L. O. **2000**, *289*, 2068–2075.
- (101) Al-Ghussain, L. *Environ. Prog. Sustain. Energy* **2019**, *38*, 13–21.
- (102) Logan, C. A. *BioScience* **2014**, *60*, 819–828.
- (103) Feely, R. A.; Doney, S. C.; Cooley, S. R. *Oceanography* **2015**, *22*, 36–47.
- (104) Carleton, T. A.; Hsiang, S. M.. *Science* **2016**, *353*, 9387–9402.
- (105) Eberle, U.; Müller, B.; Von Helmholt, R. *Energy Environ. Sci.* **2012**, *5*, 8780–8798.
- (106) Robert, E.; Heinz, H.; Jean-Francois, L.; Laura, L.; Heiko, M.; David, R. *Well-To-Wheels Analysis of Future Automotive*, **2014**.
- (107) Sordakis, K.; Tang, C.; Vogt, L. K.; Junge, H.; Dyson, P. J.; Beller, M.; Laurencyzy, G. *Chem. Rev.* **2018**, *118* (2), 372–433.
- (108) Rowsell, J. L. C.; Yaghi, O. M. *Angew. Chem. Int. Ed.* **2005**, *44*, 4670–4679.

- (109) Thommes, M.; Kaneko, K.; Neimark, A. V.; Olivier, J. P.; Rodriguez-Reinoso, F.; Rouquerol, J.; Sing, K. S. W. *Pure Appl. Chem.* **2015**, *87*, 1051–1069.
- (110) Desjonqueres, M. C.; Spanjaard, D. *Concepts in Surface Physics*, Springer Science & Business Media, **1996**.
- (111) Dalebrook, A. F.; Gan, W.; Grasmann, M.; Moret, S.; Laurency, G.. *Chem. Commun.* **2013**, *49*, 8735–8757.
- (112) Pukazhselvan, D.; Kumar, V.; Singh, S. K. *Nano Energy* **2012**, *1*, 566–589.
- (113) Markiewicz, M.; Zhang, Y. Q.; Bösmann, A.; Brückner, N.; Thöming, J.; Wasserscheid, P.; Stolte, S. *Energy Environ. Sci.* **2015**, *8*, 1035–1045.
- (114) Gianotti, E.; Taillades-Jacquín, M.; Rozière, J.; Jones, D. J. *ACS Catal.* **2018**, *8*, 4660–4680.
- (115) Taube, M.; Rippin, D. W.; Cresswell, D. L.; Knecht, W. *Int. J. Hydrogen Energy* **1983**, *8*, 213–225.
- (116) Schildhauer, T.; Newson, E.; Müller, S.. *J. Catal.* **2001**, *198*, 355–358.
- (117) “Chiyoda Corporation” can be found under <https://www.chiyodacorp.com/en> accessed 11/10/2022.
- (118) “Hydrogenious Technologies GmbH, Erlangen, Germany” can be found under <https://hydrogenious.net>, accessed 11/10/2022
- (119) “H2 industries” can be found under <https://h2-industries.com>, accessed 11/10/2022.
- (120) Pez, G. P.; Scott, A. R.; Cheng, H.; Bagzis, L. D.; Appleby, J. B. Hydrogen Storage by Reversible Hydrogenation of Pi-Conjugated Substrates. US7101530B2, **2003**.
- (121) Moores, A.; Poyatos, M.; Luo, Y.; Crabtree, R. H. *New J. Chem.* **2006**, *30*, 1675–1678.
- (122) Clot, E.; Eisenstein, O.; Crabtree, R. H. *Chem. Commun.* **2007**, *22*, 2231–2233.
- (123) Sotoodeh, F.; Smith, K. J. *Ind. Eng. Chem. Res.* **2010**, *49*, 1018–1026.

- (124) Sotoodeh, F.; Huber, B. J. M.; Smith, K. J. *Appl. Catal. A Gen.* **2012**, 419–420, 6
- (125) Sotoodeh, F.; Smith, K. J. *J. Catal.* **2011**, 279, 36–47.
- (126) Gleichweit, C.; Amende, M.; Schernich, S.; Zhao, W.; Lorenz, M. P. A.; Höfert, O.; Brückner, N.; Wasserscheid, P.; Libuda, J.; Steinrück, H. P.; Papp, C. *ChemSusChem* **2013**, 6, 974–977.
- (127) Pez, G., Scott, A., Cooper, A., Cheng, H. Hydrogen Storage by Reversible Hydrogenation of Pi-Conjugated Substrates. US7101530, **2006**.
- (128) Wang, Z.; Tonks, I.; Belli, J.; Jensen, C. M. *J. Organomet. Chem.* **2009**, 694, 2854–2857.
- (129) Stark, K.; Keil, P.; Schug, S.; Müller, K.; Wasserscheid, P.; Arlt, W. *J. Chem. Eng. Data* **2016**, 61, 1441–1448.
- (130) Xie, Y.; Milstein, D. *ACS Appl. Energy Mater.* **2019**, 2, 4302–4308.
- (131) Yamaguchi, R.; Ikeda, C.; Takahashi, Y.; Fujita, K. I. *J. Am. Chem. Soc.* **2009**, 131, 8410–8412.
- (132) Deraedt, C.; Ye, R.; Ralston, W. T.; Toste, F. D.; Somorjai, G. A. *J. Am. Chem. Soc.* **2017**, 139, 18084–18092.
- (133) Moromi, S. K.; Siddiki, S. M. A. H.; Kon, K.; Toyao, T.; Shimizu, K. H. *Catal. Today* **2017**, 281, 507–511.
- (134) Wu, J.; Talwar, D.; Johnston, S.; Yan, M.; Xiao, J. *Angew. Chemie - Int. Ed.* **2013**, 2, 6983–6987.
- (135) Ryabchuk, P.; Agapova, A.; Kreyenschulte, C.; Lund, H.; Junge, H.; Junge, K.; Beller, M. *Chem. Commun.* **2019**, 55, 4969–4972.
- (136) Jaiswal, G.; Subaramanian, M.; Sahoo, M. K.; Balaraman, E. *ChemCatChem.* **2019**, 11, 2449–2457.
- (137) Mikami, Y.; Ebata, K.; Mitsudome, T.; Mizugaki, T.; Jitsukawa, K.; Kaneda, K. *ChemInform.* **2011**, 82, 1371–1377.

- (138) Jaiswal, G.; Landge, V. G.; Jagadeesan, D.; Balaraman, E. *Nat. Commun.* **2017**, *8*, 2147–2160.
- (139) Bera, A.; Bera, S.; Banerjee, D. *Chem. Commun.* **2021**, *57*, 13042–13058.
- (140) Chen, Y.; Jiang, J. *Sustain. Energy Fuels* **2021**, *5*, 6478–6487.
- (141) Liu, J.; Guo, F.; Cui, F.; Zhu, J.; Liu, X.; Ullah, A.; Wang, X.; Quan, Z. *New J. Chem.* **2022**, *46*, 1791–1799.
- (142) Zheng, M.; Shi, J.; Yuan, T.; Wang, X. *Angew. Chem. Int. Ed.* **2018**, *57*, 5487–5491.
- (143) Massey, R.; Jacobs, M. *Global Chemicals Outlook – Towards Sound Management of Chemicals*, **2013**.
- (144) Clark, J.; Deswarte, F. *Introduction to Chemicals from Biomass Wiley Series in Renewable Resources*, **2015**.
- (145) Lim, D. S. W.; Anderson, E. A. *Org. Lett.* **2011**, *13*, 4806–4809.
- (146) Fleming, I.; Barbero, A.; Walter, D. *Chem. Rev.* **1997**, *97*, 2063–2192.
- (147) Flann, C. J.; Overman, L. E. *J. Am. Chem. Soc.* **1987**, *109*, 6115–6118.
- (148) Hatanaka, Y.; Hiyama, T. *J. Organic Chem.* **1989**, *54*, 268–270.
- (149) Miura, K.; Hondo, T.; Okajima, S.; Hosomi, A. *Tetrahedron Lett.* **1996**, *37*, 487–490.
- (150) Luh, T.-Y.; Liu, S.-T. *Synthetic Applications of Allylsilanes and Vinylsilanes*, In *The Chemistry of Organic Silicon Compounds*, **2009**.
- (151) Overman, L. E.; Bell, K. L. S. *J. Am. Chem. Soc.* **1981**, *103*, 1851–1853.
- (152) Murakami, K.; Yorimitsu, H.; Oshima, K.. *J. Org. Chem.* **2009**, *74*, 1415–1417.
- (153) Hirano, K.; Yorimitsu, H.; Oshima, K. *J. Am. Chem. Soc.* **2007**, *129*, 6094–6095.
- (154) Zanardi, A.; Mata, J. A.; Peris, E. *Eur. J. Inorg. Chem.* **2011**, *3*, 416–421.
- (155) Karstedt, B. D. *Platinum-vinylsiloxanes*, US3715334, **1973**.

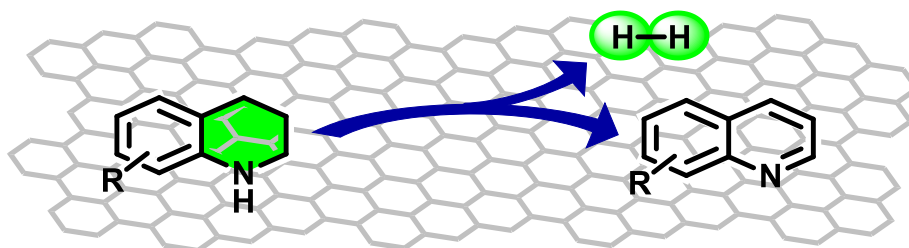
- (156) Stein, J.; Lewis, L. N.; Gao, Y.; Scott, R. A. *J. Am. Chem. Soc.* **1999**, *121*, 3693–3703.
- (157) Markó, I. E.; Stérin, S.; Busine, O.; Mignani, G.; Branlard, P.; Tinant, B.; Declercq J. -P. *Science* **2002**, *298*, 204–206.
- (158) Berthon-Gelloz, G.; Schumers, J. M.; De Bo, G.; Markó, I. E. *J. Org. Chem.* **2008**, *73*, 4190–4197.
- (159) Fernández, G.; Pleixats, R. *Catalysts* **2020**, *10*, 1–18.
- (160) Jankowska-Wajda, M.; Bartlewicz, O.; Szepecht, A.; Zajac, A.; Smiglak, M.; Maciejewski, H. *RSC Adv.* **2019**, *9*, 29396–29404.
- (161) Zhao, J.; Gui, Y.; Liu, Y.; Wang, G.; Zhang, H.; Sun, Y. 'an; Fang, S. *Catal. Letters* **2017**, *147*, 1127–1132.
- (162) Fouché, M.; Rooney, L.; Barrett, A. G. M. *J. Org. Chem.* **2012**, *77*, 3060–3070
- (163) Rossi, R. *Synthesis (Stuttg.)*. **1977**, *12*, 817–836.
- (164) Odinkov, V. *Chem. Nat. Compd.* **2000**, *36*, 11–39.
- (165) Smith, A. B.; Beauchamp, T. J.; Lamarche, M. J.; Kaufman, M. D.; Qiu, Y.; Arimoto, H.; Jones, D. R.; Kobayashi, K. *J. Am. Chem. Soc.* **2000**, *122*, 8654–8664.
- (166) Tallarico, J. A.; Randall, M. L.; Snapper, M. L. *Tetrahedron* **1997**, *53*, 16511–16520.
- (167) Malcolmson, S. J.; Meek, S. J.; Sattely, E. S.; Schrock, R. R.; Hoveyda, A. H. *Nature* **2008**, *456*, 933–937.
- (168) Yu, M.; Wang, C.; Kyle, A. F.; Jakubec, P.; Dixon, D. J.; Schrock, R. R.; Hoveyda, A. H. *Nature* **2011**, *479*, 88–92.
- (169) Endo, K.; Grubbs, R. H. *J. Am. Chem. Soc.* **2011**, *133*, 8525–8527.
- (170) Neveselý, T.; Wienhold, M.; Molloy, J. J.; Gilmour, R. *Chem. Rev.* **2022**, *122*, 2650–2694.

- (171) Kudo, E.; Sasaki, K.; Kawamata, S.; Yamamoto, K.; Murahashi, T. S. *Nat. Commun.* **2021**, *12*, 1–8.
- (172) Chen, C.; Dugan, T. R.; Brennessel, W. W.; Weix, D. J.; Holland, P. L. *J. Am. Chem. Soc.* **2014**, *136*, 945–955.
- (173) Kojoori, R. K. *J. Chem. Soc. Pakistan* **2016**, *38*, 1121–1128.
- (174) Zhang, W.; Wang, F.; Li, X.; Liu, Y.; Liu, Y.; Ma, J. *Appl. Surf. Sci.* **2017**, *404*, 398–408.
- (175) Dubuis, R.; Lindlar, H. *Org. Synth.* **1966**, *46*, 89–91.
- (176) Cheng, J.; Deming, T. J. Stereoselective Synthesis of Z-Alkenes. In *Stereoselective Alkene Synthesis*; Springer, **2012**.
- (177) Oger, C.; Balas, L.; Durand, T.; Galano, J. M. *Chem. Rev.* **2013**, *113*, 1313–
- (178) Garbe, M.; Budweg, S.; Papa, V.; Wei, Z.; Hornke, H.; Bachmann, S.; Scalone, M.; Spannenberg, A.; Jiao, H.; Junge, K.; Beller, M. *Catal. Sci. Technol.* **2020**, *10*, 3994–4001.
- (179) Lu, Y.; Feng, X.; Takale, B. S.; Yamamoto, Y.; Zhang, W.; Bao, M. *ACS Catal.* **2017**, *7*, 8296–8303.
- (180) Delgado, J. A.; Godard, C. *Progress in the Selective Semi-Hydrogenation of Alkynes by Nanocatalysis*, Springer, **2020**.
- (181) Corma Canos, A.; Iborra, S.; Velty, A. *Chem. Rev.* **2007**, *107*, 2411–2502.
- (182) Besson, M.; Gallezot, P.; Pinel, C. *Chem. Rev.* **2014**, *114*, 1827–1870.
- (183) Huber, G. W.; Iborra, S.; Corma, A. *Chem. Rev.* **2006**, *106*, 4044–4098.
- (184) Zhang, Z.; Huber, G. W. *Chem. Soc. Rev.* **2018**, *47*, 1351–1390.
- (185) Ramanna, M.; Subhosh, G.; Madakka, M. Comparative Biochemistry and Kinetics of Microbial Lignocellulolytic Enzymes. In *Recent Developments in Applied Microbiology and Biochemistry*, Elsevier Inc., **2019**.
- (186) Byadgi, S. A.; Kalburgi, P. B. *Procedia Environ. Sci.* **2016**, *35*, 555–562.

- (187) Gargulak, J. D.; Lebo, S. E.; McNally, T. J. Lignin. In *Kirk-Othmer Encyclopedia of Chemical Technology*; John Wiley & Sons, **2015**.
- (188) Chatterjee, C.; Pong, F.; Sen, A. *Green Chem.* **2015**, *17*, 40–71.
- (189) Takkellapati, S.; Li, T.; Gonzalez, M. A. *Clean Technol. Environ. Policy* **2018**, *20*, 1615–1630.
- (190) “Food Standards Agency” can be found under <https://www.food.gov.uk>, accessed 11/11/2022.
- (191) Levy, J. K.; Crawford, P. C.; Appel, L. D.; Clifford, E. L. *Am. Vet. Med. Assoc.* **2008**, *69*, 140–143.
- (192) Kodsangma, A.; Homsaard, N.; Nadon, S.; Rachtanapun, P. *Carbohydr. Polym.* **2020**, *242*, 116421–116428.
- (193) Ma, S.; Li, W.; Zhang, S.; Ge, D.; Yu, J.; Shen, X. *Constr. Build. Mater.* **2015**, *91*, 138–144.
- (194) Thermodynamics, J. C.; Antonick, P. J.; Hu, Z.; Fujita, Y.; Reed, D. W.; Das, G.; Wu, L.; Shivaramaiah, R.; Kim, P.; Eslamimanesh, A.; Lencka, M. M.; Jiao, Y.; Anderko, A.; Navrotsky, A.; Riman, R. E. *J. Chem. Thermodyn.* **2019**, *132*, 491–496.
- (195) Borja, P.; Mata, J. A.; Vicent, C.; Baya, M. *Green Chem.* **2018**, *20*, 4094–4101.
- (196) Ramachandran, S.; Fontanille, P.; Pandey, A.; Larroche, C. *Food Technol. Biotechnol.* **2006**, *44*, 185–195.
- (197) Mirescu, A.; Berndt, H.; Martin, A.; Pru, U. *Appl. Catal. A Gen.* **2007**, *317*, 204–209.

CHAPTER 2:

Reduced Graphene Oxides as Carbocatalysts in Acceptorless Dehydrogenation of N-Heterocycles



ABSTRACT

The catalytic properties of graphene-derived materials are evaluated in acceptorless dehydrogenation of N-heterocycles. Among them, reduced graphene oxides (rGOs) are active (quantitative yields in 23 h) under mild conditions (130 °C) and act as efficient heterogeneous carbocatalysts. rGO exhibits reusability and stability at least during eight consecutive runs. Mechanistic investigations supported by experimental evidence (i.e. organic molecules as model compounds, purposely addition of metal impurities and selective functional group masking experiments) suggest a preferential contribution of ketone carbonyl groups as active sites for this transformation.

ACS Catalysis, **2021**, *11*, 14688 – 14693 (DOI: 10.1021/acscatal.1c04649)

2.1 INTRODUCTION

Metal-free catalysts might play an important role in the design of sustainable and environmentally friendly chemical transformations.¹⁻⁴ The actual dependence of catalysis on metals, often precious and rare, is no longer sustainable owing to the cost, limited abundance, and depletion of metal sources. Development of metal-free catalysts based on abundant elements is a promising area of research. Organocatalysis is a well-established field in which well-defined active sites are present in organic molecules.⁵⁻⁷ Parallel to this, the use of heterogeneous carbonaceous materials is gaining interest, but the area is in its earlier development in terms of understanding the reaction mechanisms, architecture of the active sites and engineering of materials with single sites.⁸⁻¹⁰ In recent years we have witnessed a rapid development of graphene-type materials as catalysts.^{11,12} Defective graphenes have shown catalytic activity in oxidation,^{13,14} reduction^{15,16} and coupling reactions.^{17,18}

In parallel, the hydrogenation and dehydrogenation of N-heterocycles is an important reaction from the synthetic viewpoint. N-heterocycles are found in many highly added-value organic compounds. They are also considered as potential Liquid Organic Hydrogen Carriers (LOHCs) for hydrogen storage and release.¹⁹⁻²¹ One advantage of N-heterocycles as LOHCs compared to cycloalkanes is the reduction of dehydrogenation enthalpy facilitating hydrogen release.²²⁻²⁴ The success of H₂ storage in organic compounds depends on the development of efficient, stable and affordable catalysts.²⁵⁻²⁷ However, to the best of our knowledge, acceptorless dehydrogenation (ADH) of tetrahydroquinolines using metal-free catalysts has not been reported. Previous examples describe the use of advanced nanostructures (e.g. nanodiamonds) or activated mesoporous carbons in acceptorless gas-phase dehydrogenation of alkanes at high temperatures (> 500 °C).²⁸⁻³⁰ Alternatively, graphene oxide (GO) or activated carbon (AC) have been used in the oxidative dehydrogenation of N-heterocycles with the concomitant formation of water or hydrogen peroxide (Figure 2.1).³¹⁻³⁵ In this manuscript, we describe the activity of reduced graphene oxides (rGOs) as efficient and reusable carbocatalysts for the ADH of tetrahydroquinolines with the production of molecular hydrogen, a key reaction for on-board hydrogen release. Our research provides a general scope of the metal-free ADH carbocatalysts as well as evidence of the active sites responsible for this transformation.

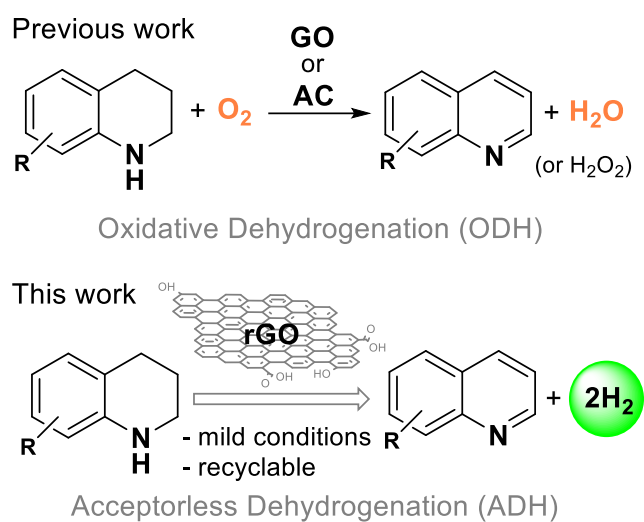
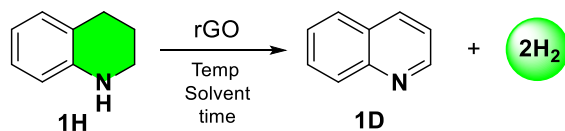


Figure 2.1 Differences between oxidative (ODH) and acceptorless dehydrogenation (ADH) of N-heterocycles. The latter is important for H₂ storage. In ADH, H₂ gas is released while in ODH hydrogen is transferred to oxygen and released as H₂O. (**GO**: Graphene oxide, **AC**: Activated carbon, **rGO**: reduced graphene oxide).

2.2 RESULTS AND DISCUSSION

The performance of **rGO** as carbocatalyst in ADH of N-heterocycles was first evaluated using 1,2,3,4-tetrahydroquinoline (THQ, **1H**) as model substrate under oxygen-free conditions (Tables 2.1 and S2.1). Our first concern was to find out whether **rGO** was acting as a true carbocatalyst or as a stoichiometric reagent.³⁶ First of all, we confirmed that dehydrogenation of THQ did not occur without **rGO** (Table 2.1, entry 1). In the presence of **rGO**, quinoline is obtained under different solvents and reaction conditions indicating that the process is general. ADH of **1H** afforded quinoline (**1D**) with the concomitant release of two molecules of H₂. Hydrogen was qualitatively analyzed using a micro GC. The ADH of N-heterocycles is an endergonic reaction in contrast to the ODH. The driving force of ADH is the removal of hydrogen from the reaction media. In fact, when the dehydrogenation reaction is carried out in a closed system, no product formation occurred (Table 2.1, entry 8). Then, the influence of catalyst loading in the dehydrogenation of 8-methoxytetrahydroquinoline (**7H**) was assessed (Figure S2.1). The apparent reaction rates depended on the amount of **rGO** and the reaction profiles suggest a catalytic nature for the reaction. For instance, lowering the catalyst loading to 5 mg, instead of using 15 mg as in the standard conditions, considerably decreased the apparent reaction rate, but still a good yield (68 %) could be obtained after 23 h. The selectivity and the presence of other reaction products was evaluated through analogous experiments using deuterated *o*-dichlorobenzene (*o*-DCB) and analyzing the reaction mixture without any purification process (Figures S2.2).

By monitoring the reaction progress by ¹H NMR spectroscopy it could be seen how the starting substrate (**3H**) is converted to the corresponding dehydrogenated product (**3D**) without the formation of other products. This confirmed the high selectivity of ADH of THQs towards quinolines using **rGO** as carbocatalyst.

Table 2.1. Catalytic activity of rGO in ADH of 1,2,3,4-tetrahydroquinoline (**1H**) under various reaction conditions.

Entry	Solvent	T (°C)	Conv. (%)	Yield (%)
1^a	<i>o</i> -DCB	130	5	1
2	<i>o</i> -DCB	130	91	85
3	<i>o</i> -DCB	110	78	67
4	DMF	130	74	58
5	toluene	110	14	9
6	<i>n</i> -decane	130	81	64
7	DIPB	130	79	58
8^b	<i>o</i> -DCB	130	10	n.d.

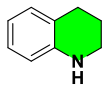
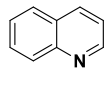
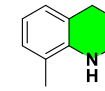
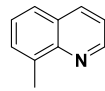
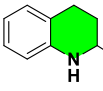
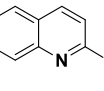
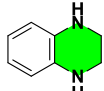
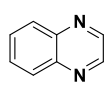
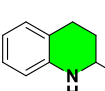
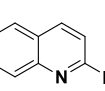
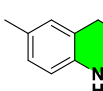
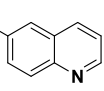
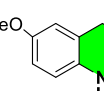
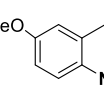
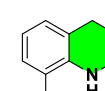
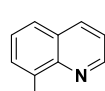
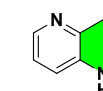
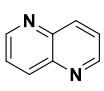
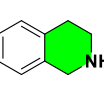
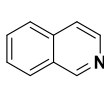
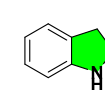
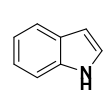
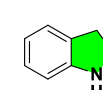
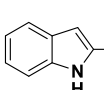
Reaction conditions: 1,2,3,4-tetrahydroquinoline (0.15 mmol), **rGO** (15 mg), solvent (1 mL) for 23 h. Evolution of starting material (conversion) obtained by GC/FID using 1,3,5-trimethoxybenzene as internal standard and product formation (yield) obtained by ¹H NMR analysis. [a] Without **rGO**. [b] Closed system. *o*-DCB: ortho dichlorobenzene; DMF: N,N-dimethylformamide; DIPB, 1,3-diisopropylbenzene.

Reaction scope

Next, we investigated the scope and limitations of N-heterocycle dehydrogenation using **rGO** as carbocatalyst (Table 2.2). The reactions were monitored by GC and the activity was compared using apparent reaction rates (Figure S2.3-S2.6 and Table S2.2). **rGO** is an efficient carbocatalyst for a variety of substituted THQs and indolines. Methyl (**3H**) or phenyl (**5H**) substitution at the 2-position of THQ showed similar rates and afforded quantitative yields after 23 h. Introduction of different groups at the 6-position (**6H** and **7H**) does not influence the formation of quinolines and similar reaction rates were obtained. A substantial limitation in ADH of THQ substituted at the 8-position was observed. The presence of a methyl (**2H**) or a phenyl (**8H**) reduced the yield of **2D** and **8D** to 56 and 50 %, respectively, probably due to steric effects. The same procedure was used for dehydrogenation of

tetrahydroisoquinoline (**10H**). Under these conditions, full conversion of **10H** was also obtained, but only 15 % yield corresponds to isoquinoline (**10D**), the rest (about 70 % yield) being the monodehydrogenated product. Monitoring of the temporal reaction profile indicates that double dehydrogenation of **10H** requires longer reaction times (Figure S2.5). A fast reaction and quantitative conversion was obtained for tetrahydroquinoxaline (**4H**) containing two nitrogen groups (92 % conv. in 8h). This result agrees with previous theoretical calculations revealing that the dehydrogenation is thermodynamically favored by increasing the number of nitrogen atoms in the N-heterocycles.²³ An important limitation was found for tetrahydronaphthyridine (**9H**) due to product degradation, while a good conversion of 76 % was observed, in contrast, the product **9D** could only be obtained in a low yield (32 %). Further studies using five-membered ring N-heterocycles (indolines) showed faster reactions. For instance, indoline (**11H**) and 2-methylindoline (**12H**) were fully dehydrogenated to the corresponding indole (**11D**) or 2-methylindole (**12D**) in less than 10 h.

Table 2.2 Scope of ADH of N-heterocycles.

Substrate	Product	Substrate	Product	Substrate	Product
 1H , Conv. 91%	 1D , Yield 85%	 2H , 66%	 2D , 59%	 3H , 91%	 3D , 87%
 4H , 100%	 4D , 82%	 5H , 96%	 5D , 91%	 6H , 100%	 6D , 93%
 7H , 100%	 7D , 91%	 8H , 56%	 8D , 50%	 9H , 74%	 9D , 32%
 10H , 100%	 10D , 15%	 11H , 100%	 11D , 86%	 12H , 100%	 12D , 73%

Reaction conditions: Substrate (0.15 mmol), 15 mg of **rGO**, *o*-DCB (1 mL) at 130 °C for 23 h. The number under the starting material corresponds to conversion obtained by GC/FID and the number under the product corresponds to the isolated product yield after purification. See SI for the reaction profiles and details. H, (hydrogenated); D (dehydrogenated).

Recyclability study

The performance of **rGO** as carbocatalyst was further evaluated by recycling experiments. The temporal reaction profile provides valuable information of activity and stability. The **rGO** was removed from the solution after each run by decantation, washed with MeOH and reused without any preactivation process. The data presented in Figure 2.2 are the average of two independent reactions. These results show some decrease in activity from run 1 to run 2 and then, from run 4 to 6. However, the activity is recovered from runs 7 and 8. These fluctuations are due to the imperfect experimental working procedure with **rGO**, rather than a real tendency to deactivation. In any case, the catalytic activity of **rGO** is maintained for eight consecutive runs. It is worth mentioning that we have not observed any sign of catalyst deactivation. This fact suggests that **rGO** is a stable carbocatalyst. After the recycling experiments the **rGO** spent in the reaction was analyzed by HRTEM, XPS, elemental analysis and Raman spectroscopy to determine any change in the morphology and composition (Figures S2.7 – S2.9). The only subtle difference is the presence of more wrinkles in the spent **rGO** carbocatalyst. We believe that the presence of these wrinkles is not directly related to the catalytic activity but a consequence of the use of **rGO** in multiple experiments. XPS spectra of the C1s and O1s bands for the fresh and spent **rGO** show a similar peak-shape and at the same binding energy (Figure S2.9). Deconvolution provides similar contributions of different bonding modes (C-C, C-N, C-O, C=O and HO-C=O) for the fresh and spent **rGO**. The oxygen/carbon ratio for the fresh **rGO** sample was 0.12 and for the spent **rGO** (8 runs) was 0.13. These results confirm that during the catalytic reaction there is not an increase or decrease of oxygen content. Elemental composition by combustion analyses, confirmed that the oxygen/carbon ratio is maintained after exhaustive recycling. The Raman spectra provided the characteristic graphene pattern with D, G and 2D bands. The relative intensity (I_D/I_G) of D and G bands is preserved after eight runs indicating the high stability of **rGO**. (Figure S2.7). The available characterization data before and after the recycling experiment indicates that **rGO** is not altered during dehydrogenation of N-heterocycles.

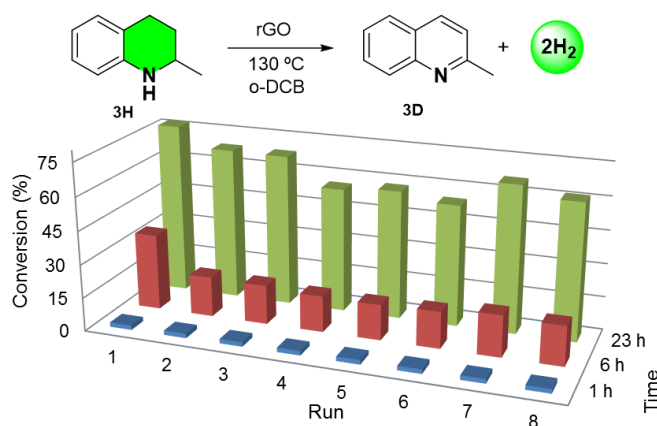


Figure 2.2 Activity of **rGO** as carbocatalyst for ADH of N-heterocycles. Reaction conditions: Tetrahydroquinoline (**3H**, 0.3 mmol), catalyst loading (30 mg of **rGO**), *o*-DCB (2.0 mL) as solvent at 130 °C. Conversion determined by GC/FID and using 1,3,5-trimethoxybenzene as internal standard.

Mechanistic studies

Mechanistic studies of catalytic reactions using carbonaceous materials is a difficult task because of the ill-defined nature of the active sites.³⁷ To get information about the catalytic active sites of **rGO**, experiments were performed to address influence of residual metals, use of organic molecules as models of the active centres and selective masking of functional groups. We first assessed the catalytic activity of different graphene-related materials including **rGO** from different commercial suppliers. The results (Figure S2.10) showed that graphene (**G**) and graphite are not active in the dehydrogenation of N-heterocycles. **GO** is highly active at low conversions, but then it deactivates fast and after a prolonged reaction time only 63 % yield is obtained. On the contrary, all **rGO** materials used show a remarkable activity independently if they are obtained by thermal or chemical reduction. This observation indicates that the presence of vacancies or holes, which are more common in thermal **rGO**, or the presence of adventitious sites, N atoms in chemical reduction by hydrazine, are not necessary for the catalytic activity. The results derived from different carbonaceous materials indicate that the functional groups and the sp² character of the basal plane of carbonaceous materials play a role as active sites in the catalytic reaction.

Then, we analysed the potential catalytic activity of metal impurities in the carbonaceous materials. Carbonaceous materials are predominantly obtained from graphite that contains several metal impurities present at trace levels.^{38–40} These impurities could have an impact in the catalytic properties of graphene. In addition, the preparation of **GO** and **rGO** involves the use of oxidant/reducing agents, some of which can contain metals that may remain in the final samples even at low concentrations. Common metal impurities found in **rGO** are iron and manganese. We evaluated the catalytic activity in dehydrogenation of N-heterocycles by adding known amounts of these metals in minute concentrations. The reaction progress in three parallel reactions containing: no added metal, with 0.5 mg of M^{2+} and with 1 mg of M^{2+} were monitored (Figures S2.11 and S2.12). The results show that the three curves overlapped for Mn^{2+} or Fe^{2+} suggesting that the catalytic effect induced by the presence of these metal ions at these concentrations is negligible.

We also used a series of organic molecules as models of the active sites to assess the role of different functional groups (-OH, -COOH and C=O) in ADH of N-heterocycles (Figure S2.13). The use of simple organic molecules for mimicking the role oxygenated groups at the surface of carbon materials is gaining interest, due to the relevant information provided.^{41,42} The results show that model molecules containing carboxylic acids and carbonyl groups promote somehow dehydrogenation of N-heterocycles (Table S2.4). For instance, the yield of 2-methyltetraquinoline (**3D**) is 19 and 34 % when using benzoic acid (**A**) and pyrene-4,5-dione (**H**), respectively. Other compounds like benzoquinone and phenol also exhibit some activity. The results also suggested that the chemical environment of the functional groups is important, as we observed differences between functional groups attached to benzene or pyrene scaffolds. The activity of the model molecules suggests that carboxylic acids, hydroxy and carbonyl groups present on **rGO** are potential catalytic active sites. We then used modified **rGO** samples in which certain functional groups have been selectively masked to provide further information on active sites. Carboxylic acids, ketone and phenol groups of **rGO** were selective masked using established procedures (Figure 2.14).^{43,44} The catalytic activity of the parent **rGO** and the masked materials **rGO**^{COOH}, **rGO**^{CO} and **rGO**^{OH} (superscript indicates the masked group) was evaluated in dehydrogenation of tetrahydroquinaldine (**3H**). The results reveal that samples without carboxylic groups or phenolic moieties exhibit lower apparent reaction rates than unprotected **rGO**. A more remarkable decrease in the dehydrogenation rates occurs upon masking the carbonyl groups (Figure S2.15). The results of masking experiments suggest that the

carbonyl groups are the prevalent active sites that together with lesser activity of carboxylic and hydroxyl groups are responsible for the performance of **rGO**.

Previous studies on the use of **rGO** as carbocatalyst have already claimed the role of carbonyl groups (quinone type) as active sites.^{41,45,46} Based on present experimental evidence, a plausible mechanism for ADH of N-heterocycles is proposed in which the role of carbonyl groups is emphasized as previously observed in ODH (Figure 2.3).⁴⁷⁻⁴⁹ According to this proposal, dehydrogenation of N-heterocycles would occur with the concomitant reduction of carbonyl groups that in a subsequent step would release molecular hydrogen

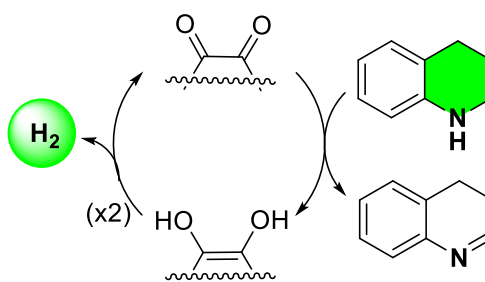


Figure 2.3 Plausible mechanism in dehydrogenation of N-heterocycles showing the role of carbonyl groups.

2.3 CONCLUSIONS

Graphene oxide (**GO**) is an efficient metal-free carbocatalyst for oxidative dehydrogenation reactions (OHD). In this manuscript, reduced graphene oxide (**rGO**) behaves as a suitable carbocatalyst to promote, without metal assistance, a more challenging thermodynamically uphill reaction, namely acceptorless dehydrogenation of N-heterocycles (ADH). H_2 must be removed from the system, in order to precede the reaction, while the catalyst has to be very efficient in establishing equilibrium concentrations. **rGOs** obtained from diverse synthetic methodologies are equally active as catalysts promoting dehydrogenation of a wide range of N-heterocycles. Available catalytic data indicate that possible metal impurities are not involved in the process and that the most likely active sites are quinone-like carbonylic groups. In this way, the present results represent a step forward towards the sustainability for on-board hydrogen release that could be applicable in massive scale without mining or depletion of limited metal resources.

2.4 SUPPORTING INFORMATION

This section contains the most relevant data of the article supporting information. To see the complete version, we invite you to download the PDF version of the article at the publisher website (<https://pubs.acs.org/doi/10.1021/acscatal.1c04649>)

General considerations

Reagents and solvents

N-heterocycles were purchased from commercial suppliers and used without further purification. Anhydrous solvents were dried using a solvent purification system or purchased from commercial suppliers and stored over molecular sieves. Solvents were deoxygenated using the freeze-pump-thaw methodology and kept under an atmosphere of nitrogen.

Instrumentation

Nuclear magnetic resonance (NMR) spectra were recorded on Bruker spectrometers operating at 300 or 400 MHz (^1H NMR) and 75 or 100 MHz ($^{13}\text{C}\{^1\text{H}\}$ NMR), respectively, and referenced to SiMe_4 (δ in ppm and J in Hertz). NMR spectra were recorded at room temperature with the appropriate deuterated solvent. Elemental Analysis was carried out in a TruSpec Micro Series. High-resolution images of transmission electron microscopy (HRTEM) and high-angle annular dark-field (HAADF-STEM) images of the samples were obtained using a Jem-2100 LaB6 (JEOL) transmission electron microscope coupled with an INCA Energy TEM 200 (Oxford) energy dispersive X-Ray spectrometer (EDX) operating at 200 kV. Samples were prepared by drying a droplet of a MeOH dispersion on a carbon-coated copper grid. X-ray photoelectron spectra (XPS) were acquired on a Kratos AXIS ultra DLD spectrometer with a monochromatic Al $K\alpha$ X-ray source (1486.6 eV) using a pass energy of 20 eV. To provide a precise energy calibration, the XPS binding energies were referenced to the C1s peak at 284.6 eV. Gas chromatography (GC) analyses were obtained on a shimadzu GC-2010 apparatus equipped with a FID detector, and using a Teknokroma column (TRB-5MS, 30 m x 0.25 mm x 0.25 μm).

Synthesis of graphenes

Reduced graphene oxide (**rGO**): The employed reduced graphene oxide in dehydrogenation reactions of N-heterocycles was obtained from a commercial

supplier (Graphenea). The same batch of **rGO** was used for all experiments to assure reproducibility. The **rGO** is produced by oxidation of graphite using the Hummer's method.⁵⁰ Then is chemically reduced using an organic reducing agent under basic conditions. Properties: Specific surface area 423 – 498 m²/g; Electrical conductivity: 667 S/m; Density 0.06 – 0.09 g/cm³.

Graphene oxide (**GO**): It was prepared from graphite powder (natural, universal grade, 200 mesh, 99,9995%) by the Hummer's method.⁵⁰ Briefly, graphite is oxidized using potassium permanganate under strong acidic conditions (sodium nitrite and sulfuric acid). Exfoliation is performed using ultrasounds.

Thermal reduced graphene oxide (**rGO^t**): The **rGO^t** was obtained by thermal reduction of **GO**. The **GO** (prepared by the Hummer's method) was heated in a furnace under inert atmosphere (Ar) at 200 °C (5 °C/min) for 4 h. Removal of functional groups produces a black material known as thermally reduced graphene oxide (**rGO^t**) that has been previously described.⁵¹

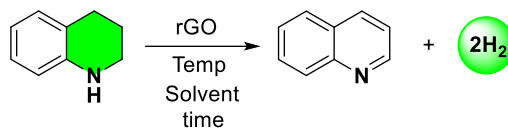
Graphene (**G**): **G** was prepared according to a literature procedure literature.⁵² Commercial alginate, after purification by dissolution in aqueous solution and filtration under pressure, was pyrolyzed as powder on a ceramic crucible at 900 °C (5 °C/min) under an argon flow for 4h. The carbonaceous residue was submitted to sonication (250 W) for 30 min in water. The suspension was decanted, and the solid residue discarded. The suspension was freeze-dried and the graphenic material resuspended before using as a catalyst.

Catalytic dehydrogenation reactions

All catalytic experiments were carried out under an atmosphere of nitrogen using dry and deoxygenated solvents. In a typical procedure, the carbocatalyst was filled into a dry Schlenk flask (20 mL) connected to condenser containing a bubbler filled with mineral oil to exclude air from the reaction system and allowing the release of hydrogen gas. Solvent, substrate and 1,3,5-trimethoxybenzene as a standard were added under a nitrogen flux. The mixture was stirred at 130 °C (bath temperature) for at least 23h. The reaction progress was monitored by gas chromatography taking aliquots at selected intervals.

Optimization of reaction conditions

Table S2.1 Optimization of reaction conditions in dehydrogenation of 1,2,3,4-tetrahydroquinoline.



Entry	rGO (mg)	Substrate (mmol)	Solvent	T (°C)	Time (h)	Conv. (%)	Yield (%)
1	-	0.1	<i>o</i> -DCB (2mL)	130	23	5	1
2	20	0.1	<i>o</i> -DCB (2mL)	130	23	100	85
3	10	0.3	<i>o</i> -DCB (2mL)	130	23	41	35
4	15	0.15	<i>o</i> -DCB (1mL)	130	23	91	85
5	15	0.15	<i>o</i> -DCB (1mL)	110	23	78	67
6	15	0.15	DMF(1mL)	130	23	74	58
7	15	0.15	toluene (1mL)	110	23	14	9
8	15	0.15	n-butanol (1mL)	120	23	18	12
9	15	0.15	n-decane (1mL)	130	23	81	64
10	15	0.15	DIPB (1mL)	130	23	79	58
11 ^a	15	0.15	<i>o</i> -DCB (1mL)	130	23	10	n.d.
12 ^b	15	0.15	<i>o</i> -DCB (1mL)	130	32	99	90
13 ^c	15	0.15	<i>o</i> -DCB (1mL)	130	30	90	84

Reaction conditions: 1,2,3,4-tetrahydroquinoline (0.15 mmol), **rGO**, solvent for 23 h. Evolution of starting material (conversion) obtained by GC/FID using 1,3,5-trimethoxybenzene as an internal standard and product formation (yield) obtained by ¹H NMR analysis [a] Closed system. *o*-DCB, ortho dichlorobenzene; DMF, N,N-dimethylformamide; DIPB, 1,3-diisopropylbenzene. [b] Under aerobic conditions. [c] Under aerobic conditions in a closed system.

Influence of catalyst loading

The influence of catalyst loading in dehydrogenation of N-heterocycles was evaluated using 6-methoxytetrahydroquinoline (**7H**) as model substrate. The catalytic reaction was monitored by gas chromatography using different amounts of **rGO** as carbocatalyst.

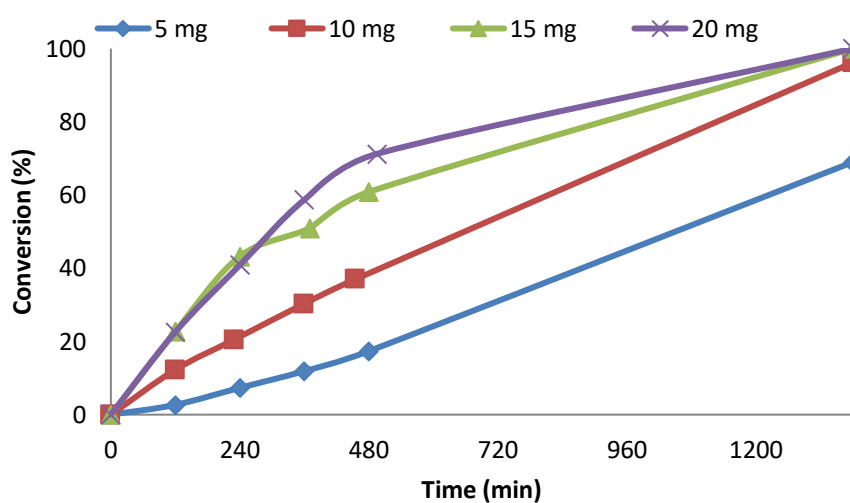
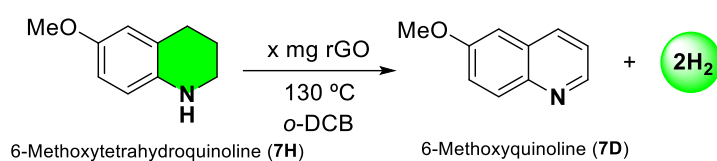


Figure S2.1 Reaction progress profiles: Influence of catalyst loading in dehydrogenation of **7H**. Conditions: Substrate (0.15 mmol), **rGO** (x mg), *o*-DCB (1 mL) at 130 °C. Conversion by GC/FID.

Selectivity study in the conversion of 6-Methyl-tetrahydroquinoline (6H)

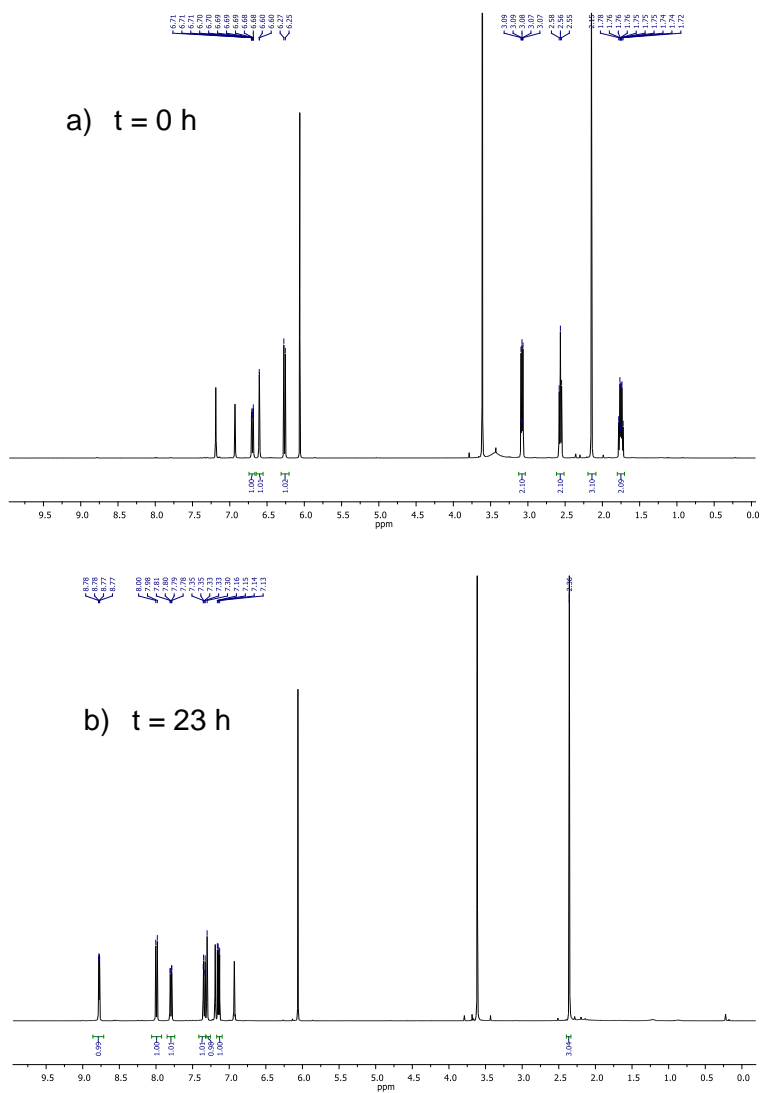
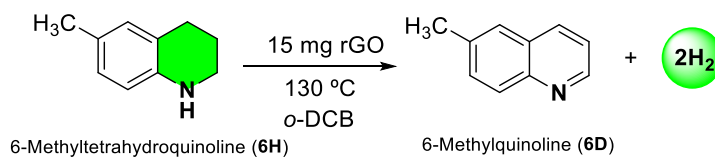


Figure S2.2 Acceptorless dehydrogenation of 6H. Initial ^1H NMR spectrum (a) and after $t = 23$ h reaction (b) using 1,3,5-trimethoxybenzene (signals at 3.61 and 6.06 ppm) as an internal standard. Residual *o*-DCB solvent signals at 6.93 and 7.19 ppm.

Scope and limitations: Reaction progress profiles

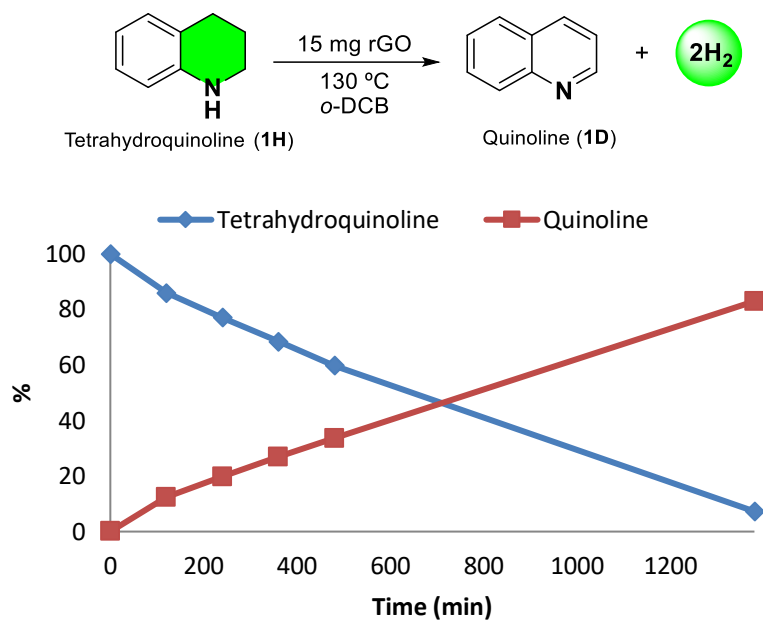


Figure S2.3 Reaction progress profile in the conversion of 1H to 1D.

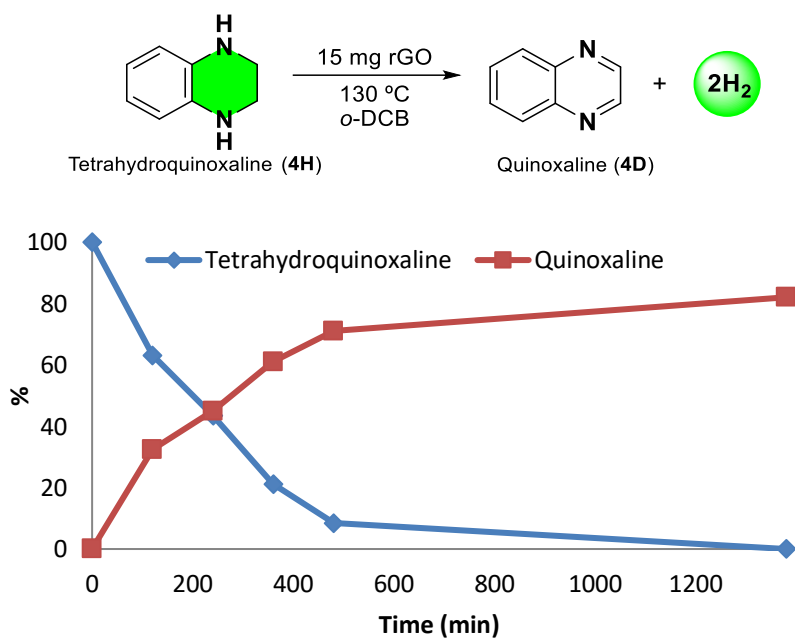


Figure S2.4 Reaction progress profile in the conversion of 4H to 4D.

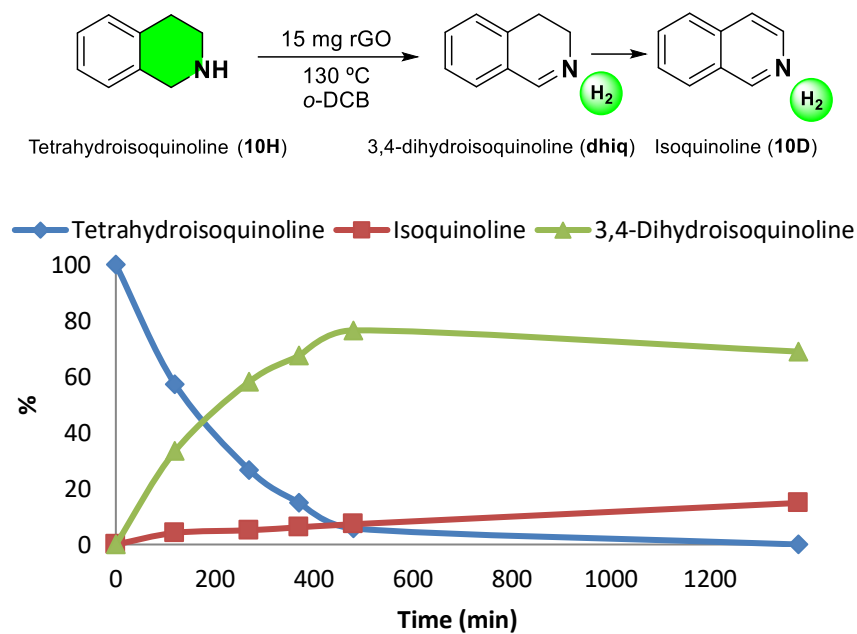


Figure S2.5 Reaction progress profile in the conversion of 10H to 10D and dhiq.

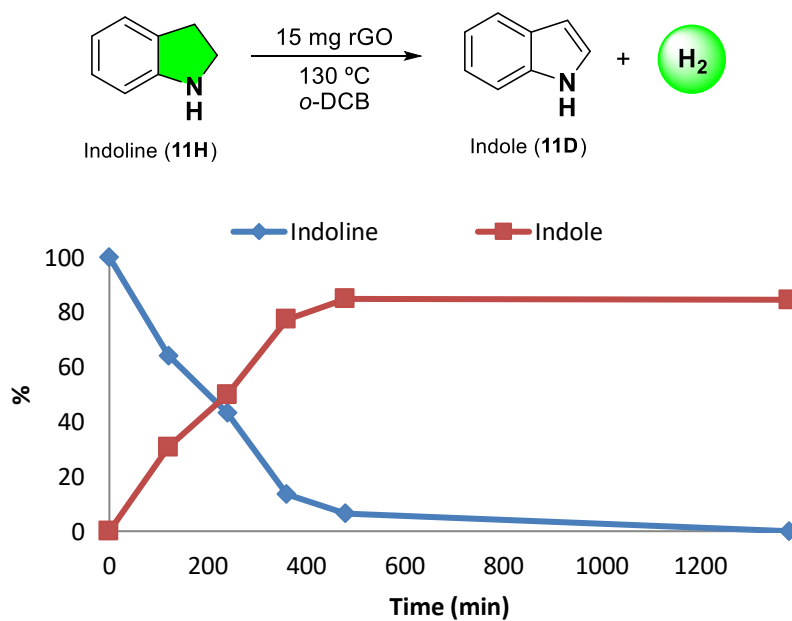
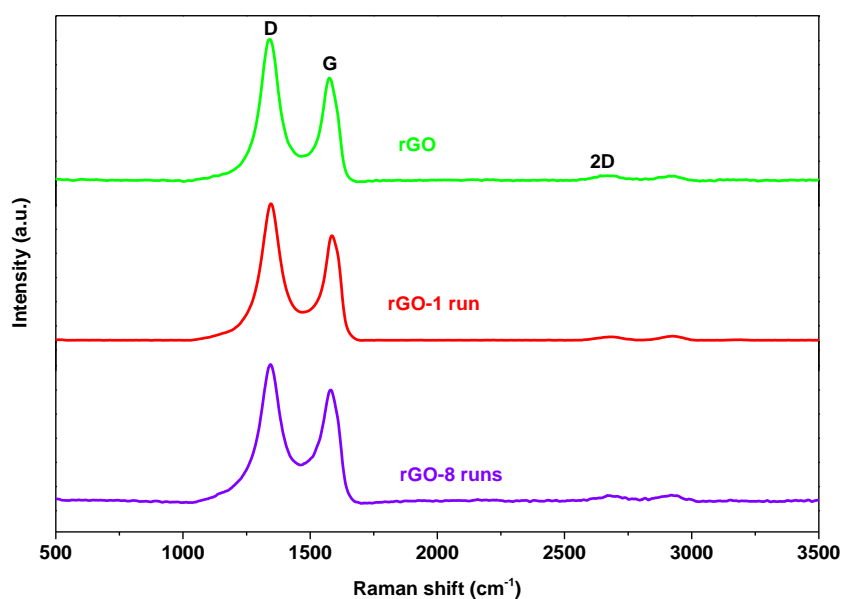


Figure S2.6 Reaction progress profile in the conversion of 11H to 11D.

Table S2.2 Comparison of the initial conversion rates in ADH of N-heterocycles for substrates included in table 2.

Entry	Substrate	Conversion rate (mmol g _{cat} ⁻¹ h ⁻¹)	Entry	Substrate	Conversion rate (mmol g _{cat} ⁻¹ h ⁻¹)
1	1H	1.086E-5	7	7H	1.920E-5
2	2H	4.172E-6	8	8H	2.559E-6
3	3H	1.673E-5	9	9H	-
4	4H	2.864E-5	10	10H	3.655E-5
5	5H	8.679E-6	11	11H	2.665E-5
6	6H	1.263E-5	12	12H	4.271E-5

Recycling experiment: Fresh and spent rGO characterization.**Figure S2.7** Raman spectra of rGO during the recycling experiment.

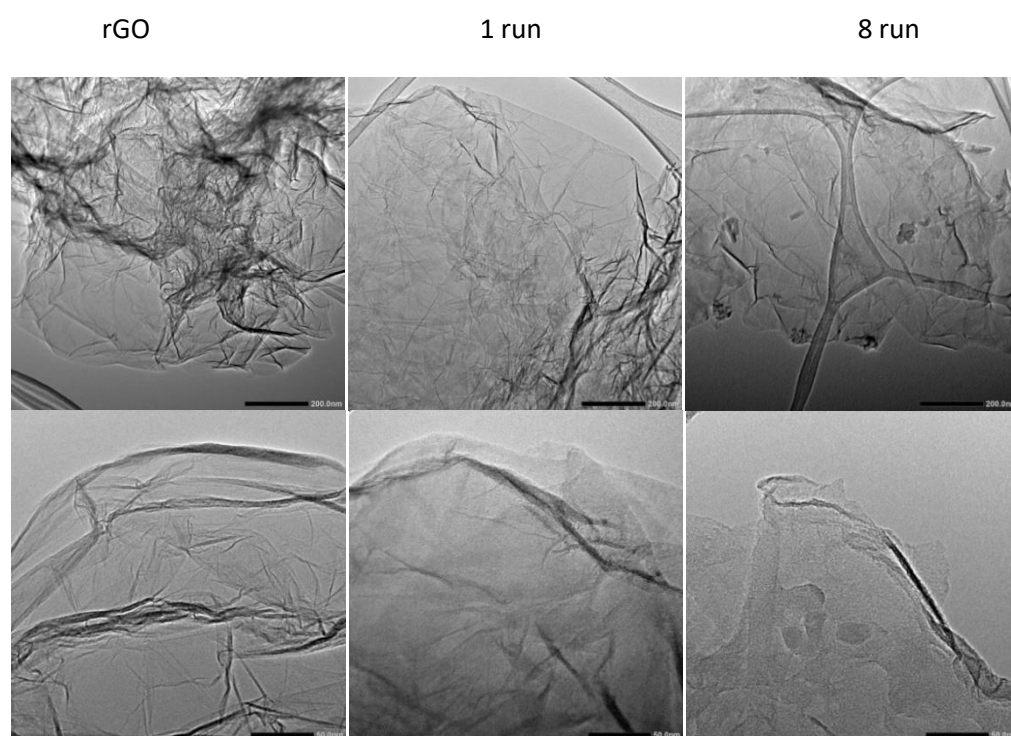


Figure S2.8 HRTEM images of rGO at different magnifications at selected runs.

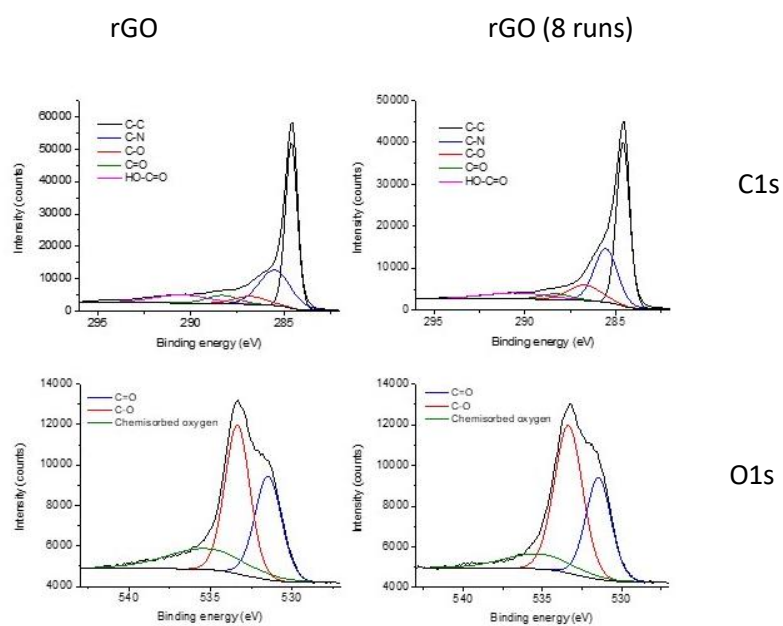


Figure S2.9 XPS analysis of fresh and 8 runs rGO. Binding energies of C1s and O1s.

Catalytic properties of graphene materials in dehydrogenation of N-heterocycles

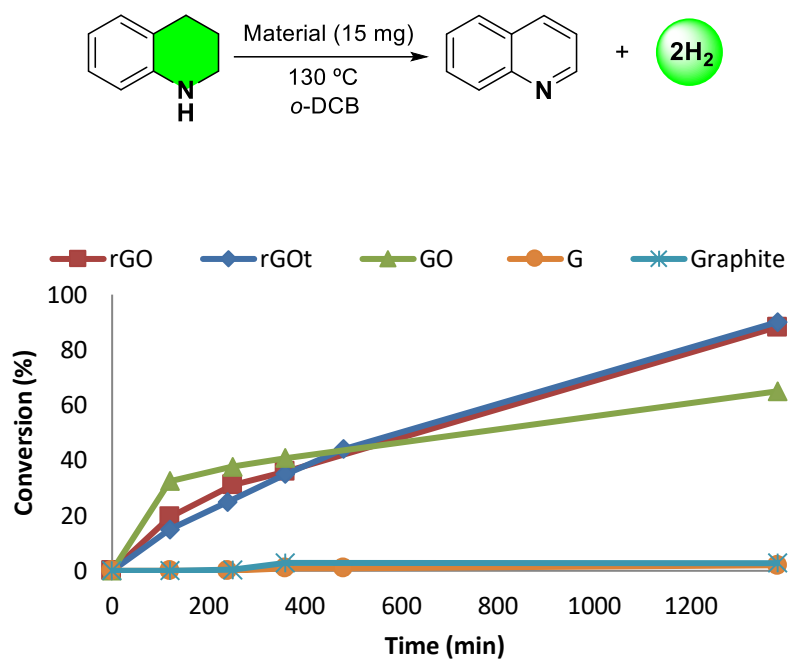


Figure S2.10 Reaction progress profile in dehydrogenation of tetrahydroquinoline (**1H**) to quinoline (**1D**) using different graphene-related materials.

Influence of metal ions in the catalytic properties of rGO

Table S2.3 ICP/MS analysis of iron and manganese in rGO

Catalyst	Mn (ppm)	Mn (wt%)	Fe (ppm)	Fe (wt%)
rGO	2400	0.2400	420	0.420

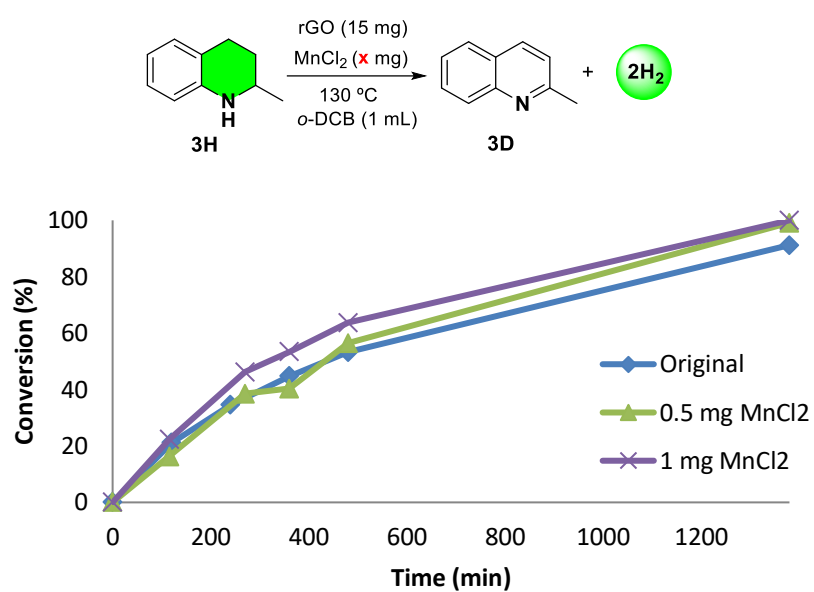


Figure S2.11 Reaction progress profile in dehydrogenation of **3H** into **3D** under standard conditions with the addition of different amounts of Mn²⁺.

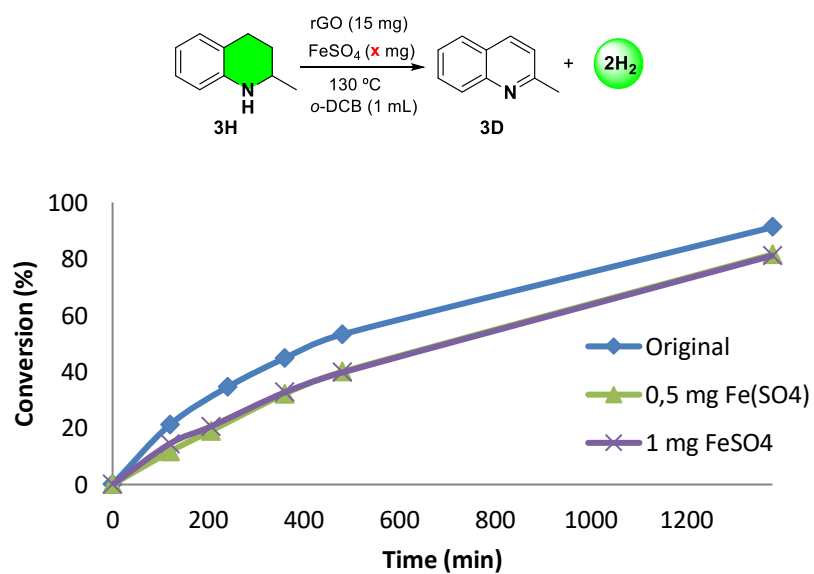


Figure S2.12 Reaction progress profile in dehydrogenation of **3H** into **3D** under standard conditions with the addition of different amounts of Fe²⁺.

Functional groups: Model molecules as carbocatalyst

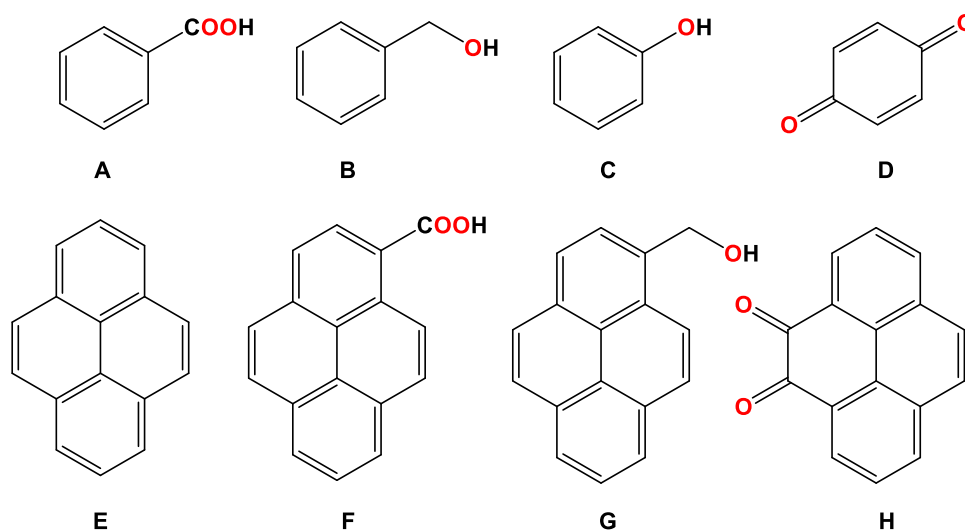
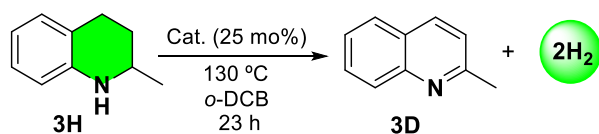


Figure S2.13 Model molecules used as carbocatalyst for dehydrogenation of N-heterocycles.

Table S2.4 Catalytic properties of model compounds in dehydrogenation of 2-methyltetrahydroquinoline (**3H**).

Entry	Cat.	Yield
1	-	<1
2	A	19
3	B	<1
4	C	9
5	D	8
6	E	<1
7	F	9
8	G	<1
9	H	34

Conditions: Anaerobic conditions using N_2 . 2-methyltetrahydroquinoline (0.15 mmol), o-dichlorobenzene (1 mL), $T=130\text{ }^\circ\text{C}$ and model molecule (25 mol%). Conversion and yield determined by GC/FID using trimethoxybenzene as an internal standard.

Masking experiments

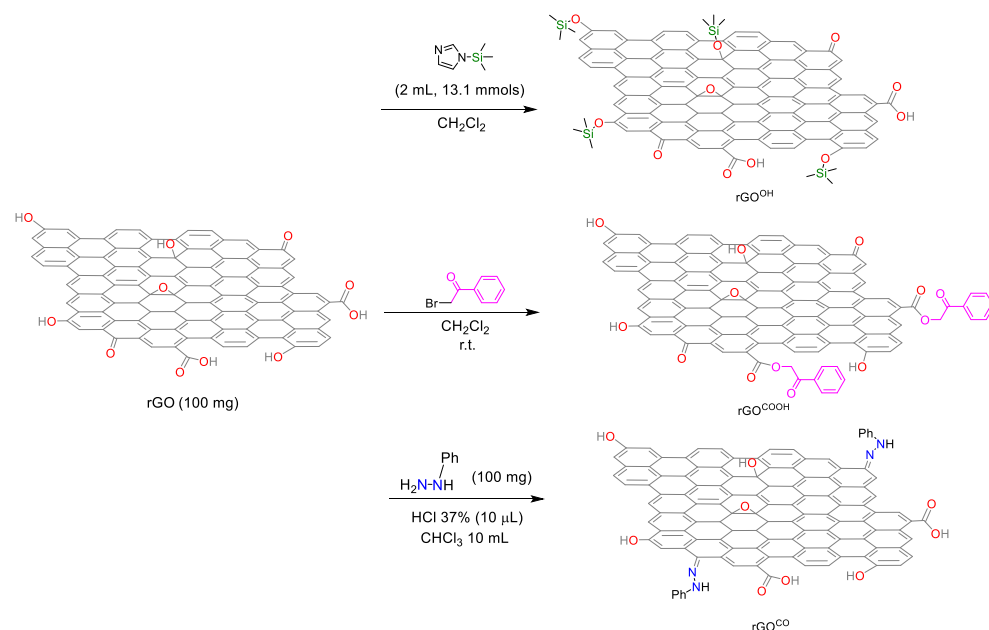


Figure S2.14 Synthesis of masked rGO derivatives.

Masking of phenol type groups (rGO^{OH})

rGO^{OH} was synthesized by adapting a previously described procedure.⁴⁶ rGO (100 mg) was dispersed in 10 mL of dry CH_2Cl_2 and in an ultrasonic bath for 30 min. Then 200 μ L of trimethylsilylimidazole (1.31 mmol) was added and the mixture was stirred under N_2 for 12 h at 60 $^\circ$ C. The suspension was filtered out and washed with CH_2Cl_2 , water and acetone giving a black solid.

Masking of carboxylic acid groups (rGO^{COOH})

rGO^{COOH} was synthesized adapting a procedure previously described.⁴⁵ 2-bromo-1-phenylethanone (200 mg, 1 mmol) and 100 mg rGO were mixed in 5 mL of dry CH_2Cl_2 and stirred at room temperature for 5 h under N_2 in the dark. The mixture was filtered out washed with CH_2Cl_2 , water and acetone to remove the physical adsorbed molecules of 2-bromo-1-phenylethanone, giving a black solid.

Masking of ketonic carbonyl groups (rGO^{CO})

rGO^{CO} was synthesized adapting a procedure previously described.⁴⁵ Phenylhydrazine (200 mg, 1.81 mmol) and 10 μ L HCl acid (37 %) were dissolved in 10 ml of dry CH_2Cl_2 . Then, 100 mg rGO was added to the solution and was stirred for 72h under N_2 . The mixture was filtered out, washed with CH_2Cl_2 , water and acetone to remove the physical adsorbed molecules of phenyl hydrazine, giving a black solid.

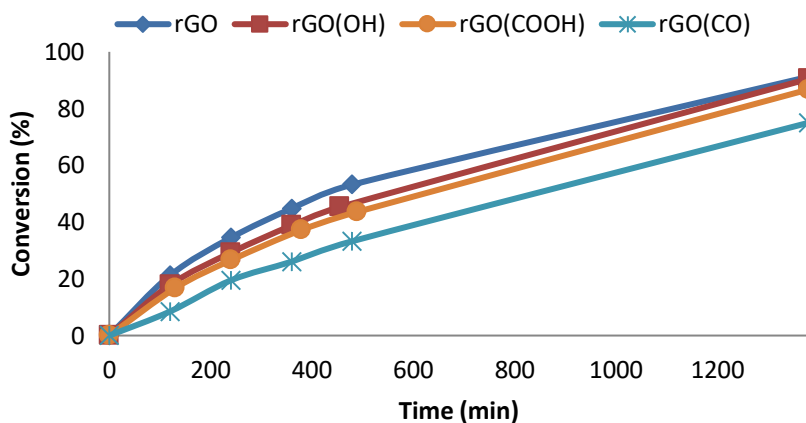
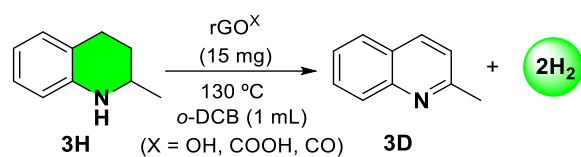


Figure S2.15 Reaction progress profile in dehydrogenation of **3H** into **3D** under standard conditions using masked rGO derivatives.

2.5 REFERENCES

- (1) Dalko, P. I.; Moisan, L. *Angew. Chem. Int. Ed.* **2004**, *43*, 5138–5175.
- (2) MacMillan, D. W. C. *Nature* **2008**, *455*, 304–308.
- (3) Su, D. S.; Wen, G.; Wu, S.; Peng, F.; Schlögl, R. *Angew. Chem. Int. Ed.* **2017**, *56*, 936–964.
- (4) Figueiredo, J. L.; Pereira, M. F. R. *Catal. Today* **2010**, *150*, 2–7.
- (5) Chua, C. K.; Pumera, M. *Chem. A Eur. J.* **2015**, *21*, 12550–12562.
- (6) Dreyer, D. R.; Bielawski, C. W. *Chem. Sci.* **2011**, *2*, 1233.
- (7) Titirici, M.-M.; White, R. J.; Brun, N.; Budarin, V. L.; Su, D. S.; del Monte, F.; Clark, J. H.; MacLachlan, M. J. *Chem. Soc. Rev.* **2015**, *44*, 250–290.
- (8) Espinosa, J. C.; Navalón, S.; Primo, A.; Moral, M.; Sanz, J. F.; Álvaro, M.; García, H. *Chem. A Eur. J.* **2015**, *21*, 11966–11971.
- (9) Navalon, S.; Dhakshinamoorthy, A.; Alvaro, M.; Antonietti, M.; García, H. *Chem. Soc. Rev.* **2017**, *46*, 4501–4529.
- (10) Lombardi, L.; Bandini, M. *Angew. Chem. Int. Ed.* **2020**, *59*, 20767–20778.
- (11) Navalon, S.; Dhakshinamoorthy, A.; Alvaro, M.; Garcia, H. *Chem. Rev.* **2014**, *114*, 6179–6212.
- (12) Su, C.; Loh, K. P. *Acc. Chem. Res.* **2013**, *46*, 2275–2285.
- (13) Axet, M. R.; Dechy-Cabaret, O.; Durand, J.; Gouygou, M.; Serp, P. *Coord. Chem. Rev.* **2016**, *308*, 236–345.
- (14) Dreyer, D. R.; Jia, H.-P.; Bielawski, C. W. *Angew. Chem. Int. Ed.* **2010**, *49*, 6813–6816.
- (15) Espinosa, J. C.; Navalón, S.; Álvaro, M.; García, H. *ChemCatChem* **2016**, *8*, 2642–2649
- (16) Machado, B. F.; Serp, P. *Catal. Sci. Technol.* **2012**, *2*, 54–75.

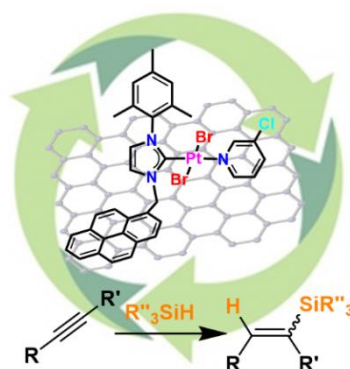
- (17) Gao, Y.; Ma, D.; Wang, C.; Guan, J.; Bao, X. *Chem. Commun.* **2011**, 47, 2432–2434.
- (18) Hu, H.; Xin, J. H.; Hu, H.; Wang, X. *Nano Res.* **2015**, 8, 3992–4006.
- (19) Acocella, M. R.; Mauro, M.; Falivene, L.; Cavallo, L.; Guerra, G. *ACS Catal.* **2014**, 4, 492–496.
- (20) Su, C.; Acik, M.; Takai, K.; Lu, J.; Hao, S. J.; Zheng, Y.; Wu, P.; Bao, Q.; Enoki, T.; Chabal, Y. J.; Loh, K. P. *Nat. Commun.* **2012**, 3, 1–9.
- (21) Preuster, P.; Papp, C.; Wasserscheid, P. *Acc. Chem. Res.* **2017**, 50, 74–85.
- (22) Crabtree, R. H. *Energy Environ. Sci.* **2008**, 1, 134–138.
- (23) Zheng, J.; Zhou, H.; Wang, C.-G.; Ye, E.; Xu, J. W.; Loh, X. J.; Li, Z. *Energy Storage Mater.* **2021**, 35, 695–722.
- (24) Crabtree, R. H. *ACS Sustain. Chem. Eng.* **2017**, 5, 4491–4498.
- (25) Clot, E.; Eisenstein, O.; Crabtree, R. H. *Chem. Commun.* **2007**, 22, 2231–2233.
- (26) Zhang, Y.; Wang, J.; Zhou, F.; Liu, J. *Catal. Sci. Technol.* **2021**, 11, 3990–4007.
- (27) Rao, P. C.; Yoon, M. *Energies* **2020**, 13, 6040.
- (28) Sinigaglia, T.; Lewiski, F.; Santos Martins, M. E.; Mairesse Siluk, J. C. *Int. J. Hydrogen Energy* **2017**, 42, 24597–24611.
- (29) Teichmann, D.; Arlt, W.; Wasserscheid, P. *Int. J. Hydrog. Energy* **2012**, 37, 18118–18132.
- (30) Zhang, J.; Su, D. S.; Blume, R.; Schlögl, R.; Wang, R.; Yang, X.; Gajović, A. *Angew. Chem. Int. Ed.* **2010**, 49, 8640–8644.
- (31) Liu, L.; Deng, Q.-F.; Liu, Y.-P.; Ren, T. Z.; Yuan, Z. Y. *Catal. Commun.* **2011**, 16, 81–85.
- (32) Liu, L.; Deng, Q.-F.; Agula, B.; Ren, T.Z.; Liu, Y.P.; Zhao-rigetü, B.; Yuan, Z.Y. *Catal. Today* **2012**, 186, 35–41.
- (33) Zhang, J.; Chen, S.; Chen, F.; Xu, W.; Deng, G.-J.; Gong, H. *Adv. Synth. Catal.* **2017**, 359, 2358–2363.

- (34) Hayashi, M. *System. Chem. Rec.* **2008**, *8*, 252–267.
- (35) Kawashita, Y.; Hayashi, M. *System. Molecules* **2009**, *14*, 3073–3093.
- (36) Enders, L.; Casadio, D. S.; Aikonen, S.; Lenarda, A.; Wirtanen, T.; Hu, T.; Hietala, S.; Ribeiro, L. S.; Pereira, M. F. R.; Helaja, J. *Catal. Sci. Technol.* **2021**, *11*, 5962–5972.
- (37) Pereira, M. F. R.; Órfão, J. J. M.; Figueiredo, J. L. *Appl. Catal. A Gen.* **1999**, *184*, 153–160.
- (38) Presolski, S.; Pumera, M. *Angew. Chemie Int. Ed.* **2018**, *57*, 16713–16715.
- (39) Navalón, S.; Herance, J. R.; Álvaro, M.; García, H. *Mater. Horiz.* **2018**, *5*, 363–378.
- (40) Ambrosi, A.; Chee, S. Y.; Khezri, B.; Webster, R. D.; Sofer, Z.; Pumera, M. *Angew. Chem. Int. Ed.* **2012**, *51*, 500–503.
- (41) Wang, L.; Ambrosi, A.; Pumera, M. *Angew. Chem. Int. Ed.* **2013**, *52*, 13818–13821.
- (42) Ambrosi, A.; Chua, C. K.; Khezri, B.; Sofer, Z.; Webster, R. D.; Pumera, M. *Proc. Natl. Acad. Sci.* **2012**, *109*, 12899–12904.
- (43) Wu, S.; Wen, G.; Liu, X.; Zhong, B.; Su, D. S. *ChemCatChem* **2014**, *6*, 1558–1561.
- (44) Zhang, J.; Wang, X.; Su, Q.; Zhi, L.; Thomas, A.; Feng, X.; Su, D. S.; Schlögl, R.; Müllen, K. *J. Am. Chem. Soc.* **2009**, *131*, 11296–11297.
- (45) Qi, W.; Liu, W.; Zhang, B.; Gu, X.; Guo, X.; Su, D. *Angew. Chemie Int. Ed.* **2013**, *52*, 14224–14228.
- (46) Sánchez-Page, B.; Jiménez, M. V.; Pérez-Torrente, J. J.; Passarelli, V.; Blasco, J.; Subias, G.; Granda, M.; Álvarez, P. *ACS Appl. Nano Mater.* **2020**, *3*, 1640–1655.
- (47) Espinosa, J. C.; Navalón, S.; Álvaro, M.; García, H. *ChemCatChem* **2016**, *8*, 2642–2648.

- (48) Wang, Y.; Xie, Y.; Sun, H.; Xiao, J.; Cao, H.; Wang, S. *ACS Appl. Mater. Interfaces* **2016**, *8*, 9710–9720.
- (49) Wendlandt, A. E.; Stahl, S. S. *J. Am. Chem. Soc.* 2014, *136* (34), 11910–11913.
- (50) Hummers, W. S.; Offeman, R. E. *J. Am. Chem. Soc.* **1958**, *80*, 1339.
- (51) Espinosa, J. C.; Álvaro, M.; Dhakshinamoorthy, A.; Navalón, S.; García, H. *ACS Sustain. Chem. Eng.* **2019**, *7* (19), 15948–15956.
- (52) Trandafir, M.-M.; Florea, M.; Neațu, F.; Primo, A.; Parvulescu, V. I.; García, H. *ChemSusChem* **2016**, *9* (13), 1565–1569.

CHAPTER 3:

A Platinum molecular complex immobilised on the surface of graphene as active catalyst in alkyne hydrosilylation



ABSTRACT

A platinum complex bearing a N-heterocyclic carbene (NHC) ligand functionalised with a pyrene-tag is immobilised onto the surface of reduced graphene oxide (rGO). The hybrid material composed of an organometallic complex and a graphene derivative is readily available in a single-step process under mild reaction conditions. This methodology preserves the inherent properties of the active catalytic centre and the support. The platinum hybrid material is an efficient catalyst in hydrosilylation of alkynes and can be recycled and reused without significant loss of activity due to its high stability. Interestingly, the catalytic activity of the platinum complex is not affected by diffusion problems after immobilisation. The influence of graphene in hydrosilylation of alkynes is discussed in terms of activity and selectivity.

3.1 INTRODUCTION

Hydrosilylation of alkynes represents a direct approach for the synthesis of carbon-silicon bonds.¹⁻⁴ These compounds are useful industrial intermediates for the production of fine chemicals, silicones, lubricants, coatings and fine chemicals.^{5,6} Among all the active metals in hydrosilylation reactions, platinum stands out in terms of activity and selectivity. As example, highly active Karstedt⁷ and Speier⁸ catalysts are present in several industrial processes (Figure 3.1). However, they bear limited stability against oxygen and moisture under catalytic conditions forming platinum species that can taint the products. To circumvent this problem, Markó *et al*, introduced a series of N-heterocyclic carbene ligand (NHC) based platinum complexes (Figure 3.1).⁹⁻¹² These homogeneous catalysts have shown remarkable efficiency and selectivity in the hydrosilylation of alkynes under aerobic conditions, but they cannot be easily isolated and used in multiple runs.¹³⁻¹⁸ Hence, seeking new effective alternatives for catalysts endurance is highly encouraging. In this context, immobilisation of molecular metal complexes onto supports enables the development of hybrid materials with specific and controllable properties relevant for ulterior catalytic applications.¹⁹⁻²² Metal complexes can be anchored onto supports by means of strong covalent bonds to avoid leaching during the catalytic reactions. This immobilisation process normally requires several synthetic steps and lacks of complete control in the way the metal sites are tethered to supports.²³⁻²⁵ Some of them have recently been applied for the hydrosilylation of terminal alkynes.²⁶⁻²⁸ On the contrary, the use of non-covalent interaction for the immobilisation of well-defined complexes onto graphene allows the preparation of hybrid materials in a single step with controllable metal positions at specific sites.²⁹⁻³² This approach is complementary to homogeneous systems, since allows the easy recovery of the catalysts, and at the same time provides mechanistic information regarding catalysts resting state. In addition, the immobilisation of metal complexes facilitates the precise control of the catalytic active sites.³³⁻³⁵ Based on our experience on the preparation of different supported catalysts, we envisioned that the incorporation of a molecular platinum catalyst onto the surface of graphene could result beneficial for the hydrosilylation reaction of alkynes by: i) decreasing the kinetics of the deactivation pathways, ii) hampering the interaction with external agents and iii) increasing the catalyst activity by facilitating the interactions between the catalyst and the substrates.

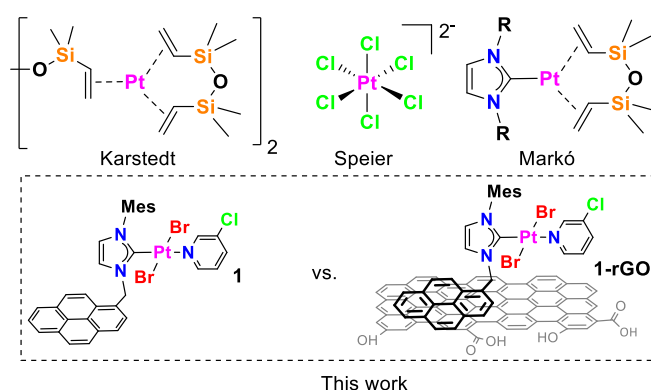
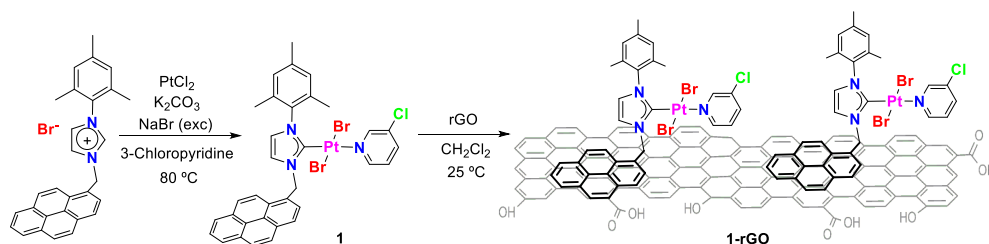


Figure 3.1 Active platinum catalytic systems for hydrosilylation.

Herein, in this chapter, we describe a contrastive study of the structural and catalytic properties of a molecular platinum type PEPPSI complex **1** (PEPPSI = pyridine-enhanced precatalyst preparation, stabilisation and initiation) and its related derivative immobilised onto the surface of reduced graphene oxide (rGO) by non-covalent interactions **1-rGO** (Figure 3.1). The hybrid catalytic material is obtained in a single step starting from an organometallic complex and the carbonaceous material.



Scheme 3.1 Synthesis of the platinum complex **1** and the hybrid material **1-rGO**.

The catalytic performance of both, molecular system and the hybrid material were evaluated towards the hydrosilylation reaction of alkynes. Metal complex **1** is a competent catalyst towards terminal and internal alkynes displaying moderate regioselectivity, having a preferential inclination for β versus the α isomer. In parallel, the catalytic activity of **1** was matched by the hybrid material **1-rGO**, which displayed a greater stability but present the advantage that can be recycled and reused for up to ten runs without significant loss of activity.

3.2 RESULTS AND DISCUSSION

Synthesis and characterization of 1 and 1-rGO

The platinum molecular complex **1** and the related hybrid material **1-rGO** immobilized onto graphene were synthesised as described in Scheme 3.1. The aim of this study is the evaluation of the catalytic properties in hydrosilylation from a homogeneous and heterogeneous approach. Initially, molecular Pt-NHC complex **1** was prepared by applying the same methodology described for the palladium PEPPSI type complexes.³⁶⁻³⁸ Imidazolium salt functionalised with a pyrene polyaromatic tag³⁹ used as ligand precursor was treated with PtCl₂, 3-chloropyridine, K₂CO₃ as base and excess of NaBr to avoid halide scrambling. Complex **1** was isolated in 70% yield and fully characterised by NMR spectroscopy, ESI-MS spectrometry, elemental analysis and thermogravimetric analysis (Figure S3.1). The complete characterisation at the molecular level facilitates the monitoring of the changes that the complex undergoes during the immobilisation process and the catalytic experiments. Coordination of the NHC ligand to platinum is confirmed by the disappearance of the acidic signal of the imidazolium salt in the ¹H NMR spectra at 9.36 ppm. ¹³C NMR spectra showed the characteristic signal for Pt–C_{carbene} at 148.3 ppm although the satellites corresponding to the coupling with ¹⁹⁵Pt could not be observed due to their low intensity. Positive ion ESI mass spectrum analysis (ESI-MS) in acetonitrile of complex **1** shows a base peak for [M – Br + CH₃CN]⁺ at *m/z* = 830.3 and a less intense peak for [M – Br – (3-Cl-Pyridine) + 2CH₃CN]⁺ at *m/z* = 757.3. The presence of these fragments confirms the proposed molecular composition of complex **1** based on the mass/charge relation and the isotopic pattern. In addition, it reveals the lability of the 3-chloropyridine ligand, as expected for PEPPSI-type complexes. Metal–halide bond-breaking is a common ionisation mechanism for neutral complexes under ESI conditions and L-type ligands correlate with ease metal-ligand substitution. The molecular structure of complex **1** was confirmed by single-crystal X-ray diffraction.⁴⁰ The structure analysis reveals a platinum centre with two trans bromides, a 3-chloropyridine and the NHC ligand in square-planar coordination environment (Figure 3.2).

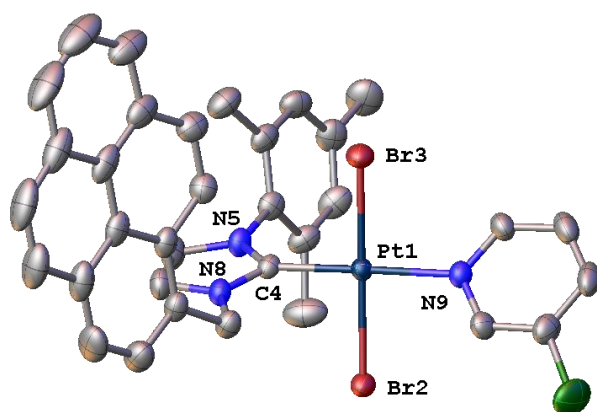


Figure 3.2 Molecular structure of compound **1**. Ellipsoids are at 50% probability level. Hydrogen atoms and crystallisation solvent (dichloromethane) have been omitted for clarity. Selected bond lengths [Å] and angles [°]: Pt(1) - C(4) 1.962(3), Pt(1) - Br(2) 2.4266(3), Pt(1) - Br(3) 2.4173(4), Pt(1) - N(9) 2.097(3), Br(2) - Pt(1) - Br(3) 176.945(13), N(9) - Pt(1) - C(4) 178.55(12), N(9) - Pt(1) - Br(2) 89.76(8), C(4) - Pt(1) - Br(2) 89.37(9).

The hybrid organometallic-graphene material **1-rGO** was obtained by applying an immobilisation methodology previously reported by our research group.^{30,41,42} It is based in the establishment of non-covalent π -type interactions between the polyaromatic pyrene tag and the **rGO**. The tethering of the molecular complex involves mixing complex **1** with reduced graphene oxide (**rGO**) in dichloromethane at room temperature, followed by 30 minutes sonication in a water bath. Finally, the mixture is stirred at room temperature for 24 h. The exact platinum content on the hybrid material **1-rGO** was determined by digestion of the samples in hot mixture of HCl/HNO₃ followed by ICP-MS analysis. The results obtained by ICP-MS analysis accounted for 4.6 wt% of **1** in the hybrid material **1-rGO**.

The characterisation of the platinum hybrid material **1-rGO** was performed using High Resolution Transmission Microscopy (HRTEM) and X-ray Photoelectron Spectroscopy (XPS). HRTEM images of **1-rGO** at different magnifications (Figure 3.3 a, b) show the characteristic 2D morphology of graphene and the absence of metal nanoparticles. Elemental mapping by Energy-Dispersive X-ray Spectroscopic analysis (EDX) of **1-rGO** (Figure 3.3 c) confirms the elemental composition of the molecular complex **1** (Pt, N, Br and Cl) and the homogeneous distribution of platinum in the hybrid materials (Fig. 3.3d). In parallel to this, the surface of hybrid material **1-rGO**,

was characterised and analysed by means of XPS. This technique provides relevant information related to the elemental composition and oxidation states. In our case, a comparative analysis of complex **1** and hybrid material **1-rGO** facilitates the interpretation of the results. A survey XPS analysis of **1** shows the presence of platinum, nitrogen, bromide and chloride (Figure 3.4). As expected for the molecular complex **1**, the two peaks of Pt4f confirm the +2 oxidation state at binding energies of 72.7 and 76.0 eV.⁴³ A high-resolution XPS analysis of **1** and **1-rGO** shows the characteristic core-level peaks of Pt 4f, Br 3d, N 1s and Cl 2p at the same binding energies for the molecular complex and the hybrid material (Figure 3.4). These results confirm the tethering of the molecular complex **1** onto the surface of graphene. The nature of the complex is not altered during the harness process. Additionally, we have evidence of the exact nature and composition of the platinum species deposited onto the graphene surface.

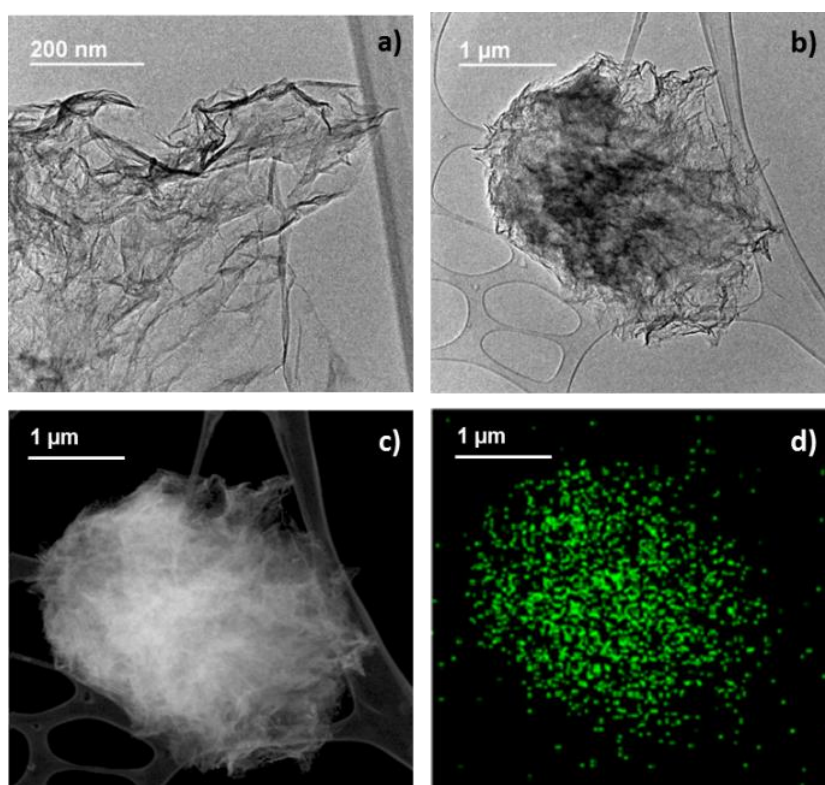


Figure 3.3 HRTEM images of **1-rGO** at different magnifications (a, b). STEM images (c) and EDS elemental mapping (d) images showing the homogeneous distribution of platinum on the hybrid material **1-rGO**.

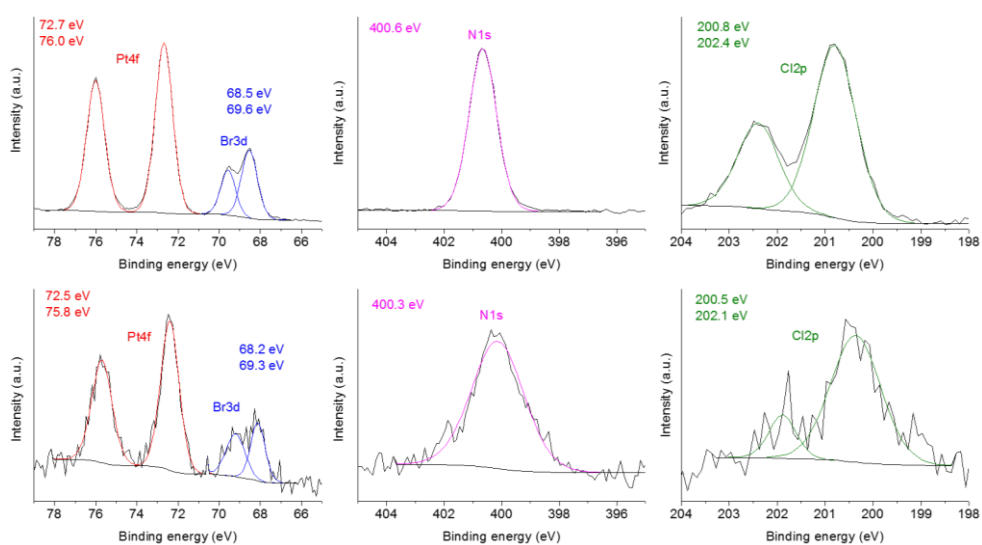
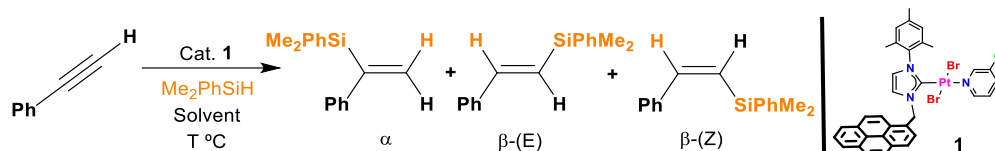


Figure 3.4 XPS analysis of the core-level peaks Pt4f, Br3d N1s and Cl2p for complex **1** (top) and hybrid material **1-rGO** (bottom).

Catalytic applications

The catalytic properties of the molecular platinum complex **1** and the hybrid material **1-rGO** were studied in the hydrosilylation reaction of internal and terminal alkynes. Optimisation of reaction conditions was carried out using phenyl acetylene and dimethylphenylsilane as model substrates (Table 3. 1).

Table 3.1 Optimization of reaction conditions for the hydrosilylation of phenyl acetylene



Entry	Cat mol%	Solvent	T (°C)	Time (h)	Conv (%) ^a	Sel ^a (α/β)
1	-	Toluene	50	3	0	-
2	-	Toluene	80	3	0	-
3	1	Toluene	30	3	0	-
4	1	Toluene	50	3	0	-
5	1	Toluene	65	3	5	30/70
6	1	Toluene	80	3	40	33/67
7	1	Toluene	90	3	76	32/68
8	1 ^b	Toluene	80	3	29	33/67
9	0.5	Toluene	80	3	34	32/68
10	0.5	Toluene	80	6.5	69	35/65
11	0.5	Toluene	80	24	≥99	32/68
12	0.5	Acetonitrile	80	3	8	40/60
13	0.5	1,4-Dioxane	80	3	74	41/59
14	0.5	1,2-Dichloroethane	80	3	10	40/60

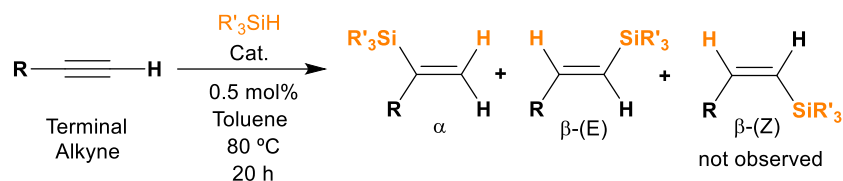
Conditions: 0.3 mmol of alkyne, 0.31 mmol of silane and 0.3 mmol of anisole used as internal standard. Aerobic conditions. [a] conversion of alkyne and selectivity determined by GC analyses. [b] KPF₆ (3 mol%) was used as additive.

Control experiments at two different temperatures 50 and 80 °C respectively were carried out to confirm that the metal complex is required in the hydrosilylation reaction. No conversion was observed when the reaction was performed in the absence of the platinum catalyst **1** (Table 3.1, entry 1, 2). Then, we evaluated the activity of the catalyst varying the temperature (Table 3.1, entries 3 - 7). Using 1 mol% of catalyst, the reaction does not occur below 50 °C and it is very slow at 65 °C (3h, 5% yield). Increasing the temperature to 80 – 90 °C affords moderate to good conversions after 3h. According to these results, the lowest temperature to study

the hydrosilylation reaction under reasonable experimental conditions was 80 °C. The addition of a halide abstractor (KPF₆) did not improve the catalytic outcomes (Table 3.1, entry 8). Reduction of catalyst loading to 0.5 mol% allows to monitor the reaction into a reasonable time-scale of 24h (Table 3.1, entries 9 - 11). The influence of catalyst loading in hydrosilylation is described using reaction progress profiles in the supporting information (Figure S3.3). We evaluated the solvent influence and observed that hydrosilylation also took place with solvents other than toluene such as Acetonitrile, 1,4-dioxane and 1,2-dichloroethane (Table 3.1, entries 12 - 14). It is worth mentioning that although higher activity was observed when using 1,4-dioxane, lower selectivity was obtained (Entry 13). The influence of the presence of air or moisture was assessed. However, no significant catalytic difference in the presence of air was observed, suggesting a relative high stability of catalysts precursor and intermediates versus oxygen and moisture. The optimal results in terms of activity and selectivity for the study of hydrosilylation reaction were obtained using a catalyst loading of 0.5 mol%, toluene as solvent at 80 °C under aerobic conditions.

Next, we studied the scope and limitations in hydrosilylation of different terminal and internal alkynes under these reaction conditions. We first explored the hydrosilylation of aryl (Table 3.2, entry 1-5) and alkyl terminal alkynes (Table 3.2, entry 6-14) using complex **1** and the hybrid material **1-rGO**. Both catalytic systems are competent in the hydrosilylation of alkynes affording quantitative yields after 20 h reaction. Preliminary comparison experiments of **1** vs. **1-rGO** for different substrates reveal that the catalytic activity is maintained or slightly improved (Vide infra). We have observed that substrate scope is preserved after immobilization (Table 3.2, entries 2, 7, 10, 13). Improvement of α/β regioselectivity is a difficult task in hydrosilylation. In our case, we have observed that the average regioselectivity is 40/60 for the α/β -addition products (Table 3.2) and that is maintained after catalysts immobilization. The best results were obtained in the case of 1-hexyne displaying a regioselectivity ratio of 25/75 for the α/β -addition products using catalysts **1-rGO** (Table 3.2, entry 10). Interestingly a very high stereoselectivity towards the β (E) versus the β (Z)-addition product was observed. In fact, no formation of β (Z)-isomer was detected in any case.

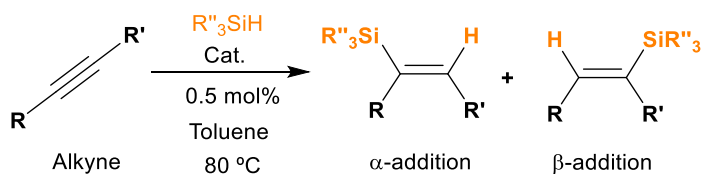
Table 3.2 Hydrosilylation of terminal alkynes



Entry	R	R' ₃ SiH	Cat	Yields (%)	Sel.(%) ^a α/β(E)/β(Z)
1	Ph	Me ₂ PhSiH	1	91	35/65/0
2	Ph	Me ₂ PhSiH	1-rGO	96	43/57/0
3	Ph	Et ₃ SiH	1	94	65/35/0
4	p-tolyl	Me ₂ PhSiH	1	80	30/70/0
5	p-tolyl	Et ₃ SiH	1	92	65/35/0
6	Benzyl	Me ₂ PhSiH	1	≥99	40/60/0
7	Benzyl	Me ₂ PhSiH	1-rGO	≥99	32/68/0
8	Benzyl	Et ₃ SiH	1	93	42/58/0
9	n-Hex	Me ₂ PhSiH	1	94	30/70/0
10	n-Hex	Me ₂ PhSiH	1-rGO	94	25/75/0
11	n-Hex	Et ₃ SiH	1	≥99	38/62/0
12	(CH ₂) ₃ CN	Me ₂ PhSiH	1	82	37/63/0
13	(CH ₂) ₃ CN	Me ₂ PhSiH	1-rGO	90	39/61/0
14	(CH ₂) ₃ CN	Et ₃ SiH	1	87	35/65/0

Reaction conditions: 0.3 mmol of alkyne, 0.31 mmol of silane, 0.5 mol% of catalyst (based on Pt), T = 80 °C, 20h and 1 mL of toluene. Aerobic conditions. [a] Yields were determined with GC using anisole as a standard and selectivity by ¹H NMR.

Then, we studied the performance of complex **1** and the hybrid material **1-rGO** in hydrosilylation of a variety of internal alkynes using different silanes (Table 3.3), resulting an efficient catalyst. Yields over 90% were obtained for internal alkynes in ca. 3 h, much faster than the previously observed for the terminal alkynes. The regioselectivity for non-symmetric internal alkynes favours the addition of the silyl group at the C atom bound next to the phenyl group (defined as the α-addition product). We have observed that the regioselectivity is controlled by sterics imposed by the alkyne rather than the nature of the silane. For instance, the hydrosilylation of the small ethyl phenyl acetylene gave moderate selectivities (Table 3, entries 1 – 2). In contrast, when using a more steric demanding trimethylsilane phenyl acetylene the regioselectivity was 100% and only the α isomer was observed (Table 3, entries 5 – 7). These results suggest that steric factors of the internal alkyne dominate the selectivity of the reaction.

Table 3.3 Hydrosilylation of internal alkynes

Entry	R	R'	R'' ₃ SiH	Cat	t (h)	Yields (%)	Sel.(%) ^a (α/β)
1	Ph	Et	Me ₂ PhSiH	1	2.5	99	82/18
2	Ph	Et	Et ₃ SiH	1	4	≥99	81/19
3	Ph	nPr	Me ₂ PhSiH	1	2	93	84/16
4	Ph	nPr	Et ₃ SiH	1	3	≥99	79/21
5	Ph	(CH ₃) ₃ Si	Me ₂ PhSiH	1	2.5	86	100/0
6	Ph	(CH ₃) ₃ Si	Me ₂ PhSiH	1-rGO	2.5	87	100/0
7	Ph	(CH ₃) ₃ Si	Et ₃ SiH	1	6	96	100/0
8	Ph	Ph	Me ₂ PhSiH	1	1	≥99	- ^b
9	Ph	Ph	Et ₃ SiH	1	6	92	- ^b
10	nPr	nPr	Me ₂ PhSiH	1	1.5	≥99	- ^b
11	nPr	nPr	Me ₂ PhSiH	1-rGO	1.5	≥99	- ^b
12	nPr	nPr	Et ₃ SiH	1	3.5	95	- ^b
13	MeO(CH ₂) ₂	MeO(CH ₂) ₂	Me ₂ PhSiH	1	4	92	- ^b
14	MeO(CH ₂) ₂	MeO(CH ₂) ₂	Me ₂ PhSiH	1-rGO	3	95	- ^b
15	MeO(CH ₂) ₂	MeO(CH ₂) ₂	Et ₃ SiH	1	6	98	- ^b

Regioselectivity (α/β) vs. the Ph group except for symmetric alkynes. E/Z isomerism not determined. Reaction conditions: 0.3 mmol of alkyne, 0.31 mmol of silane, 0.5 mol% of catalyst, T = 80 °C and 1 mL of toluene. Aerobic conditions. [a] Yields were determined with GC using anisole as a standard and selectivity by ¹H NMR. [b] Only one regioisomer is possible.

Next, different competition experiments were carried out to explore the selectivity of alkyne hydrosilylation in the presence of other substrates bearing different functional groups such as alkenes, aldehydes, and nitriles (Figure S3.4 – S3.6). It was found that the platinum catalyst **1** produced the hydrosilylation of alkynes without altering any of the other substrates bearing aldehydes, alkenes or nitriles. It is important to note that the kinetics of hydrosilylation are strongly affected by the presence of other functionalities and in particular the induction time is completely different. The results suggest that complex **1** is a competent catalyst in the hydrosilylation of alkynes also in the presence of other functional groups.

We assessed the effect of catalyst loading in the hydrosilylation of 1-phenyl-1-butyne with dimethylphenylsilane using **1** (Figure S3.3). The reaction progress profiles showed that quantitative yields are obtained for catalyst loadings between 2 – 0.01 mol%. These experiments reveal that the induction time is dependent of the catalyst loading. The maximum catalyst turnover number (TON) of 9.3×10^3 was obtained at 0.01 mol% loading after 24h. The best catalyst turnover frequency (TOF) at 50% conversion reached a remarkable 380 h^{-1} and was achieved when using a catalyst loading of 0.01 mol%. These results reveal that **1** is a robust and stable catalyst. To analyse the nature of the catalytic active species we performed poisoning experiments (ESI). We used poly(4-vinylpyridine) (PVP)⁴⁴ as an scavenger of Pt(II) molecular species and Hg (Mercury test)⁴⁵ as an scavenger of Pt nanoparticles.⁴⁶ The addition of Hg increases the time of the induction period from 50 to ca. 100 min (Compare Figure S3.2 vs S3.7). The results reveal that the addition of mercury had no effect in hydrosilylation but the addition of PVP completely inhibits the reaction (Figure S3.7). The poisoning experiments suggest that the catalytic active species are homogeneous in nature.

Once we studied the reaction scope and limitations of complex **1** and the hybrid material **1-rGO**, we explored the catalytic properties of both systems by means of reaction progress profiles in the hydrosilylation of phenyl acetylene (Figure 3.5). These experiments provide valuable information of apparent reaction rates, induction time and influence of the support in the catalytic reaction. Both reactions were carried out under the exact conditions and using the same catalyst loading (0.5 mol%). The reaction progress profiles reveal that the supported catalyst is more active than the molecular version in terms of reaction rates (TOF) and product formation (TON). For instance, the yield is ca. 80% for the hybrid material **1-rGO** and 56% for the molecular complex **1** after 5h. Importantly, immobilization of **1** onto graphene aided to reduce the induction period significantly as shown in the reaction profile (Figure 3.5). These results indicate that the activity of catalyst **1** is not affected by diffusion problems when supported onto graphene. In general, diffusion problems are especially important when using supported catalysts onto porous materials. The 2D structure of graphene avoids or at least limits the problems related to diffusion issues. We have observed that this process is general, and it has been experienced for other catalytic systems using graphene as support.⁴⁷⁻⁵³ The catalytic activity of the molecular platinum complex improves when supported onto graphene.

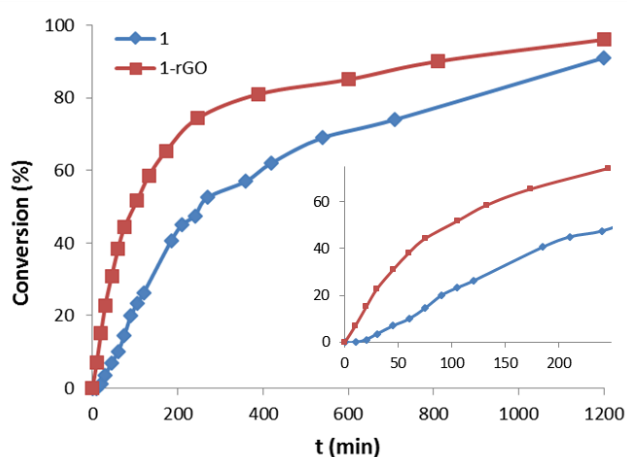


Figure 3.5 Reaction progress profile in the hydrosilylation of phenylacetylene using catalysts **1** and **1-rGO**. Reaction conditions: 0.3 mmol of phenylacetylene, 0.31 mmol of PhMe_2SiH , 0.5 mol% of catalyst (based on Pt), $T = 80^\circ\text{C}$ and 1 mL of toluene. Conversion by GC analysis using anisole as a standard.

A common problem generally encountered in supported catalysis is the release of the catalytic active species into the solution during the reaction, known as the “boomerang effect”.^{54,55} In order to evaluate the mechanism of action in the immobilisation of molecular species onto graphene we performed hot filtration experiments.⁵⁶ We used catalyst **1-rGO** (0.5 mol%) in the hydrosilylation of phenylacetylene and dimethylphenylsilane as a model reaction. After 2 h reaction (GC conversion 54%), half of the reaction mixture was separated by filtration at 80°C . The GC analysis after 15 h indicates a slight increment for the filtrate vs. quantitative conversion in the case of the supported catalysts **1-rGO**. Preliminary results in the hot filtration test support the absence of catalytic species in solution due to the release of the molecular complex from the surface of graphene. These results suggest that the catalytic process is heterogeneous in nature and take place at the surface of graphene.

Recyclability study

In view of the good results of complex **1** in the hydrosilylation of alkynes, we decided to test the recyclability properties of the hybrid material **1-rGO** to determine the influence of the support.⁵⁷ Recycling experiments were carried out using phenylacetylene and dimethylphenylsilane as the model substrates. The reactions were performed using the conditions described in the general procedure (Table 3.1), the reaction progress was monitored by GC and the selectivity by ¹H NMR. After each run, the mixture was cooled down to room temperature. The solid catalyst was isolated by decantation, washed thoroughly with toluene (3 x 5 mL) and used again in another run. The reaction progress profiles allow comparing the apparent reaction rates is a direct method to observe catalyst deactivation. The hydrosilylation of phenylacetylene with dimethylphenylsilane was monitored for ten runs. The reaction progress profiles reveal that the hybrid material **1-rGO** was reused up to ten times (Figure 3.6a). The reaction progress profiles overlapped for seven runs within the experimental error (<10%). Run 6 should be considered as an outlier because the catalyst activity is even lower than for runs 7, 8 and 9 (Figure 3.6a, green line with triangles). This artefact is most probably due to an experimental error in the GC measurement. In order to evaluate the mechanism of the deactivation process, the platinum content in the solution of each run was analysed by ICP-MS. The results reveal that the platinum content in the solutions corresponding to runs 1 – 10 is very low. These results suggest that deactivation of the hybrid material **1-rGO** is produced by catalyst manipulation during the recycling experiments. It is important to note that we have not observed a sharp catalyst deactivation. In addition, the selectivity of hydrosilylation is not affected in the recycling experiments (Figure 3.6b). The α : β addition product ratio is maintained ca. 40:60 (at 5h reaction) during all runs. Interestingly, the β -(Z) product is not observed in any run. These results suggest that the nature of the catalytic active species is preserved from batch to batch. We believe that these results are excellent in terms of recycling especially if we consider the catalyst loading used of 0.5 mol%.

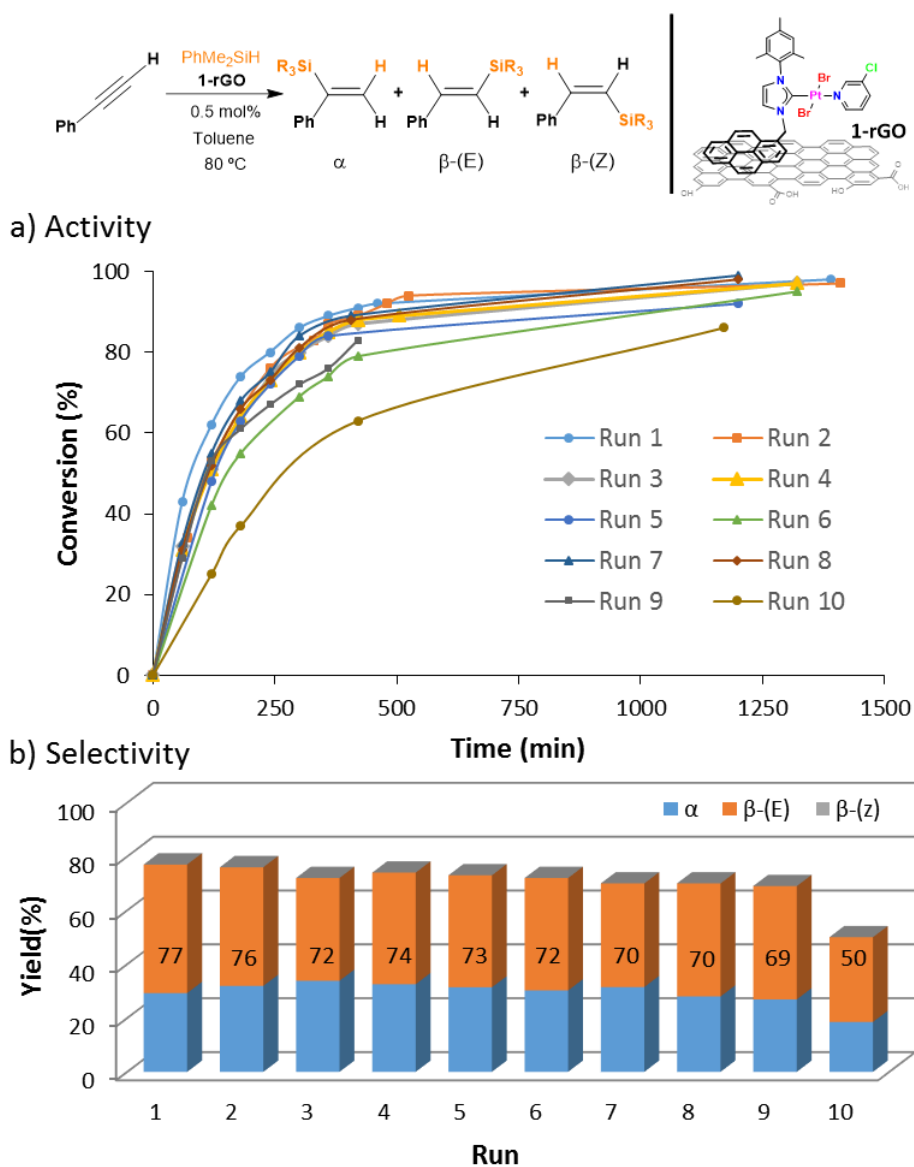


Figure 3.6 Recycling properties of **1-rGO** in hydrosilylation. a) Activity using reaction progress profiles for runs 1 to 10. b) Selectivity in the hydrosilylation of phenylacetylene at 5h reaction. Conversions determined by GC analysis and selectivity by ¹H NMR.

We analysed the hybrid catalytic material **1-rGO** after the recycling experiments in order to explore the changes of the support and complex **1** and get important information about the reaction mechanism and/or deactivation pathways. After ten

catalytic runs, HRTEM images of the hybrid material **1-rGO** showed that the morphology of the graphene is maintained after the reactions. The only difference that we noticed was the presence of more wrinkles as consequence of the usage of the hybrid material in the catalytic experiments (Figure 3.7). The dark field STEM images confirmed the absence of platinum nanoparticles and the EDS elemental mapping showed the homogeneous distribution of platinum on the hybrid material **1-rGO** after ten catalytic runs as it was in the initial material. These results agree with the poisoning experiments indicating that platinum nanoparticles are not involved in the hydrosilylation reaction.

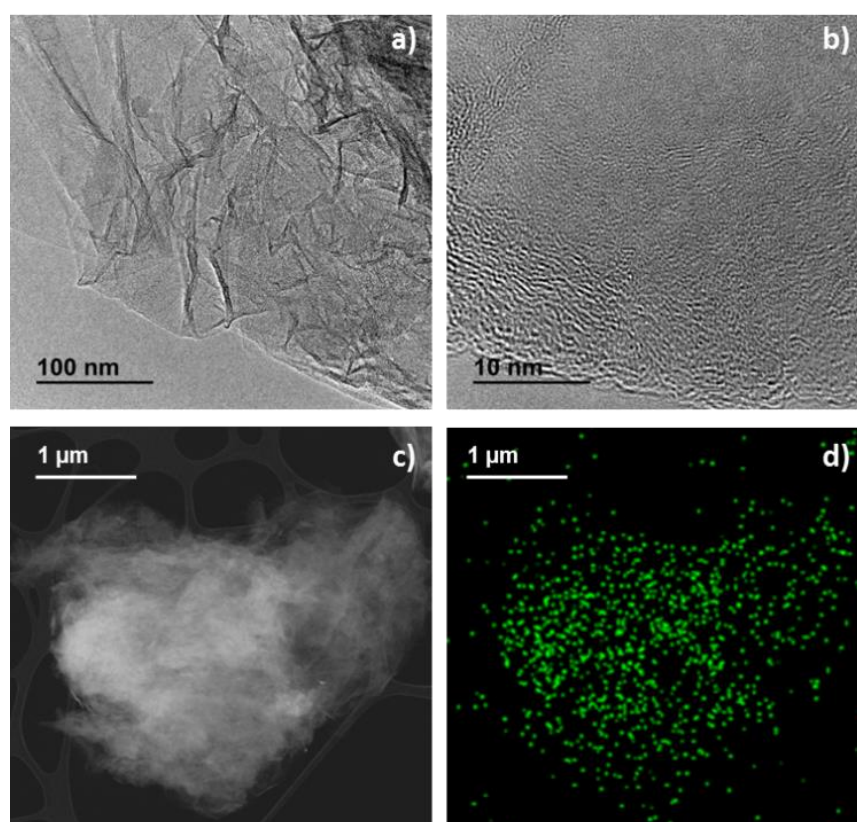


Figure 3.7 HRTEM images of **1-rGO** at different magnifications (a,b) after ten catalytic runs. STEM image showing the absence of platinum nanoparticles (c) and EDS elemental mapping (d) image shows the homogeneous distribution of platinum on the hybrid material **1-rGO** after ten catalytic runs.

XPS analysis comparison of the hybrid material **1-rGO** before and after ten catalytic runs (Figure 3.8) displayed the expected peaks corresponding at Pt4f, Br3d and N1s at the same binding energies. The high-resolution XPS analysis for the core-level peak of Pt4f, which appears as a doublet, indicates the presence of platinum only in the +2 oxidation state. These results demonstrate that after ten catalytic runs the platinum species observed are like the initial ones. XPS analysis also suggests that the nature and composition of catalyst resting state should be similar to the complex **1**. Thus, the hybrid material **1-rGO** is a robust solid catalyst that can be reused maintaining the selectivity in hydrosilylation.

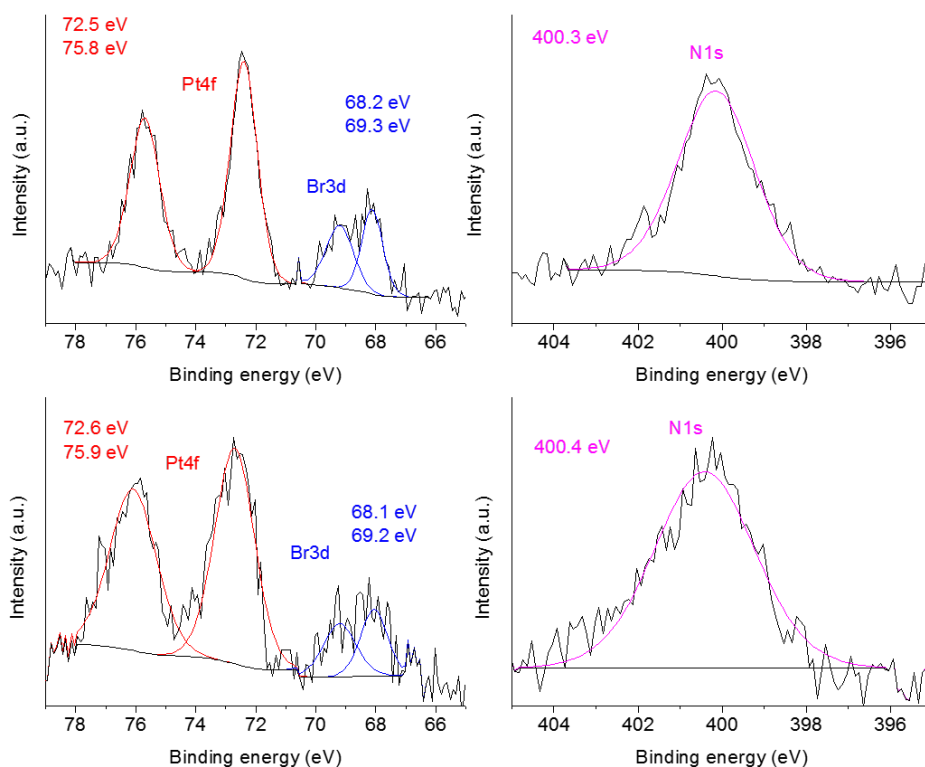


Figure 3.8 XPS analysis comparison of the hybrid material **1-rGO** before (top) and after ten catalytic runs (bottom).

3.3 CONCLUSIONS

A direct method for the immobilisation of metal complexes onto the surface of graphene by non-covalent interactions allows the precise control of the catalytic properties of the corresponding hybrid material. The structure of the metal complex and the properties of the support are not altered during the immobilisation process due to mild conditions used. The hybrid material contains metal sites homogeneously distributed and not only located at edges of defects. The catalytic studies with the molecular platinum complex **1** and the hybrid material **1-rGO** in the hydrosilylation reaction of alkynes reveal some of the advantages of the immobilisation. The catalytic activity and stability of the molecular complex **1** is maintained when anchored onto graphene while greater reaction rates were observed. Most probably the support prevents some deactivation pathways and aid to bring in close proximity substrates with the metal sites at the surface of graphene facilitating their interaction. Nevertheless, the platinum hybrid material (**1-rGO**) is an efficient catalyst in hydrosilylation of alkynes allowing recycling and reuse. This work represents a clear example of the catalytic benefits observed in the immobilisation of metal complexes onto graphene. The catalytic improvement in terms of activity and stability may inspire future research in development of efficient supported catalysis.

3.4 SUPPORTING INFORMATION

This section contains the most relevant data of the article supporting information. To see the complete version, we invite you to download the PDF version of the article at the publisher website (<https://chemistry-europe.onlinelibrary.wiley.com/doi/full/10.1002/ejic.202000356>).

General considerations

Reagents and solvents

Anhydrous solvents were dried using a solvent purification system or purchased from commercial suppliers and stored over molecular sieves

Instrumentation

Nuclear magnetic resonance (NMR) spectra were recorded on Bruker spectrometers operating at 300 or 400 MHz (^1H NMR) and 75 or 100 MHz ($^{13}\text{C}\{^1\text{H}\}$ NMR), respectively, and referenced to SiMe_4 (δ in ppm and J in Hertz). NMR spectra were recorded at room temperature with the appropriate deuterated solvent. Elemental analyses were carried out in a TruSpec Micro Series. Electrospray Mass Spectra (ESI-MS) were recorded on a MicroMass Quatro LC instrument. Methanol was used as mobile phase and nitrogen was used as the drying and nebulizing gas. High-resolution images of transmission electron microscopy (HRTEM) and high-angle annular dark-field (HAADF-STEM) images of the samples were obtained using a Jem-2100 LaB6 (JEOL) transmission electron microscope coupled with an INCA Energy TEM 200 (Oxford) energy dispersive X-Ray spectrometer (EDX) operating at 200 kV. Samples were prepared by drying a droplet of a MeOH dispersion on a carbon-coated copper grid. X-ray photoelectron spectra (XPS) were acquired on a Kratos AXIS ultra DLD spectrometer with a monochromatic Al $K\alpha$ X-ray source (1486.6 eV) using a pass energy of 20 eV. To provide a precise energy calibration, the XPS binding energies were referenced to the C1s peak at 284.6 eV. GC analyses were obtained on a Shimadzu GC-2010 apparatus equipped with a FID detector, and using a Teknokroma column (TRB-5MS, 30 m x 0.25 mm x 0,25 μm).

Catalysts synthesis

Synthesis of **1**: Platinum chloride (200 mg, 0.75 mmol), imidazolium salt functionalised with a pyrene-tag (361.3 mg, 0.75 mmol), potassium carbonate (521.3 mg, 3.75 mmol) and sodium bromide (780,0 mg, 7,5 mmol) were added to a Schlenk flask under nitrogen atmosphere. Then, 2.2 mL of 3-chloropyridine were added, and the mixture was stirred at 80 °C for 43 h. After solvent removal, the crude product was purified by column chromatography. The pure compound **1** was eluted using CH₂Cl₂ and was precipitated as a yellow solid from a mixture of CH₂Cl₂/hexane in 69 % yield. Full characterization of complex **1** is Figure S3.1.

Synthesis of **1-rGO**: In a round-bottom flask were introduced 180 mg of **rGO** and 100 mL of CH₂Cl₂. The suspension was introduced in ultra-sounds for 30 minutes. Then, 25 mg of compound **1** was added to the exfoliated graphene, and the mixture was sonicated for 5 extra min. Next, the suspension was stirred at room temperature for 12 hours. The mixture was filtered and washed with CH₂Cl₂ (3 x 25 mL) obtaining a black solid (material **1-rGO**). The filtrates were combined and evaporated to dryness under reduced pressure. The presence of unsupported complex **1** was analysed by ¹H NMR using anisole as internal standard. Integration of the characteristic signal of anisole accounts for a first indication of the complex amount deposited onto **rGO**. The exact amount of complex supported was determined by ICP-MS analysis. Digestion of the materials was performed in a microwave oven using nitric and hydrochloric acids (3:1). This analysis shows that the quantity of complex **1** in the material **1-rGO** is 4.55% in weight.

Catalytic hydrosilylation experiments

A pyrex© tube with a stirring bar is charged with 0.3 mmol of alkyne, 0.31 mmol of hydrosilane, catalyst and 1 mL of toluene as solvent. The tube is then introduced in a preheated 80 °C oil bath. Yields and conversions were determined by GC and/or ¹H NMR analysis using anisole or 1,3,5-trimethoxybenzene as internal standard. Recycling experiments were carried out under the same reaction conditions as described in the general procedure. After completion of each run (24 h), the reaction mixture was allowed to reach room temperature and the catalyst was isolated by decantation. The solid was washed thoroughly with toluene (3 x 5 mL) and toluene (3 x 5 mL) and reused in the following run.

Catalyst characterization

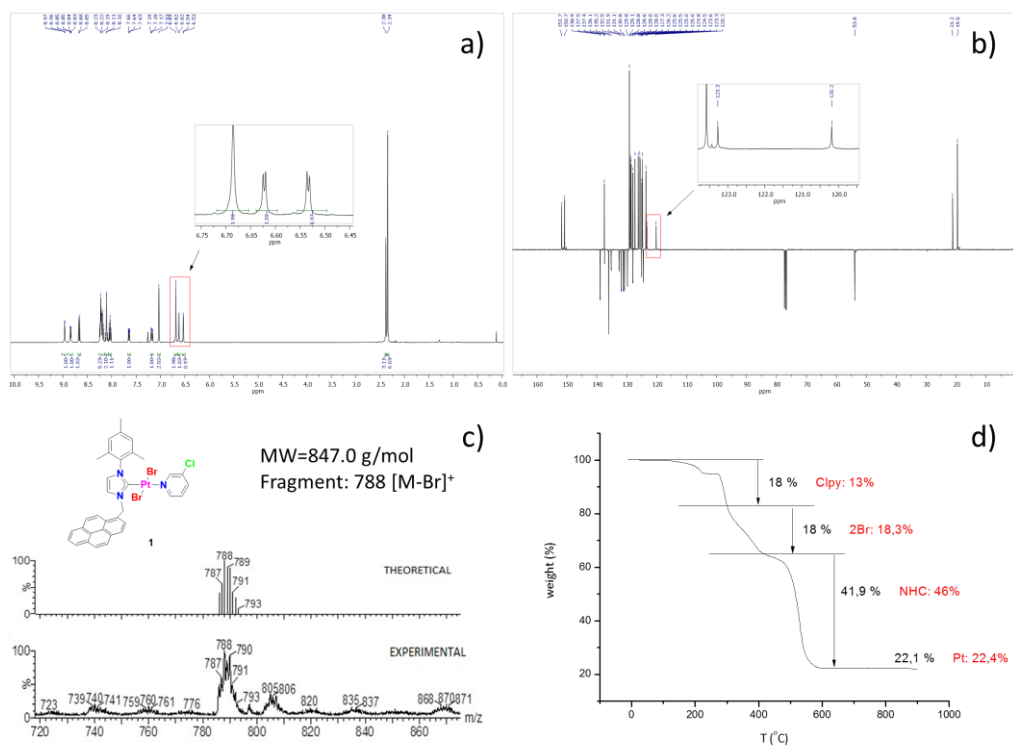


Figure S3.1 ^1H NMR spectrum (a), APT spectrum (b), ESI/MS spectrum (c) and thermogravimetric analysis (d) of complex **1**.

Kinetic analysis of hydrosilylation reaction

General procedure for the catalytic hydrosilylation of alkynes: In a general catalytic experiment, a pyrex tube equipped with a stirring bar is charged with 0.3 mmol of alkyne, 0.31 mmol of hydrosilane, catalyst and 1 mL of toluene as solvent. The pyrex tube is then introduced in a preheated 80 °C oil bath. Yields and conversions were determined by GC and/or ¹H NMR analysis using anisole or 1,3,5-trimethoxybenzene as internal standard.

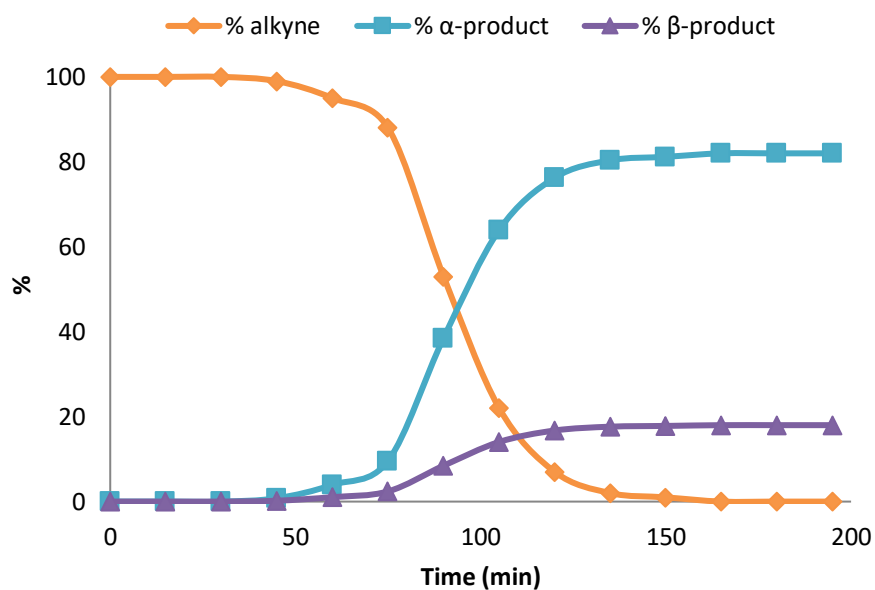
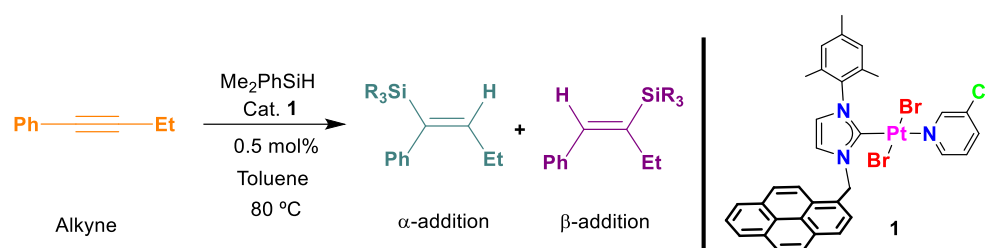


Figure S3.2 Hydrosilylation of 1-phenyl-1-butyne with dimethylphenylsilane.

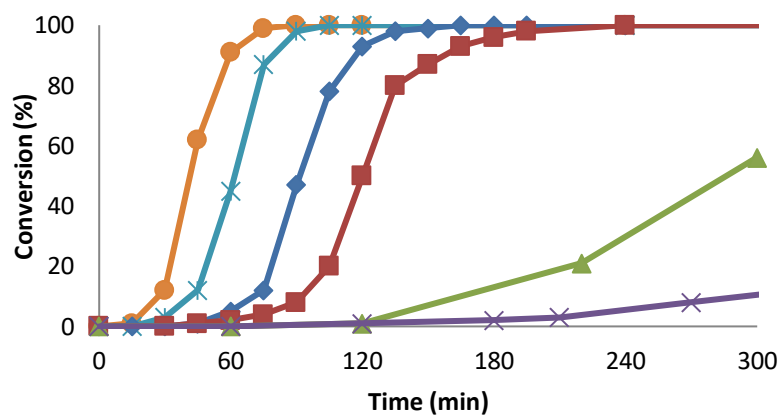
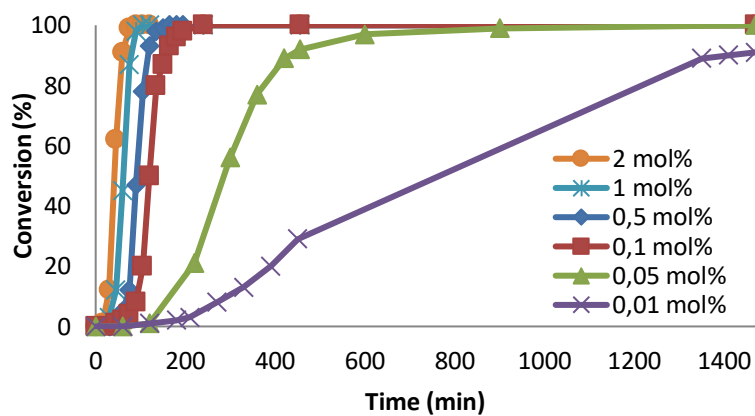
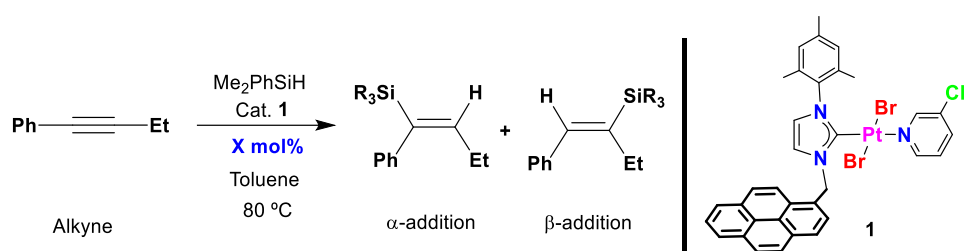


Figure S3.3 Hydrosilylation of 1-phenyl-1-butyne with dimethylphenylsilane using cat. **1** at different loadings. Zoom of $t = 0 - 300$ min (down).

Competitive experiments

General procedure for competitive catalytic hydrosilylation: In a general catalytic experiment, a pyrex tube equipped with a stirring bar is charged with 0.3 mmol of alkyne, 0.3 mmol of competitive molecule, 0.62 mmol of dimethylphenylsilane, catalyst and 1.5 mL of toluene as solvent. The pyrex tube is then introduced in a preheated 80 °C oil bath. Yields and conversions were determined by GC and/or ¹H NMR analysis using anisole or 1,3,5-trimethoxybenzene as internal standard.

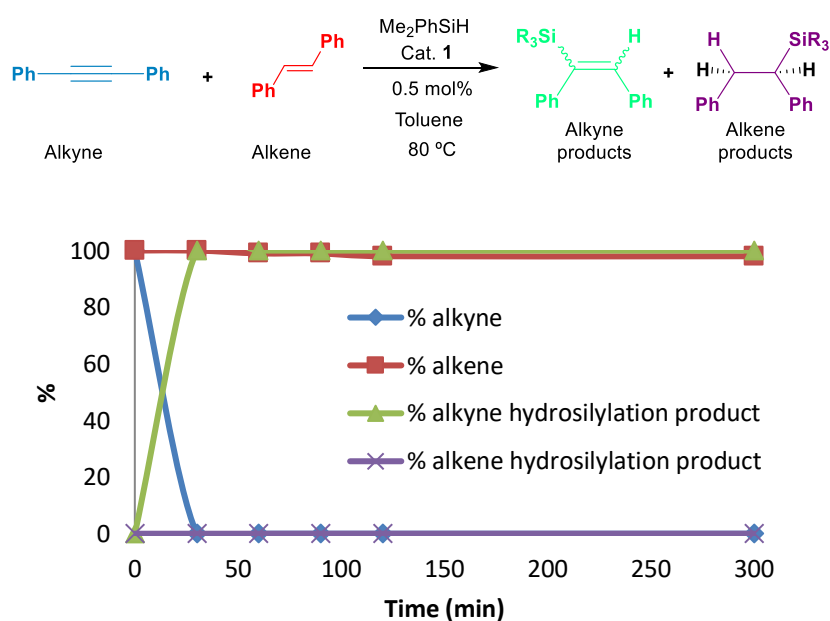


Figure S3.4 Hydrosilylation of diphenylacetylene in the presence of (E)-stilbene.

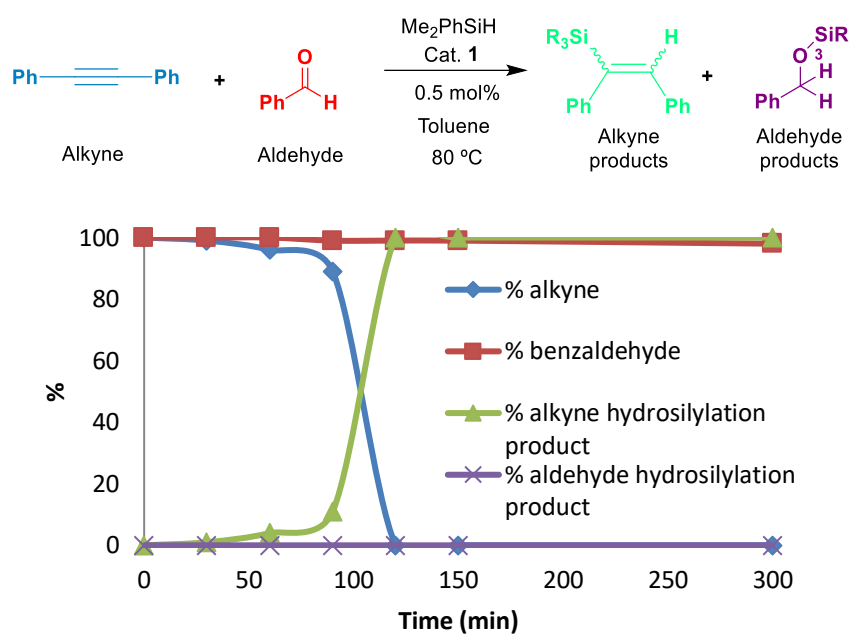


Figure S3.5 Hydrosilylation of diphenylacetylene in the presence of benzaldehyde.

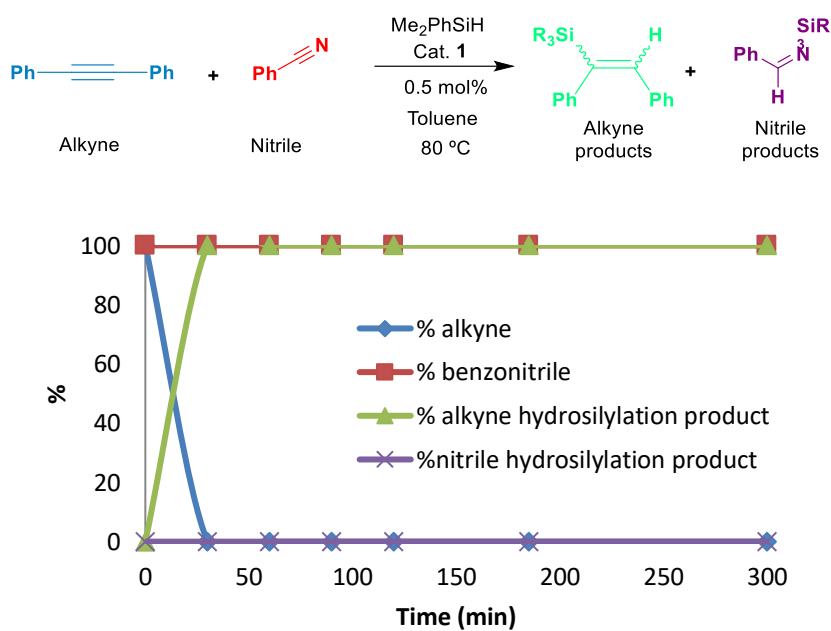


Figure S3.6 Hydrosilylation of diphenylacetylene in the presence of benzonitrile.

Poisoning experiments

Poisoning experiments using P4VP (poly(4-vinylpyridine)) as an scavenger of Pt(II) molecular species and the Hg drop test as an scavenger of Pt nanoparticles. Scavengers added after 90 min. reaction to assure the formation of the catalytic active species.

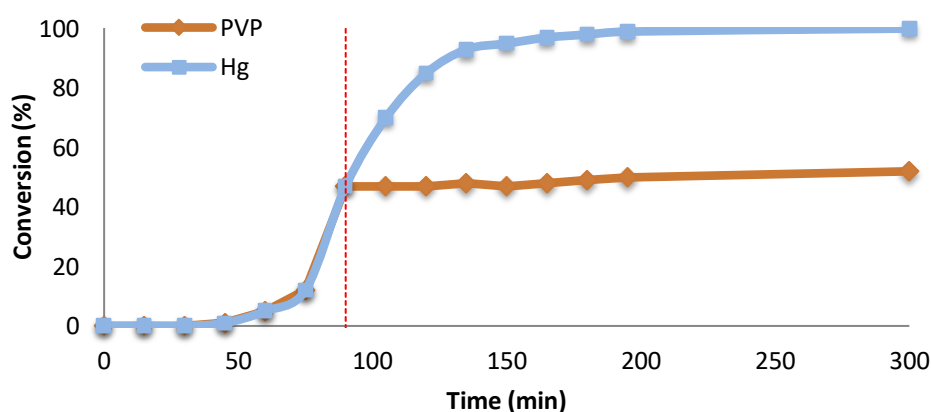
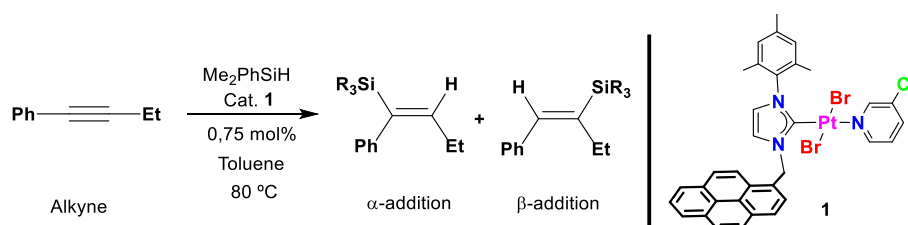


Figure S3.7 Poisoning experiments in the hydrosilylation of alkynes catalysed by **1**. The addition of PVP (poly(4-vinylpyridine)) used as a scavenger of Pt(II) molecular species inhibits the reaction. The addition of Hg (Mercury test) used as a scavenger of Pt nanoparticles does not have any significant effect in hydrosilylation. Both experiments suggest that the catalytic active species are homogeneous in nature.

3.5 REFERENCES

- (1) Marciniak, B.; Maciejewski, H.; Pietraszuk, C.; Pawluć, P. *Appl. Homog. Catal. with Organomet. Compd.*, Wiley, **2017**, pp. 569–620.
- (2) Marciniak, B. *Springer Netherlands*, Dordrecht, **2008**, pp. 53–86.
- (3) Lewis, L. N.; Stein, J.; Gao, Y.; Colborn, R.E.; Hutchins, G. *Platinum Metals Rev.* **1997**, *41*, 66–75.
- (4) Meister, T.K.; Riener, K.; Gigler, P.; Stohrer, J.; Herrmann, W. A.; Kühn, F. E. *ACS Catal.* **2016**, *6*, 1274–1284.
- (5) Nakajima, Y.; Shimada, S. *RSC Adv.* **2015**, *5*, 20603–20616.
- (6) Troegel, D.; Stohrer, J. *Coord. Chem. Rev.* **2011**, *255*, 1440–1459.
- (7) Karstedt, B.; Gen. Electr. Company, U.S. Pat. No. 3775452A 1973.
- (8) Speier, J.L.; Webster, J. A.; Barnes, G. H. *J. Am. Chem. Soc.* **1957**, *79*, 974–979.
- (9) Markó, I. E.; Stérin, S.; Buisine, O.; Mignani, G.; Branlard, P.; Tinant, B.; Declercq, J.P. *Science* **2002**, *298*, 204–206.
- (10) Berthon-Gelloz, G.; Buisine, O.; Brière, J. F.; Michaud, G.; Stérin, S.; Mignani, G.; Tinant, B.; Declercq, J. P.; Chapon, D.; Markó, I. E. *J. Organomet. Chem.* **2005**, *690*, 6156–6168.
- (11) Dierick, S.; Markó, I. E.; *N-Heterocyclic Carbenes Eff. Tools Organomet. Synth.* Wiley, **2014**, 9783527334, 111–150.
- (12) Dierick, S.; Vercruyse, E.; Berthon-Gelloz, G.; Markó, I. E.; *Chem. Eur. J.* **2015**, *21*, 17073–17078.
- (13) Crabtree, R. H.; *Chem. Rev.* **2012**, *112*, 1536–1554.
- (14) Taige, M.A.; Ahrens, S.; Strassner, T. *J. Organomet. Chem.* **2011**, *696*, 2918–2927.
- (15) Bolbat, E.; Suarez-Alcantara, K.; Canton, S. E.; Wendt, O. F. *Inorg. Chim. Acta* **2016**, *445*, 129–133.

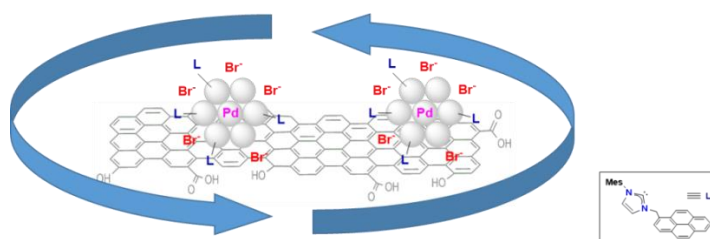
- (16) Chay, R. S.; Rocha, B. G. M.; Pombeiro, A. J. L.; Kukushkin, V. Y.; Luzyanin, K. V. *ACS Omega* **2018**, *3*, 863–871.
- (17) Žak, P.; Bolt, M.; Kubicki, M.; Pietraszuk, C. *Dalton Trans.* **2018**, *47*, 1903–1910.
- (18) Silbestri, G. F.; Flores, J. C.; de Jesús, E. *Organometallics* **2012**, *31*, 3355–3360.
- (19) Ye, R.; Zhao, J.; Wickemeyer, B. B.; Toste, F. D.; Somorjai, G. A. *Nat. Catal.* **2018**, *1*, 318–325.
- (20) Zhong, R.; Lindhorst, A. C.; Groche, F. J.; Kühn, F. E. *Chem. Rev.* **2017**, *117*, 1970–2058.
- (21) Wang, W.; Cui, L.; Sun, P.; Shi, L.; Yue, C.; Li, F. *Chem. Rev.* **2018**, *118*, 9843–9929.
- (22) Benaglia, M. Ed. , *Recoverable and Recyclable Catalysts*, John Wiley & Sons, Ltd, Chichester, UK, **2009**.
- (23) Axet, M. R.; Dechy-Cabaret, O.; Durand, J.; Gouygou, M.; Serp, P.; *Coord. Chem. Rev.* **2016**, *308*, 236–345.
- (24) Axet, M. R.; Durand, J.; Gouygou, M.; Serp, P. *Surface Coordination Chemistry on Graphene and Two-Dimensional Carbon Materials for Well-Defined Single Atom Supported Catalysts*, Elsevier Inc., **2019**.
- (25) Gladysz, J. A. *Pure Appl. Chem.* **2001**, *73*, 1319–1324.
- (26) Xu, C.; Huang, B.; Yan, T.; Cai, M. *Green Chem.* **2018**, *20*, 391–397.
- (27) Naganawa, Y.; Maegawa, Y.; Guo, H.; Gholap, S. S.; Tanaka, S.; Sato, K.; Inagaki, S.; Nakajima, Y. *Dalton Trans.* **2019**, *48*, 5534–5540.
- (28) Chen, L.; Ali, I. S.; Sterbinsky, G. E.; Gamler, J. T. L.; Skrabalak, S. E.; Tait, S. L.; *ChemCatChem* **2019**, *11*, 2843–2854.
- (29) Sabater, S.; Mata, J. A. *Non-Covalent Interact. Synth. Des. New Compd.*, John Wiley & Sons Inc, Hoboken, NJ, **2016**, pp. 313–326.
- (30) Sabater, S.; Mata, J.A.; Peris, E.; *ACS Catal.* **2014**, *4*, 2038–2047.

- (31) Georgakilas, V.; Otyepka, M.; Bourlinos, A. B.; Chandra, V.; Kim, N.; Kemp, K.C.; Hobza, P.; Zboril, R.; Kim, K.S. *Chem. Rev.* **2012**, *112*, 6156–6214.
- (32) Georgakilas, V.; Tiwari, J. N.; Kemp, K. C.; Perman, J.A.; Bourlinos, A.B.; Kim, S.; Zboril, R. *Chem. Rev.* **2016**, *116*, 5464–5519.
- (33) Maishal, T. K.; Alauzun, J.; Basset, J. M.; Copéret, C.; Corriu, R. J. P.; Jeanneau, E.; Mehdi, A.; Reyé, C.; Veyre, L.; Thieuleux, C. *Angew. Chem. Int. Ed.* **2008**, *47*, 8654–8656.
- (34) Samantaray, M.K.; Alauzun, J.; Gajan, D.; Kavitate, S.; Mehdi, A.; Veyre, L.; Lelli, M.; Lesage, A.; Emsley, L.; Copéret, C. *J. Am. Chem. Soc.* **2013**, *135*, 3193–3199.
- (35) Copéret, C.; Comas-Vives, A.; Conley, M.P.; Estes, D.P.; Fedorov, A.; Mougél, V.; Nagae, H.; Núñez-Zarur, F.; Zhizhko, P. A. *Chem. Rev.* **2016**, *116*, 323–421.
- (36) Valente, C.; Çalimsiz, S.; Hoi, K. H.; Mallik, D.; Sayah, M.; Organ, M. G. *Angew. Chem. Int. Ed.* **2012**, *51*, 3314–3332.
- (37) Bouché, M.; Bonnefont, A.; Achard, T.; Bellemin-Laponnaz, S. *Dalton Trans.* **2018**, *47*, 11491–11502.
- (38) Bouché, M.; Dahm, G.; Wantz, M.; Fournel, S.; Achard, T.; Bellemin-Laponnaz, S. *Dalton Trans.* **2016**, *45*, 11362–11368.
- (39) Ventura-Espinosa, D.; Sabater, S.; Mata, J. A. *J. Catal.* **2017**, *352*, 498–504.
- (40) Dolomanov, O. V.; Bourhis, L. J.; Gildea, R.J.; Howard, J. A. K.; Puschmann, H. *J. Appl. Crystallogr.* **2009**, *42*, 339–341.
- (41) Sabater, S.; Mata, J. A.; Peris, E.; *Organometallics* **2015**, *34*, 1186–1190.
- (42) Mata J. A.; Peris, E.; Sabater, S. Soporte de Catalizadores En Derivados de Grafeno. Spain Pat. No P201331680, **2015**.
- (43) Peuckert, M.; Coenen, F. P.; Bonzel, H. P.; *Electrochim. Acta* **1984**, *29*, 1305–1314.
- (44) Richardson, J. M.; Jones, C. W. *Adv. Synth. Catal.* **2006**, *348*, 1207–1216.

- (45) Foley, P.; DiCosimo, R.; Whitesides, G.M. *J. Am. Chem. Soc.* **1980**, *102*, 6713–6725.
- (46) Crabtree, R. H. *Chem. Rev.* **2015**, *115*, 127–150.
- (47) Ventura-Espinosa, D.; Carretero-Cerdán, A.; Baya, M.; García, H.; Mata, J. A. *Chem. Eur. J.* **2017**, *23*, 10815–10821.
- (48) Ventura-Espinosa, D.; Sabater, S.; Carretero-Cerdán, A.; Baya, M.; Mata, J. A. *ACS Catal.* **2018**, *8*, 2558–2566.
- (49) A. Mollar-Cuni, D. Ventura-Espinosa, S. Martín, Á. Mayoral, P. Borja, J. A. Mata, *ACS Omega* 2018, *3*, 15217–15228.
- (50) Ventura-Espinosa, D.; Vicent, C.; Baya, M.; Mata, J. A. *Catal. Sci. Technol.* **2016**, *6*, 8024–8035.
- (51) Ventura-Espinosa, D.; Marzá-Beltrán, A.; Mata, J. A. *Chem. Eur. J.* **2016**, *22*, 17758–17766.
- (52) Ballestin, P.; Ventura-Espinosa, D.; Martín, S.; Caballero, A.; Mata, J. A.; Pérez, P. J. *Chem. A Eur. J.* **2019**, *25*, 9534–9539.
- (53) Ventura-Espinosa, D.; Martín, S.; Mata, J.A. *J. Catal.* **2019**, *375*, 419–426.
- (54) Vriamont, C.; Devillers, M.; Riant, O.; Hermans, S. *Chem. Eur. J.* **2013**, *19*, 12009–12017.
- (55) Bayram, E.; Linehan, J. C.; Fulton, J. L.; Roberts, J. S.; Szymczak, N. K.; Smurthwaite, T. D.; Özkar, S.; Balasubramanian, M.; Finke, R. G.; *J. Am. Chem. Soc.* **2011**, *133*, 18889–18902.
- (56) Phan, N. T. S.; Van Der Sluys, M.; Jones, C. W. *Adv. Synth. Catal.* **2006**, *348*, 609–679.
- (57) Conley, M. P.; Copéret, C. *Top. Catal.* **2014**, *57*, 843–851.

CHAPTER 4:

Stabilization of nanoparticles produced by hydrogenation of Palladium-NHC complexes on the surface of graphene and implications in catalysis



ABSTRACT

Palladium nanoparticles have been obtained by decomposition of well-defined palladium complexes non-covalently anchored onto the surface of reduced graphene oxide. Morphological analysis by microscopy showed the presence of small palladium nanoparticles homogeneously distributed on the support. Characterization by XPS confirmed that the palladium nanoparticles contain Pd(2+) and Pd(0) oxidation states stabilized by N-heterocyclic carbene (NHC) and bromide ligands. The catalytic properties of the nanoparticles with and without the support have been evaluated in the hydrogenation of alkynes. Supported palladium nanoparticles showed an increased activity versus the non-supported ones and could be recycled up to ten times without loss of catalytic activity. The composition of the palladium nanoparticles is different for each catalytic cycle indicating a dynamic process and the formation of different catalytic active species. On the contrary, the unsupported palladium nanoparticles showed limited activity caused by decomposition and could not be recycled. The role of the support has been investigated. The results indicate that the support influences the stability of palladium nanoparticles.

ACS Omega, **2018**, 3, 15217-15228 (DOI: 10.1021/acsomega.8b02193)

4.1 INTRODUCTION

Palladium plays a major role in the synthesis of value chemicals and pharmaceuticals by carbon-carbon coupling and hydrogenation catalytic reactions.¹⁻⁹ The nature of the catalytic active species is under continuous debate and different types have been proposed as key intermediates including molecular complexes, clusters, single-atoms and nanoparticles.¹⁰⁻¹⁴ Among them, palladium nanoparticles have received increase attention because they are observed in many catalytic processes and serve as a class of highly active catalysts.¹⁵⁻¹⁸ An important limitation in the use of nanoparticles arise from deactivation by sintering or agglomeration. Functionalization of metal nanoparticles with organic ligands confers stability and controls the size and distribution.¹⁹⁻²¹ These properties markedly regulate the catalytic applications of metal nanoparticles. However, even the functionalized nanoparticles suffer dynamic changes at the surface during the catalytic reactions and single atoms and/or metal clusters are released to the reaction media forming new species.²² If the generation of the new species is not reversible, the original nanoparticles evolve into the formation of different metal nanoparticles with different catalytic properties. As an alternative, the use of supports is a complementary approach to increase the stability of metal nanoparticles functionalized with organic ligands.²³⁻²⁷ The use of stabilizing ligands in combination with supports increases the potential catalytic applications of the systems especially in the recycling and reuse of metal nanoparticles.

Palladium nanoparticles functionalized with NHC ligands have a great potential for catalytic applications. In parallel, ligand-free palladium nanoparticles have been immobilized onto graphene. However, the combination of palladium nanoparticles functionalized with organic ligands and supported over graphene is unexplored.^{28,29} In this manuscript, we discuss the preparation of palladium nanoparticles (Pd-NPs) stabilized by N-heterocyclic carbene (NHC) ligands by decomposition of well-defined organometallic complexes.³⁰⁻³² The catalytic properties of the Pd-NPs are evaluated in the hydrogenation of alkynes as a benchmark reaction. We describe the influence of graphene as a support for the Pd-NPs and the potential benefits in the catalytic applications. The use of NHC ligands as stabilizers and graphene as support allows reusing and recycling the palladium nanoparticles. The modular approach, starting from molecular complexes, nanoparticles and immobilization, allows an in-deep characterization of the materials and offers the opportunity to study the influence of the individual components in the design of hybrid catalytic systems.

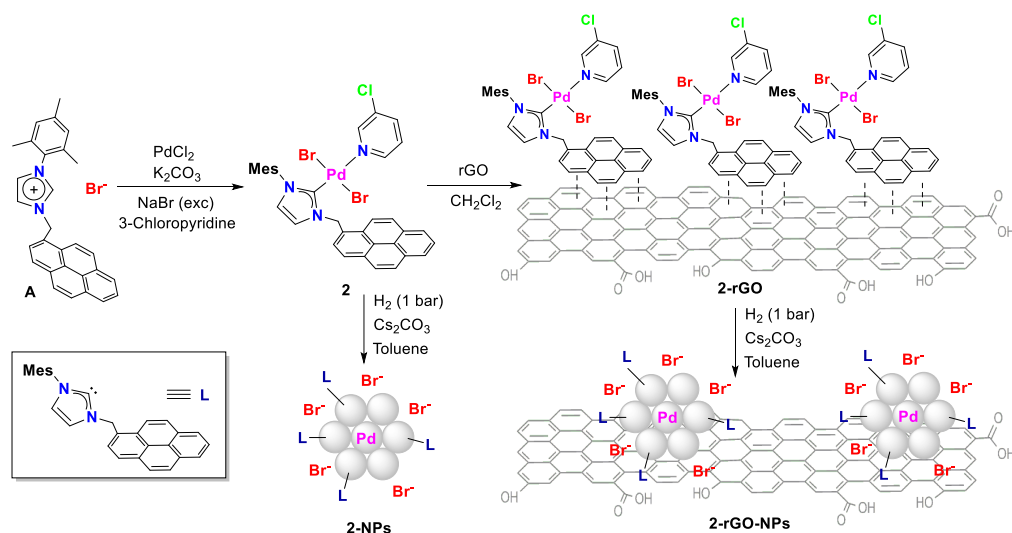
4.2 RESULTS AND DISCUSSION

Synthesis, immobilisation and characterization of 2 and 2-rGO

The palladium complex **2** at the molecular level or supported onto reduced graphene oxide (**2-rGO**) was used for the synthesis of free and supported palladium nanoparticles (Scheme 4.1). Complex **2** was obtained by the methodology described for the palladium PEPPSI type complexes.³³ The imidazolium salt **A** was reacted with palladium (II) chloride and potassium carbonate in 3-chloropyridine to afford complex **2** in good yield. An excess of sodium bromide was added to the reaction media to avoid halide scrambling in the final product. Complex **2** was fully characterized by NMR spectroscopy, ESI-MS spectrometry, elemental analysis, X-ray photoelectron spectroscopy (XPS), UV/Vis absorption spectroscopy and thermogravimetric (TG) analysis (Figure S4.1). We observed that TG analysis is a valuable characterization technique for palladium PEPPSI type complexes because shows the sequential mass losses assigned to the different palladium ligands (Figure S4.2). The molecular structure of **2** was confirmed by X-ray spectroscopy (Figure 4.1a). The palladium shows a distorted squared-planar environment with the bromide ligands in trans position. The crystal packing reveals that the pyrene-tag of different molecules are close in proximity showing π -stating interactions with an interplanar distance of 3.5 Å (Figure 4.1b).

The immobilization of complex **2** onto graphene for obtaining the hybrid material **2-rGO** was carried out as previously described.^{34,35} This methodology allows a controlled grafting of molecular complexes on the surface of reduced graphene oxide (**rGO**). The immobilization conditions are mild so it is expected that the properties of the **rGO** and the metal complex are preserved. The pyrene tag permits the formation of π -interactions with graphene that retain the molecular complex attached to the material. The π -stating interactions are considered weak but their multiplicity, such in the case of graphene, grants the efficient immobilization of molecular complexes. This is evidenced by the formation of short-distance interactions at the molecular level as the ones found in the crystal packing of complex **2**. We have previously observed that ruthenium, iridium and gold molecular complexes containing a pyrene group form strong π -stating interactions with reduced graphene oxide. The catalytic properties reveal that these interactions are maintained during the recycling experiments.³⁶⁻⁴¹

Characterization of **2-rGO** was performed by HRTEM, XPS, UV/vis, TG and the exact amount of complex **2** onto graphene was analyzed by ICP/MS analysis (Figure 4.2 and S4.3). The result of the ICP/MS analysis accounted for a 5.5 % w/w of **2** onto the graphene surface. X-ray photoelectron spectroscopy (XPS) analysis was used for the characterization of complex **2** and the hybrid material **2-rGO**. This technique provides valuable information of elemental composition and oxidation states. XPS analysis of **2** showed the presence of palladium, nitrogen, bromide and carbon. As expected for the molecular complex, the binding energies of Pd confirm the +2 oxidation state. A comparative XPS analysis of **2** and **2-rGO** shows the characteristic core-level peaks of Pd 3d, Br 3d, N 1s and Cl 2p at the same binding energy for the molecular complex and the hybrid material (Figure 4.2). The XPS analysis confirms the immobilization of molecular complex **2** onto the surface of graphene. All these techniques suggest that properties of the **rGO** and the palladium complex **2** are preserved during the formation of the hybrid material **2-rGO**. In addition, we know the exact nature and composition of the palladium species deposited onto the surface of graphene.



Scheme 4.1 Synthesis of palladium complex **2**, immobilization onto **rGO** (**2-rGO**) and synthesis of free palladium nanoparticles (**2-NPs**) and supported onto **rGO** (**2-rGO-NPs**).

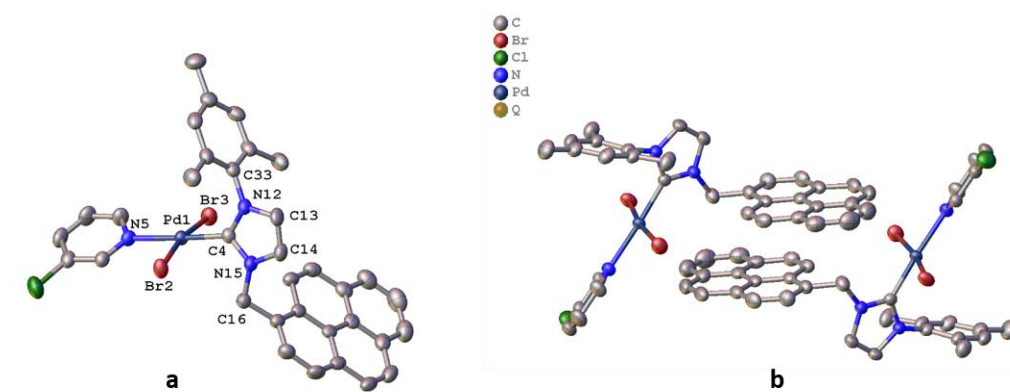


Figure 4.1 Molecular structure of complex **2** (a) X-ray packing view of **2** showing an interplanar distance between the pyrene tags of 3.5 Å (b).

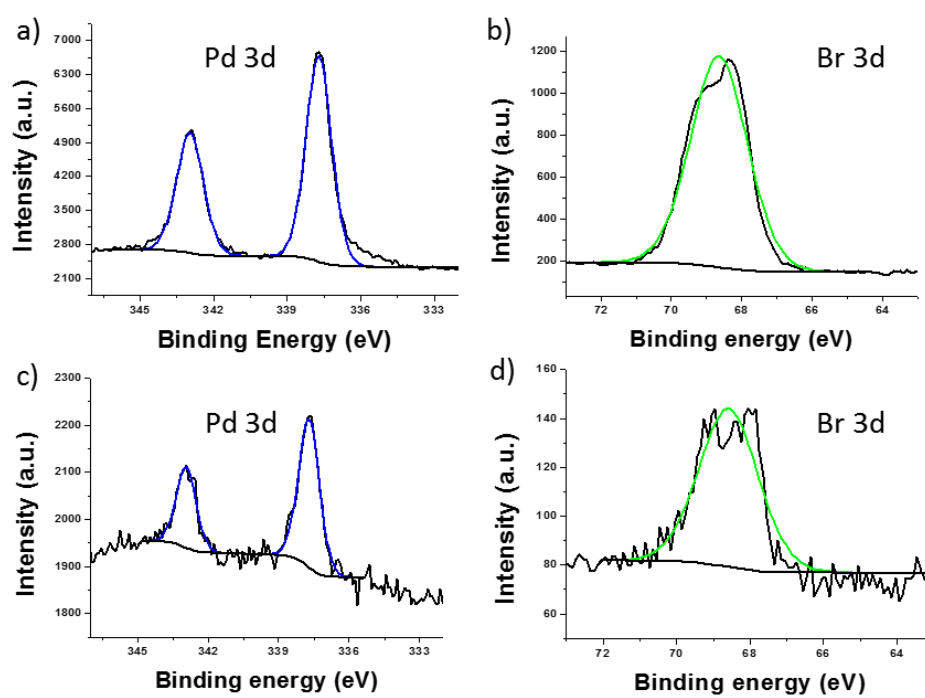


Figure 4.2 Comparative XPS analysis of the core-level peak of Pd 3d and Br 3d for complex **2** (a, b) and hybrid material **2-rGO** (c, d). See SI for details of other core-level peaks.

Synthesis and characterization of 2-NPs and 2-rGO-NPs

We observed a change in color of the solution when exposing the molecular complex **2** to hydrogen under basic conditions. The initial pale-yellow solution of **2** in toluene darkens in 20 min and after 3 h there is a black precipitate (Figure 4.3). This black precipitate corresponds to the formation of palladium nanoparticles (**2-NPs**). Decomposition of the palladium complex [Pd(NHC)(Br)₂(Cl-Py)] leads to the formation of palladium nanoparticles stabilized by NHC ligands from an organometallic approach as previously described.⁴²⁻⁴⁷ The presence of ligands avoids aggregation and controls the size of the nanoparticles. The HRTEM images confirmed the presence of small palladium nanoparticles of an average size of 6 nm (Figure 4.4a). The XPS analysis reveals the presence of palladium, carbon, nitrogen and bromine, but no trace of chlorine. The 3-chloropyridine ligand is lost during the nanoparticle formation. This ligand is labile and decoordination of metal center is usually observed in Pd-PEPPSI catalytic reactions. High-resolution XPS analysis shows the presence of two doublets for the core-level peaks of Pd 3d, indicating the presence of Pd⁰ and Pd²⁺ oxidation states (Figure 4.4b). The results show that **2-NPs** contained palladium atoms in two oxidation states, NHC and bromide ligands. The presence of ligands in the surface of the nanoparticles avoids aggregation and confers stability. The use of NHC ligands has previously been described to stabilize palladium nanoparticles.⁴⁸⁻⁵²

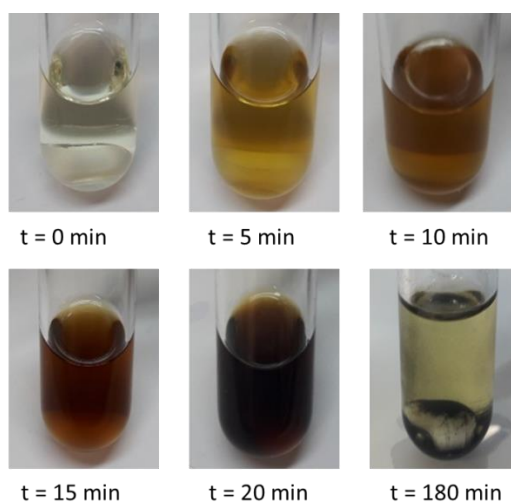


Figure 4.3 Complex **2** evolution under exposure to H₂ (1 bar) using toluene in the presence of Cs₂CO₃ at 65 °C.

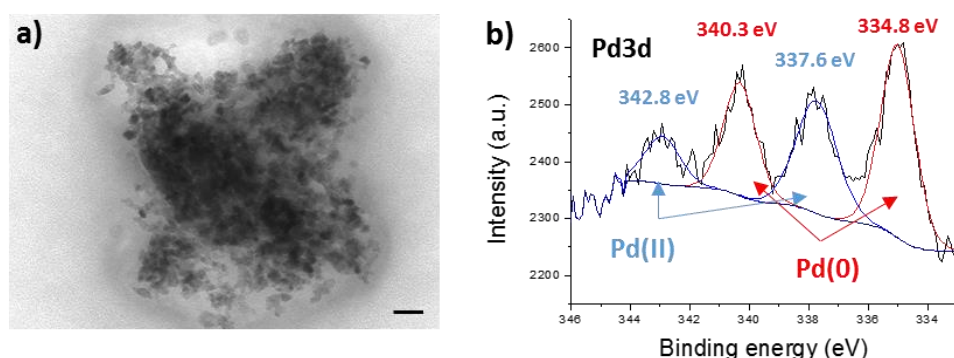


Figure 4.4 HRTEM images of **2-NPs** (a) and XPS analysis (b) showing the presence of Pd⁰ and Pd²⁺. Scale bar 20 nm.

The hybrid material **2-rGO** was exposed under the same conditions as the molecular complex **2** for the formation of palladium nanoparticles. HRTEM images of the hybrid material **2-rGO** before the exposure to hydrogen showed the single layer nature of graphene and the absence of palladium nanoparticles (Figure 4.5a). The EDS elemental mapping confirms the elemental composition of the molecular complex **2** (Pd, N, Br and Cl) and the homogeneous distribution of the complex over all the graphene surface. On the contrary, HRTEM images of the hybrid material **2-rGO** after the exposure to hydrogen showed the formation of palladium nanoparticles of an average size of 4 nm (Figure 4.5b). XPS analysis before the hydrogenation reaction confirmed the presence of only Pd²⁺ species in the **2-rGO** hybrid material (Figure 4.5c). After the exposure to H₂, XPS analysis confirms the presence of palladium, nitrogen, bromine, carbon and oxygen. More interesting is the formation of Pd⁰ oxidation state that coexists with Pd²⁺ as in **2-NPs** (Figure 4.5d). These results suggest that exposing **2-rGO** to hydrogen under basic conditions produce palladium nanoparticles of Pd²⁺ and Pd⁰ that contain NHC and bromide ligands immobilized onto graphene. The average size of the palladium nanoparticles is slightly smaller compared to the particles formed using the molecular complex **2**. Graphene is acting as a support to produce of small and well-dispersed palladium nanoparticles. We have observed that graphene acts as a nanoparticle-sponge in the in situ formation of gold particles by laser ablation. The results revealed a control of the particle size, and the gold nanoparticles obtained in the presence of graphene were smaller.⁵³ This process is general, and many reports confirm the immobilization

of metal nanoparticles on the surface of graphene by interactions of the d-metal orbitals with the π -delocalized electronic density of the graphene material.^{29,54,55}

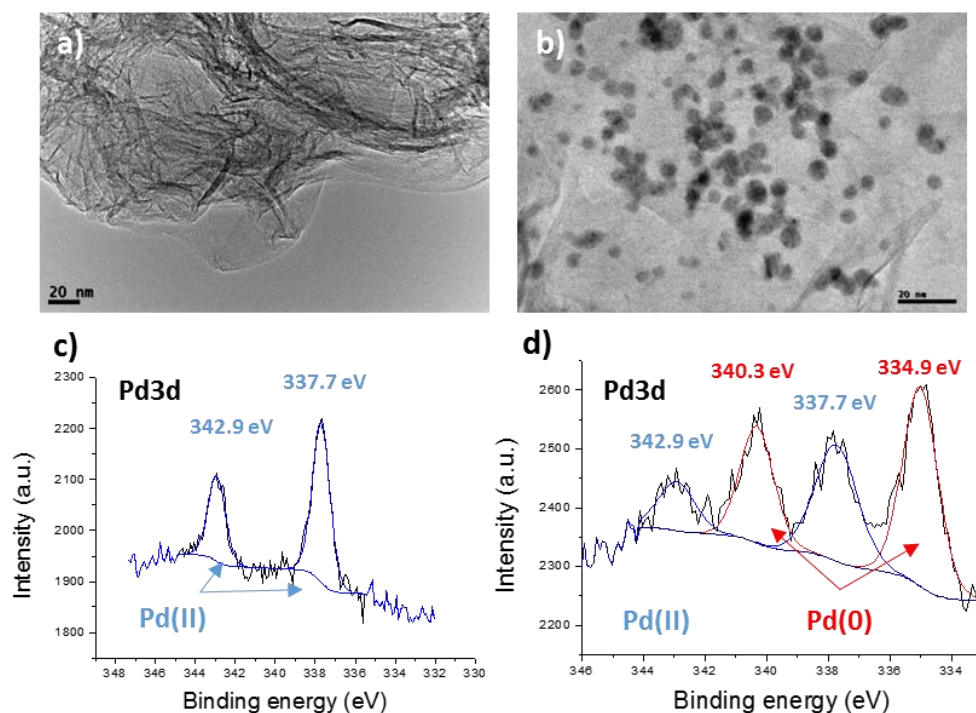


Figure 4.5 HRTEM images (top) and XPS analysis (bottom) for the core-level peaks of Pd 3d. HRTEM of **2-rGO** before (a) and after (b) the exposure to H₂. XPS analysis of **2-rGO** before (c) and after (d) the exposure to H₂ showing the characteristic peaks of Pd⁰ and Pd²⁺.

Catalytic studies

The catalytic hydrogenation of alkynes was evaluated using molecular hydrogen at low pressure with the precatalysts molecular complex **2** and the hybrid material **2-rGO**. The catalytic active palladium NPs (**2-NPs** and **2-rGO-NPs**) were generated in situ under appropriate reaction conditions. In a general procedure, a Schlenk flask was charged with the catalyst, base, alkyne and solvent. Then, a balloon of H₂ (≈ 1 bar) was connected to the system and the reaction was immersed in a pre-heated oil bath. The monitoring of the reaction and the product distribution was analyzed by GC chromatography and ¹H NMR using anisole as an internal standard. The

hydrogenation reaction is general and works for different bases and solvents. After optimization using diphenylacetylene as a model substrate, the best reaction conditions in terms of activity and selectivity are catalytic amounts of Cs_2CO_3 , dry toluene and 65 °C.

Reaction monitoring profile in the hydrogenation of 1-phenyl-1-butyne with precatalyst **2** (1 mol%) showed an induction period of 15 min. indicating the formation of the catalytic active species **2-NPs** (Figure 4.6 a). Then, the alkyne was hydrogenated to the Z-alkene in excellent yield and with good stereoselectivity (t = 1.5 h, alkyne conversion = 97 %, alkenes yield: 92 %, ratio Z/E = 95:5 and alkane yield 5%). Catalyst **2-NPs** is highly stereoselective for the cis isomer even at high alkyne conversion. When the alkyne was consumed, the E and Z alkenes were hydrogenated to the corresponding alkane. As the hydrogenation process was sequential, the formation of alkanes could be avoided by stopping the reaction at convenient time. Selective palladium catalysts in the semi-hydrogenation of alkynes are scarce and overreduction is better controlled by transfer hydrogenation methodologies.⁵⁶⁻⁶⁰ The reaction monitoring using precatalyst **2-rGO** showed an identical profile to catalyst **2-NPs** but with a longer induction period (30 min.) (Figure 4.6 b). Comparison of the catalytic activity of **2-NPs** vs **2-rGO-NPs** revealed that the reaction using catalyst **2-rGO-NPs** started later due to a longer induction period but then proceed at higher rates. This result is significantly different if we consider that catalyst **2-rGO-NPs** contains half amount of palladium of **2-NPs** (Figure 4.6 c). When the reaction was carried out at the same catalyst loading (0.5 mol%), full conversion of alkyne was not observed using **2-NPs**, indicating catalyst deactivation. These results show that immobilization of molecular complexes onto graphene lead to a more efficient catalysts and that the kinetics are not affected by diffusion problems.

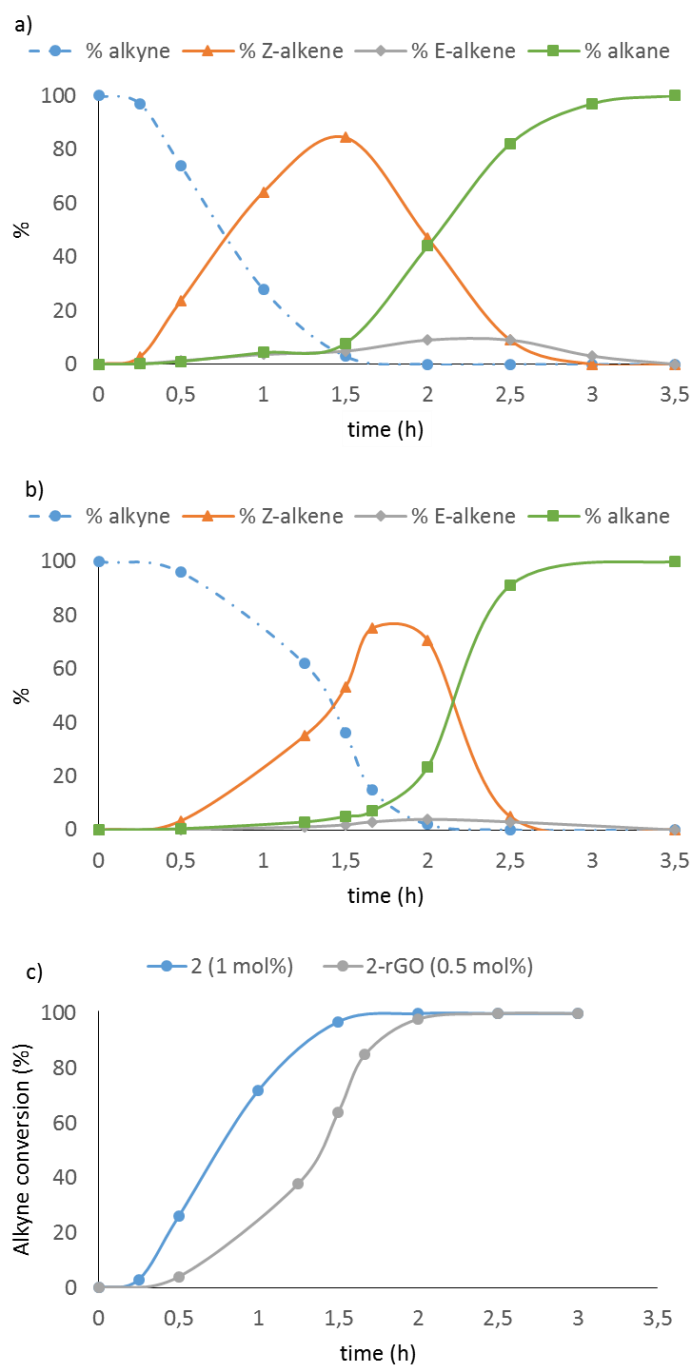


Figure 4.6 Hydrogenation of 1-phenyl-1-butyne with pre-catalysts **2** (1 mol%), (a) **2-rGO** (0.5 mol%) (b) and comparison of alkyne conversion for both pre-catalyst (c).

The nature of the catalytic active species was further analyzed by poisoning experiments using poly(4-vinylpyridine) (P4VP) as a scavenger of Pd²⁺ molecular species and the mercury drop test as a scavenger of palladium nanoparticles (Figure S4.4).^{61–66} The reactions were performed using precatalyst **2** (1.0 mol%) and 1-phenyl-1-butyne as substrate. The results showed that in the presence of poly(4-vinylpyridine) the hydrogenation rate is affected but not inhibited and after the addition of Hg drops, the reaction immediately stopped. Partial poisoning experiments suggest that the catalytic active palladium species are heterogeneous in nature and confirm that the active catalytic species are **2-NPs** and **2-rGO-NPs**. Then, we performed a Maitlis' test which implies a hot filtration to support preliminary data in the formation of nanoparticles.⁶⁷ In the hydrogenation of 1-phenyl-1-pentyne with precatalyst **2**, after 1 h reaction (GC conversion 40 %) half of the reaction mixture was filtered off through celite at 65 °C. The filtrate was maintained for 5 h under identical conditions, but GC analysis indicated that no further hydrogenation occurred (GC conversion 40%). On the contrary, the remaining mixture achieved full conversion in 2 h reaction. This experiment reinforces the heterogeneous nature of the catalytic active species.

An interesting topic to address in supported catalysis is the influence of the support. The support may only act as a medium that holds the active catalyst or may also play a role during the catalytic reaction facilitating the conversion of reagents into products.^{68–71} We explored the influence of the **rGO** support on palladium nanoparticles during hydrogenation. The experiment consisted in the monitoring of the reaction profile in the hydrogenation of 1-phenyl-1-butyne with precatalyst **2**, the hybrid material **2-rGO** and a mixture of molecular complex **2** with **rGO** for simulating the material **2-rGO** (Figure 4.7). In all cases we observed an induction period corresponding to the formation of NPs. The results revealed that precatalyst **2** did not afford full conversion and the reaction was stopped after 15.5 h. There is catalyst deactivation due to a lack of stability of **2-NPs** under the reaction conditions. In the case of the hybrid material **2-rGO** full conversion of alkyne was achieved in 2.3 h indicating again that **rGO** plays a role in the stabilization of the **2-NPs**. More interesting results were obtained by the mixture of catalyst **2** with **rGO**. The high catalytic activity of the mixture is comparable to that observed for the hybrid material **2-rGO**. The catalytic properties of complex **2** significantly increased after the addition of **rGO**. These results support that the graphene plays an important role during the catalytic experiment in the stabilization of palladium nanoparticles and avoids deactivation.

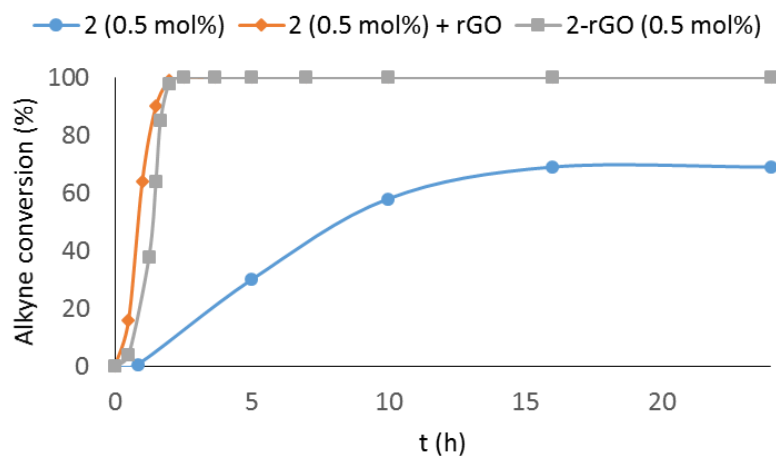
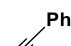
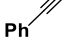
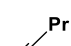
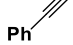
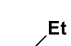
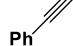
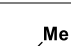
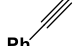



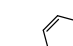


Figure 4.7 Hydrogenation of 1-phenyl-1-butyne with precatalyst **2** (blue circles), **2-rGO** (grey squares) and **2 + free rGO** (20 mg) (orange diamonds). Catalyst loading 0.5 mol% based on palladium. H₂ pressure 1 bar, Cs₂CO₃ (10 mol%) in toluene at 65 °C.

Precatalysts **2** and **2-rGO** are active in the hydrogenation of different substrates at low hydrogen pressure and short reaction times (Table 4.1). Internal alkynes were rapidly semi-hydrogenated to the corresponding alkenes with good to excellent stereoselectivity towards the Z isomer (Table 4.1, entries 1 – 8). We have not observed isomerization or migration of the Z-alkenes. Prolonged reaction time produced the hydrogenation of the alkenes to the corresponding alkanes. The complete reaction monitoring profiles are in the supporting information. The reactions are sequential and can be stopped at the appropriate time in the formation of alkene or alkane. Terminal alkynes react equally well but tend to give lower chemoselectivity at higher conversions (Table 4.1, entries 9 – 12). We noted that performing the hydrogenations using 0.5 mol% of catalyst **2** the reaction stopped at ca. 50%. On the contrary, using 0.5 mol% of catalyst **2-rGO** affords quantitative yields in short reaction times. As we have previously observed the immobilization of precatalyst **2** onto graphene plays a role in the catalytic process. The graphene does not act as a mere support. The immobilization of palladium complexes onto graphene helps in the stabilization of the catalytic active species and allows the reduction of catalyst amount.

Table 4.1 Hydrogenation substrate scope.

$\text{R} \text{---} \text{C} \equiv \text{C} \text{---} \text{R} + \text{H}_2 \xrightarrow[\text{Toluene, 65 } ^\circ\text{C}]{\text{[Cat.] Cs}_2\text{CO}_3 \text{ (10 mol\%)}} \text{R} \text{---} \text{C} = \text{C} \text{---} \text{R}$ <p style="text-align: center;">3a-3f 4a-4f</p>						
Entry	Substrate	Precatalyst (mol%)	Time (h)	Conversion ^a (%)	Yield ^a (%)	Z/E ^b
1		2 (1)	1.5	100	91	93:7
2		3a 2-rGO (0.5)	2.0	95	90	90:10
3		2 (1)	1.8	100	93	90:10
4		3b 2-rGO (0.5)	3.5	94	87	86:14
5		2 (1)	1.5	100	90	95:5
6		3c 2-rGO (0.5)	2	100	76	95:5
7		2 (1)	1	100	95	97:3
8		3d 2-rGO (0.5)	2	100	82	91:9
9		2 (1)	0.75	95	78	---
10		3e 2-rGO (0.5)	2	97	77	---
11		2 (1)	1.25	100	77	---
12		4f 2-rGO (0.5)	1.6	100	76	---

Conditions: 0.3 mmol of alkyne, 0.3 mmol of anisole used as internal standard, 1 bar of H₂ and 1 mL of Tol. Aerobic conditions [a] Conversions and Yields determined by GC. Yields calculated by the sum of alkenes. [b] Product distribution determined by ¹H NMR.

We performed competitive experiments to further evaluate the selectivity properties of precatalysts **2** and **2-rGO**. The competitive studies were carried out monitoring the hydrogenation reaction of alkynes in the presence of substrates

containing ketone, nitrile and nitro groups. In the alkyne/ketone experiment, 1-phenyl-1-butyne was mixed with acetophenone in equimolar amounts. Reaction monitoring using precatalysts **2** and **2-rGO** showed complete conversion of alkyne without ketone hydrogenation. Similar results were obtained in the case of alkyne/nitrile experiment using benzonitrile as substrate. Competition experiments show that hydrogenation of alkynes tolerates the presence of nitriles and ketones (Figure S4.10). Different results were obtained using the molecular complex **2** or the supported **2-rGO** in the competitive experiment alkyne/nitrobenzene. The hydrogenation reaction of 1-phenyl-1-butyne in the presence of nitrobenzene using precatalyst **2** was completely unselective. After 2 h reaction, the presence of aniline was already observed. The alkyne was not completely hydrogenated even after 20 h reaction. On the contrary, for the same experiment but using precatalyst **2-rGO**, we observed complete alkyne hydrogenation after 3 h reaction. The nitrobenzene was not hydrogenated and remained constant after 20 h reaction (Figure 4.8). These results suggest that the active catalytic species are different in nature for **2** or **2-rGO**.

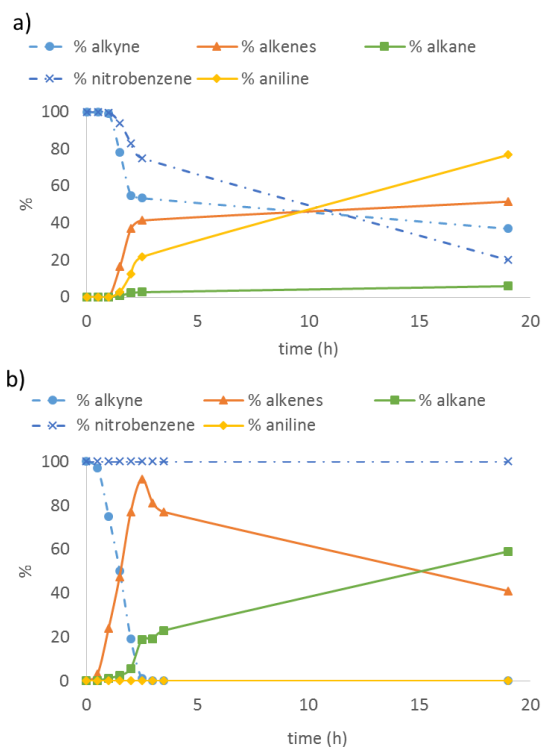


Figure 4.8 Competitive experiment in the hydrogenation of 1-phenyl-1-butyne in the presence equimolar amount of nitrobenzene using a) **2** (1 mol %) and b) **2-rGO** (0.5 mol%). Nitrobenzene is not hydrogenated when using precatalyst **2-rGO**.

Recycling studies

The main advantage of immobilization of **2** onto the surface of graphene is to recover and reuse the catalyst in multiple runs. Catalyst stability and recycling properties of the hybrid material **2-rGO** (0.5 mol%) were tested using 1-phenyl-1-butyne as substrate, dry toluene as solvent (2 mL), Cs₂CO₃ as base (10 mol%), H₂ (1 bar) and anisole as an internal standard. In the first run, we observed an induction period of 30 min and the reaction was stopped after 1 h and was analyzed by GC. At this point, we observed 100 % of alkyne conversion, 91 % alkene yield with good selectivity towards Z-alkene (Z/E, 90:10) and low over-reduction (9 %). The solid precatalyst **2-rGO** was removed from the solution by decantation washed with toluene and reused with the addition of fresh substrate, solvent, H₂ and anisole. In the next runs, we did not observe an induction period and the reaction was stopped after 1h. The catalytic active species are formed in the first run and are stabilized by the support. In the absence of the graphene support (precatalyst **2**), the catalytic active species are not stabilised and the catalytic system could not be recycled. The hybrid material **2-rGO** was reused up to ten times without observing a decrease in activity (Figure 4.9 a).

The palladium amount in the filtrate for each run was analyzed by ICP-MS. The results revealed no significant palladium content indicating the absence of palladium leaching. This result was confirmed by analyzing the palladium content in **2-rGO** after the 10th run. Digestion of the solid catalyst and ICP-MS analysis revealed that only 10 wt% of the initial palladium amount is lost by leaching during the ten recycling experiments. The stereoselectivity towards the Z-isomer and the over-reduction alkane product is maintained constant for each run within the experimental error. The results show that immobilization of **2** onto graphene leads to a robust catalytic hybrid material that is highly recyclable.

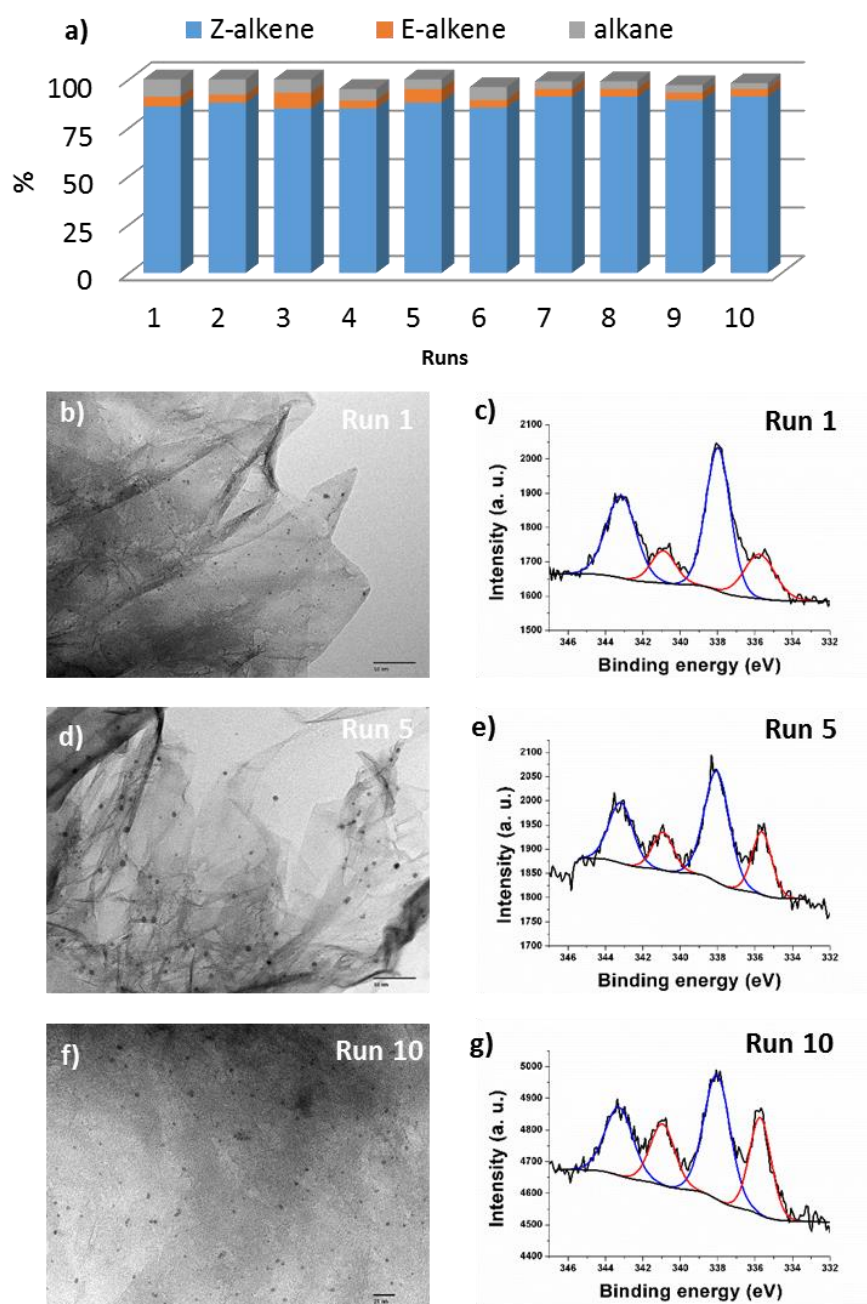


Figure 4.9 Recycling of 2-rGO in the hydrogenation of 1-phenyl-1-butyne with molecular H₂. First run 1.5 h because of the induction time and next runs 1h. (a) HRTEM image after run 1 (b), run 5 (d) and run 10 (f) and the corresponding XPS spectra of runs 1 (c), 5 (e) and 10 (g). Blue line corresponds to the Pd²⁺ core-level peaks 3d and red line corresponds to the core level peaks 3d of Pd⁰.

In order to rationalize the formation and evolution of palladium nanoparticles species we analyzed the nature of the hybrid material **2-rGO** in the recycling experiment. A small sample of the solid catalyst was taken after selected runs and was analyzed by HRTEM and XPS spectroscopy (Figure 4.9). HRTEM images confirmed the presence of palladium nanoparticles in all catalytic runs. The size and morphology of these nanoparticles is preserved during all runs of the recycling experiment. The nanoparticles are spherical with diameters in the range of 2 - 7 nm. XPS analysis confirmed that the palladium nanoparticles are composed of Pd²⁺ and Pd⁰ oxidation states. These palladium nanoparticles are decorated by the presence of NHC and Br⁻ ligands on the surface.⁷²⁻⁷⁶ XPS analysis confirms the presence of these ligands by the assignment of peaks corresponding to the N (400.6 eV) and the Br (68.6 eV). We have observed that the Pd²⁺/Pd⁰ ratio is not constant for all the experiments indicating that palladium is reduced and oxidized during the catalytic hydrogenation reactions. There is a dynamic ligand exchange that alters the surface of the Pd-NPs and in consequence the ratio of Pd²⁺/Pd⁰ oxidation states. There are precedents of dynamic ligand exchange at the surface of metal nanoparticles caused by catalytic transformations.⁷⁷⁻⁸¹ Palladium nanoparticles were further characterized by spherical aberration (C_s) corrected STEM, using a High Angle Annular Dark Field (HAADF) detector. This mode is highly advantageous over conventional TEM as the contrast is dependent on the atomic number of the elements; therefore, heavier atoms will appear much brighter in the images, helping to visualize the metallic species. Samples corresponding to runs 1 and 10 were selected for the evaluation of their morphology and to characterize the evolution of the palladium nanoparticles during the catalytic experiments. The C_s-corrected STEM data showed the presence of small crystalline palladium nanoparticles in the range of 2 up to 15 nm (Figure 4.10). Pd units were always found in the form of Icosahedral (*Ih*) or *fcc* nanoparticles.⁸²⁻⁸⁴ In addition to these entities, bright spots were identified all over the carbon support, which corresponded to cesium in the form of individual atoms. We have not observed the formation of other catalytic active species such as single palladium atoms or clusters. After analyzing the sample in the 10th run, similar conclusions could be obtained as no significant morphological differences are observed between the two materials.

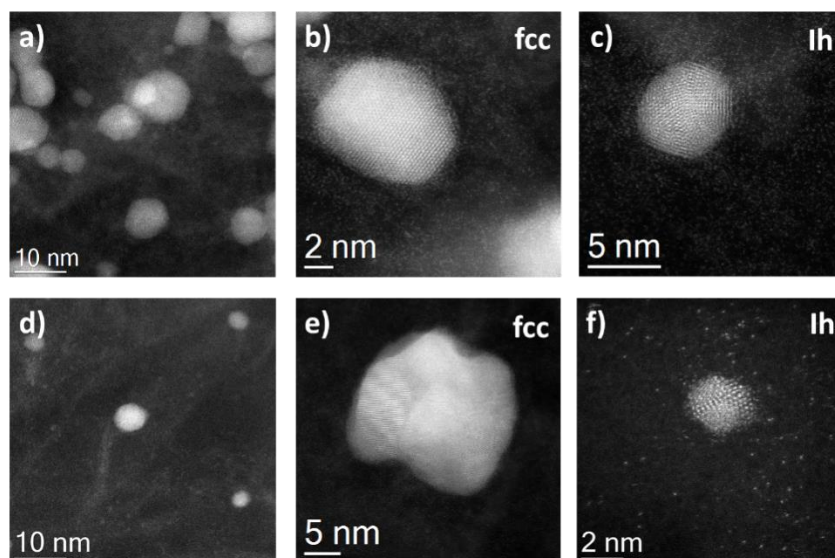


Figure 4.10 C_s -corrected STEM-HAADF images of 2-rGO after one catalytic cycle (a – c) and 10 catalytic cycles (d-f). Zooming of the Pd⁰ NPs show the fcc crystal nature of some of the nps (b and e) and the icosahedral (Ih) structures (c and f).

4.3 CONCLUSIONS

Palladium nanoparticles supported on the surface of reduced graphene oxide have been synthesized by decomposition of well-defined organometallic palladium complexes. XPS analysis reveals that the Pd-NPs are stabilized by the presence of ligands (NHC and Br) and contain palladium in two oxidation states (Pd^{2+} and Pd^0). For comparative purposes, Pd-NPs without the support were synthesized starting from the same organometallic complexes. Characterization by XPS analysis shows similar composition for these NPs in terms of ligands and palladium oxidation states. The catalytic properties in the hydrogenation of alkynes have been evaluated using the free and supported palladium nanoparticles. The results clearly indicate that immobilisation of palladium nanoparticles onto reduced graphene oxide improves the catalytic properties in terms of activity and selectivity. The palladium nanoparticles composition displays a dynamic process during the recycling experiments and different amounts of Pd^{2+} and Pd^0 oxidation states were observed. The support plays a role in the catalytic performance most probably due to stabilization of palladium nanoparticles.

4.4 SUPPORTING INFORMATION

This section contains the most relevant data of the article supporting information. To see the complete version, please visit the article website.

General considerations

Reagents and solvents

Anhydrous solvents were dried using a solvent purification system or purchased from commercial suppliers and stored over molecular sieves.

Instrumentation

Nuclear magnetic resonance (NMR) spectra were recorded on Bruker spectrometers operating at 300 or 400 MHz (^1H NMR) and 75 or 100 MHz ($^{13}\text{C}\{^1\text{H}\}$ NMR), respectively, and referenced to SiMe_4 (δ in ppm and J in Hertz). High-resolution images of transmission electron microscopy HRTEM and high-angle annular dark-field HAADF-STEM images of the samples were obtained using a Jem-2100 LaB6 (JEOL) transmission electron microscope coupled with an INCA Energy TEM 200 (Oxford) energy dispersive X-Ray spectrometer (EDX) operating at 200 kV. Samples were prepared by drying a droplet of a MeOH dispersion on a carbon-coated copper grid. X-ray photoelectron spectra (XPS) were acquired on a Kratos AXIS ultra DLD spectrometer with a monochromatic Al $K\alpha$ X-ray source (1486.6 eV) using a pass energy of 20 eV. To provide a precise energy calibration, the XPS binding energies were referenced to the C1s peak at 284.6 eV. TGA analysis were performed using a TG-STDA Mettler Toledo model TGA/SDTA851e/LF/1600 coupled to a mass spectrometer quadrupole PFEIFFER VACUUM model OmniStar GSD 320 O3, 1-300 um. bearing tungsten filament. Spherical aberration corrected (Cs-corrected) Scanning Transmission Electron Microscopy (STEM) coupled with a High Angle Annular Dark Field (HAADF) detector measurements were performed in a XFEG Titan Low base FEI 300-60 kV, operated at 300 kV. The column was fitted with a CEOS aberration corrector for the electron probe, assuring a point resolution of 0.8 Å for the current accelerating voltage. For spectroscopic analyses, the microscope was also equipped with an EDAX EDS detector and a Gatan Tridiem Energy Filter. Prior observations the sample were dispersed in ethanol and placed onto a holey carbon copper microgrids. Mass spectra were obtained using a QTOF Premier (quadrupole-hexapole-TOF) with an orthogonal Z-spray-electrospray interface (Waters, Manchester, UK). The drying gas as well as nebulizing gas was nitrogen at

a flow of 400 L/h and 80 L/h respectively. The temperature of the source block was set to 120 °C and the desolvation temperature to 150 °C. A capillary voltage of 3.5 KV was used in the positive scan mode and the cone voltage was set to 10 V to control the extent of fragmentation. Mass calibration was performed using a solution of sodium iodide in isopropanol:water (50:50) from m/z 150 to 1000 Da. Sample solutions (ca. 1×10^{-5} M) were infused via syringe pump directly connected to the interface at a flow of 10 $\mu\text{l}/\text{min}$. A 1 $\mu\text{g}/\text{mL}$ solution of Luekine-enkephaline was used as lock mass for accurate m/z determinations. The UV/Vis spectra were recorded between 250 and 600 nm by a Cary 300 Bio UV-Vis Varian spectrophotometer. The samples were suspended in CH_2Cl_2 and sonicated for 5 minutes before the measurements.

Catalysts synthesis

Synthesis of **2**: A Schlenk flask was charged with a mixture of imidazolium salt (400 mg, 0.830 mmol), palladium(II) chloride (134 mg, 0.750 mmol), potassium carbonate (521 mg, 3.77 mmol), sodium bromide (710 mg, 7.5 mmol) and 3-chloropyridine (4 mL) under a nitrogen atmosphere. The resulting suspension was stirred for 19h at 80 °C. The reaction mixture was diluted with CH_2Cl_2 and filtered through silica and celite. The resulting yellow solution was evaporated to dryness. Complex **2** was precipitated with CH_2Cl_2 /hexanes, filtered and dried (Yield. 400 mg, 68 %).

Synthesis of **2-rGO**: A suspension of 180 mg of **rGO** in 100 mL of CH_2Cl_2 was introduced in an ultrasounds bath for 30 min. Then, complex **2** (25 mg, 0,032 mmol) was added to the mixture. The suspension was stirred at room temperature for 16 hours. The black solid was isolated by filtration and washed with CH_2Cl_2 (2 x 15 mL) affording the hybrid material as a black solid. The exact amount of supported complex was determined by ICP-MS analysis. The results accounted for a 5.5 wt% of complex **2** in the hybrid material **2-rGO**.

General procedure for the catalytic hydrogenation of alkynes

In a general catalytic experiment, a 10 mL Schlenk equipped with a stirring bar is charged with 0.3 mmol of alkyne, base (Cs_2CO_3 , 10 mol %), catalyst and 2 mL of dry toluene as solvent. A balloon full of H_2 is connected to the Schlenk. The Schlenk is then introduced in a preheated 65 °C oil bath. Yields and conversions were determined by GC or ^1H NMR analysis using anisole or 1,3,5-trimethoxybenzene as an internal standard.

Complex 2 and hybrid material 2-rGO characterization

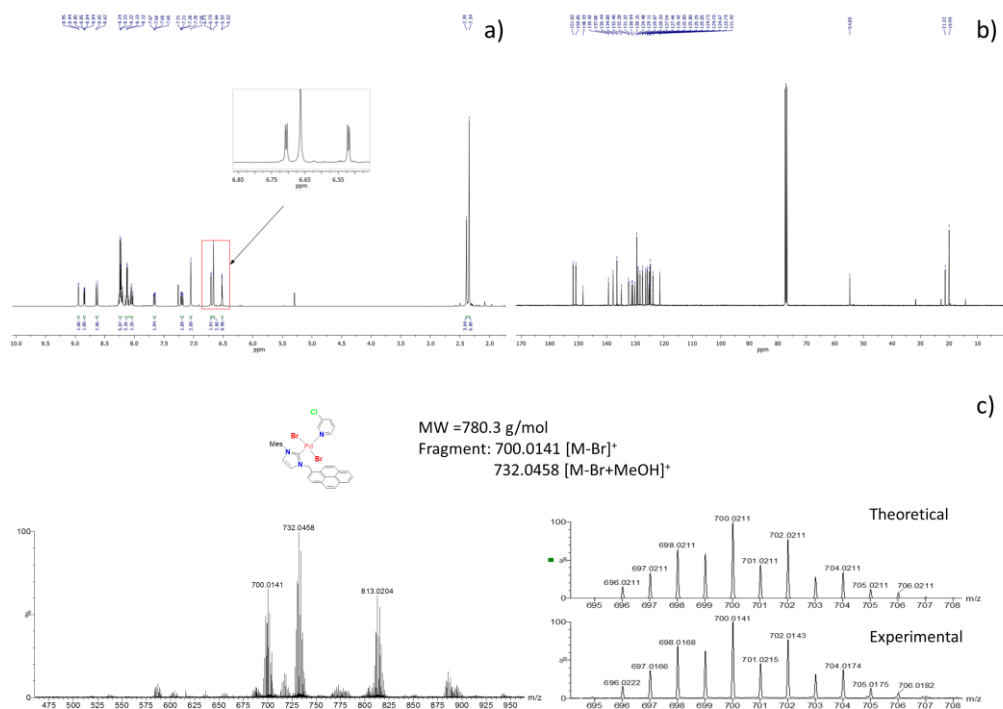


Figure S4.1 ^1H NMR spectrum (a), ^{13}C NMR spectrum (b) and HRMS spectrum (c) of complex 2.

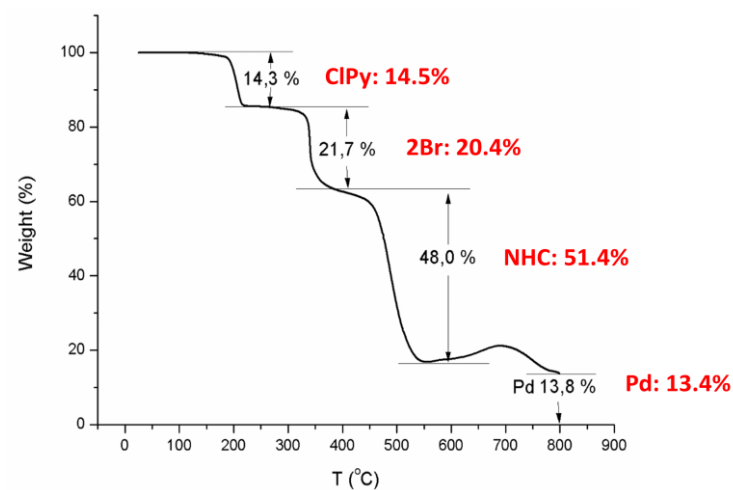


Figure S4.2 Thermogravimetric analysis of complex 2.

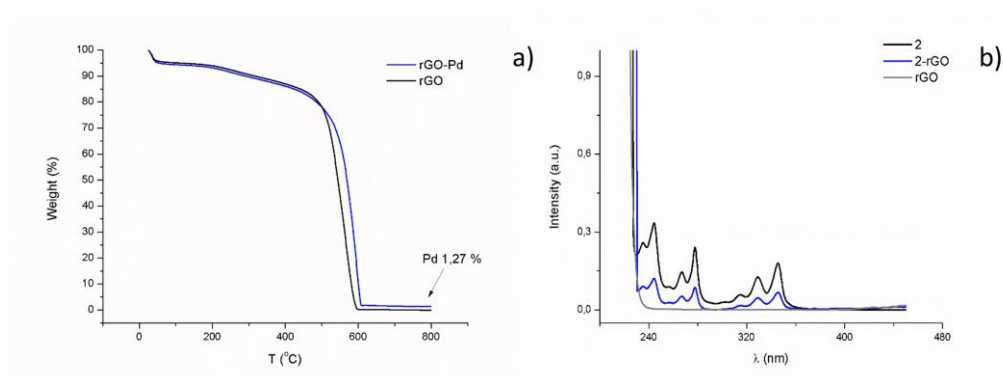


Figure S4.3 Thermogravimetric analysis of **2**-rGO a) and UV-Vis analysis comparison between **2**, **2**-rGO and rGO b).

Poisoning experiments

Poisoning experiments using P4VP (poly(4-vinylpyridine)) as an scavenger of Pd(II) molecular species and the Hg drop test as an scavenger of Pd nanoparticles. Scavengers added after 30 min reaction to assure the formation of the catalytic active species.

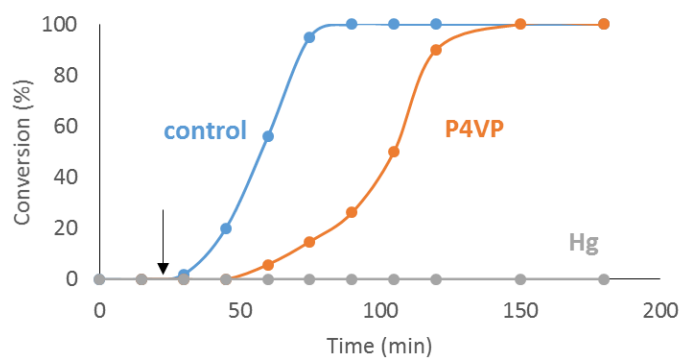
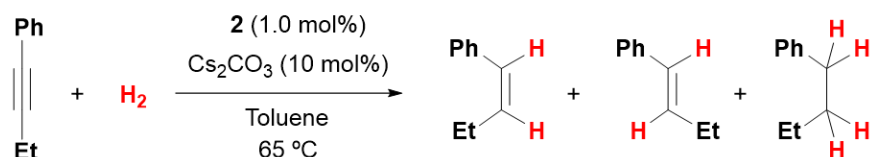


Figure S4.4 Poisoning experiments in the semihydrogenation of alkynes catalysed by **2**. The addition of PVP (poly(4-vinylpyridine)) used as a scavenger of Pd(II) and Hg (Mercury test) used as a scavenger of Pd nanoparticles.

The Maitlis hot filtration test

The Maitlis' test involves the filtration of a part of the catalytic reaction maintaining the reaction conditions and monitoring the reaction time-profile in the remaining solution and the filtrate. No catalytic activity in the filtrate suggests heterogeneous active catalytic species. In the hydrogenation of 1-phenyl-1-butyne with precatalyst **2**, after 1 h reaction (GC conversion 40 %) half of the reaction mixture was filtered off through celite at 65 °C. The filtrate was maintained for 5 h under identical conditions, but GC analysis indicated that no further hydrogenation occurred (GC conversion 40%). On the contrary, the remaining mixture achieved full conversion in 2 h reaction.

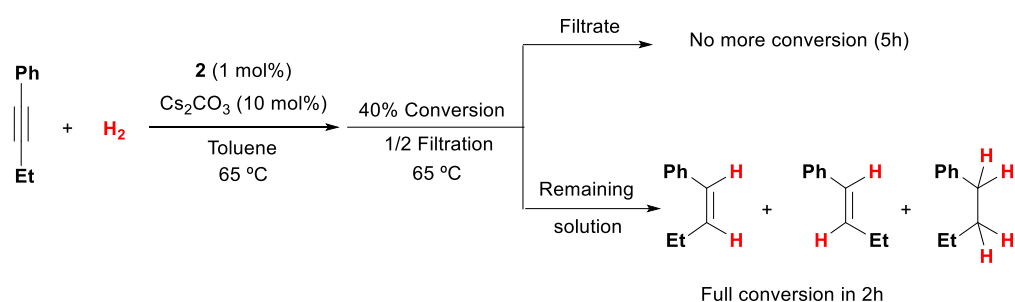
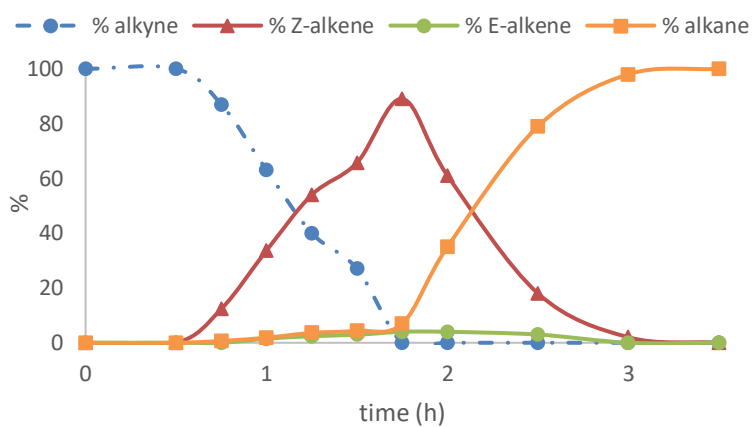
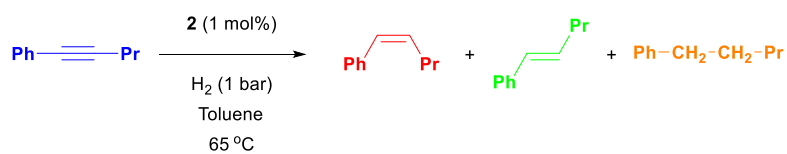
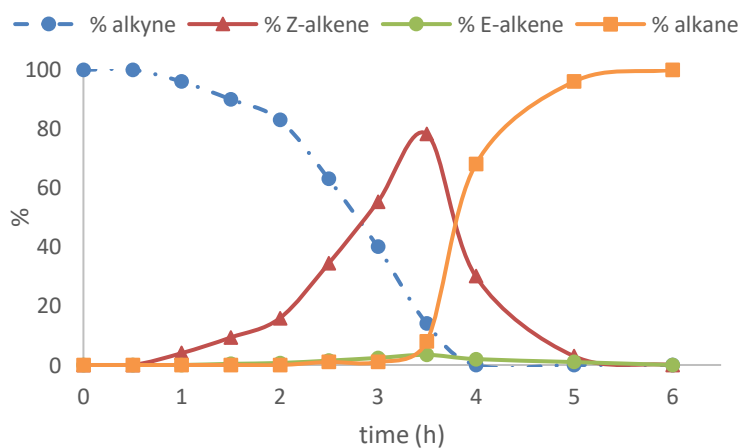
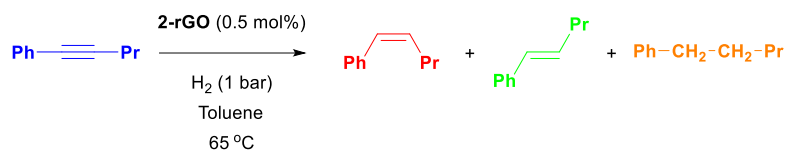


Figure S4.5 Hot filtration experiment in the semihydrogenation of alkynes reaction using **2** as catalyst.

Kinetic analysis of semihydrogenation reaction

Figure S4.6 Hydrogenation of 1-phenyl-1-pentyne with **2** (Table 4.1, entry 3)Figure S4.7 Hydrogenation of 1-phenyl-1-pentyne with **2-rGO** (Table 4.1, entry 4)

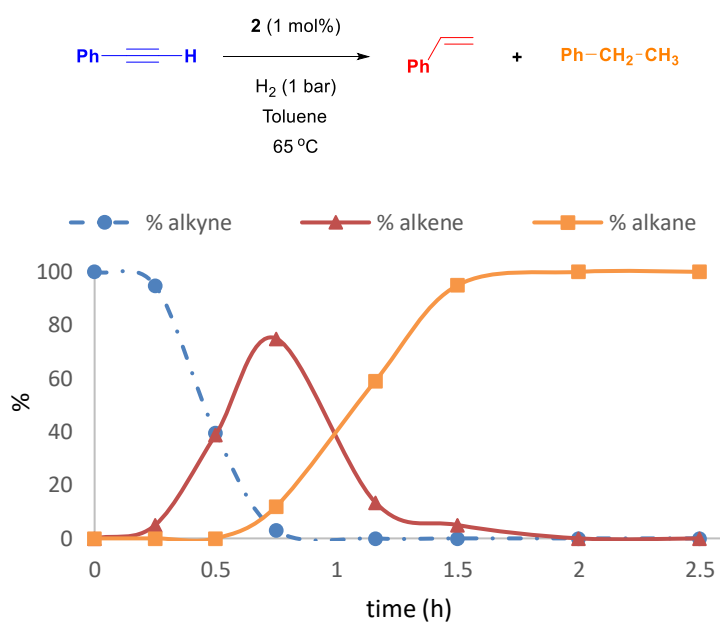


Figure S4.8 Hydrogenation of phenylacetylene with **2** (Table 4.1, entry 9).

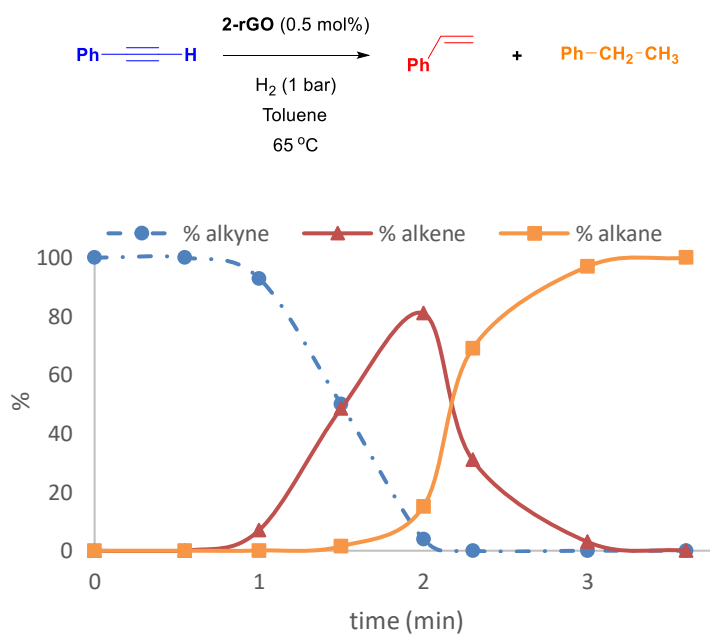


Figure S4.9 Hydrogenation of phenylacetylene with **2-rGO** (Table 4.1, entry 10).

Hydrogenation competitive experiments

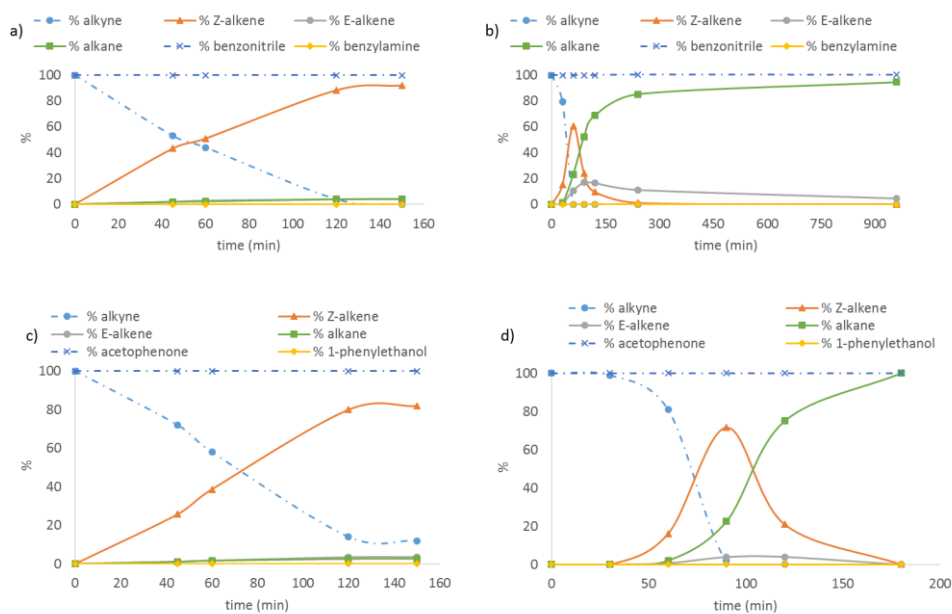


Figure S4.10 Competitive experiment in the hydrogenation of 1-phenyl-1-butyne in the presence equimolar amounts of benzonitrile using catalyst a) **2** (1 mol %) and b) **2-rGO** (0.5 mol%) or acetophenone using catalyst c) **2** (1 mol %) and d) **2-rGO** (0.5 mol%).

4.5 REFERENCES

- (1) Teschner, D.; Borsodi, J.; Wootsch, A.; Revay, Z.; Havecker, M.; Knop-Gericke, A.; Jackson, S. D.; Schlogl, R. *Science* **2008**, *320*, 86–89.
- (2) Fortman, G. C.; Nolan, S. P. *Chem. Soc. Rev.* **2011**, *40*, 5151.
- (3) Beletskaya, I. P.; Cheprakov, A. V. *Chem. Rev.* **2000**, *100*, 3009–3066.
- (4) Johansson Seechurn, C. C. C.; Kitching, M. O.; Colacot, T. J.; Snieckus, V. *Angew. Chem. Int. Ed.* **2012**, *51*, 5062–5085.
- (5) Kantchev, E. A. B.; O'Brien, C. J.; Organ, M. G. *Angew. Chem. Int. Ed.* **2007**, *46*, 2768–2813.
- (6) Sprengers, J. W.; Wassenaar, J.; Clement, N. D.; Cavell, K. J.; Elsevier, C. J. *Angew. Chem. Int. Ed.* **2005**, *44*, 2026–2029.
- (7) Torborg, C.; Beller, M. *Adv. Synth. Catal.* **2009**, *351*, 3027–3043.
- (8) Zapf, A.; Beller, M. *Top. Catal.* **2002**, *19*, 101–109.
- (9) Mata, J. A.; Poyatos, M. *Curr. Org. Chem.* **2011**, *15*, 3309–3324.
- (10) Chun, Y. S.; Shin, J. Y.; Song, C. E.; Lee, S. *Chem. Commun.* **2008**, 7345, 942–944.
- (11) Ott, L. S.; Finke, R. G. *Coord. Chem. Rev.* **2007**, *251*, 1075–1100.
- (12) Astruc, D.; Lu, F.; Aranzaes, J. R. *Angew. Chem. Int. Ed.* **2005**, *44*, 7852–7872.
- (13) Aiken, J. D.; Finke, R. G. *J. Mol. Catal. A Chem.* **1999**, *145*, 1–44.
- (14) Reetz, M. T.; de Vries, J. G. *Chem. Commun.* **2004**, *14*, 1559–1563.
- (15) Górna, M.; Szulmanowicz, M. S.; Gniewek, A.; Tylus, W.; Trzeciak, A. M. *J. Organomet. Chem.* **2015**, *785*, 92–99.
- (16) Ferry, A.; Schaepe, K.; Tegeder, P.; Richter, C.; Chepiga, K. M.; Ravoo, B. J.; Glorius, F. *ACS Catal.* **2015**, *5*, 5414–5420.
- (17) Richter, C.; Schaepe, K.; Glorius, F.; Ravoo, B. J. *Chem. Commun.* **2014**, *50*, 3204–3207.

- (18) Planellas, M.; Pleixats, R.; Shafir, A. *Adv. Synth. Catal.* **2012**, *354*, 651–662.
- (19) Putta, C.; Sharavath, V.; Sarkar, S.; Ghosh, S. *RSC Adv.* **2015**, *5*, 6652–6660.
- (20) Luska, K. L.; Moores, A. *Adv. Synth. Catal.* **2011**, *353*, 3167–3177.
- (21) Pontes da Costa, A.; Nunes, D. R.; Tharaud, M.; Oble, J.; Poli, G.; Rieger, J. P. *ChemCatChem* **2017**, *9*, 2167–2175.
- (22) Narayanan, R.; El-Sayed, M. A. *J. Am. Chem. Soc.* **2003**, *125*, 8340–8347.
- (23) Sankar, M.; Dimitratos, N.; Miedziak, P. J.; Wells, P. P.; Kiely, C. J.; Hutchings, G. J. *Chem. Soc. Rev.* **2012**, *41*, 8099–8139.
- (24) White, R. J.; Luque, R.; Budarin, V. L.; Clark, J. H.; Macquarrie, D. J. Supported Metal Nanoparticles on Porous Materials. Methods and Applications. *Chem. Soc. Rev.* **2009**, *38*, 481–494.
- (25) Gallon, B. J.; Kojima, R. W.; Kaner, R. B.; Diaconescu, P. L. *Angew. Chem. Int. Ed.* **2007**, *46*, 7251–7254.
- (26) Wildgoose, G. G.; Banks, C. E.; Compton, R. G. *Small* **2006**, *2*, 182–193.
- (27) Pachón, L. D.; Rothenberg, G. *Appl. Organomet. Chem.* **2008**, *22*, 288–299.
- (28) Shi, X.; Cai, C. *New J. Chem.* **2018**, *42*, 2364–2367.
- (29) Scheuermann, G. M.; Rumi, L.; Steurer, P.; Bannwarth, W.; Mulhaupt, R. *J. Am. Chem. Soc.* **2009**, *131*, 8262–8270.
- (30) Marion, N.; Nolan, S. P. *Acc. Chem. Res.* **2008**, *41*, 1440–1449.
- (31) Meiries, S.; Le Duc, G.; Chartoire, A.; Collado, A.; Speck, K.; Arachchige, K. S. A.; Slawin, A. M. Z.; Nolan, S. P. *Chem. Eur. J.* **2013**, *19*, 17358–17368.
- (32) Fantasia, S.; Egbert, J. D.; Jurčík, V.; Cazin, C. S. J.; Jacobsen, H.; Cavallo, L.; Heinekey, D. M.; Nolan, S. P. *Angew. Chem. Int. Ed.* **2009**, *48*, 5182–5186.
- (33) Valente, C.; Pompeo, M.; Sayah, M.; Organ, M. G. *Org. Process Res. Dev.* **2014**, *18*, 180–190.
- (34) Sabater, S.; Mata, J. A.; Peris, E. *ACS Catal.* **2014**, *4*, 2038–2047.
- (35) Sabater, S.; Mata, J. A.; Peris, E. *Organometallics* **2015**, *34*, 1186–1190.

- (36) Ventura-Espinosa, D.; Marzá-Beltrán, A.; Mata, J. A. *Chem. Eur. J.* **2016**, *22*, 17758–17766.
- (37) Ventura-Espinosa, D.; Vicent, C.; Baya, M.; Mata, J. A. *Catal. Sci. Technol.* **2016**, *6*, 8024–8035.
- (38) Ventura-Espinosa, D.; Carretero-Cerdán, A.; Baya, M.; García, H.; Mata, J. A. *Chem. Eur. J.* **2017**, *23*, 10815–10821.
- (39) Ventura-Espinosa, D.; Sabater, S.; Carretero-Cerdán, A.; Baya, M.; Mata, J. A. *ACS Catal.* **2018**, *8*, 2558–2566.
- (40) Ventura-Espinosa, D.; Sabater, S.; Mata, J. A. *J. Catal.* **2017**, *352*, 498–504.
- (41) Ruiz-Botella, S.; Peris, E. *Chem. Eur. J.* **2015**, *21*, 15263–15271.
- (42) Lara, P.; Rivada-Wheelaghan, O.; Conejero, S.; Poteau, R.; Philippot, K.; Chaudret, B. *Angew. Chem. Int. Ed.* **2011**, *50*, 12080–12084.
- (43) Dassenoy, F.; Philippot, K.; Ould Ely, T.; Amiens, C.; Lecante, P.; Snoeck, E.; Mosset, A.; Casanove, M.-J.; Chaudret, B. *New J. Chem.* **1998**, *22*, 703–712.
- (44) Pan, C.; Dassenoy, F.; Casanove, M.-J.; Philippot, K.; Amiens, C.; Lecante, P.; Mosset, A.; Chaudret, B. *J. Phys. Chem. B* **1999**, *103*, 10098–10101.
- (45) Ely, T. O.; Pan, C.; Amiens, C.; Chaudret, B.; Dassenoy, F.; Lecante, P.; Casanove, M.-J.; Mosset, A.; Respaud, M.; Broto, J.-M. *J. Phys. Chem. B* **2000**, *104*, 695–702.
- (46) Vidoni, O.; Philippot, K.; Amiens, C.; Chaudret, B.; Balmes, O.; Malm, J.-O.; Bovin, J.-O.; Senocq, F.; Casanove, M.-J. *Angew. Chem. Int. Ed.* **1999**, *38*, 3736–3738.
- (47) Gonzalez-Galvez, D.; Lara, P.; Rivada-Wheelaghan, O.; Conejero, S.; Chaudret, B.; Philippot, K.; van Leeuwen, P. W. N. M. *Catal. Sci. Technol.* **2013**, *3*, 99–105.
- (48) Asensio, J. M.; Tricard, S.; Coppel, Y.; Andrés, R.; Chaudret, B.; de Jesús, E. *Angew. Chem. Int. Ed.* **2017**, *56*, 865–869.
- (49) Asensio, J. M.; Tricard, S.; Coppel, Y.; Andrés, R.; Chaudret, B.; de Jesús, E. N-Heterocyclic Carbenes. *Chem. Eur. J.* **2017**, *23*, 13435–13444.
- (50) Baquero, E. A.; Tricard, S.; Flores, J. C.; de Jesús, E.; Chaudret, B. *Angew. Chem. Int. Ed.* **2014**, *53*, 13220–13224.

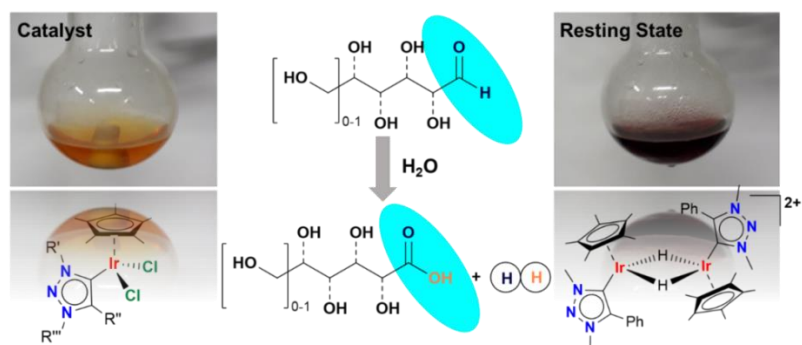
- (51) Baquero, E. A.; Tricard, S.; Coppel, Y.; Flores, J. C.; Chaudret, B.; de Jesús, E. *Dalton Trans.* **2018**, *47*, 4093–4104.
- (52) Canseco-Gonzalez, D.; Gniewek, A.; Szulmanowicz, M.; Müller-Bunz, H.; Trzeciak, A. M.; Albrecht, M. *Chem. Eur. J.* **2012**, *18*, 6055–6062.
- (53) Torres-Mendieta, R.; Ventura-Espinosa, D.; Sabater, S.; Lancis, J.; Mínguez-Vega, G.; Mata, J. A. *Sci. Rep.* **2016**, *6*, 30478.
- (54) Navalon, S.; Dhakshinamoorthy, A.; Alvaro, M.; Garcia, H. *Coord. Chem. Rev.* **2016**, *312*, 99–148.
- (55) Jeon, E. K.; Seo, E.; Lee, E.; Lee, W.; Um, M.-K.; Kim, B.-S. *Chem. Commun.* **2013**, *49*, 3392.
- (56) Johnson, C.; Albrecht, M. Z -Selective Alkyne Semi-Hydrogenation Catalysed by Piano-Stool N -Heterocyclic Carbene Iron Complexes. *Catal. Sci. Technol.* **2018**, *8*, 2779–2783.
- (57) Conley, M. P.; Drost, R. M.; Baffert, M.; Gajan, D.; Elsevier, C.; Franks, W. T.; Oschkinat, H.; Veyre, L.; Zagdoun, A.; Rossini, A. *Chem. Eur. J.* **2013**, *19*, 12234–12238.
- (58) Sluijter, S. N.; Warsink, S.; Lutz, M.; Elsevier, C. J. *Dalton Trans.* **2013**, *42*, 7365–7372.
- (59) Drost, R. M.; Bouwens, T.; van Leest, N. P.; de Bruin, B.; Elsevier, C. J. *ACS Catal.* **2014**, *4*, 1349–1357.
- (60) Hauwert, P.; Boerleider, R.; Warsink, S.; Weigand, J. J.; Elsevier, C. J. *J. Am. Chem. Soc.* **2010**, *132*, 16900–16910.
- (61) Crabtree, R. H. *Chem. Rev.* **2012**, *112*, 1536–1554.
- (62) Drost, R. M.; Rosar, V.; Marta, S. D.; Lutz, M.; Demitri, N.; Milani, B.; de Bruin, B.; Elsevier, C. J. *ChemCatChem* **2015**, *7*, 2095–2107.
- (63) Klingelhöfer, S.; Heitz, W.; Greiner, A.; Oestreich, S.; Förster, S.; Antonietti, M. *J. Am. Chem. Soc.* **1997**, *119*, 10116–10120.
- (64) Foley, P.; DiCosimo, R.; Whitesides, G. M. *J. Am. Chem. Soc.* **1980**, *102*, 6713–6725.
- (65) Weck, M.; Jones, C. W. *Inorg. Chem.* **2007**, *46*, 1865–1875.
- (66) Richardson, J. M.; Jones, C. W. *Adv. Synth. Catal.* **2006**, *348*, 1207–1216.

- (67) Phan, N. T. S.; Van Der Sluys, M.; Jones, C. W. *Adv. Synth. Catal.* **2006**, *348*, 609–679.
- (68) Samantaray, M. K.; Alauzun, J.; Gajan, D.; Kavitate, S.; Mehdi, A.; Veyre, L.; Lelli, M.; Lesage, A.; Emsley, L.; Copéret, C. *J. Am. Chem. Soc.* **2013**, *135*, 3193–3199.
- (69) Maishal, T. K.; Alauzun, J.; Basset, J.-M.; Copéret, C.; Corriu, R. J. P.; Jeanneau, E.; Mehdi, A.; Reyé, C.; Veyre, L.; Thieuleux, C. *Angew. Chem. Int. Ed.* **2008**, *47*, 8654–8656.
- (70) Conley, M. P.; Copéret, C. *Top. Catal.* **2014**, *57*, 843–851.
- (71) Copéret, C.; Comas-Vives, A.; Conley, M. P.; Estes, D. P.; Fedorov, A.; Mougél, V.; Nagae, H.; Núñez-Zarur, F.; Zhizhko, P. A. *Chem. Rev.* **2016**, *116*, 323–421.
- (72) Dupont, J.; Scholten, J. D. *Chem. Soc. Rev.* **2010**, *39*, 1780–1804.
- (73) Migowski, P.; Dupont, J. *Chem. Eur. J.* **2007**, *13*, 32–39.
- (74) Scholten, J. D.; Leal, B. C.; Dupont, J. *ACS Catal.* **2012**, *2*, 184–200.
- (75) Cassol, C. C.; Umpierre, A. P.; Machado, G.; Wolke, S. I.; Dupont, J. *J. Am. Chem. Soc.* **2005**, *127*, 3298–3299.
- (76) Umpierre, A. P.; Machado, G.; Fecher, G. H.; Morais, J.; Dupont, J. *Adv. Synth. Catal.* **2005**, *347*, 1404–1412.
- (77) Pan, C.; Pelzer, K.; Philippot, K.; Chaudret, B.; Dassenoy, F.; Lecante, P.; Casanove, M.J. *J. Am. Chem. Soc.* **2001**, *123*, 7584–7593.
- (78) Eremin, D. B.; Ananikov, V. P. *Coord. Chem. Rev.* **2017**, *346*, 2–19.
- (79) Astakhov, A. V.; Khazipov, O. V.; Chernenko, A. Y.; Pasyukov, D. V.; Kashin, A. S.; Gordeev, E. G.; Khrustalev, V. N.; Chernyshev, V. M.; Ananikov, V. P. *Organometallics* **2017**, *36*, 1981–1992.
- (80) Khazipov, O. V.; Shevchenko, M. A.; Chernenko, A. Y.; Astakhov, A. V.; Pasyukov, D. V.; Eremin, D. B.; Zubavichus, Y. V.; Khrustalev, V. N.; Chernyshev, V. M.; Ananikov, V. P. *Organometallics* **2018**, *37*, 1483–1492.
- (81) Yakukhnov, S. A.; Pentsak, E. O.; Galkin, K. I.; Mironenko, R. M.; Drozdov, V. A.; Likholobov, V. A.; Ananikov, V. P. *ChemCatChem* **2018**, *10*, 1869–1873.
- (82) Wang, X.; Choi, S.-I.; Roling, L. T.; Luo, M.; Ma, C.; Zhang, L.; Chi, M.; Liu, J.; Xie, Z.; Herron, J. A. *Nat. Commun.* **2015**, *6*, 7594–7604.

- (83) Li, C.; Sato, R.; Kanehara, M.; Zeng, H.; Bando, Y.; Teranishi, T. S. *Angew. Chem. Int. Ed.* **2009**, *48*, 6883–6887.
- (84) Xing, X.; Hermann, A.; Kuang, X.; Ju, M.; Lu, C.; Jin, Y.; Xia, X.; Maroulis, G. *Sci. Rep.* **2016**, *6*, 19656.

CHAPTER 5:

Selective conversion of various monosaccharaides into sugar acids by additive-free dehydrogenation in water



ABSTRACT

Abundant sugars of five and six carbon atoms are promising candidates for the production of valuable platform chemicals. In this chapter, we describe the catalytic dehydrogenation of several pentoses and hexoses into their corresponding sugar acids with the concomitant formation of molecular hydrogen (H₂). This biomass transformation is promoted by highly active and selective catalysts based on iridium(III) complexes containing a 1,2,3-triazolylidene (trz) as ligand. Monosaccharides are converted into sugar acids in an easy and sustainable manner using only catalyst and water, and in contrast to previously reported procedures, in the absence of any additive. The reaction is therefore very clean, and moreover highly selective, which avoids the tedious purification and product separation. Mechanistic investigations using ¹H NMR and UV-vis spectroscopies and ESI mass spectrometry (ESI-MS) indicates the formation of an unprecedented diiridium-hydride as dormant species that correspond to the catalyst resting state.

ChemCatChem. **2020**, *12*, 376-3752 (DOI: 10.1002/cctc.202000544)

5.1 INTRODUCTION

Biomass represents an abundant and natural renewable feedstock for the preparation of initial platform chemicals.¹⁻⁴ The growing interest in the production of bio-sourced chemicals lies in the circular character of carbon which represents a neutral carbon process. Replacing the use of fossil fuels with transformation of biomass is a major challenge for reduction of global CO₂ emissions.⁵⁻⁹ The initial platform chemicals obtained from biomass are sustainable intermediates for the production of specific chemicals.¹⁰⁻¹³ Carbohydrates are abundant in nature and constitute one of the major components of plant biomass.^{14,15} Among them, monosaccharides of five and six carbon rings are the basic units of cellulose and hemicellulose. Conversion of these sugars, particularly D-Glucose and D-Xylose, represents an interesting biomass source for the preparation of initial platform chemicals.¹⁶⁻²⁰ Oxidation of sugars into the corresponding sugar acids produces useful chemical intermediates with applications in food, pharmaceutical and other specific industries. Traditionally, oxidation of sugars is carried out by enzymatic or heterogeneous catalysts.^{21,22} The main limitation for these approaches is a rigorous control of the reaction conditions to avoid pH variations, oxygen pressure and stability of the natural catalysts. For the conversion of sugars, there is a need to develop selective transformations avoiding tedious separation or purification techniques. Unsurprisingly, therefore, most catalysts for the conversion of carbohydrates is restricted to materials and enzymes. The use of homogeneous catalysts for the conversion of sugars is scarce even though these types of catalysts generally lead to highly selective transformations.^{23,24} One of the reasons for this underdeveloped chemistry is the frequently found poor stability and solubility of well-defined organometallic species in aqueous media. However, recent developments have indicated substantial progress of organometallic chemistry in water,²⁵⁻²⁸ thus providing new opportunities for biomass transformation in aqueous media with homogeneous catalysts.

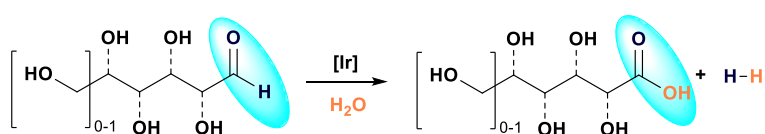


Figure 5.1 Selective dehydrogenation of sugars into sugar acids without additives.

Prompted by this expansion of organometallic chemistry into aqueous media, we decided to explore the potential of iridium complexes as homogeneous catalysts for the conversion of glucose. In a preliminary work, we demonstrated the formation of gluconic acid using homogeneous Cp*Ir complexes with imidazole-based N-heterocyclic carbene (NHC) ligands.²⁹ This transformation is formally an oxidation of glucose but is better described as a dehydrogenative coupling of glucose and water with the simultaneous formation of molecular hydrogen (H₂). Starting from glucose, the process is highly selective towards the formation of gluconic acid but requires strong acidic conditions. In this context, modulation of well-defined organometallic species with suitable ligands offers an attractive methodology to increase activity and selectivity in the activation of functional groups. Here, we demonstrate that the introduction of 1,2,3-triazolydene (trz) ligands induces a substantial improvement of the catalytic properties of these iridium complexes in the conversion of sugars into sugar acids (Figure 5.1). The enhanced catalytic competence allows to omit the harsh acid additives and significantly broadens the substrate scope to efficient dehydrogenative coupling of other carbohydrates. Moreover, this approach provided relevant mechanistic insights into this transformation.

5.2 RESULTS AND DISCUSSION

Catalytic studies

The catalytic conversion of sugars into sugar acids was tested using a series of Cp*Ir(carbene)Cl₂ complexes containing different carbene ligands (Figure 5.2). Complex **3**, containing an Arduengo-type N-heterocyclic carbene ligand (NHC), was used for comparative purposes. Complexes **4-6** contain a triazole-derived ligand with different substituents that modulate the electronic and the steric properties. The 1,2,3-triazolylidene ligands do not possess a neutral resonance structure and are therefore more polar. Moreover, iridium-(trz) complexes were observed to be highly water-soluble,^{30,31} which may be due in parts to the polar structure, and in other parts due the presence of a backbone nitrogen for potential hydrogen bonding.³² Complex **6** contains a carbohydrate wingtip group which has been introduced to probe whether hydrogen bonding to sugar substrates favours the catalytic process.

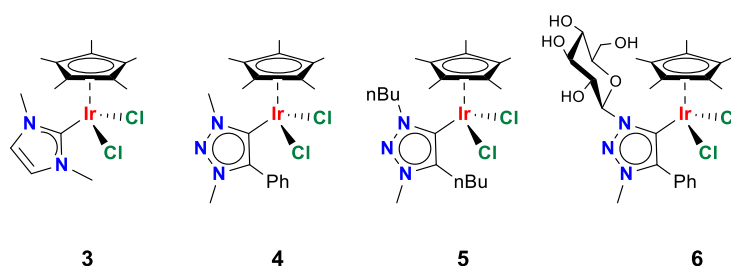


Figure 5.2 Iridium complexes used in the catalytic dehydrogenation of sugars featuring an NHC ligand (**3**) and 1,2,3- triazolylidene (trz) ligands (**4-6**), respectively.

In a first set of experiments, we evaluated the catalytic activity of complexes **4-6** in the conversion of glucose to gluconic acid. The experimental set-up consists of the addition of the iridium complex to a solution of glucose in deionised water. The mixture is heated to reflux and the progress of the reaction and selectivity is monitored by NMR spectroscopy and HPLC chromatography. As a representative example, the reaction progress for the conversion of glucose to gluconic acid was profiled using complex **4** as catalyst precursor (Figure 5.3 a). The mass balance confirms that all glucose is converted to gluconic acid. Product analysis by NMR spectroscopy and MS does not show the formation of any other by-products. Interestingly, and contrary to our previous observations using complex **3**, complex **4** performs better without additives. A >90% conversion of glucose is observed

without the addition of H_2SO_4 after 7.5h. In contrast, the addition of acid (0.25 equiv.) reduced the conversion to 65% (Figure 5.3 b).

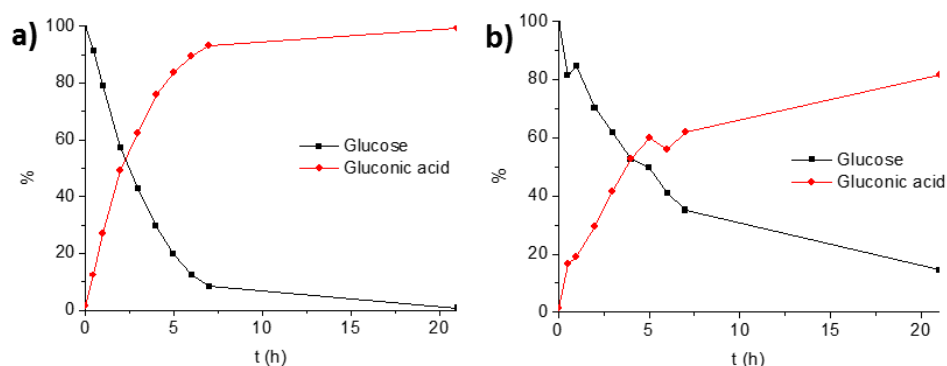
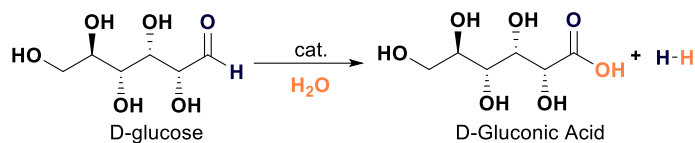


Figure 5.3 Reaction profile monitored by HPLC-MS/MS of glucose conversion (black squares) and gluconic acid formation (red diamonds) using catalytic quantities of complex **4** (2 mol%) at 110 °C (bath temperature). Glucose (0.44 mmol) in 5 mL H_2O : without additives (a) and with 0.25 eq. of H_2SO_4 (b).

These results prompted us to study the catalytic activity of **3-6** in the conversion of glucose to gluconic acid with and without additives (Table 5.1). Control experiments revealed that the presence of iridium complexes is required for the production of gluconic acid and hydrogen. We have not observed uncatalysed sugar degradation under neutral or acidic conditions at 110 °C (Table 5.1, entry 1). Monitoring substrate conversion over time using catalyst **6** showed high initial rates that, however, rapidly slowed down. This is an indication of catalyst deactivation by limited stability (Figures S5.1 and S5.2). In order to study the process of catalyst deactivation we performed thermal stability tests by ^1H NMR spectroscopy. Solutions of complex **4** and **5** in D_2O (10 mM) are stable at 100 °C for at least 2 h without noticeable decomposition whereas complex **6** completely decomposes under these conditions into undefined products. Reducing the temperature to 80 °C increases stability and we have not observed degradation for up to 1 h. These results show that catalyst **4** and **5** containing alkyl or aryl N-substituents are stable at the optimal catalytic conditions but catalyst **6** decomposes rapidly, which accounts for the drop of the catalytic activity for this complex. Conversion of glucose at lower temperatures (80 °C) is feasible, though requiring longer reaction times to achieve full conversion (Table 5.1, entry 6).

Table 5.1 Glucose dehydrogenation using catalyst **3-6**

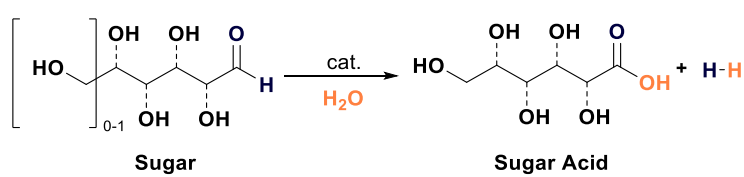


Entry	Cat	Additive H ₂ SO ₄ (Eq.)	T (°C)	Conv (%) ^a	Yield (%) ^a
1	-	-	110	-	-
2^b	3	-	110	44	44
3^b	3	0.25	110	100	88
4	4	-	110	100	100
5	4	0.25	110	81	81
6	4	-	80	90	71
7	5	-	110	65	65
8	6	-	110	35	33
9	6	0.25	110	51	45

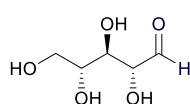
Reaction conditions: Glucose (80 mg, 0.44 mmol), catalyst loading (2 mol%), deionised H₂O (5 mL) for 20h. [a] Conversions and yields determined by ¹H NMR spectroscopy and HPLC-MS/MS. [b] Data from reference 29.

In view of the excellent conversion of glucose to gluconic acid by dehydrogenation we decided to explore the catalytic activity of complexes **3–6** towards other C5 and C6 sugars (Figure 5.4). A range of pentoses (D-ribose, D-xylose and L-arabinose), hexoses (D-mannose and D-galactose) as well as 2-deoxy-D-glucose are converted in water to the corresponding sugar acids by dehydrogenation with the formation of molecular hydrogen (H₂). The formation of H₂ was qualitatively analysed by gas chromatography using a TCD detector. The set-up for the catalytic experiments only requires the addition of the catalysts into an aqueous solution of the carbohydrate. However, it is important to note that the reaction mixture should be maintained under constant reflux in an open system, since the continuous release of hydrogen gas from the reaction mixture facilitates conversion to the sugar. The reaction is not sensitive to the presence of oxygen indicating the high stability of catalysts under the reaction conditions. Catalysts **3–5** are highly active in the production of sugar acids, the isolated yields are >90% in most cases. As noted for glucose conversion, complex **3** requires the addition of additives for better catalytic performance, which compromises yields to some extent. In contrast, no additives are necessary when employing complexes **4** and **5** containing a 1,2,3-triazolylidene ligand, and isolation

of the product is therefore particularly simple. Analysis of the crude product by ^1H NMR spectroscopy revealed highly selective oxidation of the C1 position and clean formation of the corresponding sugar acids and therefore, no further purification was required (Figure S5.3 to Figure S5.6). Of note, product analysis in the case of D-glucose or D-xylose by NMR spectroscopy under neutral or acidic conditions is complicated by the presence of different species due to the acid/base equilibria coupled with partial lactonisation. However, in basic media, these equilibria are shifted and only one set of signals is observed.

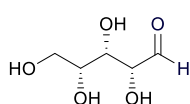


Cat X: Conversion (Yield)



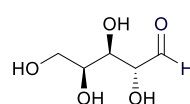
D-xylose

Cat 3*: 100% (80%)
 Cat 4: 99% (98%)
 Cat 5: 99% (99%)



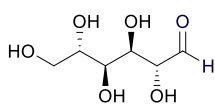
D-ribose

Cat 3*: 100% (87%)
 Cat 4: 100% (93%)
 Cat 5: 100% (95%)



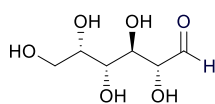
D-Arabinose

Cat 3*: 100% (91%)
 Cat 4: 100% (91%)
 Cat 5: 100% (91%)



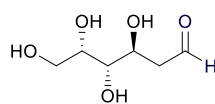
D-Galactose

Cat 3*: 100% (92%)
 Cat 4: 100% (94%)
 Cat 5: 98% (85%)



D-glucose

Cat 3*: 100% (88%)
 Cat 4: 100% (100%)
 Cat 5: 65% (65%)



2-Deoxy-D-glucose

Cat 3*: 100% (87%)
 Cat 4: 99% (90%)
 Cat 5: 99% (92%)

Figure 5.4 Reaction scope using catalyst **3**, **4** and **5**. Reaction conditions: Sugar (0.44 mmol), catalyst loading (2 mol%), deionised H_2O (5 mL) at 110 °C for 20h. Conversions and yields determined by ^1H NMR spectroscopy and HPLC-MS/MS for selected experiments. *Additive 0.25 eq. of H_2SO_4 .

Monitoring of the reaction progress was performed by ^1H NMR spectroscopy, using L-arabinose as a model substrate with catalyst **4** (Figure 5.5). The results show that the conversion of L-arabinose into L-arabinoic acid is very fast at the initial stages and then slows down and proceeds slowly. For instance, yields are higher than 50% after 4 h and after 8 h the yields are close to 80%. This is the general trend observed in the conversion of all the sugars tested either by ^1H NMR spectroscopy (Figure 5.5) or HPLC/MS (Figure 5.3) suggesting a first order reaction in catalyst.

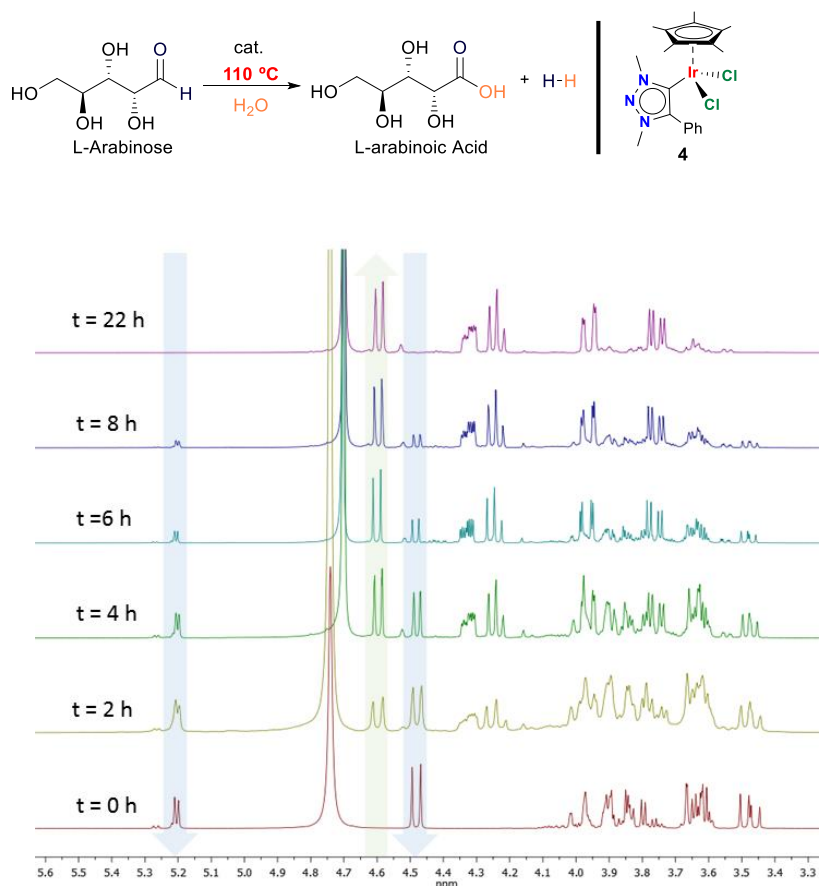
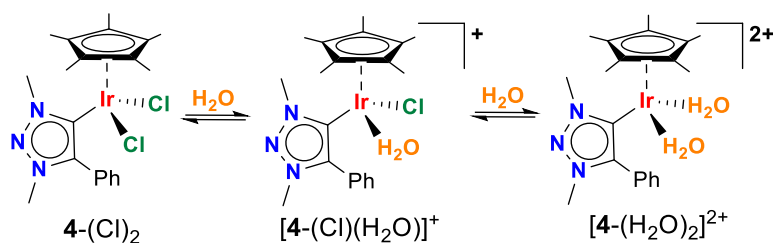


Figure 5.5 Time-resolved conversion monitored by ^1H NMR spectroscopy. L-Arabinose (0.44 mmol) conversion into L-Arabinoic acid using catalyst **4** (2 mol%) without additives in H_2O (5 mL). Samples were taken at appropriate time, dried under reduced pressure and dissolved in D_2O for NMR analysis. Signals highlighted in green are diagnostic for determining yields, and resonances highlighted in blue for conversions.

Mechanistic investigations

In order to gain mechanistic insight into the conversion of sugars we first addressed the chemical speciation of iridium complexes in water using pre-catalyst **4** as representative complex. Catalyst **4** is soluble in water and forms an orange solution. The solubility of **4** in water is promoted by the polar nature of the 1,2,3-triazolylidene ligand and a facile chloride-water ligand exchange at iridium (Scheme 5.1) as identified by the chemical speciation determined from ESI-MS and NMR spectroscopy.³³ Aqueous solutions of **4** were stirred and aliquots were extracted at different time intervals, diluted with water to a final concentration of 5×10^{-4} M (based on the initial Ir concentration), and directly introduced to the mass spectrometer. The ESI-MS of **4** in water (Figure 5.6) shows two intense signals containing the hydroxo-ligated species $[\text{Cp}^*\text{Ir}(\text{trz})(\text{OH})]^+$ (m/z 518.2) and $[\text{Cp}^*\text{Ir}(\text{trz})(\text{OH})(\text{H}_2\text{O})]^+$ at m/z 536.2, the latter coexisting with $[\text{Cp}^*\text{Ir}(\text{trz})\text{Cl}]^+$. Even though species $[\text{Cp}^*\text{Ir}(\text{trz})(\text{OH})(\text{H}_2\text{O})]^+$ and $[\text{Cp}^*\text{Ir}(\text{trz})\text{Cl}]^+$ overlap in the MS, they could be unambiguously identified on the basis of their distinctive collision induced dissociation (CID) spectra (Figure S5.7). In the lower m/z region, we also observed doubly-charged species of formula $[\text{Cp}^*\text{Ir}(\text{trz})]^{2+}$ (m/z 250.6, not shown) attributed to the generation of the diaqua complex $[\text{Cp}^*\text{Ir}(\text{trz})(\text{H}_2\text{O})_2]^{2+}$ containing labile H_2O ligands that are removed upon ionisation under ESI conditions.



Scheme 5.1 Equilibrium of complex **4** in water.

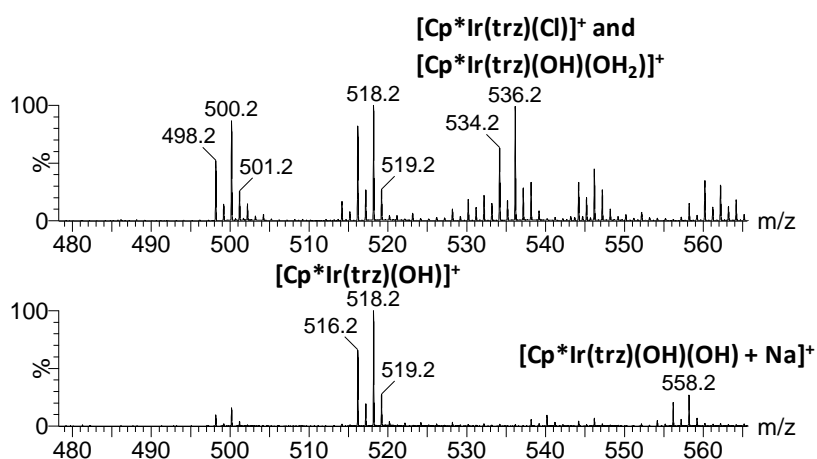


Figure 5.6 ESI mass spectra of complex **4** recorded in water (top) and water with NaOH 10^{-3} M (bottom). The peak at m/z 500.2 is attributed to a product ion from species at m/z 518.2 and 536.2.

Further support for the solvolysis equilibrium depicted in Scheme 5.1 is provided by recording the ESI-MS of **4** at higher pH. Under these conditions, it is expected that iridium-bound water molecules in complexes $[\text{Cp}^*\text{Ir}(\text{trz})(\text{H}_2\text{O})_2]^{2+}$ are deprotonated to hydroxo ligands which are not removed under positive-mode ESI conditions. Figure 5.6 displays the ESI mass spectrum of aqueous solutions in the presence of NaOH (10^{-3} M solution). Species $[\text{Cp}^*\text{Ir}(\text{trz})(\text{OH})]^+$ (m/z 518.2) and $[\text{Cp}^*\text{Ir}(\text{trz})(\text{OH})_2 + \text{Na}]^+$ (m/z 558.2) were detected by their m/z values, isotopic composition and CID spectra (Figures S5.8 and S5.9). Analysis of this solvolysis equilibrium by ^1H NMR spectroscopy using complex **4** in D_2O , revealed the presence of a single set of signals for the Cp^* and the 1,2,3-triazolylidene ligand, which is consistent with fast equilibria on the NMR time scale.

Furthermore, we monitored the progress of the catalytic conversion of sugars by NMR and UV/Vis spectroscopies and by ESI-MS. The combination of these orthogonal techniques provides insights into the identity of intermediate species relevant to the mechanism.^{34,35} Notably, the conversion of sugars is accompanied by a diagnostic change of colour of the reaction solution from orange to deep-red when using complexes **3-5**. The deep-red colour is formed at initial stages and maintained during the entire catalytic reaction. This change in colour was analysed in more detail using L-arabinose as model substrate and complex **4** as the pre-catalyst

(Figures 5.7a and 5.7b). The initially orange colour originates from two broad absorptions at 340 nm and about 400 nm, the latter observed only as a shoulder. The spectrum of the deep-red coloured solution during conversion of L-arabinose features two distinct absorption bands at 445 and 545 nm. Monitoring the reaction by ESI-MS revealed a signal at m/z 501.2, which is maintained during the course of the reaction. The mass/charge value and the simulated isotopic pattern distribution support the formation of a dicationic diiridium-hydride species (Figure 5.7d). Other signals confirmed the reaction progress as indicated by the observation of signals corresponding to deprotonated arabinic acid-bound complex formulated as $[\text{Cp}^*\text{Ir}(\text{trz})(\text{C}_5\text{O}_6\text{H}_9)]^+$ at m/z 666.2 (Figure 5.7d) and in the negative scan mode the signal attributed to deprotonated arabinic acid at m/z 165. The presence of a hydride species was further confirmed by monitoring the catalytic reaction by ^1H NMR spectroscopy using L-arabinose and 10 mol% of pre-catalyst **4**. The spectra showed a characteristic signal in the hydride region at -16.8 ppm, integrating for two hydrogen nuclei. Based on these data and the ESI-MS analysis, we postulate a dimetallic species **7** as intermediate with molecular formula $[\text{Cp}^*(\text{trz})\text{Ir}(\mu\text{-H})_2\text{Ir}(\text{trz})\text{Cp}^*]^{2+}$, which contains two $[\text{Cp}^*\text{Ir}(\text{trz})]$ fragments bridged by two hydride ligands. Similar diiridium-hydride species have been described before using N-heterocyclic carbene ligands.^{36,37} In order to further characterise this species, we synthesised the diiridium-hydride complex **7** as a triflate salt starting from **4** by chloride abstraction and exposure to H_2 (Figure S5.10 and S5.11). Characterisation by ESI-MS and ^1H NMR spectroscopy showed the same ion fragment (m/z 501.2) and isotopic distribution and a hydride resonance at -16.8 ppm, in excellent agreement with the data of the intermediate formed during the catalytic reaction. The molecular structure of complex **7** was unambiguously elucidated by single crystal X-ray diffraction (Figure 5.7c). Most strikingly, the isolated complex **7** is catalytically competent in the dehydrogenative transformation of L-arabinose and achieves activity comparable to those observed with complex **4**, suggesting an identical or at least closely related catalytically active species. In addition, the UV/Vis spectrum of **7** in water shows two characteristic bands at 445 and 545 nm, commensurate with the diagnostic features of the catalytic solution (Figure 5.8, see also discussion above). These data therefore suggest that the diiridium-hydride complex **7** is a relevant species in the reaction mechanism as an off-cycle catalyst resting state. Most probably, cleavage of the diiridium-hydride species provides an iridium monohydride intermediate, which can bind the carbohydrate or water and subsequently release a carbohydrate/water proton and the metal-bound hydride as H_2 .

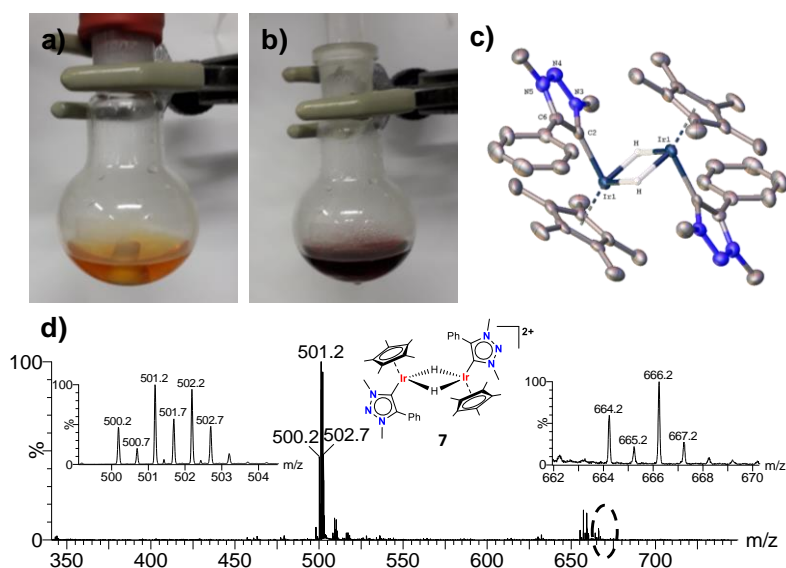


Figure 5.7 Initial orange solution in H₂O of L-arabinose with catalyst **4** (a) and characteristic deep-red solution after 30 min. at 110 °C (b). ORTEP structure from single crystal X-ray diffraction of complex **7** (hydrogen atoms except hydrides and counterions (**4** CF₃SO₃⁻) omitted for clarity). (c) ESI-MS of the deep-red solution showing a base peak at 501.2 m/z that fits with [Cp*(trz)Ir(μ-H)₂Ir(trz)Cp*]²⁺ and a minor peak (m/z 666.2) due to the deprotonated arabinic acid-bound complex formulated as [Cp*Ir(trz)(C₅O₆H₉)]⁺(d).

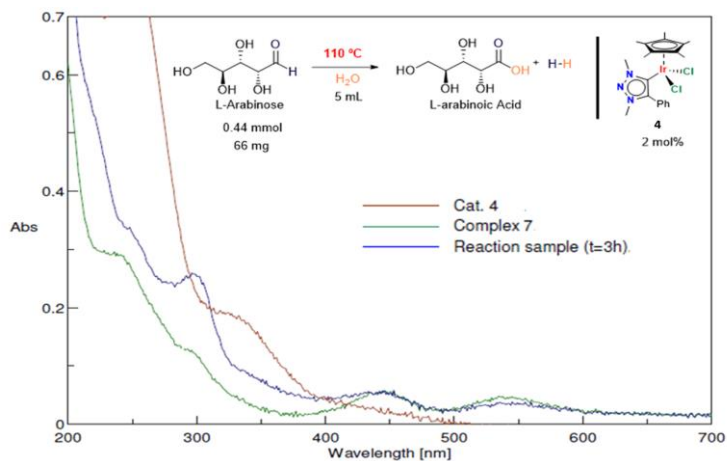
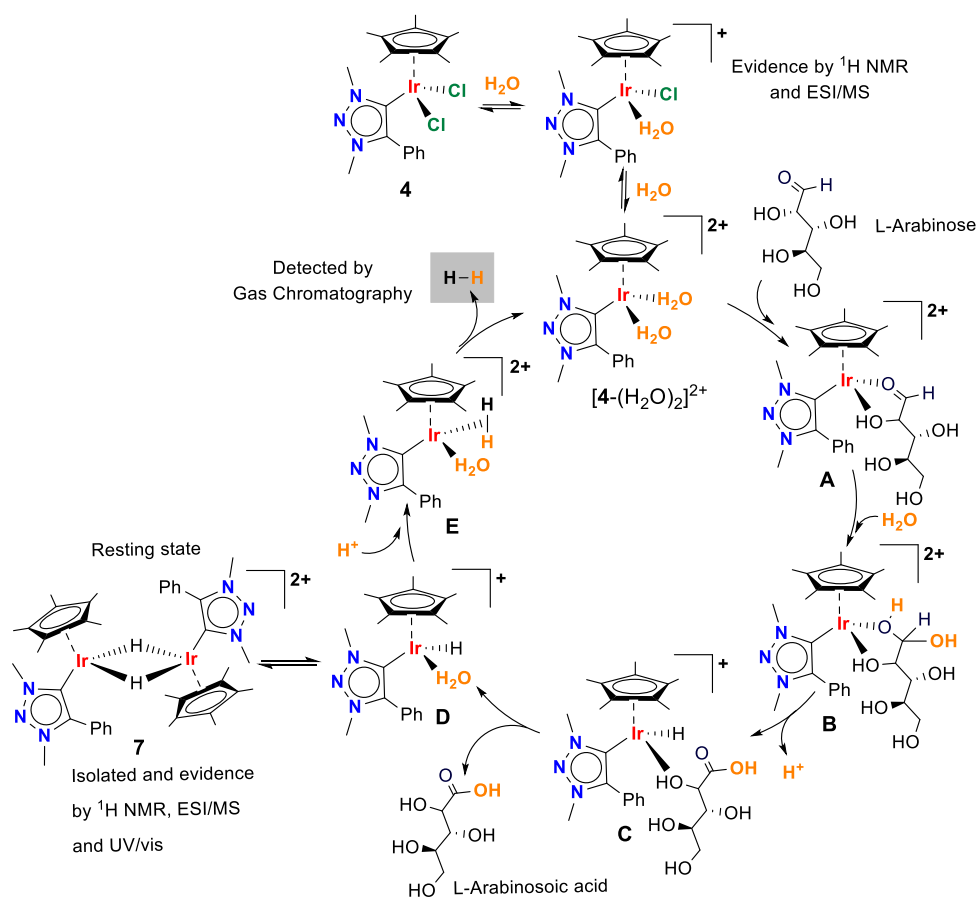


Figure 5.8 UV/vis spectra of the solutions (H₂O) from the catalytic conversion of L-arabinose. The bands at 445 nm and 545 nm are identical for the catalytic reaction (blue line) and for the independently prepared diiridium-hydride species **7** (green line).

A plausible mechanism for the conversion of sugars into sugar acids is proposed based on previous results²⁹ and complemented by the new experimental evidence from this work (Scheme 5.2). Iridium complexes of general formula $[\text{Cp}^*\text{IrL}(\text{Cl})_2]$ ($\text{L} = \text{NHC}$ or triazolylidene) undergo water/halide ligand exchange forming the aqua complexes that are the active catalytic species (Scheme 5.1). The labile H_2O ligands are substituted by L-arabinose most probably in a chelate coordination via the carbonyl and a hydroxyl group (A). Such chelation may rationalise the selectivity of the oxidation, which does not affect any of the primary or secondary alcohol units. Intermediate (A) featuring 1,2,3-triazolylidene as ancillary ligand was not observed by ESI-MS; however, for the NHC pre-catalyst **3** and glucose, intermediate (A) was readily observed. The enhanced stability of the sugar-bound intermediate (A) in the case of the NHC-based catalyst correlates with the reduced catalytic activity of this complex towards the sugar acid formation.³⁸ The coordinated L-arabinose undergoes nucleophilic attack by water at the aldehyde, producing a gem-diol species (B). These species have been postulated as key intermediates in the conversion of alcohols or aldehydes to carboxylic acids or esters in aqueous media.³⁹⁻⁴⁸ The gem-diol species releases a solvated proton, forms an iridium-hydride by β -hydride elimination and delivers the L-arabinoic acid product (C,D). The iridium-hydride species is in equilibrium with the diiridium-hydride (**7**) which corresponds to the catalyst resting state. In the final stage, the iridium hydride is protonated by the previously released proton to form (E). We speculate that this protonation step is greatly accelerated by the trz ligand due to the potentially basic N2 site of this ligand,^{32,49} which enables an intramolecular and hence fast proton shuttle mechanism from N2 to the iridium-bound hydride. Such intramolecular proton transfer is not feasible with NHC complexes and may therefore rationalise the need for a strong acid as additive with those ligands, but not with triazole-derived carbenes. Formation of (E) induces the release of molecular hydrogen and regeneration of the initial diaqua species $[\mathbf{4}-(\text{H}_2\text{O})_2]^{2+}$.

Selective conversion of various monosaccharides into sugar acids by additive-free dehydrogenation in water



Scheme 5.2 Mechanistic proposal for the conversion of sugars to sugar acids and molecular hydrogen.

5.3 CONCLUSIONS

Iridium complexes bearing 1,2,3-triazolylidene ligands are efficient catalysts for the conversion of sugars into sugar acids without additives and using water as solvent. This transformation produces molecular hydrogen as a valuable by-product along with the selective formation of sugar acids. The conversion of sugars represents an interesting biomass transformation for the production of initial platform chemicals in a sustainable manner. The reaction is highly selective and does not require purification of the sugar acid products. Moreover, the catalysts are highly promiscuous and convert a variety of carbohydrate substrates, which contrasts the typically highly substrate-specific mode of operation of enzymes. Noticeably, high conversion and selectivity proceeds without any additional acid using trz complexes, which is a common requirement for sugar dehydrogenation in the presence of its NHC congeners. Mechanistic studies support the formation of a diiridium-hydride as catalyst resting state in the conversion of sugars to sugar acids. These results provide useful guidelines for further optimisation of this valuable biomass transformation.

5.4 SUPPORTING INFORMATION

This section contains the most relevant data of the article supporting information. To see the complete version, we invite you to download the PDF version of the article at the publisher website.

General considerations

Reagents and solvents

D-glucose (99 %), D-gluconic acid (50 % aq. sol), D-ribose (98%), D-xylose (99%), L-arabinose (99%), D-mannose (99%), D-Galactose (98%) and 2-deoxy-D-glucose (99%) were purchased from commercial suppliers and used as received. HPLC-grade water was obtained from distilled water passed through a Milli-Q water purification system. Anhydrous solvents were dried using a solvent purification system or purchased from commercial suppliers and stored over molecular sieves

Instrumentation

Nuclear magnetic resonance (NMR) spectra were recorded on Bruker spectrometers operating at 400 MHz (^1H NMR) and 100 MHz ($^{13}\text{C}\{^1\text{H}\}$ NMR) respectively, and referenced to SiMe_4 (δ in ppm and J in Hz). NMR spectra were recorded at room temperature with the appropriate deuterated solvent. UV/Vis spectra were recorded on a Jasco spectropolarimeter at room temperature using MiliQ water as solvent. Hydrogen was analysed using gas chromatography with a GS-MOL 15 meters column ID 0.55 mm TCD from J&W Scientific, using N_2 as carrier gas. HRMS studies were conducted on a QTOF Premier instrument with an orthogonal Z-spray-electrospray interface (Waters, Manchester, UK) operating in the V-mode at a resolution of ca. 10000 (FWHM). The drying and cone gas was nitrogen set to flow rates of 300 and 30 L/h, respectively. A capillary voltage of 3.5 kV was used in the positive ESI(+) scan mode. The cone voltage was adjusted to a low value (typically $U_c = 5\text{--}15$ V) to control the extent of fragmentation in the source region. Chemical identification of the Ir-containing species was facilitated by the characteristic isotopic pattern at natural abundance of Ir and it was carried out by comparison of the isotope experimental and theoretical patterns using the MassLynx 4.1 software. Sample preparation was carried out as follows: i) for aqueous speciation studies, aqueous solutions of pre-catalysts were stirred and aliquots were extracted at the required time intervals and ii) for the study of the progress of the catalytic reaction, aqueous solutions of pre-catalysts were stirred under catalytic conditions and aliquots were

extracted at the required time intervals. In both cases, samples were diluted with water to a final concentration of 5×10^{-4} M (based on the initial Ir concentration) and directly introduced to the mass spectrometer. HPLC-ESI-MS/MS experiments were carried out in a Waters Acquity UPLC system was interfaced to a triple quadrupole mass spectrometer Xevo TQS (Waters) equipped with an orthogonal Z-spray electrospray ionisation interface (ESI). Single crystal X-ray analysis were carried out on a SuperNova dual source equipped with a CCD Atlas detector diffractometer (Agilent Technologies). At the end of the reaction, the solvent was evaporated and the crude product was analysed by $^1\text{H-NMR}$ spectroscopy without further purification. In the case of D-gluconic and D-xylonic acids the pH was adjusted to 12 by adding NaOH for NMR characterization

Catalysts synthesis

Catalysts **3-6** were synthesized according to reported procedures.⁵⁰⁻⁵²

Catalytic dehydrogenation reactions

In a typical reaction, iridium catalyst (2 mol%) was added to a sugar solution (0.44 mmol) in deionised H_2O (5 mL). The reaction vessel was connected to a reflux condenser and was introduced in a pre-heated oil bath at 110°C for the appropriate time (standard time 20h). Reaction monitoring was carried out following two methodologies: for the quantification of glucose/gluconic acid, a previously described method based on reverse-phase UHPLC coupled to ESI-MS/MS was used. For the rest of sugars and sugar acids, different aliquots (400 μL) were directly extracted from the Schlenk tube with a syringe. The solvent was removed under reduced pressure and the residue was redissolved in D_2O for ^1H NMR analysis.

Kinetics study of catalyst 6

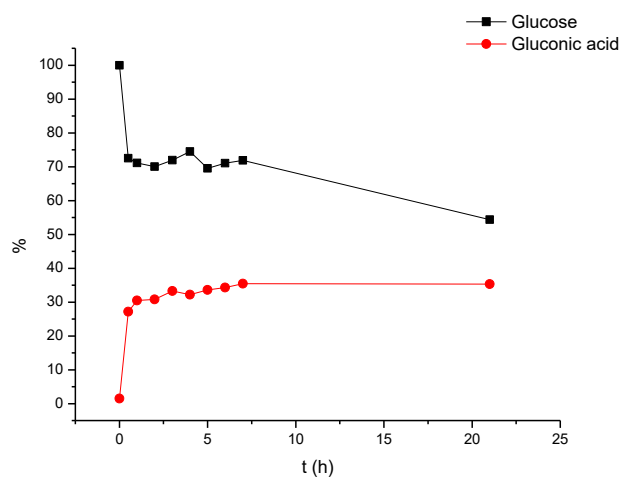


Figure S5.1. HPLC reaction monitoring. Complex 6 (2 mol%), glucose (0.44 mmol), H₂O (20 mL) at 110 °C.

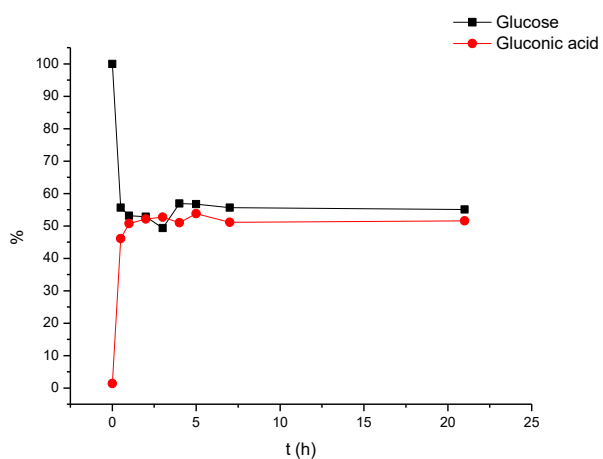


Figure S5.2. HPLC reaction monitoring. Catalyst 4 (2 mol%), H₂SO₄ additive (0.11 mmol, 0.25 eq.), glucose (0.44 mmol), H₂O (20 mL) at 110 °C.

Product characterization

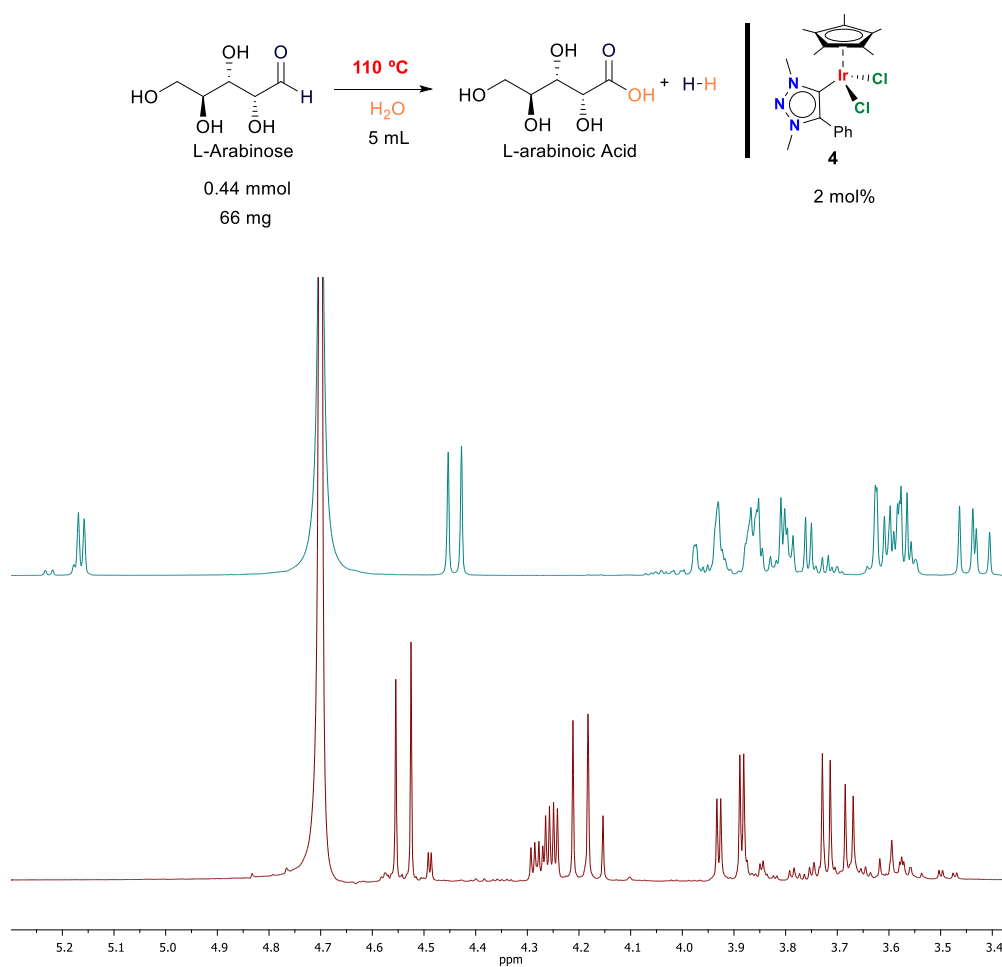
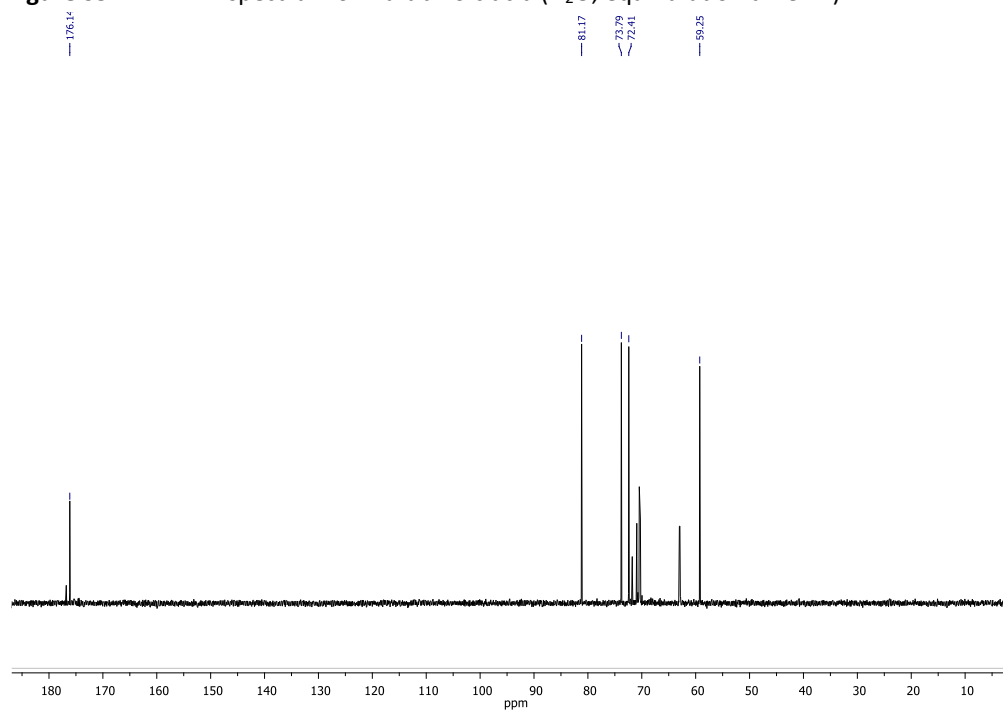
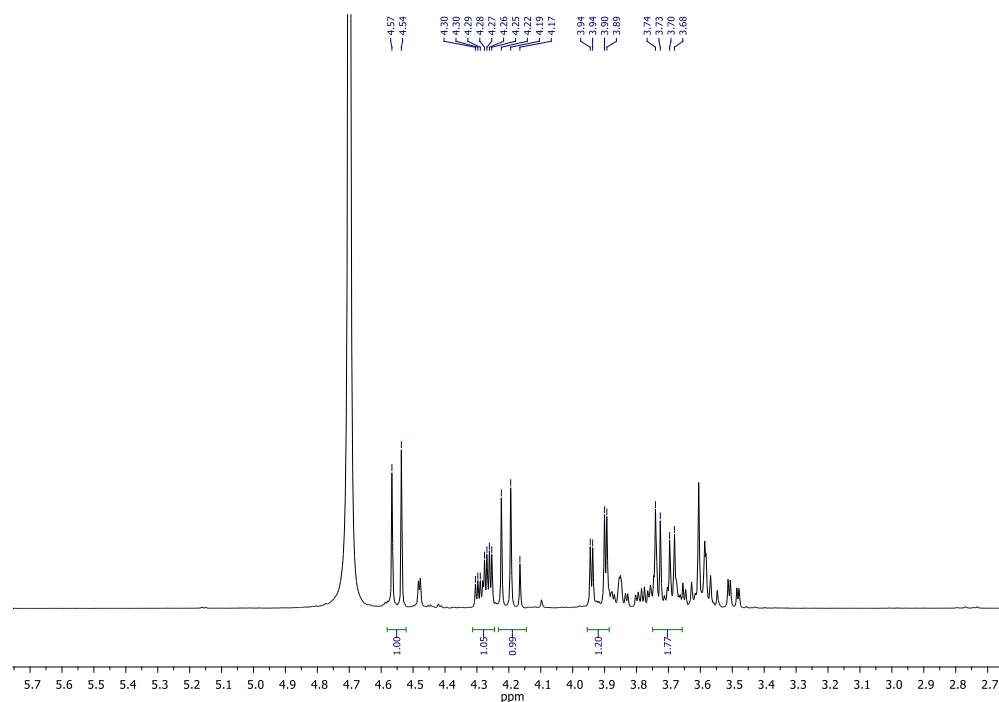


Figure S5.3 Top: ¹H NMR spectra of L-arabinose (400 MHz, D₂O, equilibration time 2h). Bottom: ¹H NMR spectrum (400 MHz, D₂O) of reaction crude with complex **4** (t = 20h).



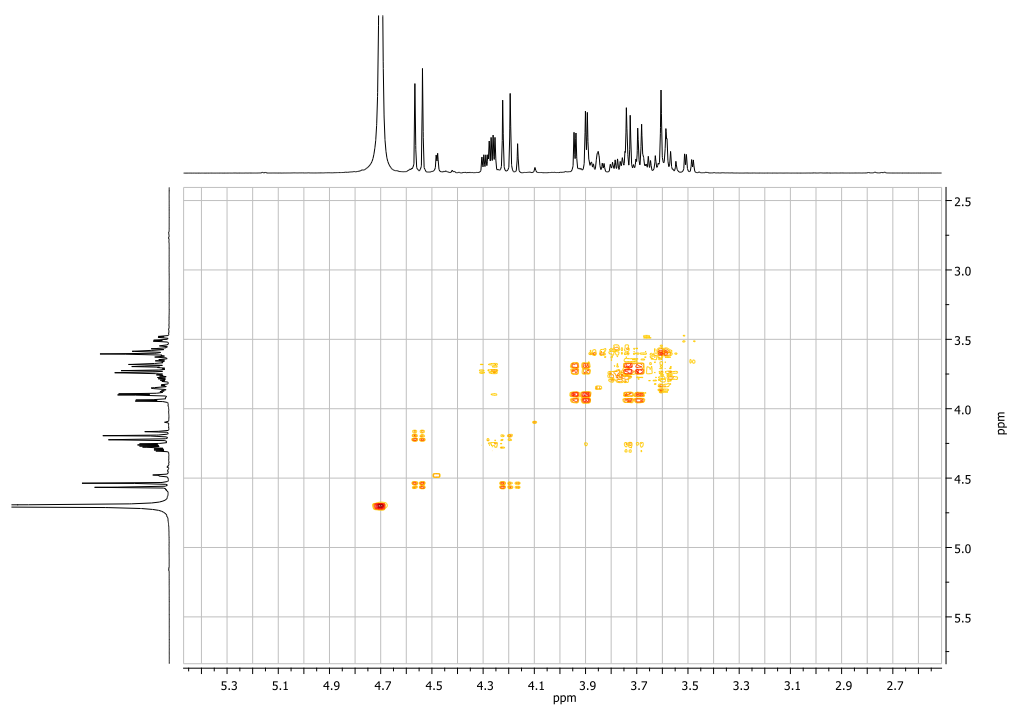


Figure S5.5 ^1H - ^1H COSY spectrum of L-arabinoic acid (D_2O).

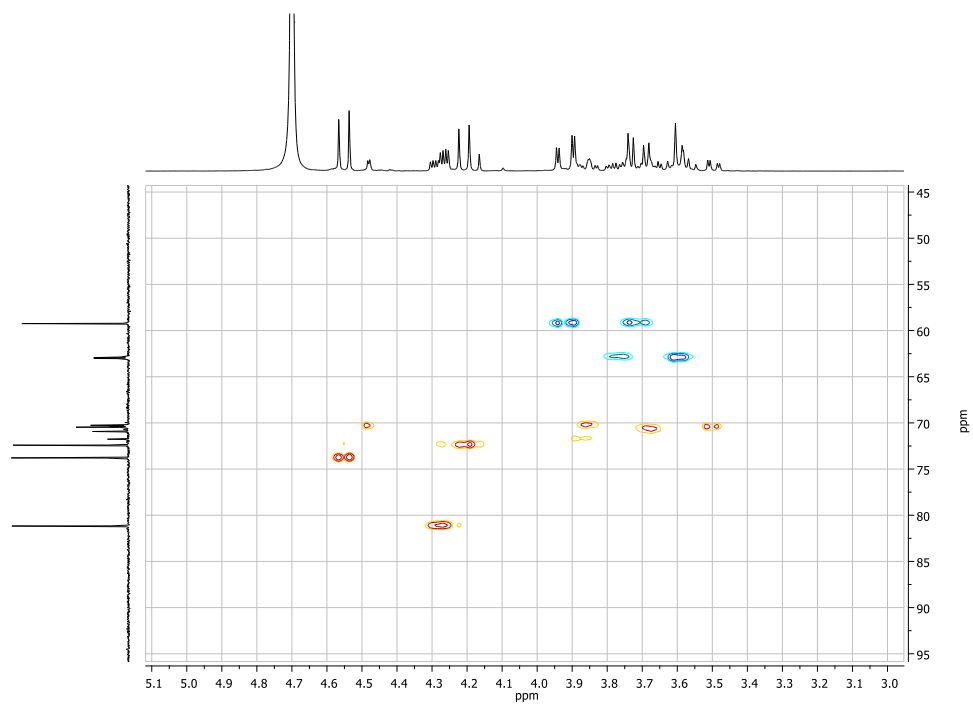


Figure S5.6 ^1H $^{13}\text{C}\{^1\text{H}\}$ HSQC spectrum of L-arabinoic acid (D_2O).

Electrospray Ionisation Mass Spectrometry (ESI-MS) and Collision Induced Dissociation (CID) experiments.

ESI-MS studies were conducted on a QTOF Premier instrument with an orthogonal Z-spray-electrospray interface (Waters, Manchester, UK) operating in the W-mode at a resolution of ca. 15000 (FWHM). The drying and cone gas was nitrogen set to flow rates of 300 and 30 L/h, respectively. A capillary voltage of 3.5 kV was used in the positive ESI(+) scan mode. The cone voltage was adjusted to a low value (typically $U_c = 5\text{--}15$ V) to control the extent of fragmentation in the source region. Chemical identification of the Ir-containing species was facilitated by the characteristic isotopic pattern at natural abundance of Ir and it was carried out by comparison of the isotope experimental and theoretical patterns using the MassLynx 4.1. For CID experiments, the cations of interest were mass-selected using the first quadrupole (Q1) and interacted with argon in the T-wave collision cell at variable collision energies (Elaboratory = 3 -15 eV). The ionic products of fragmentation were analyzed with the time-of-flight analyzer. The isolation width was 1Da and the most abundant isotopomer was mass-selected in the first quadrupole analyzer.

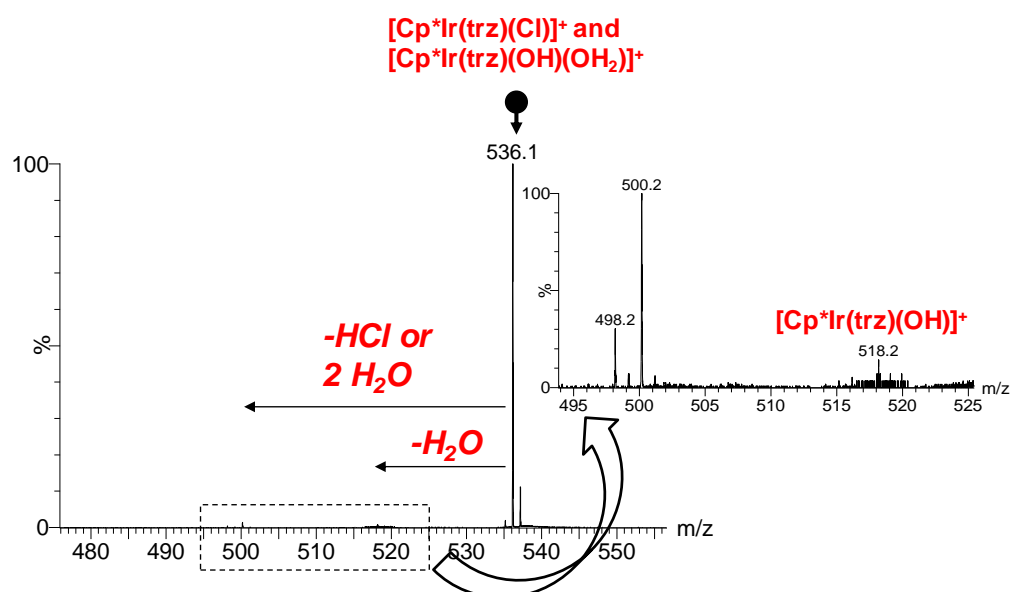


Figure S5.7 CID mass spectrum of mass-selected species at m/z 536 recorded at low collision energy $E_{lab} = 5$ eV showing the losses of $\Delta m = 18$ and 36. The inset shows an expanded region in the m/z 495-525 range where the product ions are observed.

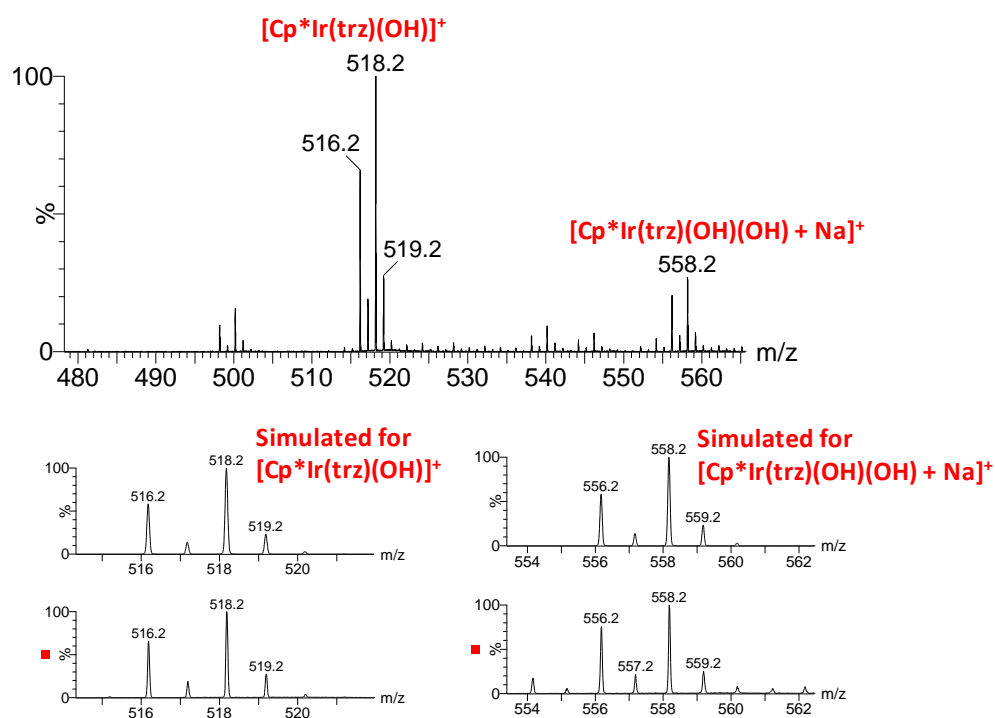


Figure S5.8 ESI mass spectrum of compound 4 in aqueous NaOH 10⁻³ M (top) together with the comparison between the calculated and experimental isotopic pattern for [Cp*Ir(trz)(OH)]⁺ and [Cp*Ir(trz)(OH)(OH) + Na]⁺

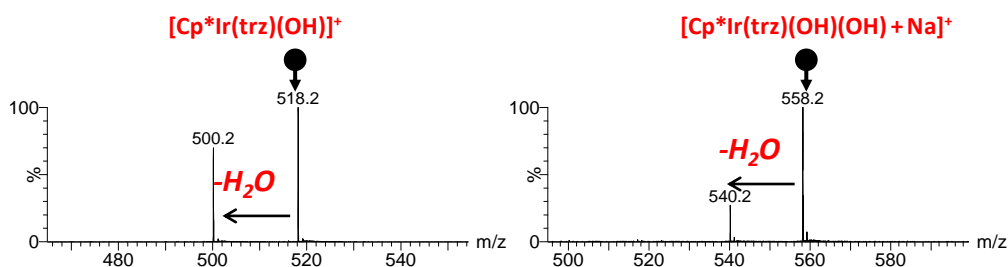


Figure S5.9 CID mass spectrum of mass-selected species at m/z 518 and 552 recorded at low collision energy $E_{\text{lab}} = 10$ eV showing the losses of $\Delta m = 18$ consistent with the presence of hydroxo groups.

Synthesis and characterization of 7

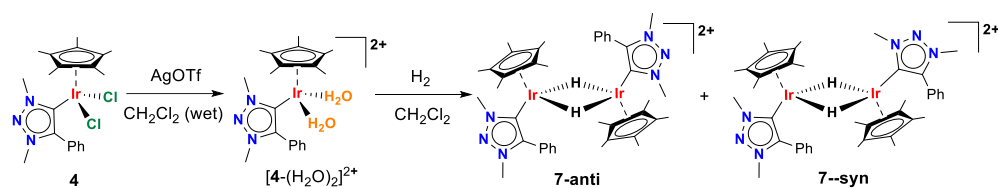


Figure 5.10 Synthesis of diiridium dihydride 7.

The synthesis of complex 7 was carried out in a two step-process. Complex 4 (60 mg, 0.1 mmol) and silver triflate (54 mg, 0.2 mmol) were suspended in 5 mL of CH₂Cl₂ (wet). The mixture was protected from light using aluminum foil and was stirred overnight. The resulting suspension was filtered through Celite© and the solvent was removed under reduced pressure to afford complex [4-(H₂O)₂](OTf)₂ (75.9 mg, 91% yield). ¹H NMR (400 MHz, CD₃OD, 298K) δ: 1.91 (s, 15H, Cp*), 3.93 (s, 3H, N-CH₃), 4.11 (s, 3H, N-CH₃), 7.43-7.64 (m, 5H, CH). Complex 5 was prepared starting from a solution of complex [2-(H₂O)₂](OTf)₂ (75.9 mg, 0.09 mmol) in 20 mL of CH₂Cl₂ and bubbling H₂(g) for 1h. The solvent was reduced to 6 mL under vacuum and complex 7 precipitated upon addition of hexanes (27.8 mg, 47% yield). Suitable crystals for X-ray diffraction were obtained by slow diffusion of hexane into a concentrated CH₂Cl₂ solution of 7. Complex 7 is obtained as a mixture of two isomers (syn and anti with respect to the orientation of the triazolylidene substituents), which were separated by fractional crystallisation using CH₂Cl₂/hexane mixtures. ¹H NMR_{anti} (400 MHz, CD₃OD, 298K) δ: 1.17 (s, 30H, Cp*), 4.20 (s, 6H, N-CH₃), 4.31 (s, 6H, N-CH₃), 7.65-7.86 (s, 10H, CH), and -16.82 (s, 2H, Ir-H). ¹³C NMR_{anti} (100 MHz, CD₃OD, 298K) δ: 9.6 (Cp*), 39.1 (N-CH₃), 42.6 (N-CH₃), 97.5 (Cp*), 127.7 (Ph), 130.4 (Ph), 130.7 (Ph), 131.7 (Ph), 131.9 (Ph), 132.0 (Ph), 145.7 (C-Ph), 155.6 (C-Ir).

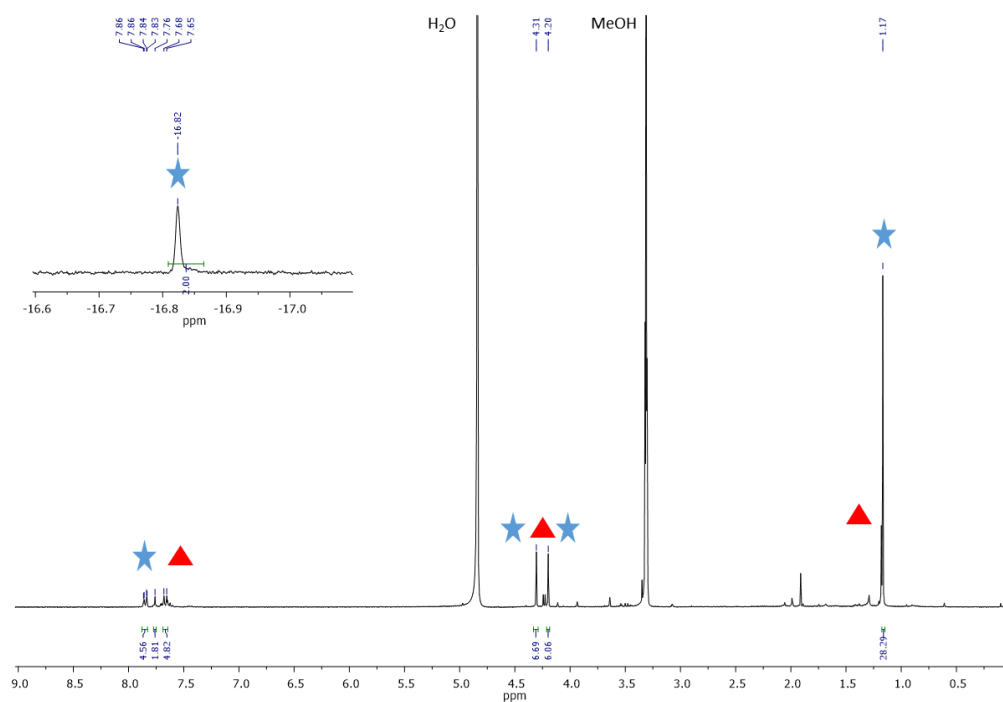


Figure S5.11 ^1H NMR spectrum in CD_3OD of diiridium dihydride **7-anti** (Blue stars). Small signals (red triangles) correspond to the **7-syn** isomer.

5.5 REFERENCES

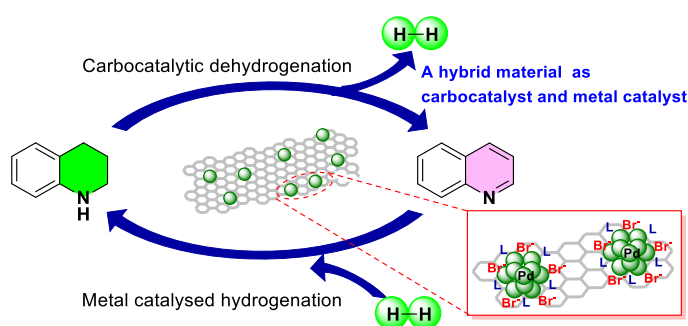
- (1) Corma, A.; Iborra, S.; Velty, A. *Chem. Rev.* **2007**, *107*, 2411–2502.
- (2) Besson, M.; Gallezot, P.; Pinel, C. *Chem. Rev.* **2014**, *114*, 1827–1870.
- (3) Sheldon, R. A. *Green Chem.* **2014**, *16*, 950–963.
- (4) Yabushita, M.; Kobayashi, H.; Fukuoka, A. *Appl. Catal. B Environ.* **2014**, *145*, 1–9.
- (5) Gallezot, P. *Green Chem.* **2007**, *9*, 295–302.
- (6) Gallezot, P. *ChemSusChem* **2008**, *1*, 734–737.
- (7) Gallezot, P. *Chem. Soc. Rev.* **2012**, *41*, 1538–1558.
- (8) He, J.; Li, H.; Saravanamurugan, S.; Yang, S. *ChemSusChem* **2019**, *12*, 347–378.
- (9) H. Choudhary, S. Nishimura, K. Ebitani, *Appl. Catal. B Environ.* **2015**, *162*, 1–10.
- (10) Mika, L. T.; Cséfalvay, E.; Németh, Á. *Chem. Rev.* **2018**, *118*, 505–613.
- (11) Climent, M. J.; Corma, A.; Iborra, S. *Green Chem.* **2011**, *13*, 520–540.
- (12) Climent, M. J.; Corma, A.; Iborra, S. *Chem. Rev.* **2011**, *111*, 1072–1133.
- (13) Mirescu, A.; Prüße, U. *Appl. Catal. B Environ.* **2007**, *70*, 644–652.
- (14) Makhubela, B. C. E.; Darkwa, J. *Johnson Matthey Tech. Rev.* **2018**, *62*, 4–31.
- (15) Mager, N.; Meyer, N.; Léonard, A. F.; Job, N.; Devillers, M.; Hermans, S. *Appl. Catal. B Environ.* **2014**, *148*, 424–435.
- (16) Chatterjee, C.; Pong, F.; Sen, A. *Green Chem.* **2015**, *17*, 40–71.
- (17) Deuss, P. J.; Barta, K.; de Vries, J. G. *Catal. Sci. Technol.* **2014**, *4*, 1174–1196.
- (18) Esteban, J.; Yustos, P.; Ladero, M. *Catalysts* **2018**, *8*, 637–676.
- (19) Bhaumik, P.; Dhepe, P. L. *RSC Green Chem.* **2016**, pp. 1–53.

- (20) Sutton, A. D.; Kim, J. K.; Wu, R.; Hoyt, C. B.; Kimball, D. B.; Silks, L. A.; Gordon, J. C. *ChemSusChem* **2016**, *9*, 2298–2300.
- (21) Kusema, B.T; Murzin, D. Y. *Catal. Sci. Technol.* **2013**, *3*, 297–307.
- (22) Ramachandran, S.; Fontanille, P.; Pandey, A.; Larroche, C. *Food Technol. Biotechnol.* **2006**, *44*, 185–195.
- (23) Crabtree, R.H. *Handbook of Green Chemistry, Green Catalysis, Heterogeneous Catalysis*, WILEY-VCH Verlag, **2009**.
- (24) Thananattananachon, T.; Rauchfuss, T. B. *ChemSusChem* **2010**, *3*, 1139–1141.
- (25) Schaper, L. A.; Hock, S. J.; Herrmann, W.; Kühn, F. E. *Angew. Chem. Int. Ed.* **2013**, *52*, 270–289.
- (26) Velazquez, H. D.; Verpoort, F. *Chem. Soc. Rev.* **2012**, *41*, 7032–7060.
- (27) De, S.; Udvardy, A.; Czégéni, C.E.; Joó, F. *Coord. Chem. Rev.* **2019**, *400*, 213038–213069.
- (28) Vivancos, A.; Segarra, C.; Albrecht, M. *Chem. Rev.* **2018**, *118*, 9493–9586.
- (29) Borja, P.; Vicent, C.; Baya, M.; García, H.; Mata, J. A. *Green Chem.* **2018**, *20*, 4094–4101.
- (30) Woods, J. A.; Lalrempuia, R.; Petronilho, A.; McDaniel, N. D.; Müller-Bunz, H.; Albrecht, M.; Bernhard, S. *Energy Environ. Sci.* **2014**, *7*, 2316–2328.
- (31) Petronilho, A.; Woods, J. A.; Mueller-Bunz, H.; Bernhard, S.; Albrecht, M. *Chem. Eur. J.* **2014**, *20*, 15775–15784.
- (32) Tulchinsky, Y.; Iron, M. A.; Botoshansky, M.; Gandelman, M. *Nat. Chem.* **2011**, *3*, 525–531.
- (33) Petronilho, A.; Llobet, A.; Albrecht, M. *Inorg. Chem.* **2014**, *53*, 12896–12901.
- (34) Theron, A.; Wu, Y.; Yunker, L. P. E.; Hesketh, A. V.; Pernik, I.; Weller, A. S.; McIndoe, J. S. *ACS Catal.* **2016**, *6*, 6911–6917.
- (35) Scott, S. L. *ACS Catal.* **2019**, *9*, 4706–4708.
- (36) Hanasaka, F.; Fujita, K.; Yamaguchi, R. *Organometallics* **2005**, *24*, 3422–3433.

- (37) Lehman, M. C.; Gary, J. B.; Boyle, P. D.; Sanford M. S.; Ison, E. A. *ACS Catal.* **2013**, *3*, 2304–2310.
- (38) Wassenaar, J.; Jansen, E.; van Zeist, W. J.; Bickelhaupt, F. M.; Siegler, M. A.; Spek, A. L.; Reek, J. N. H. *Nat. Chem.* **2010**, *2*, 417–421.
- (39) Balaraman, E.; Khaskin, E.; Leitus, G.; Milstein, D. *Nat. Chem.* **2013**, *5*, 122–125.
- (40) Kawahara, R.; Fujita, K.; Yamaguchi, R. *J. Am. Chem. Soc.* **2012**, *134*, 3643–3646.
- (41) Trincado, M.; Banerjee, D.; Grützmacher, H. *Energy Environ. Sci.* **2014**, *7*, 2464–2503.
- (42) Ventura-Espinosa, D.; Vicent, C.; Baya, M.; Mata, J. A. *Catal. Sci. Technol.* **2016**, *6*, 8024–8035.
- (43) Zweifel, T.; Naubron, J. V.; Grützmacher, H. *Angew. Chem. Int. Ed.* **2009**, *48*, 559–563.
- (44) Gunanathan, C.; Milstein, D. *Science* **2013**, *341*, 1229712–1229712.
- (45) Li, H.; Hall, M.B.; *J. Am. Chem. Soc.* **2014**, *136*, 383–95.
- (46) Rodríguez-Lugo, R. E.; Trincado, M.; Vogt, M.; Tewes, F.; Santiso-Quinones, G.; Grützmacher, H. *Nat. Chem.* **2013**, *5*, 342–347.
- (47) Vicent, C.; Gusev, D. G. *ACS Catal.* **2016**, *6*, 3301–3309.
- (48) Spasyuk, D.; Vicent, C.; Gusev, D. G. *J. Am. Chem. Soc.* **2015**, *137*, 3743–3746.
- (49) Keitz, B. K.; Bouffard, J.; Bertrand, G.; Grubbs, R. H. *J. Am. Chem. Soc.* **2011**, *133*, 8498–8501.
- (50) Xiao, X. Q.; Jin, G. X. *J. Organomet. Chem.* **2008**, *693*, 3363–3368.
- (51) Petronilho, A.; Rahman, M.; Woods, J. A.; Al-Sayyed, H.; Müller-Bunz, H.; Don MacElroy, J. M.; Bernhard, S.; Albrecht, M. *Dalton Trans.* **2012**, *41*, 13074–13080.
- (52) Pretorius, R.; Olguín, J.; Albrecht, M. *Inorg. Chem.* **2017**, *56*, 12410–12420.

CHAPTER 6:

Dual role of graphene as support of ligand- stabilized palladium nanoparticles and carbocatalyst for (de)hydrogenation of N-heterocycles



ABSTRACT

The hybrid material composed of palladium nanoparticles (PdNPs) functionalized with N-heterocyclic carbene ligands (NHCs) immobilized onto the surface of reduced graphene oxide (**rGO**) results an efficient catalytic material towards hydrogenation and dehydrogenation of N-heterocycles. The **rGO** plays a dual role by acting as a carbocatalyst in acceptorless dehydrogenation of N-heterocycles and as a support for the palladium nanoparticles. The mild conditions used in both transformations represent a potential application of this system for hydrogen storage technologies in the form of liquid organic hydrogen carriers (LOHCs). At the same time, the hybrid material is a robust and efficient catalytic platform that can be recovered and reused in up to eight runs in both transformations without significant deactivation. The use of a single solid catalyst that is recyclable in hydrogen conversion and reconversion through (de)hydrogenation of N-heterocycles paves the way for the development of efficient hydrogen storage materials.

Carbon **2022**, (CARBON-D-22-04236, under revision)

6.1 INTRODUCTION

The principle of microscopic reversibility states that catalytic reactions are essentially reversible as the potential energy surface does not depend on the direction of the reaction.¹⁻³ Herein, the mechanism is the same (but reversed) for both, the forward and backward version of the reaction. They have the same energy path and transition state, but different activation energy and binding affinity substrate-catalyst. As a result, catalysts are efficient in only one direction specially in the thermally activated reactions. Although there are reported examples in the literature where a single catalyst is efficient in both processes, still they are predominantly limited to electro and enzymatic catalysis.⁴⁻⁸ In parallel, both the hydrogenation and dehydrogenation of N-heterocycles are considered fundamental organic transformations since this class of molecules are relevant in the preparation of drugs and biologically active intermediates.⁹⁻¹³ Hydrogenation of N-heterocycles is favored by thermodynamics being an exergonic reaction although not entropically favored by the conversion of H₂ gas.¹⁴⁻¹⁷ On the contrary, dehydrogenation of N-heterocycles is endergonic but entropically favored and requires the removal of H₂ gas from the reaction media to proceed, which experimentally is translated in the used of high reaction temperatures and working under systems that allow the release of hydrogen.¹⁸⁻²²

The combination of such reversible reactions could potentially be used for hydrogen storage using organic molecules. These are the basis of the Liquid Organic Hydrogen Carrier (LOHC) technologies that enables to store hydrogen in the liquid form.²³⁻²⁷ The conversion of hydrogen gas into a liquid in LOHCs represent an attractive alternative for hydrogen storage when compared to traditional high-pressure or liquified technologies.²⁸⁻³⁰ N-heterocycles are suitable candidates to fulfill all the technical requirements for efficient LOHCs displaying lower enthalpy in the dehydrogenation process when compared with cyclic alkanes.³¹⁻³⁶ Thus, the availability of a single catalytic platform for hydrogen release and up-take using N-heterocycles as LOHCs is considered as a valuable and promising alternative to overcome the current technological shortcomings.

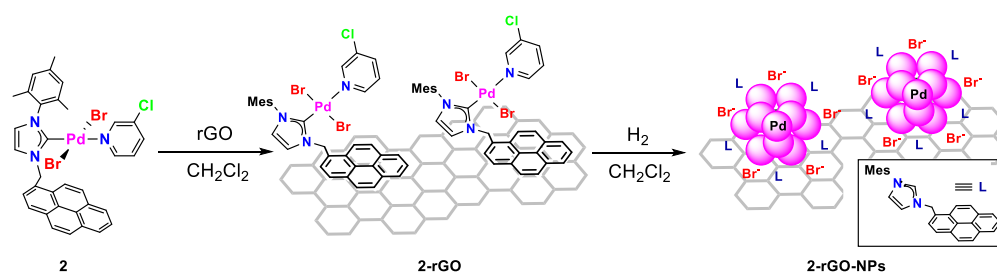
Herein we describe the synthesis of a reversible catalytic system based on a hybrid material. The material is prepared using a bottom-up approach starting from a well-defined N-heterocyclic carbene palladium molecular complex which contains a pyrene tag that facilitates the π -interactions with rGO. Decomposition of the immobilized complex onto the surface of graphene results in the formation of

palladium nanoparticles (PdNPs) featuring homogeneous size, shape, and composition affording the hybrid material (**2-rGO-NPs**). The catalytic performance of **2-rGO-NPs** was evaluated in (de)hydrogenation of N-heterocycles. The PdNPs are the active sites in hydrogenation using H₂ and the **rGO** acts as a carbocatalyst in acceptorless dehydrogenation of N-heterocycles. The stabilization of the PdNPs by NHC ligands and the use of graphene as support enables the **2-rGO-NPs** to be used and recycled in sequential (de)hydrogenation reactions up to eight cycles. To the best of our knowledge, the combination of MNPs and a carbocatalyst into a single catalytic hybrid material has no precedent and the particularity of this performance is attributed to the dual role played by graphene.

6.2 RESULTS AND DISCUSSION

Catalysts synthesis and characterization

Ligand-stabilized palladium nanoparticles anchored onto graphene used in (de)hydrogenation of N-heterocycles were prepared in a two-step process starting from the palladium complex **2** (Scheme 6.1). The design of an N-heterocyclic carbene ligand containing a polyaromatic tag allows the immobilization of complex **2** onto graphene by π -interactions.^{38–40} This methodology facilitates the preparation of **2-rGO** with a controlled composition of the precursor species used for the formation of palladium nanoparticles. The presence of the polyaromatic tag is responsible for the immobilization of molecular species and metal nanoparticles onto graphene. We have previously observed that ruthenium,^{41–43} iridium⁴⁴, platinum⁴⁵ and gold^{46,47} molecular complexes containing a pyrene tag form strong π -stacking interactions with reduced graphene oxide. The catalytic properties revealed that these interactions are maintained during recycling experiments. We have not observed deactivation promoted by leaching, which confirmed the importance of the polyaromatic group in the stability of metal species anchored onto graphene derivatives.^{48,49} Exposure of the hybrid material **2-rGO** to hydrogen under mild conditions induce the formation of palladium nanoparticles anchored onto graphene (**2-rGO-NPs**). Decomposition of the metal complexes for the formation of metal nanoparticles is a well established procedure first developed by Chaudret.^{50–55} This organometallic approach allows the formation of metal nanoparticles stabilized by the presence of ligands. The ligands (NHCs) avoid aggregation and control the size and morphology of the metal nanoparticles.^{56–58}



Scheme 6.1 Bottom-up synthesis of ligand-stabilized palladium nanoparticles supported onto graphene.

The exact nature and composition of palladium nanoparticles onto graphene was determined by microscopic, spectroscopic, and analytical techniques starting from the molecular palladium complex (**2**), its immobilized version (**2-rGO**) to the final hybrid material (**2-rGO-NPs**). Supporting information contains detailed characterization information of all species. NMR spectroscopy and high-resolution mass spectrometry (HR/MS) provides full characterization of **2**. Morphological analysis of **2-rGO** by HRTEM microscopy displays the characteristic bidimensional nature of graphene and the absence of metal aggregates in the form of palladium nanoparticles. EDX analysis reveal the presence of palladium (also N, Br and Cl) homogeneously distributed on the surface of graphene confirming the presence of complex **2** onto the surface of **rGO**. On the contrary, morphological analysis of **2-rGO-NPs** is completely different and shows the presence of metal aggregates (Figure 6.1). These metal aggregates correspond to spherical palladium nanoparticles of an average size of 1.98 ± 0.81 nm (Figure 6.1d). XPS analysis of **2-rGO-NPs** display peaks (C, N and Br) at binding energies corresponding to the NHC ligand (Figure S6.1) confirming its presence of ligand in the final hybrid material. We have not observed the presence of Cl indicating that the 3-chloropyridine ligand is lost during the nucleation and growing of metal nanoparticles. This is not unexpected as the 2-chloropyridine ligand is labile and likely to dissociate from the metal center. Interestingly, the high-resolution XPS analysis for the core-level peaks of Pd 3d displays two doublets confirming the presence of Pd(0) and Pd(2+) oxidation states (Figure 6.1e). Our approach to the formation of metal nanoparticles onto the surface of graphene represents a convenient bottom-up approach for the preparation of hybrid materials with an exhaustive control on composition and interaction between the different components. We propose a model for the **2-rGO-NPs** material that consists of reduced graphene oxide decorated with small and spherical palladium nanoparticles. The Pd NPs contain Pd(0) atoms at the core and Pd(+2) ions at the surface coordinated to NHC and Br ligands.

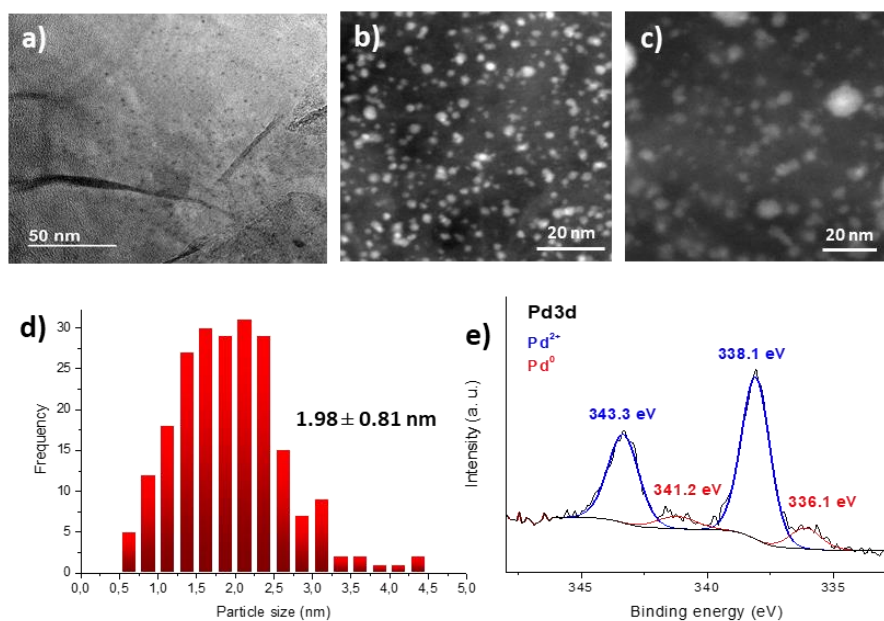


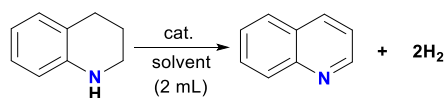
Figure 6.1 Characterization of **2-rGO-NPs** a) HRTEM image, b) STEM image, c) histogram (n = 450) and d) XPS analysis for the core-level peak of Pd 3d.

Dehydrogenation of N-heterocycles

The activity of **2-rGO-NPs** as catalyst for dehydrogenation of N-heterocycles was initially assessed using 1,2,3,4-tetrahydroquinoline as model substrate (Table 6.1). Dehydrogenation is endergonic and requires high temperatures to proceed. For this reason, we first evaluated the reaction without any catalyst (entry 1). No conversion or trace of quinoline was detected by gas chromatography (GC/FID) analysis indicating the need of a catalysts and highlighting the stability of 1,2,3,4-tetrahydroquinoline under the reaction conditions. Control experiments using only the molecular palladium **2** exclude this complex as a competent catalyst for this transformation and reveal that graphene species are required to promote dehydrogenation of tetrahydroquinolines (entry 2). In fact, when using reduced graphene oxide (**rGO**) a yield of 80% of quinoline is obtained indicating that graphene acts as an efficient carbocatalyst as we and others have previously observed for this and related carbonaceous materials.^{59–63} Comparison of the catalytic activity of **rGO** with palladium in the form of molecular species (**2-rGO**) or nanoparticles (**2-rGO-NPs**) reveal that no significant differences are observed

(Entries 3 – 5). These results reinforce the role of **rGO** as carbocatalyst and points out that the palladium species do not have any effect in the catalytic dehydrogenation of tetrahydroquinolines. The dehydrogenation of 1,2,3,4-tetrahydroquinoline proceeds using different solvents such as toluene, *p*-xylene or 1,2-DCB (Figure S6.2). However, low to moderate activity was observed when toluene was used as solvent (entries 6 – 7), but it was significantly superseded with *p*-xylene (entries 8 – 9). Still, the best results of 70% conversion in 9 h (and 100% in 23 h) were obtained when using 1,2-DCB (entries 5, 10). The reaction temperature strongly influences the catalytic activity. For instance, at 130 °C full conversion to quinoline was obtained in 23 h (entry 10). In contrast, when the reaction was carried out at 110 °C the conversion lowers to 60% (entry 11) and requires 48 h to reach full conversion (entry 12). Furthermore, it was observed that the dehydrogenation of N-heterocycles was negligible at 100 °C or below (entry 13). In addition, we have observed that dehydrogenation of 1,2,3,4-tetrahydroquinoline does not evolve when using a closed system that impedes the release of H₂ (entry 14).

Table 6.1 Dehydrogenation of 1,2,3,4-tetrahydroquinoline.



Entry	Cat.	Solvent	T (°C)	Time (h)	Conv. (%)
1	-	1,2-DCB	130	23	-
2	2	1,2-DCB	130	7	5
3	rGO	1,2-DCB	130	9	80
4	2-rGO	1,2-DCB	130	9	82
5	2-rGO-NPs	1,2-DCB	130	9	83
6	2-rGO-NPs	toluene	130	9	40
7	2-rGO-NPs	toluene	130	23	60
8	2-rGO-NPs	<i>p</i> -xylene	130	9	71
9	2-rGO-NPs	<i>p</i> -xylene	130	23	99
10	2-rGO-NPs	1,2-DCB	130	23	100
11	2-rGO-NPs	1,2-DCB	110	23	60
12	2-rGO-NPs	1,2-DCB	110	48	100
13	2-rGO-NPs	1,2-DCB	100	23	5
14 ^a	2-rGO-NPs	1,2-DCB	130	20	7

Reaction conditions: 1,2,3,4-tetrahydroquinoline (0.10 mmol), catalyst loading (38 mg), solvent (2 mL). Conversion determined by GC using 1,3,5-trimethoxybenzene as internal standard. a) reaction performed in a closed vessel.

To further explore the catalytic properties of **2-rGO-NPs**, dehydrogenation of 1,2,3,4-tetrahydroquinoline was evaluated at different catalyst loadings at 130 °C in 1,2-DCB (Figure 6.2). Assessment of catalyst loading provides valuable information regarding the implication of the catalyst in the kinetics of the process. Using a catalyst loading of 45 mg, 1,2,3,4-tetrahydroquinoline is quantitatively dehydrogenated (95%) in 9 h. Notably, lowering the catalyst loading to 28 mg affords quantitative yields in 23 h highlighting the stability of the catalyst. We used these data to establish the order in catalyst using variable time normalization analysis

(VTNA); a graphical method that uses reaction progress profiles.^{64–66} The results suggest a first-order dependence in catalyst, providing evidence that these species are involved in the rate-determining step of the reaction and that the diffusion factors do not play an important role (Figure S6.3).

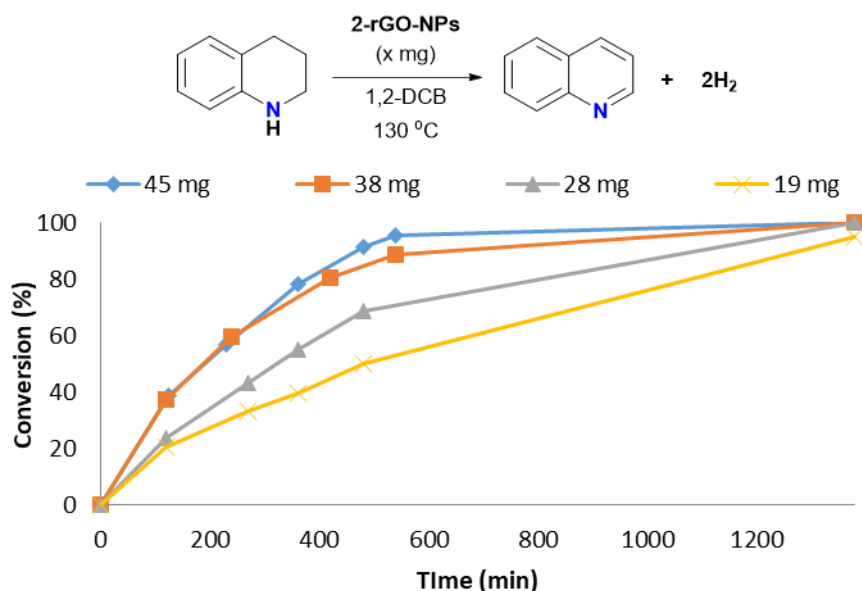


Figure 6.2 Influence of catalyst loading in dehydrogenation of N-heterocycles. Conditions: 0.1 mmol of 1,2,3,4-tetrahydroquinoline, 2 mL 1,2-DCB, 130 °C and catalyst. Conversion determined by GC using 1,3,5-trimethoxybenzene as an internal standard.

The scope of dehydrogenation was studied using different N-heterocycles and monitoring the yield/conversion of the reaction vs. time (Figure 6.3). Palladium nanoparticles anchored onto graphene (**2-rGO-NPs**) is an efficient catalyst for dehydrogenation of different N-heterocycles such as substituted tetrahydroquinolines, tetrahydroquinoxaline and indoline. The good relationship between conversion/yield implies that all substrate is converted into the corresponding product emphasizing the selectivity of the reaction. The dehydrogenation of substituted tetrahydroquinolines reached quantitative yields (>95%) in 23 h. Indoline is also dehydrogenated in ca. 23 h but initial rates are faster and 80% yield is achieved in 6 h. However, the reaction is faster for tetrahydroquinoxaline that reached quantitative yield in 8h. The reaction progress profiles indicate that the catalysts **2-rGO-NPs** is stable under the conditions and no deactivation is observed.

Dual role of graphene as support of ligand-stabilized palladium nanoparticles and carbocatalyst for (de)hydrogenation of N-heterocycles

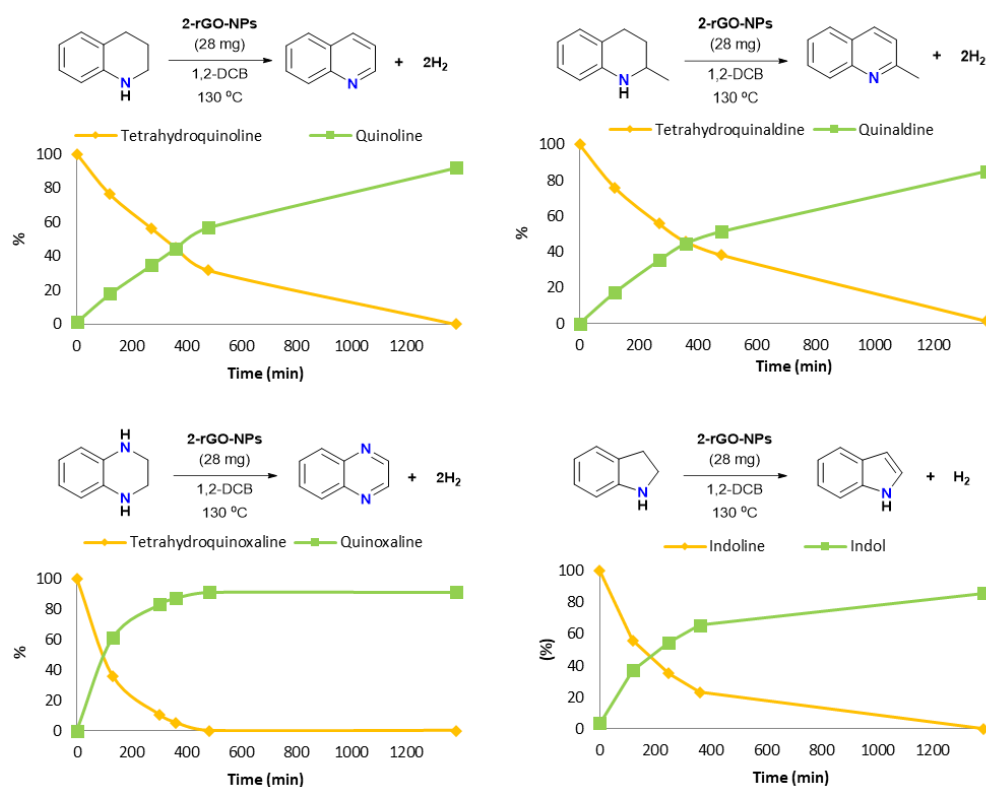


Figure 6.3 Dehydrogenation of N-heterocycles catalyzed by 2-rGO-NPs. Conditions: 0.1 mmol of substrate, 2 mL of 1,2-DCB, 130 °C and 28 mg of cat. Conversion and yield determined by GC analysis using 1,3,5-trimethoxybenzene as an internal standard.

The recycling properties and stability of catalyst 2-rGO-NPs were assessed using 1,2,3,4-tetrahydroquinoline as model substrate under standard conditions (Figure 6.4). After each run, the solid catalyst was isolated by centrifugation and washed with 1,2-DCB, ethyl-acetate and n-pentane. Once the catalyst was air-dried, it was reused in a subsequent run without any regeneration process. Reaction progress profiles shows a considerable decrease of activity for the second run although still quantitative conversion was obtained after 23 h. Then, activity was maintained within experimental error up to ten runs with a gradual deactivation. For instance, the conversion for run 3 is 42% after 8 h and for run 7 the conversion is 39%. It is important to note that an abrupt decay in conversion vs. time plot, implies fast catalyst deactivation by means of different processes such as decomposition, sintering or formation of inactive species. In our case, the gradual deactivation of the catalysts could be due to an experimental error in the treatment of the catalyst from run to run. The heterogeneous nature of the catalyst was assessed by hot filtration

experiments confirming that no active species are released from the solid into solution (Figure S6.4). The recycling experiments reveal that catalyst **2-rGO-NPs** is stable and can be easily isolated and reused in multiple runs.

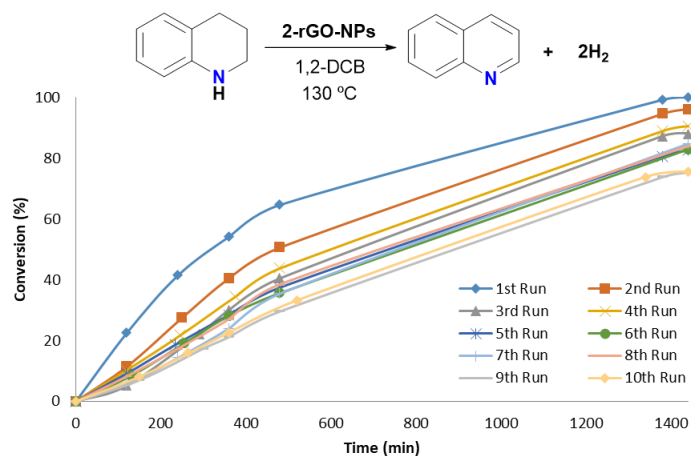


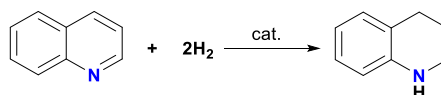
Figure 6.4 Recycling properties of 1-rGO-NPs in dehydrogenation of 1,2,3,4-tetrahydroquinoline. Conversion determined by GC analysis using 1,3,5-trimethoxybenzene as internal standard.

Hydrogenation of N-heterocycles

After having assessed the catalytic properties of the hybrid material **2-rGO-NPs** in dehydrogenation of N-heterocycles, we explored the potential of this material in the hydrogenation of quinolines (i.e., the reverse reaction). In a first set of reactions the activity of **2-rGO-NPs** as catalyst precursor in hydrogenation was assessed using quinoline as model substrate (Table 6.2). Blank experiments revealed that the presence of the catalyst is required for hydrogenation of quinoline (entry 1). We assessed the activity of **rGO** in quinoline hydrogenation under various conditions. The results show that **rGO** used as support of PdNPs is not active in hydrogenation (entry 2). Our studies in (de)hydrogenation of N-heterocycles establish that **rGO** is an efficient carbocatalyst in dehydrogenation but not in the reverse hydrogenation reaction. The hydrogenation of N-heterocycles and particularly quinoline, requires the presence of PdNPs as active catalytic sites. For instance, we have observed that hydrogenation of quinoline using **2-rGO-NPs** as catalyst is solvent dependent. While conversions were zero or very low using 1,2-DCB, toluene or water as solvents (entries 3 – 5), a high yield of tetrahydroquinoline (95%) was obtained when using EtOH (entry 6). The use of other alcohols such as iPrOH, were also very convenient

for hydrogenation of quinoline providing quantitative yields under the same reaction conditions (entry 8). We assessed the involvement of a transfer hydrogenation process instead of a direct hydrogenation using molecular hydrogen. We ruled out the participation of transfer hydrogenation as the reaction conversion was negligible when using a H₂ pressure of 1 bar. The best results were obtained when using an alcohol as solvent (EtOH or *i*PrOH) at 70 °C and a hydrogen pressure of 15 bar. Then, we assessed the scope and limitations of **2-rGO-NPs** in hydrogenation of various N-heterocycles under the optimized conditions (Table 6.3). The catalytic hydrogenation provides quantitative yields with high selectivity in most cases in just 6 h reaction. We have just observed low yields in the case of indoline (entry 4) and 8-phenylquinoline. At this point we do not have a proper explanation for such observations but our results agree with previous reports in the hydrogenation of these substrates.⁸ Nevertheless, hydrogenation of quinolines is a fast, general and selective transformation using **2-rGO-NPs** as catalyst.

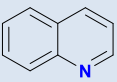
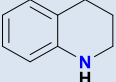
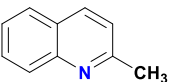
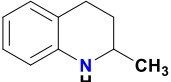
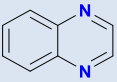
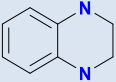
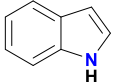
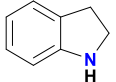
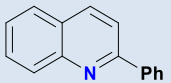
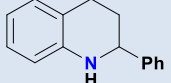
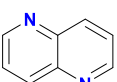
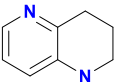
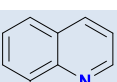
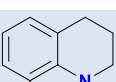
Table 6.2 Hydrogenation of quinoline under various conditions



Entry	Cat.	Loading (mol%)	Solvent	Yield (%) ^a
1	-	-	EtOH	0
2	rGO	20 mg	EtOH	0
3	2-rGO-NPs	1.5	1,2-DCB	0
4	2-rGO-NPs	1.5	toluene	3
5	2-rGO-NPs	1.5	H ₂ O	10
6	2-rGO-NPs	1.5	EtOH	95
7	2-rGO-NPs	1.5	<i>i</i> PrOH	100
8	2-rGO-NPs	1	<i>i</i> PrOH	75
9	2-rGO-NPs	0.75	<i>i</i> PrOH	68
10	2-rGO-NPs	0.5	<i>i</i> PrOH	60

Reaction conditions: quinoline (0.05 mmol), catalyst loading in mol% based on Pd, P(H₂) 15 bar, solvent (1 mL), 70 °C for 6 h. ^aYields determined by GC using 1,3,5-trimethoxybenzene as an internal standard.

Table 6.3 Reaction scope in hydrogenation of quinolines using **2-rGO-NPs**

Entry	Substrate	Product	Yield (%)
1			100
2			98
3			62
4			26
5			94
6			99
7			30

Reaction conditions: quinoline (0.05 mmol), catalyst (1.5 mol% based on Pd), P(H₂) 15 bar, ⁱPrOH (1 mL), for 6h. ^aYields determined by GC using 1,3,5-trimethoxybenzene as an internal standard.

Sequential hydrogenation/dehydrogenation of N-heterocycles

Once the properties of **2-rGO-NPs** as a carbocatalyst in dehydrogenation and as a metal-based catalyst in hydrogenation of N-heterocycles have been established, we evaluated its ability in (de)hydrogenation cycles. The hybrid material **2-rGO-NPs** was reused in sequential hydrogenation and dehydrogenation reactions. After each run, the catalyst was isolated and used again without any regeneration process. The hydrogenation reaction was stopped at ca. 50% conversion (3 h) to detect any potential deactivation process in the following runs. It is important to note that

increasing the time, the reaction achieves completeness as previously described (Tables 6.2 and 6.3). The results show that when stopping the reaction after 3h the activity of **2-rGO-NPs** is maintained constant at $45\pm 4\%$ conversion (Figure 6.5b, blue bars). After each hydrogenation, the catalyst was used in a dehydrogenation reaction (Figure 6.5b, red bars). The dehydrogenation reaction was stopped also at ca. 50% conversion (6 h). The results show that the activity of **2-rGO-NPs** is maintained constant at $60\pm 5\%$ conversion. Following this procedure, after completing 4 cycles (8 runs) the hybrid material was analyzed by HRTEM microscopy (Figure 6.5c). HRTEM and STEM images show that the morphology of **2-rGO-NPs** is preserved including the bidimensional character of **rGO** and the presence of spherical palladium nanoparticles. This experiment confirms that the conditions used in both transformations do not alter the catalytic activity of **2-rGO-NPs** as carbocatalyst and as metal catalyst.

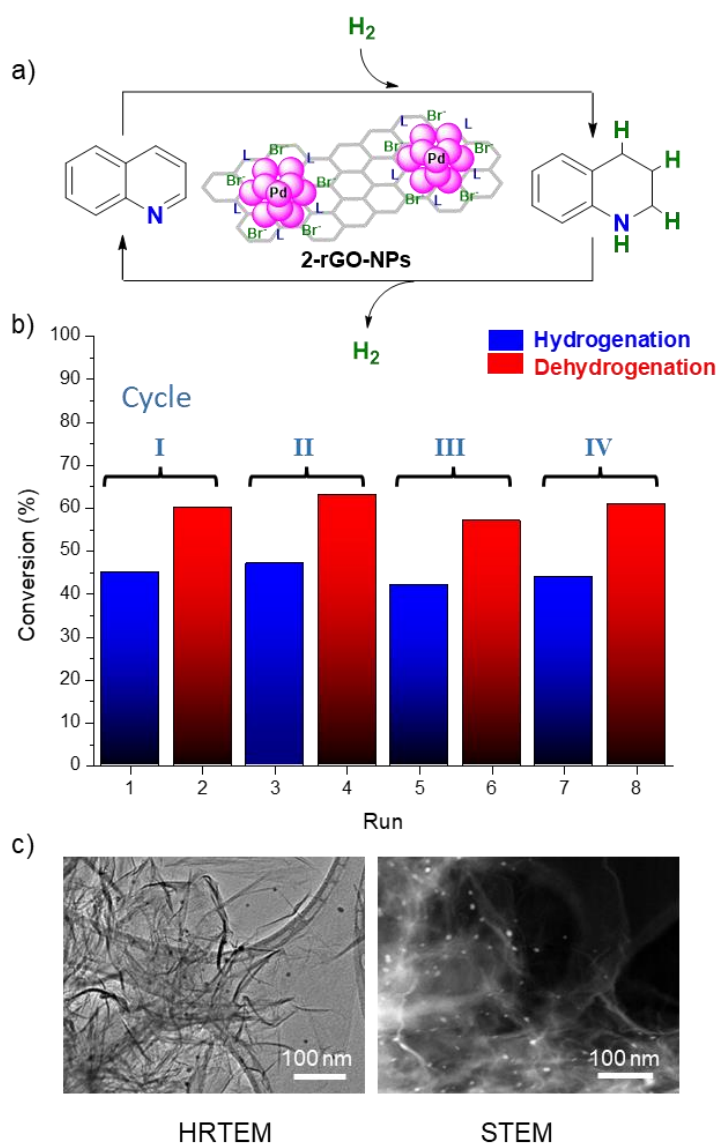


Figure 6.5 a) Reaction scheme in (de)hydrogenation cycles. b) Recycling properties of **1-rGO-NPs** in sequential hydrogenation of quinoline and dehydrogenation of 1,2,3,4-tetrahydroquinoline. Catalyst 84 mg. Hydrogenation: quinoline (0.3 mmol), $P(H_2)$ 15 bar, $iPrOH$ (6 mL), for 3h. Dehydrogenation: 1,2,3,4-tetrahydroquinoline (0.3 mmol), 6 mL 1,2-DCB, 130 °C for 6 h. Conversions determined by GC analysis using 1,3,5-trimethoxybenzene as an internal standard. c) HRTEM and STEM images of **2-rGO-NPs** after four cycles.

6.3 CONCLUSIONS

We have developed a hybrid material composed of palladium nanoparticles stabilized with N-heterocyclic carbene ligands containing a pyrene tag which are supported on the surface of reduced graphene oxide. The hybrid material is an efficient catalytic platform for acceptorless dehydrogenation and hydrogenation of N-heterocycles without additives. The catalytic system is robust and can be reused and recycled without reactivation processes for eight runs without significant loss of activity. The use of a single solid catalyst for the reversible (de)hydrogenation reaction of liquid organic compounds auspicious great potential for hydrogen storage in N-heterocycles. Further work for improving the catalyst performance at low temperatures in dehydrogenation and seeking other liquid organic hydrogen carriers for developing practical applications of hydrogen storage in the form of LOHCs are in progress.

6.4 SUPPORTING INFORMATION

This section contains the most relevant data of the article supporting information.

General considerations

Reagents and solvents

Reagents used in the preparation of catalyst were synthetic grade and used without further purification process unless otherwise stated. Palladium (II) bromide (99%), K_2CO_3 (99%), 3-chloropyridine (99%), 1,3,5-trimethoxybenzene (99%). Solvents of HPLC grade were used without further purification: CH_2Cl_2 , Diethylether, ethyl-acetate, n-pentane, iPrOH, EtOH. 1,2-DCB (1,2-Dichlorobenzene) used as solvent in dehydrogenation reactions was deoxygenated by freeze-pump-thaw method. Reduced Graphene Oxide (**rGO**) was purchase (Graphenea) and used as received. N-heterocycles are commercially available (Sigma-Aldrich) and used as received.

Instrumentation

Nuclear magnetic resonance (NMR) spectra were recorded on Bruker spectrometers operating at 300 or 400 MHz (1H NMR) and 75 or 100 MHz ($^{13}C\{^1H\}$ NMR), respectively, and referenced to $SiMe_4$ (δ in ppm and J in Hertz). Yield and conversion were determined by a GC-2010 (Shimadzu) gas chromatograph equipped with a FID and a Teknokroma (TRB-5MS; 30 m x 0.25 mm x 0.25 mm) column. High-resolution images of transmission electron microscopy HRTEM and high-angle annular dark-field HAADF-STEM images of the samples were obtained using a Jem-2100 LaB6 (JEOL) transmission electron microscope coupled with an INCA Energy TEM 200 (Oxford) energy dispersive X-Ray spectrometer (EDX) operating at 200 kV. Samples were prepared by drying a droplet of a MeOH dispersion on a carbon-coated copper grid. X-ray photoelectron spectra (XPS) were acquired on a Kratos AXIS ultra DLD spectrometer with a monochromatic Al $K\alpha$ X-ray source (1486.6 eV) using a pass energy of 20 eV. To provide a precise energy calibration, the XPS binding energies were referenced to the C1s peak at 284.6 eV.

Catalysts synthesis

Synthesis of **2**: The palladium complex was prepared by adapting a previous reported procedure described by our group.³⁷ In brief, the imidazolium salt (241 mg, 0.5 mmol), palladium(II) bromide (133 mg, 0.5 mmol), potassium carbonate (207 mg, 1.5 mmol) and 3-chloropyridine (3 mL) were introduced into a Schlenk and the resulting suspension was stirred for 20 h at 80 °C. The reaction mixture was filtered through a short pad of celite using CH₂Cl₂ and the yellow solution was evaporated to dryness. The oily precipitate was dissolved in CH₂Cl₂ and was precipitated with n-hexanes affording a yellow solid that was filtered and washed with diethyl ether. (Yield. 270 mg, 70%).

Synthesis of **2-rGO**: A suspension of 1 g of **rGO** in 560 mL of CH₂Cl₂ was introduced in an ultrasounds bath for 30 min. Then, complex **2** (160 mg, 0.21 mmol) was added to the mixture and the suspension was stirred at room temperature for 16 h. The black solid was isolated by filtration and washed with CH₂Cl₂ (3 x 100 mL) affording the hybrid material as a black solid. The exact amount of complex supported was determined by ICP-MS analysis. The results accounted for a 5.5 wt% of complex **2** in the hybrid material **2-rGO**.

Synthesis of **2-rGO-NPs**: A Schlenk flask equipped with a stirring bar was loaded with **2-rGO** (200 mg), Cs₂CO₃ (118 mg, 0.052 mmol) and toluene (24 mL). Then, a balloon of H₂ (1 bar) was connected to the Schlenk and the reaction mixture was stirred at 65 °C for 1 h. After this time, **2-rGO-NPs** were filtered, washed with toluene (3 x 30 mL), deionized water (3 x 30 mL), acetone (3 x 30 mL) and dried. **2-rGO-NPs** were characterized by HRTEM and XPS, and the exact amount of Pd on the surface of graphene was determined by ICP-MS. The results accounted for a 0.57 wt % of Pd in the hybrid material **2-rGO-NPs**.

General procedure for the catalytic dehydrogenation of N-heterocycles

In a general catalytic experiment, a 10 mL Schlenk flask equipped with a stirring bar was charged with 0.1 mmol of tetrahydroquinoline, catalyst and 2 mL of 1,2-dichlorobenzene under N₂. The reaction flask was equipped with a condenser and then introduced in a preheated 130 °C oil bath. The reaction was refluxed with stirring in an open system for 23 h. After cooling to room temperature, Yields and conversions were determined by GC and/or ¹H NMR analysis using 1,3,5-trimethoxybenzene as internal standard.

General procedure for the catalytic hydrogenation of N-heterocycles

In a general catalytic experiment, a 2 mL vial equipped with a stirring bar was charged with 0.05 mmol of N-heterocycle, catalyst and 1 mL of solvent and was introduced in an autoclave. After purging with 3 x 5 bar of H₂, the reactor was pressurized to 15 bars and heated at 70 °C for 6 h. After this time, H₂ was released, and the reactor was left to reach room temperature. Yields and conversions were determined by GC and/or ¹H NMR analysis using 1,3,5-trimethoxybenzene as an internal standard.

Recycling experiments in dehydrogenation of tetrahydroquinoline

A 25 mL schlenk equipped with a stirring bar is loaded with 0.3 mmol of tetrahydroquinoline, 84 mg of catalyst and 6 mL of 1,2-dichlorobenzene used as solvent. The balloon is then introduced in a preheated 130 °C oil-bath for 23 h. After each run, the solid catalyst is isolated, washed with 1,2-DCB (x3) and ethyl-acetate (x3) and dried with pentane (x1). The solid catalyst is then used in a next run without any regeneration process. Yields and conversions were determined by GC using 1,3,5-trimethoxybenzene as internal standard.

Recycling properties in sequential hydrogenation/dehydrogenation cycles

Hydrogenation: A 10 mL vial equipped with a stirring bar was loaded with 0.3 mmol of quinoline, **2-rGO-NPs** (1.5 mol% based on Pd, 84 mg) and 6 mL of iPrOH was introduced in an autoclave and sealed. The reactor was purged 3 times with 5 bar of H₂, then it was pressurized to 15 bars and heated at 70 °C for 3 h to achieve ca. 50% conversion. After this time, H₂ was released, and the reactor was left to reach room temperature. The solid hybrid catalyst was recovered by centrifugation, washed with iPrOH (3x 5 mL), pentane (1 x 5 mL) and dried before it was used in the subsequent dehydrogenation run. The liquid phase was analyzed by GC chromatography for determining yield and conversion using 1,3,5-trimethoxybenzene as an internal standard.

Dehydrogenation: The recovered hybrid catalyst was further used without any regeneration process in a dehydrogenation reaction completing a (de)hydrogenation cycle. A 10 mL round bottom flask equipped with a stirring bar was charged with 0.3 mmol of tetrahydroquinoline, **2-rGO-NPs** (84 mg) and 6 mL of 1,2-dichlorobenzene. The reaction flask, equipped with a condenser, was then introduced in a preheated 130 °C oil bath. The reaction was refluxed with stirring for 6 h to afford ca. 50%

conversion. After cooling to room temperature, the solid catalyst was separated by centrifugation, washed with 1,2-DCB (3 x 5 mL), ethyl-acetate (3 x 5 mL), pentane (1 x 5 mL) and dried before using in the following hydrogenation run. Yields and conversions were determined by GC using 1,3,5-trimethoxybenzene as an internal standard. The overall sequential process hydrogenation/dehydrogenation was repeated up to four cycles (eight runs) and then the solid catalyst was analyzed by HRTEM microscopy.

Molecular hydrogen determination

A 25 ml two-necked round bottom flask equipped with a stirring bar was charged with 0.2 mmol of tetrahydroquinoline, **2-rGO-NPs** (55 mg) and 4 mL of 1,2-dichlorobenzene. The reaction flask was equipped with a condenser and then introduced in a preheated 130 °C oil bath. The reaction was refluxed with stirring in a closed system. After 5 h, a 1.5 mL sample of the evolved gas was captured with a syringe and injected in a quadrupole mass spectrometer equipment (Omnistar GSD 320 03 from PFEIFER VACUUM) confirming the presence of molecular hydrogen.

Hybrid material 2-rGO-NPs characterization

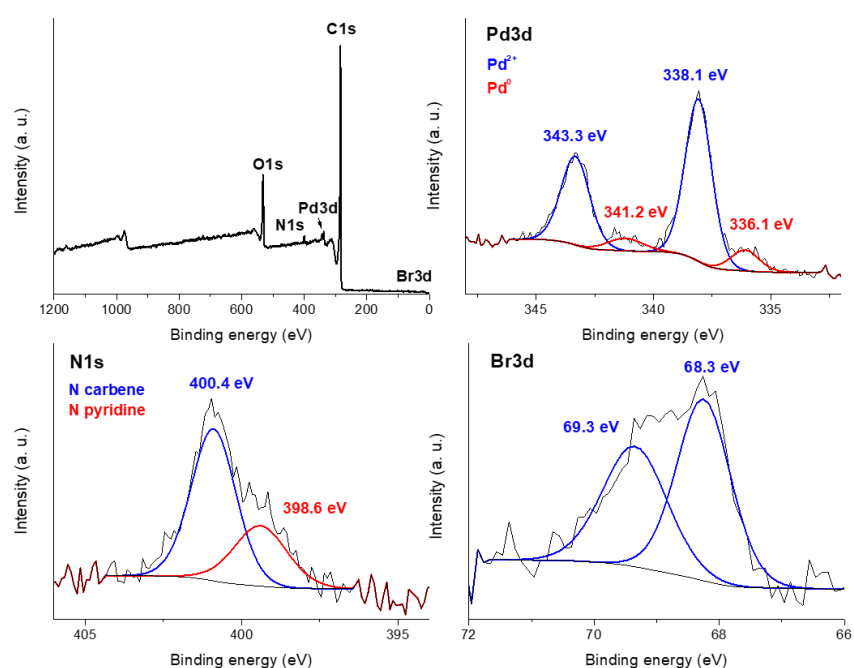


Figure S6.1 XPS analysis of **2-rGO-NPs** showing the survey spectrum and the high-resolution core-level peaks of Pd, Br and N.

Dehydrogenation of tetrahydroquinolines

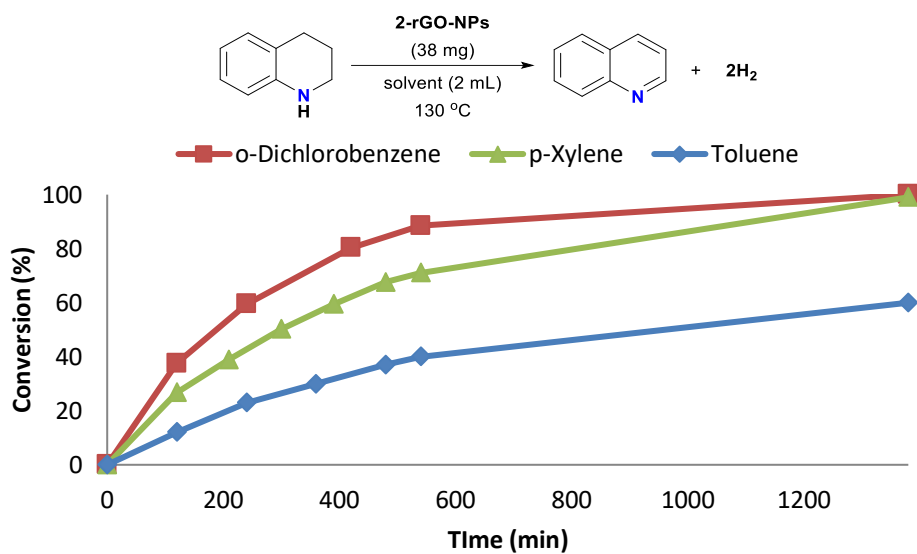


Figure S6.2 Solvent effect in acceptorless dehydrogenation of tetrahydroquinoline.

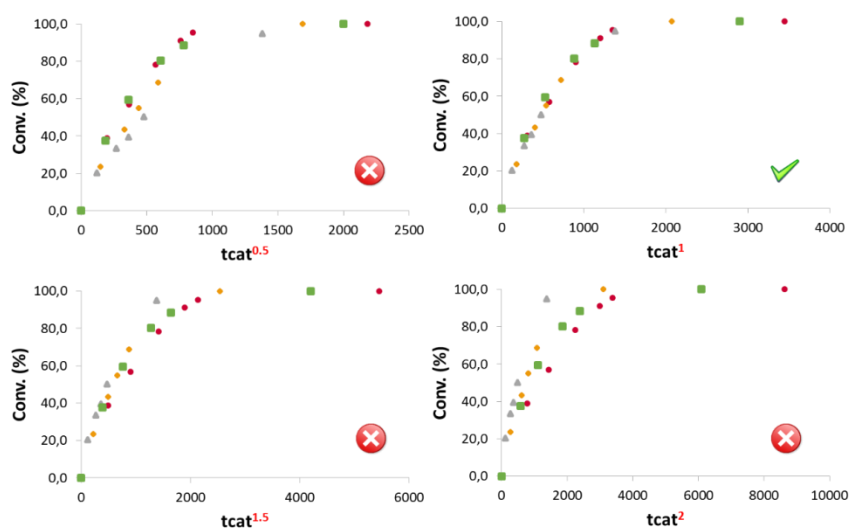


Figure S6.3 Variable time normalization analysis (VTNA) for determining the order in catalyst. The order corresponds to the representation showing the greatest overlay. In this case, the order in catalyst is 1. Data: Red circles (cat. loading 45 mg), green squares (38 mg), grey triangles (28 mg) and yellow diamonds (19 mg).

The Maitlis hot filtration test

This test predicts if during the catalytic transformation metal species are delivered into solution acting as molecular-homogeneous species. The test consists in the filtration of a part of the catalytic reaction (without solid materials) maintaining the reaction conditions and monitoring the reaction time-profile in the remaining suspension and the filtrate. No catalytic activity in the filtrate suggests that no metal species are released into the solution implying that active catalytic species are heterogeneous in nature. In the acceptorless dehydrogenation of quinoline with catalyst **1-rGO-NPs**, a balloon of 10 ml equipped with a stirring bar was charged with 0.2 mmol of tetrahydroquinoline, 56 mg of catalyst and 4 mL of 1,2-dichlorobenzene as solvent. The balloon refrigerated by water was then introduced in a preheated 130 °C oil bath. After 210 min reaction (GC conversion 35 %) half of the reaction mixture was filtered off through microfilter at 130 °C. The filtrate was maintained for 17 h under identical conditions, but GC analysis indicated that no further dehydrogenation occurred (GC conversion 38%). On the contrary, the remaining mixture achieved quantitative conversion in 17 h reaction.

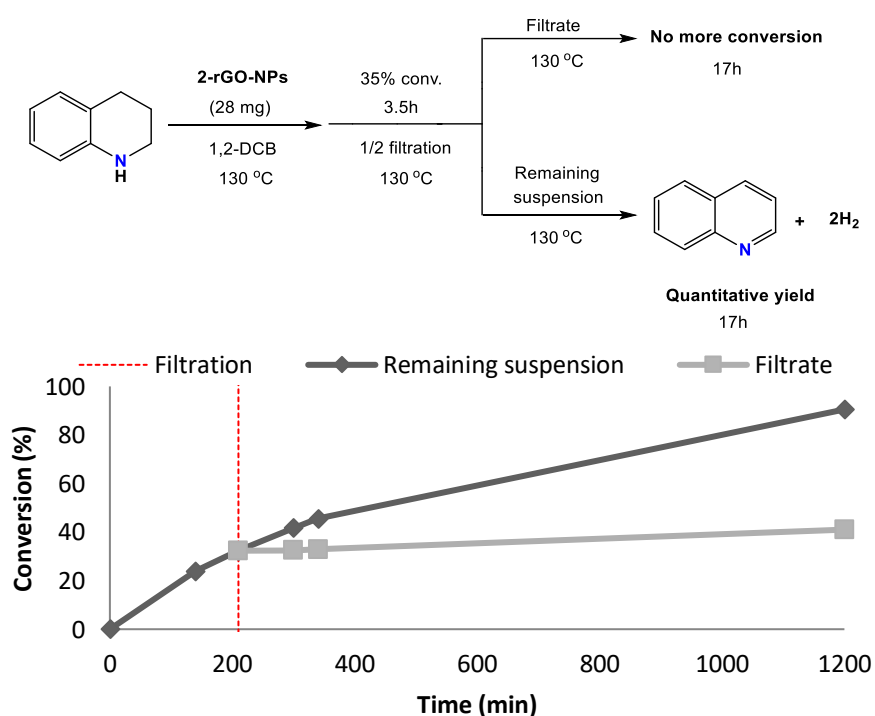


Figure S6.4 Reaction progress profile for the hot filtration experiment in dehydrogenation of 1,2,3,4-tetrahydroquinoline.

6.5 REFERENCES

- (1) Tolman, R.C. *Philos. Sci.* **1939**, *6*, 381–381.
- (2) Roduner, E. *Chem. Soc. Rev.* **2014**, *43* 8226–8239.
- (3) Astumian, R.D. *Acc. Chem. Res.* **2018**, *51*, 2653–2661.
- (4) Bonitatibus, P.J.; Chakraborty, S.; Doherty, M.D.; Siclovan, O.; Jones, W.D.; Soloveichik, G.L. *Proc. Natl. Acad. Sci.* **2015**, *112*, 1687–1692.
- (5) Yamaguchi, R.; Ikeda, C.; Takahashi, Y.; Fujita, K. *J. Am. Chem. Soc.* **2019**, *131*, 8410–8412.
- (6) Chakraborty, S.; Brennessel, W.W.; Jones, W.D. *J. Am. Chem. Soc.* **2014**, *136* 8564–8567.
- (7) Kaneda, K.; Mikami, Y.; Mitsudome, T.; Mizugaki, T.; Jitsukawa, K. *Heterocycles* **2019**, *82*, 1371–1377.
- (8) Cui, X.; Huang, Z.; van Muyden, A.P.; Fei, Z.; Wang, T.; Dyson, P.J. *Sci. Adv.* **2020**, *6*, 1–11.
- (9) Zhang, J.; Li, D.; Lu, G.; Deng, T.; Cai, C. *ChemCatChem*. **2018**, *10*, 4966–4972.
- (10) Ventura-Espinosa, D.; Mata, J.A. *Eur. J. Inorg. Chem.* **2016**, *17*, 2667–2675.
- (11) Li, H.; Jiang, J.; Lu, G.; Huang, F.; Wang, Z.-X. *Organometallics*. **2011**, *30*, 3131–3141.
- (12) Zhou, W.; Tao, Q.; Sun, F.; Cao, X.; Qian, J.; Xu, J.; He, M.; Chen, Q.; Xiao, J. *J. Catal.* **2018**, *361*, 1–11.
- (13) Xu, X.; Ai, Y.; Wang, R.; Liu, L.; Yang, J.; Li, F. *J. Catal.* **2021**, *395*, 340–349.
- (14) Zhang, X.B.; Xi, Z. *Phys. Chem. Chem. Phys.* **2011**, *13*.
- (15) Dobreiner, G.E.; Nova, A.; Schley, N.D.; Hazari, N.; Miller, S.J.; Eisenstein, O.; Crabtree, R.H. *J. Am. Chem. Soc.* **2011**, *133*, 7547–7562.
- (16) Zheng, J.; Zhou, H.; Wang, C.-G.; Ye, E.; Xu, J.W.; Loh, X.J.; Li, Z. *Energy Storage Mater.* **2021**, *35*, 695–722.

- (17) He, D.; Wang, T.; Li, T.; Wang, X.; Wang, H.; Dai, X.; Shi, F. *J. Catal.* **2021**, *400*, 397–406.
- (18) Wu, J.; Talwar, D.; Johnston, S.; Yan, M.; Xiao, J. *Angew. Chem. Int. Ed.* **2013**, *52*, 6983–6987.
- (19) Clot, E.; Eisenstein, O.; Crabtree, R.H. *Chem. Commun.* **2007**, *22*, 2231–2233.
- (20) Zhang, Y.; Wang, J.; Zhou, F.; Liu, J. *Catal. Sci. Technol.* **2021**, *11*, 3990–4007.
- (21) Kannan, M.; Barteja, P.; Devi, P.; Muthaiah, S. *J. Catal.* **2020**, *386*, 1–11.
- (22) Chen, C.; Wang, Z.-Q.; Gong, Y.-Y.; Wang, J.-C.; Yuan, Y.; Cheng, H.; Sang, W.; Chaemchuen, S.; Verpoort, F. *Carbon.* **2021**, *174*, 284–294.
- (23) Teichmann, D.; Arlt, W.; Wasserscheid, P.; Freymann, R. *Energy Environ. Sci.* **2011**, *4*, 2767–2773.
- (24) Teichmann, D.; Stark, K.; Müller, K.; Zöttl, G.; Wasserscheid, P.; Arlt, W. *Energy Environ. Sci.* **2012**, *5*, 9044–9054.
- (25) Preuster, P.; Papp, C.; Wasserscheid, P. *Acc. Chem. Res.* **2017**, *50*, 74–85.
- (26) Markiewicz, M.; Zhang, Y.Q.; Bösmann, A.; Brückner, N.; Thöming, J.; Wasserscheid, P.; Stolte, S. *Energy Environ. Sci.* **2015**, *8*, 1035–1045.
- (27) Rao, P.C.; Yoon, M. *Potential Energies.* **2020**, *13*, 6040–6063.
- (28) Modisha, P.M.; Ouma, C.N.M.; Garidzirai, R.; Wasserscheid, P.; Bessarabov, D. *Energy & Fuels.* **2019**, *33*, 2778–2796.
- (29) Sievi, G.; Geburtig, D.; Skeledzic, T.; Bösmann, A.; Preuster, P.; Brummel, O.; Waidhas, F.; Montero, M.A.; Khanipour, P.; Katsounaros, I.; Libuda, J.; Mayrhofer, K.J.J.; Wasserscheid, P. *Energy Environ. Sci.* **2019**, *12*, 2305–2314.
- (30) Cho, J.-Y.; Kim, H.; Oh, J.-E.; Park, B.Y. *Catalysts.* **2021**, *11*, 1497–1526.
- (31) Crabtree, R.H. *ACS Sustain. Chem. Eng.* **2017**, *5*, 4491–4498.
- (32) Wang, S.; Huang, H.; Bruneau, C.; Fischmeister, C. *ChemSusChem.* **2019**, *12*, 2350–2354.

- (33) Vivancos, Á.; Beller, M.; Albrecht, M. *ACS Catal.* **2018**, *8*, 17–21.
- (34) Jaiswal, G.; Subaramanian, M.; Sahoo, M.K.; Balaraman, E. *ChemCatChem.* **2019**, *11*, 2449–2457.
- (35) Zhu, T.; Yang, M.; Chen, X.; Dong, Y.; Zhang, Z.; Cheng, H. *J. Catal.* **2019**, *378*, 382–391.
- (36) Wang, B.; Yan, T.; Chang, T.; Wei, J.; Zhou, Q.; Yang, S.; Fang, T. *Carbon.* **2017**, *122*, 9–18.
- (37) Mollar-Cuni, A.; Ventura-Espinosa, D.; Martín, S.; Mayoral, Á.; Borja, P.; Mata, J.A. *ACS Omega.* **2018**, *3*, 15217–15228.
- (38) Sabater, S.; Mata, J.A.; Peris, E. *ACS Catal.* **2014**, *4*, 2038–2047.
- (39) Sabater, S.; Mata, J.A.; Peris, E. *Organometallics.*, **2015**, *34*, 1186–1190.
- (40) Axet, M.R.; Dechy-Cabaret, O.; Durand, J.; Gouygou, M.; Serp, P. *Coord. Chem. Rev.* **2016**, *308*, 236–345.
- (41) Ventura-Espinosa, D.; Carretero-Cerdán, A.; Baya, M.; García, H.; Mata, J.A. *Chem. A Eur. J.* **2017**, *23*, 10815–10821.
- (42) Ventura-Espinosa, D.; Marzá-Beltrán, A.; Mata, J.A. *Chem. A Eur. J.* **2016**, *22*, 17758–17766.
- (43) Ventura-Espinosa, D.; Vicent, C.; Baya, M.; Mata, J.A. *Catal. Sci. Technol.* **2016**, *6*, 8024–8035.
- (44) Ventura-Espinosa, D.; Sabater, S.; Carretero-Cerdán, A.; Baya, M.; Mata, J.A. *ACS Catal.* **2018**, *8*, 2558–2566.
- (45) Mollar-Cuni, A.; Borja, P.; Martín, S.; Guisado-Barrios, G.; Mata, J.A. *Eur. J. Inorg. Chem.* **2020**, *12*, 4254–4262.
- (46) Ventura-Espinosa, D.; Sabater, S.; Mata, J.A. *J. Catal.* **2017**, *352*, 498–504.
- (47) Ventura-Espinosa, D.; Martín, S.; Mata, J.A. *J. Catal.* **2019**, *375*, 419–426.
- (48) Sabater, S.; Mata, J.A. *Synth. Des. New Compd.*, John Wiley & Sons, Inc, Hoboken, NJ, **2016**, 313–326.

- (49) Ruiz-Botella, S.; Peris, E. *Chem. A Eur. J.* **2015**, *21*, 15263–15271.
- (50) Lara, P.; Rivada-Wheelaghan, O.; Conejero, S.; Poteau, R.; Philippot, K.; Chaudret, B. *Angew. Chem. Int. Ed.* **2011**, *50*, 12080–12084.
- (51) Dassenoy, F.; Philippot, K.; Ould Ely, T.; Amiens, C.; Lecante, P.; Snoeck, E.; Mosset, A.; Casanove, M.-J.; Chaudret, B. *New J. Chem.* **1998**, *22*, 703–712.
- (52) Pan, C.; Dassenoy, F.; Casanove, M.-J.; Philippot, K.; Amiens, C.; Lecante, P.; Mosset, A.; Chaudret, B. *J. Phys. Chem. B.* **1999**, *103*, 10098–10101.
- (53) Ely, T.O.; Pan, C.; Amiens, C.; Chaudret, B.; Dassenoy, F.; Lecante, P.; Casanove, M.-J.; Mosset, A.; Respaud, M.; Broto, J.-M. *J. Phys. Chem. B.* **2000**, *104*, 695–702.
- (54) Vidoni, O.; Philippot, K.; Amiens, C.; Chaudret, B.; Balmes, O.; Malm, J.-O.; Bovin, J.-O.; Senocq, F.; Casanove, M.-J. *Angew. Chem. Int. Ed.* **1999**, *38*, 3736–3738.
- (55) Gonzalez-Galvez, D.; Lara, P.; Rivada-Wheelaghan, O.; Conejero, S.; Chaudret, B.; Philippot, K.; van Leeuwen, P.W.N.M. *Catal. Sci. Technol.* **2013**, *3*, 99–105.
- (56) Asensio, J.M.; Tricard, S.; Coppel, Y.; Andrés, R.; Chaudret, B.; de Jesús, E. *Chem. A Eur. J.* **2017**, *23*, 13435–13444.
- (57) Baquero, E.A.; Tricard, S.; Flores, J.C.; de Jesús, E.; Chaudret, B. *Angew. Chem. Int. Ed.* **2014**, *53*, 13220–13224.
- (58) Asensio, J.M.; Tricard, S.; Coppel, Y.; Andrés, R.; Chaudret, B.; de Jesús, E. *Angew. Chem. Int. Ed.* **2017**, *56*, 865–869.
- (59) Su, C.; Loh, K.P. *Acc. Chem. Res.* **2013**, *46*, 2275–2285.
- (60) Mollar-Cuni, A.; Ventura-Espinosa, D.; Martín, S.; García, H.; Mata, J.A. *ACS Catal.* **2021**, *11*, 14688–14693.
- (61) Navalon, S.; Dhakshinamoorthy, A.; Alvaro, M.; Garcia, H. *Chem. Rev.*, **2014**, *114*, 6179–6212.
- (62) Machado, B.F.; Serp, P. *Catal. Sci. Technol.* **2012**, *2*, 54–75.

- (63) Duan, X.; Xiao, M.; Liang, S.; Zhang, Z.; Zeng, Y.; Xi, J.; Wang, S. *Carbon*. **2017**, *119*, 326–331.
- (64) Burés, J. *Angew. Chem. Int. Ed.* **2016**, *55*, 2028–2031.
- (65) Nielsen, C.D.T.; Burés, J. *Chem. Sci.* **2019**, *10*, 348–353.
- (66) Martínez-Carrión, A.; Howlett, M.G.; Alamillo-Ferrer, C.; Clayton, A.D.; Bourne, R.A.; Codina, A.; Vidal-Ferran, A.; Adams, R.W.; Burés, J. *Angew. Chem. Int. Ed.* **2019**, *58*, 10189–10193.

CHAPTER 7:

Conclusions

The main conclusions of the research work included in this PhD. thesis are:

- The dehydrogenation of different N-heterocycles using **rGO** as carbocatalyst has been carried out giving excellent conversions and high yields. The quinone-like groups have been proposed as possible catalytic active sites for this transformation.
- The hydrosilylation of alkynes was carried out using a PEPPSI platinum complex as catalyst giving excellent yields and good selectivities. The immobilization of the complex over **rGO** allowed its reuse several times without important losses of activity and selectivity.
- A hybrid material comprised of a palladium complex supported onto **rGO** as precatalyst catalyses the semi-hydrogenation of alkynes giving high yields towards Z-isomers under mild conditions. The heterogeneous nature of the material allowed the catalyst recycling several times maintaining its activity and selectivity. It was found that Pd NPs are produced in-situ during the reaction resulting the active catalytic species.
- A series of Ir complexes bearing NHC or MIC carbene ligands behave as efficient and selective homogeneous catalysts in dehydrogenation of monosaccharids to form the corresponding aldolic acids. A plausible reaction mechanism is proposed based on experimental evidence.
- A hybrid material based on Pd nanoparticles stabilized by a NHC ligand and supported over **rGO** have been synthesized and characterized. It was used as dual catalyst, for the dehydrogenation and hydrogenation of tetrahydroquinoline/quinoline pair to be used as LOHC.

Las principales conclusiones incluidas en esta tesis doctoral derivadas del trabajo de investigación son:

- Se ha llevado a cabo la deshidrogenación de diferentes N-heterociclos utilizando **rGO** como carbocatalizador dando como resultado conversiones excelentes y buenos rendimientos. Los grupos funcionales basados en *o*-quinonas han sido propuestos como los centros catalíticamente activos para esta transformación.
- Se ha llevado a cabo la hidrosililación de alquinos utilizando un complejo de platino PEPPSI como catalizador, dando excelentes rendimientos y altas selectividades. La inmovilización del complejo sobre **rGO** permitió su reciclaje varias veces sin pérdidas importantes de actividad ni selectividad.
- La semihidrogenación de alquinos se llevo a cabo utilizando un complejo de paladio soportado sobre **rGO** como precatalizador dando el isómero Z con altos rendimientos. Gracias a la naturaleza heterogénea del material se pudo llevar a cabo el reciclaje del catalizador varias veces sin perdidas de actividad ni selectividad. Se determino que nanoparticulas de paladio se formaban durante el transcurso de la reacción y que estas eran las responsables de la actividad catalítica.
- Una serie de complejos de Ir con un carbeno NHC o MIC como ligando actúan como catalizadores homogéneos eficientes y selectivos en la reacción de deshidrogenación de monosacáridos para obtener el correspondiente ácido aldólico. Un mecanismo de reacción plausible ha sido propuesto en base a las evidencias experimentales.
- Un material híbrido basado en nanoparticulas de paladio soportadas sobre **rGO** ha sido sintetizado y caracterizado completamente. Este material ha sido utilizado como catalizador dual en las reacciones de deshidrogenación e hidrogenación del par tetrahydroquinoleína/quinoleína con el fin de ser usado como LOHC.

APPENDIX

(Nombre) David Ventura Espinosa....., como coautor/ coautora doy mi **autorización** a (Nombre del doctorando/doctoranda) Andrés.Mollar.Cuni..... para la presentación de las siguientes publicaciones como parte de su tesis doctoral.

Relación de publicaciones:

Mollar-Cuni, A.; Ventura-Espinosa, D.; Martín, S.; García, H.; Mata, J. A.; Reduced Graphene Oxides as Carbocatalysts in Acceptorless Dehydrogenation of N-Heterocycles. ACS Catal. 2021, 11, 14688–14693.

Mollar-Cuni, A.; Ventura-Espinosa, D.; Martín, S.; Mayoral, Á.; Borja, P.; Mata, J. A.; Stabilization of Nanoparticles Produced by Hydrogenation of Palladium-N-Heterocyclic Carbene Complexes on the Surface of Graphene and Implications in Catalysis. ACS Omega 2018, 3, 15217–15228. <https://doi.org/10.1021/acsomega.8b02193>.

Asimismo, **renuncio** a poder utilizar estas publicaciones como parte de otra tesis doctoral.

Y para que conste firmo el presente documento,



Lugar, fecha y firma

Castellón 5 de diciembre de 2022

Todo ello, atendiendo al artículo 28 del Reglamento de los estudios de doctorado de la Universitat Jaume I de Castelló, regulados por el RD 99/2011, en la Universitat Jaume I (Aprobado en la sesión nº 8/2020 del Consejo de Gobierno de 02/10/2020):

“(…)

4. *En el caso de publicaciones conjuntas, todas las personas coautoras deberán manifestar explícitamente su autorización para que la doctoranda o doctorando presente el trabajo como parte de su tesis y la renuncia expresa a presentar este mismo trabajo como parte de otra tesis doctoral. Esta autorización se adjuntará como documentación en el momento del inicio de evaluación de la tesis.*

(Nombre) María Pilar Borja....., como coautor/ coautora doy mi **autorización** a (Nombre del doctorando/doctoranda) .Andrés.Mollar.Cuni.... para la presentación de las siguientes publicaciones como parte de su tesis doctoral.

Relación de publicaciones:

Mollar-Cuni, A.; Borja, P.; Martín, S.; Guisado-Barrios, G.; Mata, J. A.: A Platinum Molecular Complex Immobilised on the Surface of Graphene as Active Catalyst in Alkyne Hydrosilylation. Eur. J. Inorg. Chem. 2020, 4254–4262. <https://doi.org/10.1002/ejic.202000356>

Mollar-Cuni, A.; Ventura-Espinosa, D.; Martín, S.; Mayoral, Á.; Borja, P.; Mata, J. A.; Stabilization of Nanoparticles Produced by Hydrogenation of Palladium-N-Heterocyclic Carbene Complexes on the Surface of Graphene and Implications in Catalysis. ACS Omega 2018, 3, 15217–15228. <https://doi.org/10.1021/acsomega.8b02193>.

Mollar-Cuni, A.; Byrne, J. P.; Borja, P.; Vicent, C.; Albrecht, M.; Mata, J. A.; Selective Conversion of Various Monosaccharaides into Sugar Acids by Additive-Free Dehydrogenation in Water. ChemCatChem 2020, 12, 3746–3752. <https://doi.org/10.1002/cctc.202000544>.

Asimismo, **renuncio** a poder utilizar estas publicaciones como parte de otra tesis doctoral.

Y para que conste firmo el presente documento,

Firmado digitalmente por BORJA
USTARIZ MARIA DEL PILAR MARTINA
- 17762617Q
Nombre de reconocimiento (DN):
c=ES,
serialNumber=IDCES-17762617Q,
givenName=MARIA DEL PILAR
MARTINA, sn=BORJA USTARIZ,
cn=BORJA USTARIZ MARIA DEL PILAR
MARTINA - 17762617Q
Fecha: 2022.12.06 11:09:10 +01'00'

BORJA USTARIZ
MARIA DEL
PILAR MARTINA
- 17762617Q

Lugar, fecha y firma

Todo ello, atendiendo al artículo 28 del Reglamento de los estudios de doctorado de la Universitat Jaume I de Castelló, regulados por el RD 99/2011, en la Universitat Jaume I (Aprobado en la sesión nº 8/2020 del Consejo de Gobierno de 02/10/2020):

“(…)

4. En el caso de publicaciones conjuntas, todas las personas coautoras deberán manifestar explícitamente su autorización para que la doctoranda o doctorando presente el trabajo como parte de su tesis y la renuncia expresa a presentar este mismo trabajo como parte de otra tesis doctoral. Esta autorización se adjuntará como documentación en el momento del inicio de evaluación de la tesis.

(Nombre) Santiago Martín Solans....., como coautor/ coautora doy mi **autorización** a (Nombre del doctorando/doctoranda) .Andrés.Mollar.Cuni..... para la presentación de las siguientes publicaciones como parte de su tesis doctoral.

Relación de publicaciones:

Mollar-Cuni, A.; Ventura-Espinosa, D.; Martín, S.; García, H.; Mata, J. A.; Reduced Graphene Oxides as Carbocatalysts in Acceptorless Dehydrogenation of N-Heterocycles. ACS Catal. 2021, 11, 14688–14693.

Mollar-Cuni, A.; Borja, P.; Martín, S.; Guisado-Barrios, G.; Mata, J. A.: A Platinum Molecular Complex Immobilised on the Surface of Graphene as Active Catalyst in Alkyne Hydrosilylation. Eur. J. Inorg. Chem. 2020, 4254–4262. <https://doi.org/10.1002/ejic.202000356>

Mollar-Cuni, A.; Ventura-Espinosa, D.; Martín, S.; Mayoral, Á.; Borja, P.; Mata, J. A.: Stabilization of Nanoparticles Produced by Hydrogenation of Palladium-N-Heterocyclic Carbene Complexes on the Surface of Graphene and Implications in Catalysis. ACS Omega 2018, 3, 15217–15228. <https://doi.org/10.1021/acsomega.8b02193>.

Mollar-Cuni, A.; Martín, S.; Guisado-Barrios, G.; Mata, J. A.; Dual role of graphene as support of ligand-stabilized palladium nanoparticles and carbocatalyst for (de)hydrogenation of N-Heterocycles. Carbon, 2022, Submitted.

Asimismo, **renuncio** a poder utilizar estas publicaciones como parte de otra tesis doctoral.

Y para que conste firmo el presente documento,

MARTIN SOLANS
SANTIAGO -
17727563Z

Firmado digitalmente por MARTIN
SOLANS SANTIAGO - 17727563Z
Nombre de reconocimiento (DN): c=ES,
serialNumber=IDCES-17727563Z,
givenName=SANTIAGO, sn=MARTIN
SOLANS, cn=MARTIN SOLANS SANTIAGO
- 17727563Z
Fecha: 2022.12.01 23:03:26 +01'00'

Lugar, fecha y firma

Todo ello, atendiendo al artículo 28 del Reglamento de los estudios de doctorado de la Universitat Jaume I de Castelló, regulados por el RD 99/2011, en la Universitat Jaume I (Aprobado en la sesión nº 8/2020 del Consejo de Gobierno de 02/10/2020):

“(…)

4. En el caso de publicaciones conjuntas, todas las personas coautoras deberán manifestar explícitamente su autorización para que la doctoranda o doctorando presente el trabajo como parte de su tesis y la renuncia expresa a presentar este mismo trabajo como parte de otra tesis doctoral. Esta autorización se adjuntará como documentación en el momento del inicio de evaluación de la tesis.

(Nombre) Álvaro Mayoral....., como coautor/ coautora doy mi **autorización** a (Nombre del doctorando/doctoranda) .Andrés.Mollar.Cuni..... para la presentación de las siguientes publicaciones como parte de su tesis doctoral.

Relación de publicaciones:

Mollar-Cuni, A.; Ventura-Espinosa, D.; Martín, S.; Mayoral, Á.; Borja, P.; Mata, J. A.;
Stabilization of Nanoparticles Produced by Hydrogenation of Palladium-N-Heterocyclic Carbene
Complexes on the Surface of Graphene and Implications in Catalysis.
ACS Omega 2018, 3, 15217–15228. <https://doi.org/10.1021/acsomega.8b02193>.

Asimismo, **renuncio** a poder utilizar estas publicaciones como parte de otra tesis doctoral.

Y para que conste firmo el presente documento,

Lugar, fecha y firma

Firmado por MAYORAL
GARCIA ALVARO - ***2964**
el día 02/12/2022 con un
certificado emitido por
AC FNMT Usuarios

Todo ello, atendiendo al artículo 28 del Reglamento de los estudios de doctorado de la Universitat Jaume I de Castelló, regulados por el RD 99/2011, en la Universitat Jaume I (Aprobado en la sesión nº 8/2020 del Consejo de Gobierno de 02/10/2020):

“(…)

4. *En el caso de publicaciones conjuntas, todas las personas coautoras deberán manifestar explícitamente su autorización para que la doctoranda o doctorando presente el trabajo como parte de su tesis y la renuncia expresa a presentar este mismo trabajo como parte de otra tesis doctoral. Esta autorización se adjuntará como documentación en el momento del inicio de evaluación de la tesis.*

(Nombre) Cristian Vicent....., como coautor/ coautora doy mi **autorización** a (Nombre del doctorando/doctoranda) .Andrés.Mollar.Cuni.....para la presentación de las siguientes publicaciones como parte de su tesis doctoral.

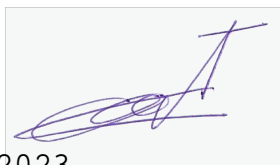
Relación de publicaciones:

Mollar-Cuni, A.; Byrne, J. P.; Borja, P.; Vicent, C.; Albrecht, M.; Mata, J. A.;
Selective Conversion of Various Monosaccharaides into Sugar Acids by Additive-Free
Dehydrogenation in Water. ChemCatChem 2020, 12, 3746–3752.
<https://doi.org/10.1002/cctc.202000544>.

Asimismo, **renuncio** a poder utilizar estas publicaciones como parte de otra tesis doctoral.

Y para que conste firmo el presente documento,

Lugar, fecha y firma



Castelló 13 gener 2023

Todo ello, atendiendo al artículo 28 del Reglamento de los estudios de doctorado de la Universitat Jaume I de Castelló, regulados por el RD 99/2011, en la Universitat Jaume I (Aprobado en la sesión nº 8/2020 del Consejo de Gobierno de 02 /10/2020):

“(…)

4. En el caso de publicaciones conjuntas, todas las personas coautoras deberán manifestar explícitamente su autorización para que la doctoranda o doctorando presente el trabajo como parte de su tesis y la renuncia expresa a presentar este mismo trabajo como parte de otra tesis doctoral. Esta autorización se adjuntará como documentación en el momento del inicio de evaluación de la tesis.

(Nombre) Martin Albrecht....., como coautor/ coautora doy mi **autorización** a (Nombre del doctorando/doctoranda) .Andrés.Mollar.Cuni..... para la presentación de las siguientes publicaciones como parte de su tesis doctoral.

Relación de publicaciones:

Mollar-Cuni, A.; Byrne, J. P.; Borja, P.; Vicent, C.; Albrecht, M.; Mata, J. A.;
Selective Conversion of Various Monosaccharaides into Sugar Acids by Additive-Free
Dehydrogenation in Water. ChemCatChem 2020, 12, 3746–3752.
<https://doi.org/10.1002/cctc.202000544>.

Asimismo, **renuncio** a poder utilizar estas publicaciones como parte de otra tesis doctoral.

Y para que conste firmo el presente documento,

Lugar, fecha y firma

Bern, 2 December 2022



Todo ello, atendiendo al artículo 28 del Reglamento de los estudios de doctorado de la Universitat Jaume I de Castelló, regulados por el RD 99/2011, en la Universitat Jaume I (Aprobado en la sesión nº 8/2020 del Consejo de Gobierno de 02 /10/2020):

“(…)

4. *En el caso de publicaciones conjuntas, todas las personas coautoras deberán manifestar explícitamente su autorización para que la doctoranda o doctorando presente el trabajo como parte de su tesis y la renuncia expresa a presentar este mismo trabajo como parte de otra tesis doctoral. Esta autorización se adjuntará como documentación en el momento del inicio de evaluación de la tesis.*

(Nombre) Joseph Byrne....., como coautor/ coautora doy mi **autorización** a (Nombre del doctorando/doctoranda) .Andrés.Mollar.Cuni.....para la presentación de las siguientes publicaciones como parte de su tesis doctoral.

Relación de publicaciones:

Mollar-Cuni, A.; Byrne, J. P.; Borja, P.; Vicent, C.; Albrecht, M.; Mata, J. A.;
Selective Conversion of Various Monosaccharaides into Sugar Acids by Additive-Free
Dehydrogenation in Water. ChemCatChem 2020, 12, 3746–3752.
<https://doi.org/10.1002/cctc.202000544>.

Asimismo, **renuncio** a poder utilizar estas publicaciones como parte de otra tesis doctoral.

Y para que conste firmo el presente documento,



Galway (Irlanda). 02/12/2022

Lugar, fecha y firma

Todo ello, atendiendo al artículo 28 del Reglamento de los estudios de doctorado de la Universitat Jaume I de Castelló, regulados por el RD 99/2011, en la Universitat Jaume I (Aprobado en la sesión nº 8/2020 del Consejo de Gobierno de 02/10/2020):

“(…)

4. En el caso de publicaciones conjuntas, todas las personas coautoras deberán manifestar explícitamente su autorización para que la doctoranda o doctorando presente el trabajo como parte de su tesis y la renuncia expresa a presentar este mismo trabajo como parte de otra tesis doctoral. Esta autorización se adjuntará como documentación en el momento del inicio de evaluación de la tesis.

(Nombre) Hermenegildo García Gómez....., como coautor/ coautora doy mi **autorización** a (Nombre del doctorando/doctoranda) .Andrés.Mollar.Cuni..... para la presentación de las siguientes publicaciones como parte de su tesis doctoral.


Relación de publicaciones:

Mollar-Cuni, A.; Ventura-Espinosa, D.; Martín, S.; García, H.; Mata, J. A.;
Reduced Graphene Oxides as Carbocatalysts in Acceptorless Dehydrogenation of N-Heterocycles.
ACS Catal. 2021, 11, 14688–14693. <https://doi.org/10.1021/acscatal.1c04649>.

Asimismo, **renuncio** a poder utilizar estas publicaciones como parte de otra tesis doctoral.

Y para que conste firmo el presente documento,

GARCIA
GOMEZ
HERMENEGILDO
O - 20402567A



Firmado digitalmente por
GARCIA GOMEZ
HERMENEGILDO -
20402567A
Fecha: 2022.12.02
10:05:58 +01'00'

Lugar, fecha y firma

Todo ello, atendiendo al artículo 28 del Reglamento de los estudios de doctorado de la Universitat Jaume I de Castelló, regulados por el RD 99/2011, en la Universitat Jaume I (Aprobado en la sesión nº 8/2020 del Consejo de Gobierno de 02/10/2020):

“(…)

4. *En el caso de publicaciones conjuntas, todas las personas coautoras deberán manifestar explícitamente su autorización para que la doctoranda o doctorando presente el trabajo como parte de su tesis y la renuncia expresa a presentar este mismo trabajo como parte de otra tesis doctoral. Esta autorización se adjuntará como documentación en el momento del inicio de evaluación de la tesis.*